UNIVERSITY OF CATANIA

Department of Electrical, Electronic and Computer Engineering

PhD Course in Systems Engineering, Energy, Information Technology and Telecommunications - XXXIII cycle

MODELING, EXPERIMENTAL ANALYSIS AND OPTIMIZATION OF FLOATING PHOTOVOLTAIC POWER PLANTS

Supervisor:

Chiar.mo Prof. Giuseppe Marco Tina

Co-supervisor:

Ing. Leonardo Merlo

Prof. Sandro Nižetić

PhD Student:

Fausto BONTEMPO SCAVO

YEAR 2021

To my parents.

STATEMENT

I hereby certify that this research paper has been composed by myself, and describes my own work, unless otherwise acknowledged in the text. All references and verbatim extracts have been quoted, and all sources of information have been specifically acknowledged. I confirm that this work is submitted for my PhD in the University of Catania and has not been submitted elsewhere in any other form for the fulfilment of any other degree or qualification.

Catania, 01.02.2021

ABSTRACT

The objective of this thesis is to explore innovative systems and FPV plant configurations, capable of increasing efficiency and reducing LCOE. In the context of the study of the integration of FPV systems in water basins, numerical models have been developed that allow to estimate the evaporation rate in relation to the characteristics of the floating systems and the occupied water surface. Models to evaluate the performances of different plant solutions (monofacial-bifacial, fixed and tracking), in active and passive cooling conditions have been implemented. An economic evaluation was carried out for each type of FPV analyzed in order to verify the competitiveness of an FPV system compared to a classic GPV. For the models validation, data collected by the floating photovoltaic experimental system, installed at the Enel Innovation Hub and Lab in Passo Martino (CT) in Italy, was used.

Results shows that, installing the FPV on 50% of the basin area, can be obtain a water saving of 73%. Thanks to the natural cooling of the modules, a gain of more than 5% can be obtained and, depending on the module technology and climatic conditions, this gain can be greater than 7%. By using bifacial modules, an energy gain ranging from 5% to 13% can be obtained, depending on the albedo. By implementing active cooling systems with a film of water, which integrate well into FPV systems, an energy gain greater than 9% can be obtained. As regards the tracking systems, for intermediate latitudes an increase higher than 47% can be obtained for Dual axis tracker. With non-evaporated water that can be sold for irrigation or in the form of electricity produced by the HPP plant, it is possible to obtain revenues greater than 3 $ / kWp in the first case and greater than 4 $ / kWp in the second case. Considering all these benefits, an FPV system can be more competitive than a classic GPV system. In fact, from the studies reported in this work it is possible to obtain an LCOE that is 20% lower than GPV.

Contents

Index of figures

Index of tables

Nomenclature

Latin symbols

A	[m^2]	Surface Area
a	[%]	Albedo
BF	[%]	Bifaciality factor
BG	[%]	Bifacial gain
C	[J/K]	Heat Capacity
C	[dimensionless]	Cloudiness function
c	[J/kg K]	Specific heat
c	[$]	Cost
CF	[%]	Capacity factor
DHI	[kWh/m^2]	Diffuse horizontal irradiation
d	[m]	Pitch or distance
E	[mm d^{-1}]	Evaporation
EE	[kWh]	Electrical energy
e_a	[kPa]	Actual vapor pressure
e_w^*	[kPa]	Saturation vapour pressure
F	[dimensionless]	View factor
f_d	[%]	Diffuse irradiation factor
FG	[%]	Floating gain
G	[W/m^2]	solar irradiance
GG	[%]	Gable gain
GHI	[kWh/m^2]	global horizontal irradiation
Gr	[dimensionless]	Grashof number
h	[W/m^2K]	Convective coefficient
h	[m]	Height
I	[A]	Current
L	[m]	Length
LW	[MJ $m^{-2}d^{-1}$]	Long wave radiation
m	[kg]	Mass
n	[year]	Life of PV plant
N	[MJ $m^{-2}d^{-1}$]	Water heat
Nu	[dimensionless]	Nusselt number
P	[W]	Power
Pr	[dimensionless]	Prandtl number
$Price$	[$]	Price
p	[m]	Perimeter of the PV module
Q	[m^3/s]	Pump flow rate
Q^*	[MJ $m^{-2}d^{-1}$]	Net radiation at the water surface
r	[%]	Discount rate
r_a	[s m^{-1}]	Aerodynamic resistance
R	[ohm]	Resistance
Ra	[dimensionless]	Rayleigh number
Re	[dimensionless]	Reynolds number
Rev	[$]	Revenue
R_b	[MJ $m^{-2}d^{-1}$]	Direct horizontal solar radiation
R_d	[MJ $m^{-2}d^{-1}$]	Diffuse horizontal solar radiation
R_s	[MJ $m^{-2}d^{-1}$]	Horizontal solar radiation

RH	[%]	Relative humidity
s	[m]	Thickness of material
S	[m^2]	Surface
SW	[MJ $m^{-2}d^{-1}$]	Short wave radiation
T	[°C]	Temperature
t	[s]	Time
TBG	[%]	Tracking gifacial gain
TG	[%]	Tracking gain
TFG	[%]	Tracking floating gain
TFBG	[%]	Tracking floating bifacial gain
u_h	[m s^{-1}]	Wind speed h meter above the ground surface
V	[V]	Voltage
Vol	[m^3]	Volume
x	[dimensionless]	Percentage of cover of water surface
Y	[h]	Equivalent operating hours
Z	[m]	Height of water basin

Greek symbols

α	[dimensionless]	Absorbance
β_0	[$°C^{-1}$]	Thermal coefficient
γ	[°]	Tilt angle
ε	[dimensionless]	Emissivity
η	[%]	Efficiency
λ	[W/m·K]	Thermal conductivity
λ	[MJ kg^{-1}]	Latent heat of vaporisation
ρ	[kg/m^3]	Density
σ	[$W/m·K^4$]	Boltzmann constant
τ	[dimensionless]	Transmissivity
Φ	[W]	Heat source
Φ	[°]	Azimuth angle

Subscripts

a	air
ap	apparent
b	Bifacial
cover	Cover
cum	Cumulated
bg	Back glass surface
bk	back
cd	Conduction
conv	Convection
COOL	Cooling
diff	difference
d	diffuse
db	dry bulb
eva	Eva material
ev	evaporation
el	*electrical*
en	*energy*
fg	Front glass surface

free	Free surface
fr	front
fl	floating
gr	Ground
g	global
in	Inlet
i	Incoming
IRR	Irrigation
l.r.	Linear regression
los	Losses
m	Monofacial
M	Module
n	Net
nw	Near water
o	Outgoing
pv	Photovoltaic
r	Radiative
rt	rooftop
ted	Back tedlar surface
w	water

Abbreviations

CAPEX	Capital expenditure
csw 1	Commercial software PVsyst
csw 2	Commercial software SAM (System Advisor Model)
CWS	Covered water surface
DoE	Design of experiments
EI	Environmental impact
EVM	Evaporation models
HDPE	High density polyethylene
HPP	Hydro power plant
LCOE	Levelized cost of electricity
NOCT	Normal Operating Cell Temperature
obj	Objective function
OPEX	Operating Expense
FPV	Floating photovoltaic
GME	Gestore dei mercati energetici
GPV	Ground photovoltaic
STC	Standard Test Conditions

1 Introduction

1.1 General background

With the emergence of several developing economies and exponential population growth, the growing demand for energy cannot be sustainably met by burning the ever-decreasing fossil fuel reserves. The use of these fuels, in fact, generates global warming and climate changes which in the long term irreversibly will damage the earth.

Renewable energies, offer an ecological and economical alternative to fossil fuels, are already playing a big role in energy production, a role which is only expected to grow further, as visible in Figure 1.

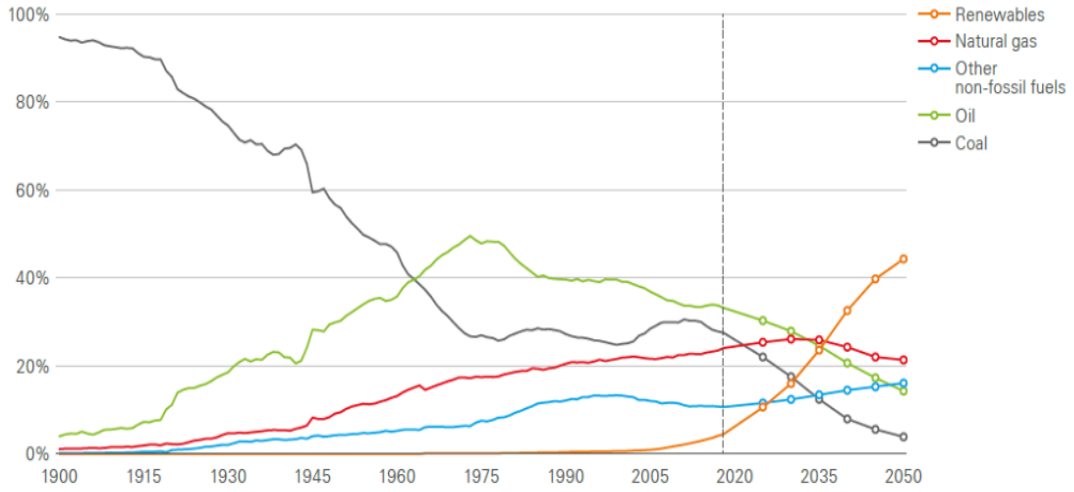

Figure 1 Global energy mix up to 2050 as forecast by BP Energy [1]

One of the methods to produce clean energy is Photovoltaic (PV). This sector has grown significantly in recent years, representing a considerable proportion of the global energy produced by renewable energy sources. By the end of 2019, total installed PV capacity reached 518.2 GW worldwide and 138 GWp in Europe [2]. A terawatt-peak could be reached shortly after 2020, according to the annual market analysis of the European PV sector association Solar Power Europe [3].

There are, however, two factors that could limit the further development of PV technology, namely:

- invasiveness and environmental impact: according to real data reported in [4] for USA, the capacity-weighted average land use for utility scale PV plants ranges between (in ha/MWac): 2.39 (fixed) ÷ 3.81 (2-axis) for medium size PV (> 1 MW, <20 MW) and 2.35 (fixed) ÷ 3.64 (1-axis) for large PV (> 20 MW).
- intermittency and availability for a limited time (between 1000 and 2000 hours per year).

In relation to the two points listed above, possible solutions have been proposed in literature: to use the concept of "agrivoltaics", that is to use the same surface of land in a synergistic way both to produce photovoltaic energy and for conventional agriculture [5], intensify the use of PV above or below water surfaces (eg lakes, reservoirs, sea). This latest technology called Floating PV, began to take hold in 2015 thanks to numerous plant projects installed around the world [6].

The solutions mentioned above become even more performing, using high efficiency modules (conversion efficiency to date it has reached values around 24% [7]) or bifacial modules that capture the solar radiation also on the rear surface [8].

In recent years bifacial technology, both in the market and in the academic environment, has aroused considerable interest so as to predict a market share of 70% in 2030 (see Figure 2) [9].

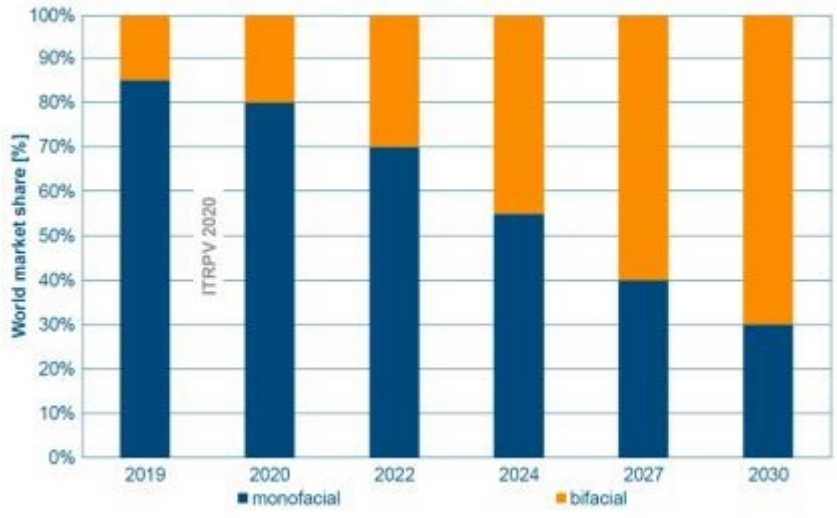

Figure 2 World development trend of PV market share between mPV and bPV technologies [9]

Numerous research studies, including simulations and experiments, on bifacial technology have been conducted in scientific settings [10]. However, to have a further

impetus, it is necessary to fill some gaps, for example: to define standards for measuring indoor performance and to define simulation models to be used to predict their performance in real plants [11].

The FPV capacity in 2018 reached a total of 1.3 GWp worldwide [12], a very significant figure as it corresponds to 0.2% of the cumulative installed capacity in the world of PV systems.

Figure 3 shows the evolution of the installed power from 2007 to 2018.

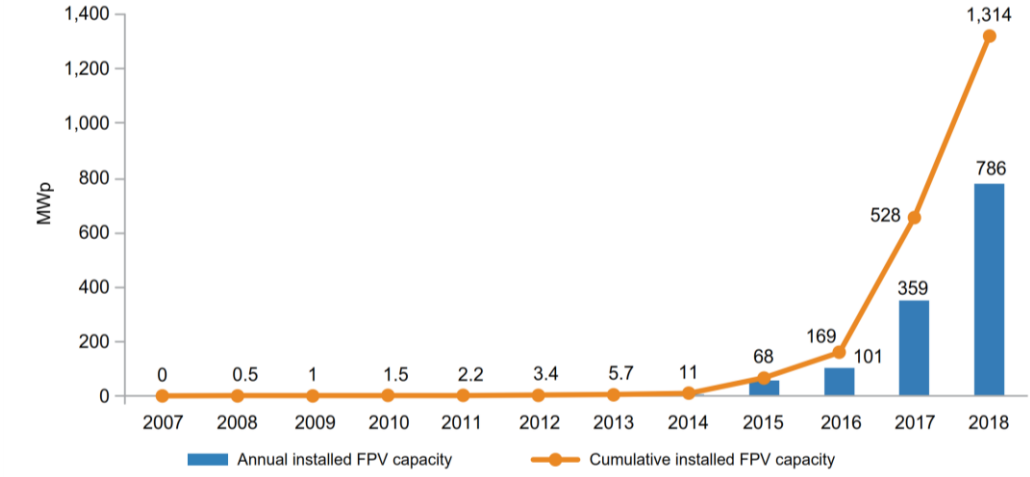

Figure 3 Global installed floating PV capacity

FPV installations therefore, open new avenues for increasing solar generation capacity, especially in countries with high population densities where there are competing uses for land availability. They have some advantages over GPV systems, including the use of existing electricity transmission infrastructures in hydroelectric power plants, compactness and modularity, proximity to demand centers (in the case of water supply tanks) and better energy yield thanks to to the cooling effects of water. The exact extent of these benefits has yet to be confirmed by larger installations, at different latitudes and over time, but in many cases they can offset the current higher capital cost. The ability to add floating solar capacity to existing hydropower plants is of particular interest, especially in the case of large hydroelectric sites which can be managed flexibly. Solar capacity can be used to increase hydroelectric production capacity and can also help optimally manage water availability. The hydroelectric source can also compensate for the variability and unpredictability of solar production.

Other potential benefits of floating solar include: reducing evaporation in water tanks, as solar panels provide shade and limit evaporative effects; the improvement of water quality, thanks to the reduction of algae growth; the reduction or elimination of the shading of the photovoltaic modules; the elimination of the need for major site preparation, such as leveling or foundation laying, which must be performed for ground installations.

In this thesis work some aspects and advantages mentioned above will be studied, with the aim of making FPV systems competitive respect to the classics PV, using innovative technologies such as bifacial modules and water active cooling techniques, which allow to reduce the cost of the energy produced.

1.2 Objectives

To achieve the objectives set during the drafting of the PhD research project, i.e. to explore innovative systems and FPV plant configurations, capable of increasing efficiency and reducing LCOE, it was first of all necessary to carry out an extensive bibliographic search of the existing literature and subsequently deepen the topics of interest, filling the gaps in the literature.

The development of the research had a modeling-experimental methodological approach. Models have been proposed for estimation of evaporation in presence of FPV systems on water basins and for performance evaluation of different plant solutions (monofacial-bifacial, fixed and tracking), in active and passive cooling conditions.

An economic evaluation was carried out for each type of FPV analyzed in order to verify the competitiveness of an FPV system compared to a classic GPV.

For the models validation, data collected by the floating photovoltaic experimental system, installed at the Enel Innovation Hub and Lab in Passo Martino (CT) in Italy, was used. The test bench description is reported in Chapter 3.

1.3 Thesis Outline

The introductory and concluding chapters of this work are respectively in Chapter 1 and Chapter 10, with Chapter 1 introducing the research work and Chapter 10 summarizing the results and contributions provided to the research, with indications for future research.

Chapter 2 presents a review of the existing literature and provides the necessary basis for tackling subsequent chapters. It contains a brief and general description of the bifacial technology (bPV) and floating (FPV) systems.

Chapter 3 describes in detail the experimental system with which the implemented models were compared.

Chapter 4 describes in detail the methodology developed to estimate the reduction of evaporation in presence of partial coverage of water basins with FPV systems.

Chapter 5 is a preliminary study of Chapter 6 and presents a multilayer temperature model for estimating the performance of mono and bifacial modules. This will be used to implement the FPV systems models.

Chapter 6 details the methodology developed to predict the performance of an FPV array under active and passive water cooling of the modules. Aspects relating to the interaction between the water surface and the FPV plant from an energy point of view are analyzed.

Chapter 7 describes in detail the methodology developed to make commercial software tools usable for FPV plant performance estimation

Chapter 8, on the basis of the methodology suggested in Chapter 7, shows the results of the yield of an FPV array in the long-term using different plant solutions, that is mono or bifacial modules and tracking systems with single horizontal or vertical axis and double axis. Therefore, it provides the energy data to be used in the economic evaluation phase of FPV systems.

Chapter 9 show comparative economic analysis on the basis of the energy performance obtained in the previous chapters and on the basis of the evaporative models that made it possible to estimate the reduction of evaporation in the presence of partial coverage of the water surface. Therefore, by calculating the LCOE of the various innovative

solutions studied, the competitiveness of an FPV system is assessed compared to a GPV system.

In Chapter 10, the results achieved and future prospects are summarized.

2 Literature review

To fully understand the work developed in this thesis it is necessary to establish a common ground of basic knowledge in several issues. This knowledge will be reached in the following sub-chapters, where the research existing up to now in the context of bifacial technology and floating systems is introduced.

2.1 Bifacial photovoltaic

Bifacial photovoltaic (bPV) technology is considered a promising alternative to the conventional monofacial PV (mPV) technology as it can generate more energy than mPV by absorbing sunlight from front and back sides.

2.1.1 Technology

Various technologies have been developed in order to increase the efficiency of the cell, those on the market are: PERC, PERL, PERT, HIT, IBC and DSBCSC [8]. The difference between the various technologies lies in the different bifaciality factor BF which ranges from 70% -80% for PERC, IBC and DSBCSC, 80-85% for PERL and PERT and 95-100% for HIT. The last one has the best performance.

The bPV modules on the market are substantially with two types of backsheet, that is glass or transparent organic material. They can also be with or without a frame.

2.1.2 Performance modelling

To predict the performance of bifacial modules, since solar energy is also captured on the rear, it is necessary to review the simulation models of traditional monofacial PV modules. In particular, the thermal, electrical, and optical models need to be reviewed.

The optical models implemented for the bifacial modules must take into account the front (G_{fr}), rear (G_{bk}) solar radiation and the albedo of the ground (a).

These models utilize different methods to calculate the rear irradiance contribution and fall into three general categories: raytracing models, view factor models and empirical models [13].

The temperature of the cells of a PV module is one of the main factors that influence the performance of a system, in fact it is necessary to know this variable in order to estimate the power produced.

The thermal models for the bifacial modules depend on the type of module (glass glass, glass-organic material with or without frame). In literature there are several studies on such topic [14] [15].

In PVsyst software, a thermal model based on the Faiman model [16] is used. Coefficients are usually equal to 25 W/m^2 K and 1.2 W/m^3 s K, respectively. Yusufoglu et al. in [17] apply NOCT method with corrected value of T_{NOCT}, assuming it 2°C higher than the corresponding value used for monofacial cell.

Energy balance models are based on energy balance equations of the modules. Solar radiation, wind speed, ambient temperature are usually the input variables.

In [18] a model in which it is possible to calculate the temperature of the various layers of the module is presented.

For the electrical characterization of a bPV, the energy produced by the rear must also be taken into account. There are three different models for calculating the power produced, namely: single-point power, characteristic point and equivalent circuit.

In [19] authors propose the equivalent circuit of Figure 4, in which the front and rear are implemented in a similar way.

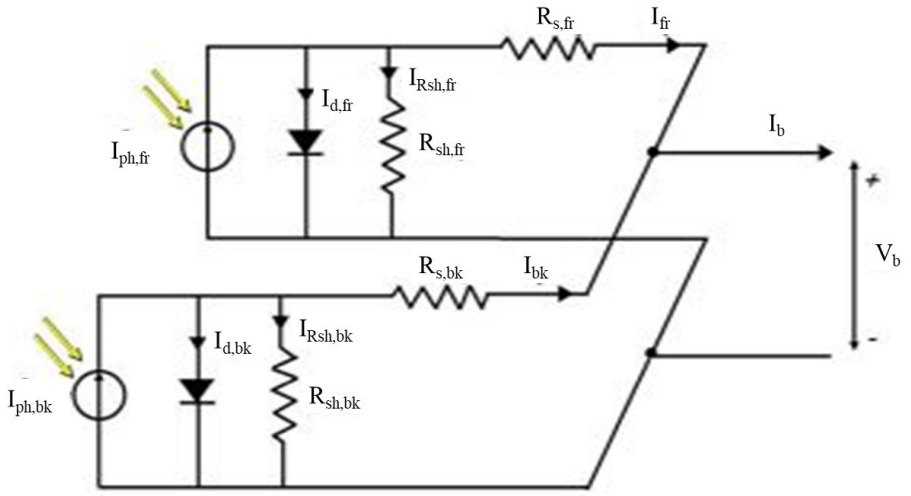

Figure 4 Equivalent circuit of bifacial cell [19]

2.1.3 Energy production and applications

The method for evaluating the energy gain of bifacial systems is to calculate the so-called bifacial gain (BG) obtained from the difference in energy produced/equivalent operating hours between a bifacial and monofacial module, normalized with respect to the energy produced/equivalent operating hours by the monofacial.

BG is defined by Eq. 1

$$BG\% = 100\frac{Y_b - Y_m}{Y_m} \quad \textbf{Eq. 1}$$

The use of bPV technology made it possible to increase the energy produced (BG=35%) for the same area occupied [20]. Specifically, high BG values, such as those listed above, can be obtained in the case of modules installed in a single row, with a high soil albedo coefficient and a height above the ground of 1.5 m and optimum tilt [21].

The efficiency of a bifacial module can be determined using the following equations.

$$\eta_{b/m-fr} = \eta_{frSTC}\left[1 - \beta_0\left(T_{pv} - T_{STC}\right) + \gamma\log\left(G_{fr}\right)\right] \quad \textbf{Eq. 2}$$

For the backside of bifacial can be calculated as:

$$\eta_{b-bk} = BF\ \eta_{frSTC}\left[1 - \beta_0\left(T_{pv} - T_{STC}\right) + \gamma\log\left(G_{bk}\right)\right] \quad \textbf{Eq. 3}$$

Where *BF* is the bifaciality factor and is defined as follows:

$$BF = \frac{\eta_{STC\ bk}}{\eta_{STC\ fr}} \quad \textbf{Eq. 4}$$

Significant advantages in terms of energy production were found on large-scale plants, in which very often the soil is treated in order to increase its albedo. Unlike systems with monofacial modules, they are also sensitive to the height above the ground/water. In addition, the energy gain, as already mentioned, are also a function of the reflection coefficients of the ground/water and the surrounding environment. Figure 5 shows the BG in function of albedo and height above ground for two different locations: El Gouna (Egypt) (Latitude: 27° N, Longitude: 33° E) and Costance (Germany) (Latitude: 47° N, Longitude: 9° E) [21].

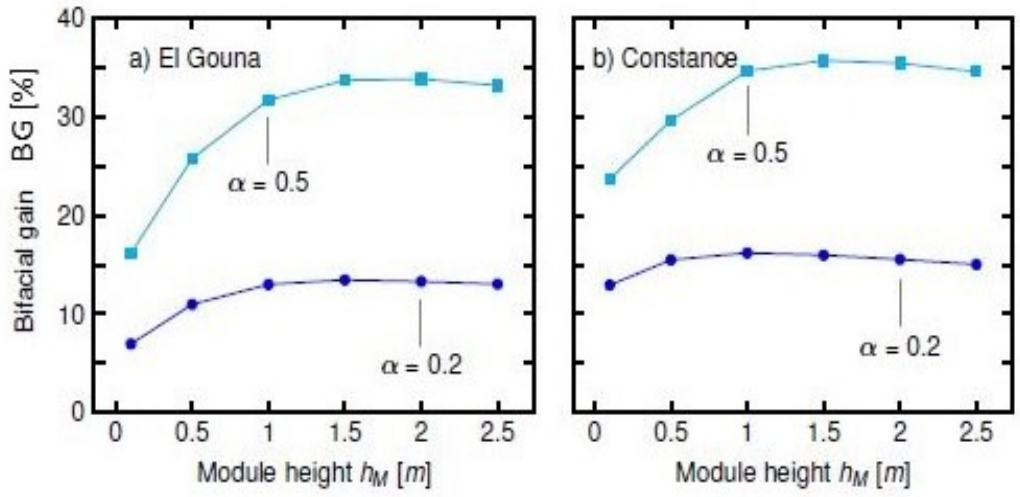

Figure 5 BG in function of module height and albedo, for El Gouna (Egypt) and Costance (Germany) [21]

The BG is also dependent on diffuse radiation. In locations with a higher diffuse irradiance factor (ratio between diffuse and global radiation) the gain due to bifaciality increases.

The physical phenomenon of this behaviour is quite intuitive since as it is well known, in the rear part of the module, there is only diffuse and reflected radiation. This causes an increase in the performance of the bifacial modules, which are also active on the back, compared to the monofacial modules with the same other climatic conditions.

Figure 6 shows the BG trend as a function of the diffuse irradiance factor for two albedo values.

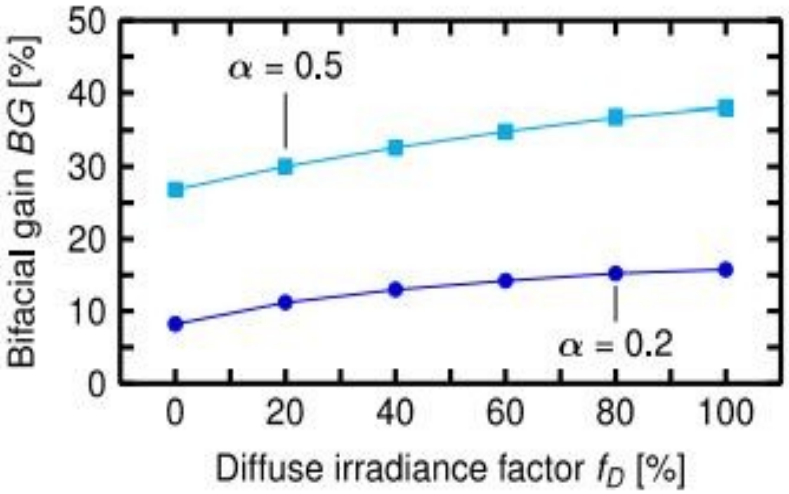

Figure 6 Bifacial gain vs diffuse irradiance factor and albedo as a parameter [21]

A comparative analysis about the main factors that impact the energy yield of mono and bifacial was addressed by Fraunhofer in [22]. A summary of the results of the comparison is reported in Table 1.

Table 1 Effect of some parameters on the energy produced by the mono and bifacial modules [22]

Yield depends on:	**m**	**b**
STC power	++	++
Module properties	+	++
Tilt angle: The bifacial module is more sensitive to tilt as it is active on both the back and front	+	++
Height: In the case of a bifacial module, the view factor of the rear also depends on the height, therefore, the energy collected is also a function of this last quantity. In the monofacial module there is no dependence on height as the rear part is not active.	0	++
Albedo: In the case of a bifacial module, the back surface is active, so the collected energy is greatly influenced by the reflected radiation. The monofacial module is not active on the rear so in the case of row installations, only the first row is sensitive to albedo	+	++
Shading effect by mounting structure: the structures of the bifacial modules must be made in such a way as to minimize the shading on the back, therefore they influence the energy yield while in the monofacial they do not.	0	+

Calculations performed by Shoukry in [21] have shown a BG up to 35% for a single rows module. By using white reflector plates under the modules, gains of 55% were achieved, and >60% for sun-belt tracking system near the Equator.

A study carried out for different locations around the world reveals that single-axis tracker installations are currently favourable in most regions of the world as they are advantageous with respect to fixed-tilt and dual-axis tracker installations. Authors found that a combination of bifacial modules with one-axis trackers produces the

cheapest electricity (LCOE 16% lower than conventional systems) by significantly boosting energy production (35% more than conventional systems) [23].

Simulations for offshore applications were carried out in [24]. The results show that the north/south facing bifacial solar panels experienced a maximum 55% of solar irradiance exposure compared to the monofacial panel when operating on the water surface. As for the east/west facing modules, it was found that a maximum 31% extra solar irradiance exposure was experienced compared to the monofacial panel when operating on the water surface.

In addition to large-scale bPV systems, bPV technology is also used for the construction of integrated PV systems (BIPV), such as the integration of vertical facades, roofs and fences (Figure 7).

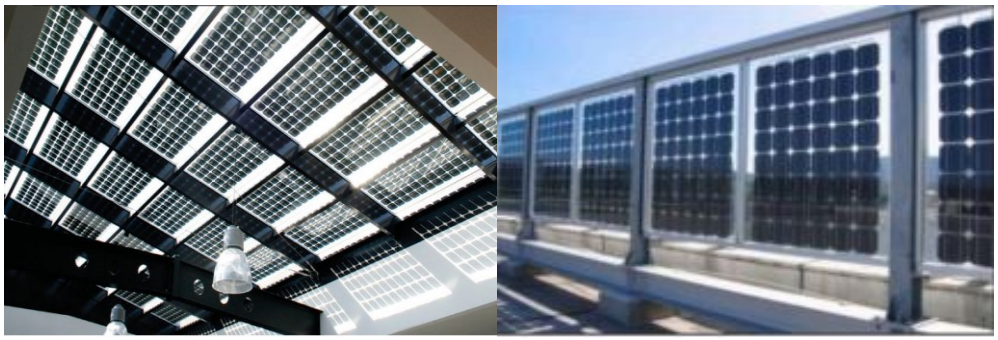

Figure 7 Roof semi-transparent and vertical barrier realized with bPV [10]

There are numerous benefits to this application. First, they not only generate electricity, but also function as conventional building materials. Moreover, they are frequently cleaned as they are part of the building and therefore the enormous cleaning costs are reduced and at the same time the performance is improved. As shown in Figure 7, they can also be installed vertically with both sides in the sun so as to capture the energy in any orientation. This is impractical with monofacial modules.

In this regard, it is good to report some results regarding performance for this type of applications. For a vertical ventilated wall, a study by Tina et al. in [25] shows that performance gains of up to 7.4% can be achieved for south facing walls with a reflective interior wall treatment. The results are based on a study developed at the laboratory of Electrical Energy Systems of the University of Catania in which the experimental plant of Figure 8 was created.

Figure 8 Building ventilated façade with integrated bifacial photovoltaic modules installed at the University of Catania (Italy)

Other common applications are the use of bPV modules to build 'noise barriers' (Figure 9) for example in highways, installed vertically and with E-W oriented facades.

Figure 9 Noise barriers with bPV [21]

The power production profile of the E-W configuration is shown in Figure 10. The diffuse fraction is set to be 0.18 and albedo is set to be 0.35, which are practical values for clear-sky conditions in Singapore. From the two curves, can be seen that the radiation received by the VMBM (Vertical mounted bifacial module) in the whole day

is 8.54 kWh, which is larger than the radiation received by the CMMM (common mounted monofacial modules with optimal tilt) that is 7.38 kWh [26].

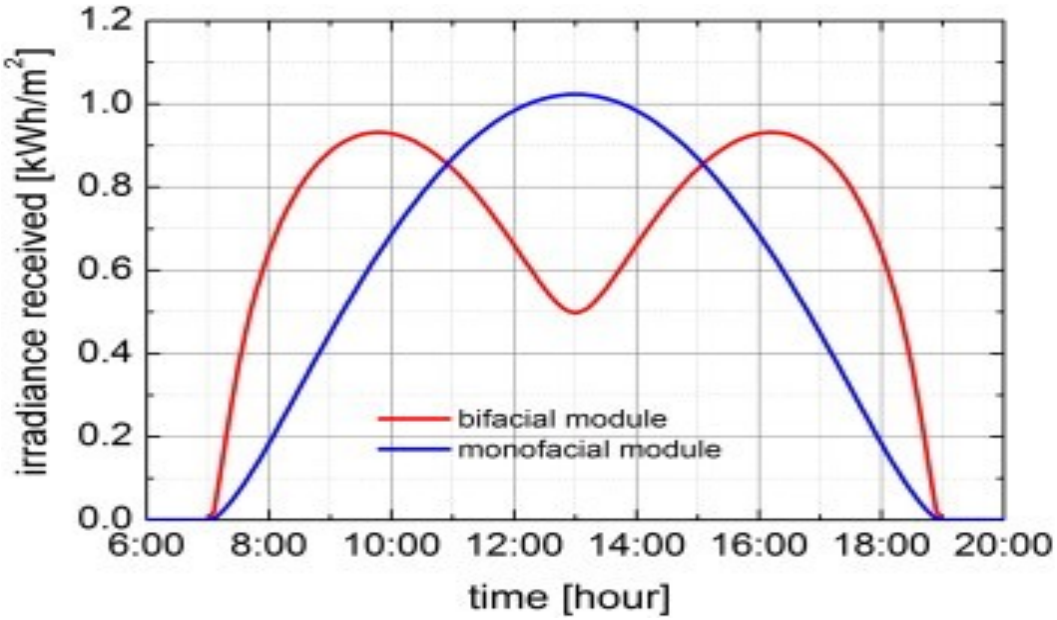

Figure 10 Simulated radiation received by a VMBM and a CMMM on a given day in Singapore [26]

Studies on E-W installation configurations were conducted in [21]. Authors shown that a module with this configuration, in certain locations, is able to obtain a gain greater than 15% compared to a classic monofacial system installed in the south.

In particular, the results summarized in the Table 2 were obtained. As can be seen, BG increases for larger albedo and is higher in Constance, due to higher amount of diffuse irradiance.

Table 2 Simulated BG of modules installed in two locations for albedo coefficients of 0.2 and 0.5.

	El Gouna		**Constance**	
BG (Monofacial south-facing vs Bifacial vertical)	a=0.2	a=0.5	a=0.2	a=0.5
	-14.88 %	-5.99 %	-4.52 %	+15.77 %

Several ongoing studies are being carried out thanks to a collaboration between the ‘Laboratory of Electrical Energy Systems’ of University of Catania and EGP at the 'Enel Innovation Hub and Lab' in Catania (IT) to evaluate the performance of the bifacial FPV modules installed on water. In the following chapters the results obtained from the experimental analysis will be shown. To increase the reflected radiation (low in the case of surfaces such as water), plans are being made to install highly reflective

components made from low-cost material. In this regard, sheets and light-colored floating spheres are being tested to evaluate the further increase in energy.

2.2 Floating photovoltaic power plants

2.2.1 Concept of floating PV plants

Solar PV modules are generally installed over ground and rooftops using rigid mounting structures. Due to the low availability of land, dense population and severe threat of deforestation interest have been directed towards the installation of PV panels over canals, lakes, reservoirs, and oceans. PV panels are installed over water bodies by making them float using suitable technology and such installations are called FPV plants. The electric power output of PV panels highly depends on incident solar radiation and the temperature of the panels. Shadow effects are negligible in FPV systems and the temperature of panels can be lowered by water with active or passive cooling techniques.

The schematic view of a FPV system is depicted in Figure 11. As shown in this figure, the main components of FPV systems are pontoon/floats, mooring systems, PV panels, and electric cables and connectors. Pontoons are devices that float by itself along with PV panels by buoyancy including a space for human accessibility. Pontoons are mostly made of high-density polyethylene (HDPE) which is UV resistant, corrosion-resistant, and has a high tensile strength [27]. The mooring system is a component that is used to keep the pontoons in the desired location, position, and prevent them from moving away. Rigid supports in the form of anchorages are provided using plinths in the bottom of the reservoir to take care of dead loads and lateral forces [28]. Generally, rigid flat-type PV panels are used in FPV systems, however, flexible panels which are adjustable according to wave movement are more attractive [29]. Trapani and Millar [30] developed a FPV array containing T3F-PV modules. In this case, they manufactured a small-scale prototype of a thin film based FPV system installed on an enclosed water body in Sudbury, Canada. The results of the 45-day operation indicated a 0.5% reduction in electric efficiency mainly because of sediment blockage on FPV modules, while an average electric improvement of 5% was reported because of the water-cooling effect for three months.

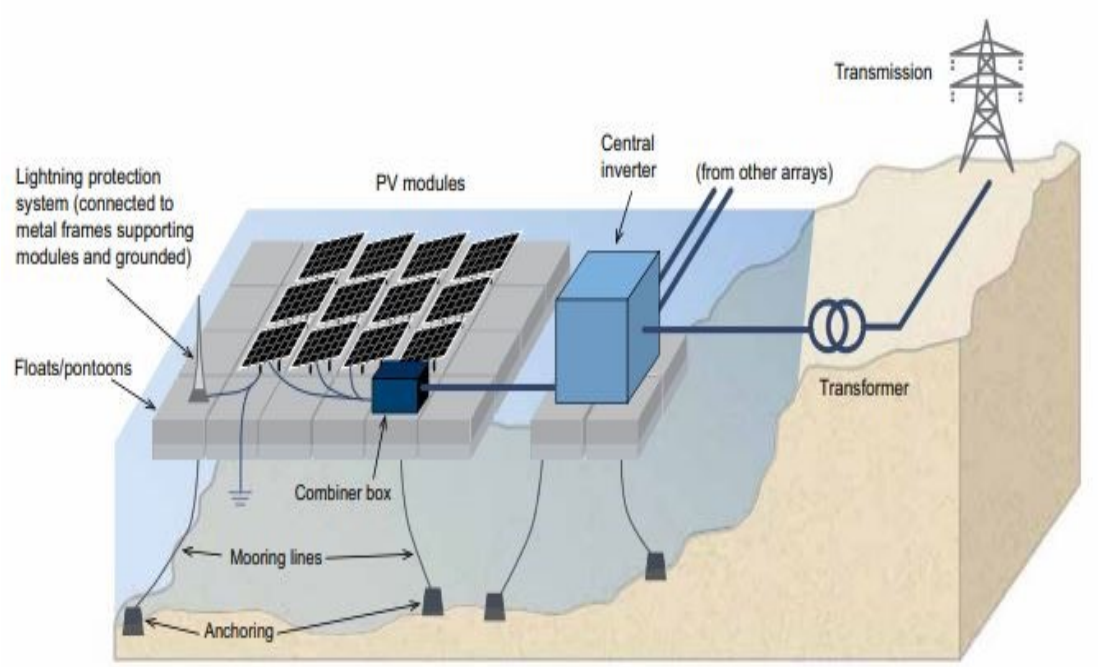

Figure 11 Schematic representation of a typical large-scale FPV system with its key components

Several technical installation proposals come from industry and research. Figure 12 shows some of the technologies proposed by industry.

In particular, Figure 12 (a) shows the suspended systems, (b) submerged/flexible systems, (c) floating systems on pontoons.

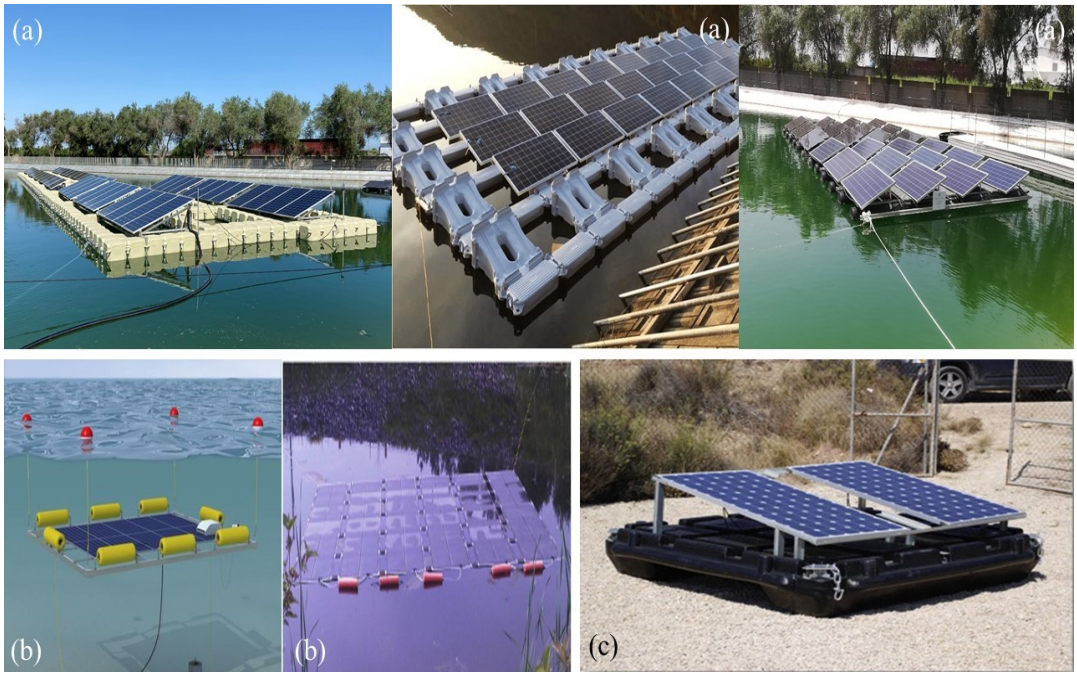

Figure 12 Design solutions of FPV in the market

Strong winds and uneven surface are two significant factors imposing threats on rigid PV panels [31]. Most of the water bodies have salinity which may affect the PV panel frames, hence polymer-based frames and supports are desired for longer life of panels. Electricity produced from FPV panels over water bodies is transported to the land through electric cables, hence waterproof, high-temperature resistance cables and junction boxes are required for the long life of the system [32] [33].

The main advantages of FPV technology can be summarized in the items below:

- Strong reduction of land occupancy. The main advantage of floating photovoltaic systems is that they do not occupy land, with the exception of the limited surfaces for the components necessary to feed energy into the grid, for example, transformers and inverters. FPV systems therefore have less impact on the environment and do not compete with areas for agricultural use. The fact of not using the land makes them cheaper because among the items of capital costs, there will certainly be no purchase of the land.
- Reduction of evaporation. The water saving effect depends on the climatic conditions and the percentage of the area covered. This effect can produces a saving of more than 20,000 m^3/year/ha, which is very useful especially in basins

for irrigation purposes or hydroelectric plants where the saved water can be fed into the turbine. Regarding this specific topic, it will be explained in more detail in the next chapters as it has been the object of study in this thesis.

- The reduction of algae growth, where there is the phenomenon of eutrophication, can be a positive effect as it improves the quality of the water.
- Installation and decommissioning. FPV systems are more compact than ground systems, as the surface on which they rest is perfectly horizontal and flat. Installation and decommissioning are simpler if compared to ground systems as there are no fixed structures and the mooring of floating systems can be carried out in a totally reversible way, unlike foundations used for a ground system.
- Cooling. Cooling can take place passively thanks to the favourable microclimate. Some studies declare an increase in energy related to passive cooling ranging from 3 to 7%. Active cooling systems that can be implemented in FPVs are simple and inexpensive. In fact, very often large quantities of water are available on site at no cost, there is no waste of water and the head required for the pumps is very small. In the case of submerged systems, no additional components are required for pumping or jets of water on the modules (electric pumps, sprinklers) and the system is passive because it does not consume energy for cooling. Regarding this specific topic, it will be explained in more detail in the next chapters as it has been the object of study in this thesis.
- Simple tracking. The floating structure allows the implementation of a simple and cheap tracking mechanism. A large floating platform can easily rotate and can perform a vertical or gable horizontal axis tracking: this can be done without wasting energy and without the need for any complex mechanical apparatus, which is needed in land-based PV plants.
- Hybridization. An FPV system can be coupled to a hydroelectric power plant. Since solar energy is anticorrelated to hydroelectric energy, water / energy storage management strategies can be adopted that increase the overall CF of the hybridized plant.
- Synergy with fishing. Several projects have been presented which couple the FPV to activities related to fish or shrimp farms, mainly in China and in the South East of Asia.

- Reduction of specific energy cost. This is a very important item, perhaps the crucial one. The evolution of the FPV technology brought the costs of the FPV plants below that of standard PV especially in the tropical regions where the land management and the maintenance of land-based plants are very expensive.

FPV plants have the following disadvantages over ground mounted PV systems [27]:

- Cannot withstand heavy waves, high tides, cyclones, and tsunami;
- They are subjected to fluctuating wind loads and vibrations hence cracking and orientation change of PV modules are possible;
- Salinity of water body can deteriorate panel component and reduce its performance;
- Transmission of sunlight into a water body is prevented and hence it may affect the aquatic ecosystem;
- Cleaning of FPV panels might be more difficult hence automatic novel cleaning mechanism needs to be designed;
- Detailed environmental impacts of FPVs are not fully known up to now.

2.2.2 Cooling

The implementation of water cooling systems is very simple and cost effective in FPV plants, as discussed above, as there is a large availability of water in the vicinity of the plant. In particular, passive cooling in FPV systems occurs naturally thanks to the favourable microclimate conditions that are created near the plant [34].

In a PV panel, some of the absorbed radiation is converted into electricity, while a part of it is converted into heat, which represents one of the reasons why PV modules have low efficiency. Specifically, the efficiency of converting solar energy to electrical energy decreases with the increase in operating PV temperature. On average, the losses of power of PV panel ranges from 0.25%/°C to 0.5%/°C [35].

In literature, there is a considerable number of studies regarding the improvement of the performance of PV modules through the use of cooling [36]. These works can be classified into two sub-categories: active and passive cooling of PV panels.

The difference between active and passive cooling is that in active systems additional energy is needed to supply the appliances used to reduce the effects of heating.

A further classification can be made in relation to the fluid or material used for cooling, that is: air, phase change material (PCM), water, metal, etc...

Active water cooling is a very advantageous technique in terms of energy gain as the physical properties of water, in particular conductivity and thermal capacity, favour a good heat exchange with the environment. Compared to air, this technique is more efficient as water is able to transport more heat per unit of mass [37].

The main active water cooling solutions proposed by the research in recent years can be categorized into two macro types:

- direct water cooling, which consists in making the water flow or spray through the nozzles, on the surface of the modules, front, rear or on both surfaces;
- indirect water cooling, which consists in circulating the water inside heat exchangers, placed in contact with the surface of the module (often the rear one).

A work that study active water cooling is conducted by Nizetic in [38]. The experimental system made it possible to spray the water on the upper and rear surfaces of the modules separately or simultaneously on both surfaces. Results show that it is possible to achieve a maximum total increase of 16.3% (net 7.7%) of the electrical power produced and a total increase of 14.1% (5.9% net) of the electrical efficiency of the panels, in circumstances of peak solar irradiation.

This technique can be easily implemented in FPV systems as low head pumps are required and there is a large availability of water near the system at no cost.

Also submersion techniques of the modules in water have been used [39] [40]. Among these proposals, there is also the FPV approach, implemented with submerged modules of the rigid or flexible type in such a way to adapt to the waves in adverse weather conditions, for example off-shore [41]. An interesting study is conducted in [42], in which authors conducted experiments on silicon PV panels immersed in fresh water. A reference PV panel exposed to air was used to compare the results. The depth of the water ranged from 4 cm to 40 cm and the specific results in relation to the relative efficiency of the PV panel are presented. According to the reported results, the reference PV panels had average operating temperatures between 70°C and 80°C, while the submerged PV panels had average temperatures around 30 °C. This implied

an increase in efficiency from 13% to 15.5%, with a maximum increase in efficiency of around 20%.

Using the water directly sprayed on the modules as a medium, it is possible to create passive cooling systems which therefore do not require electricity.

In paper [43] a passive cooling method is proposed, it uses rainwater as a cooling medium and a gas expansion device to distribute rainwater. The results of the study show that in one day, the passive cooling system reduces the temperature of the cells and increases the electrical efficiency of the PV panel by 8.3%.

Indirect passive methods often exploit the phenomenon of evaporation or high humidity near the rear of the modules. They are often integrated with other passive cooling systems that use conductive materials such as metal heat sinks. Some studies propose small systems that take advantage of the phenomenon of transpiration of plants and will be explored below.

Some systems based on the effect of evaporation are hybridized [44]. They exploited the effect of evaporation, combined with the use of condensed water from the chiller. Figure 13 shows the system studied in [44].

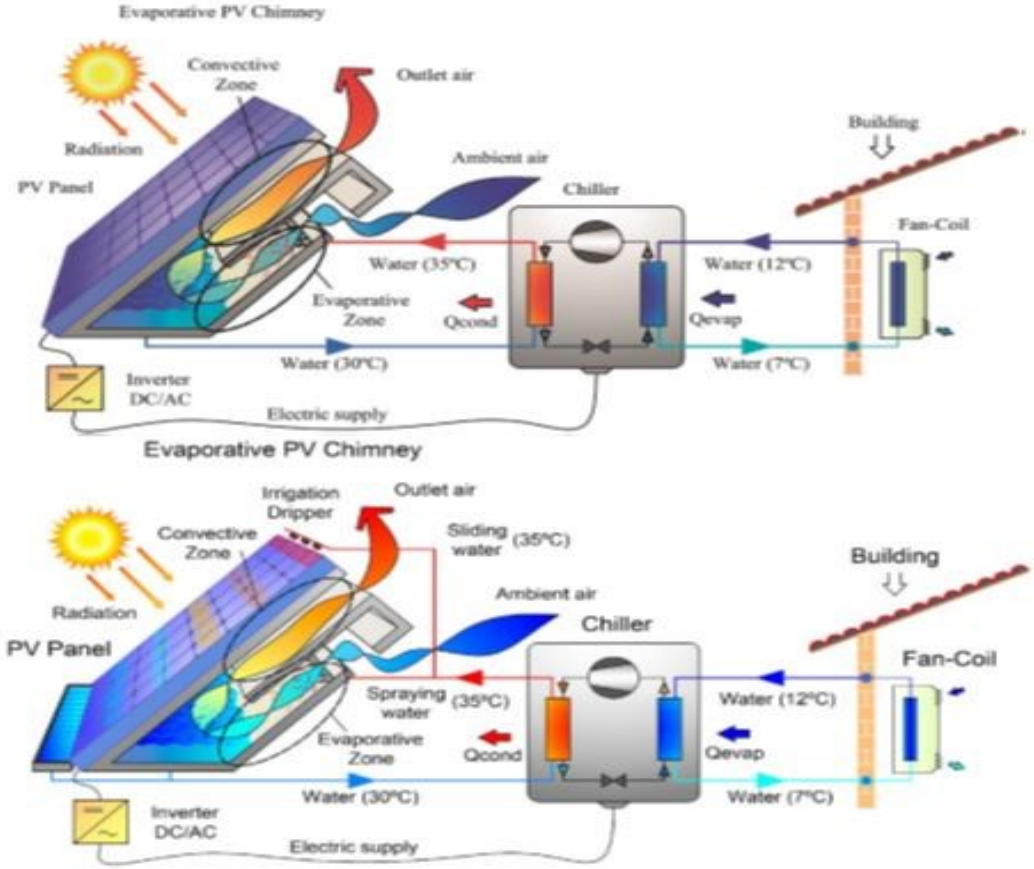

Figure 13 Evaporative PV Solar Chimney and Air conditioning system scheme [44]

A passive water cooling system based on the evaporation phenomenon is proposed by Drabionik in [45] [46]. This method combines the operating principle of ventilation cooling known from rear panel PV cooling and evaporation cooling with a bionic concept. This study takes advantage of the bionic concept that occurs in nature, in the trees. The experiments showed an efficiency increase of up to 4.8% corresponding to a low solar radiation of 575 W, while the model showed a 10% increase in efficiency for real roofing systems with incident solar radiation of 1000W.

Figure 14 shows the cooling method implemented in [46].

The methodology used in this study will be recalled in the following chapters in particular when studying the effects of cooling due to the evaporation of the water of the basin where the FPVs are installed.

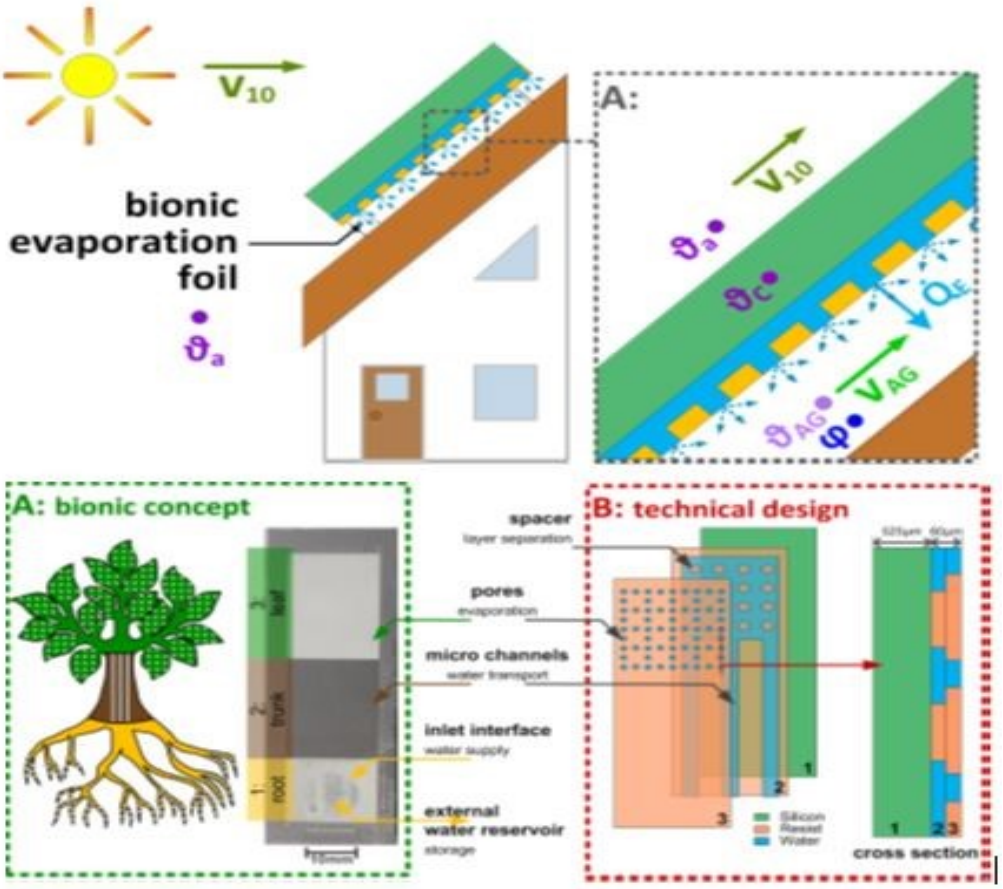

Figure 14 PV roof system with evaporative cooling [46]

Other passive cooling approach of the modules was addressed in[47], he performed CFD simulations of an FPV system with a closed loop radiator system. This study does not exploit the evaporative phenomenon but uses a passive heat exchanger that exploits the phenomenon of natural convection.

Alami [48][49], studied the physical properties, in particular, the porosity of the clay. The results showed that by applying the clay layer on the back of the module, approximately 90% of the cooling is due to evaporation especially when natural convection conditions prevail.

Studies conducted on the increase in performance due to the natural cooling of floating photovoltaic modules have been conducted by several authors. The increase in energy was due to the cooling caused by the evaporation of the water basin and the favourable microclimate around the modules.

Choi in [50] compared the energy yield of two systems installed on a water surface with one installed on the ground. He saw that thanks to the favourable microclimate

conditions, the energy yield of the modules in the water was 10% higher than those on the ground. Liu [51] through a finite element method has calculated the temperature of the modules assuming an ambient temperature near the water surface 5° lower than that on the ground. He found a difference in cell temperatures between those in the water and those on the ground, equal to 3.5° and an increase in efficiency of around 1.58-2%. Kamuyu [52] monitored a photovoltaic system installed on a water surface and pulled out a temperature model of the photovoltaic modules taking into account the environmental variables (including the water temperature) he showed that the energy yield of a system in water can increase by 14.69% compared to that on the ground thanks to favourable operating conditions.

In the studies previously analyzed, it has been seen that to obtain evaporative cooling, it is necessary to create the conditions, also using in some cases additional components such as wool, clay or other materials. In the case of systems installed on water surfaces (FPV), evaporation takes place naturally and without the aid of additional components, therefore these latter solutions lend themselves well to this cooling technique.

2.2.3 Tracking systems

The use of ground or floating tracking systems have the purpose of increasing the energy collected by the photovoltaic plants and are made with a mechanism that allows to maximize the radiation incident on the collectors.

A recent work declares that single-axis and dual-axis ground photovoltaic tracking plants, with appropriate control systems, can increase the electrical energy from 22–56%, compared to fixed PV. This window of variability in energy yield depends on the location, technology and season [53].

Two-axis systems can be implemented, ie with azimuth and tilt movements, in order to obtain maximum performance.

One-axis systems can be subdivided in the following categories:

- vertical if the system performs an azimuthal movement, with axis perpendicular to the ground/water surface;
- horizontal if the axis is parallel to the ground/water. The axis orientation can be N-S or E-W;

- tilted. The rotation axis is tilted by an angle such as to maximize the energy collected in relation to the latitude and the tracking mechanism performs an E-W rotation.

Tracking systems anchored to the ground have been studied and perfected for several years now; today the technology is quite mature and reliable. As regards the tracking for floating systems, it is necessary to take into account not only the lack of a fixed anchor but also the disturbances due to buoyancy, therefore to the presence of waves and wind.

To overcome this problem, it is necessary to find alternative technical solutions to those for ground systems, from the structural point of view and tracking algorithms.

In this regard, it is necessary to make a distinction between the different solutions proposed in literature[54]:

- Trackers inside a confinement facility whose floating platform is surrounded by an anchored structure (circle or polygon) and an appropriate electric motor makes the platform rotate with respect to the fixed structure;
- Tracking with a partial confining structure that are called external rope
- Tracking without a confining structure: using submerged reference structures or by bow thrusts;
- Tracking to a horizontal axis using the “gable” structure.

Cazzaniga in [29] suggests systems reminiscent of the carousel mechanism, in which there is a fixed part anchored to ballasts placed on the bottom, inside which rotates a mobile platform on which the photovoltaic modules are installed. The system described is shown in Figure 15.

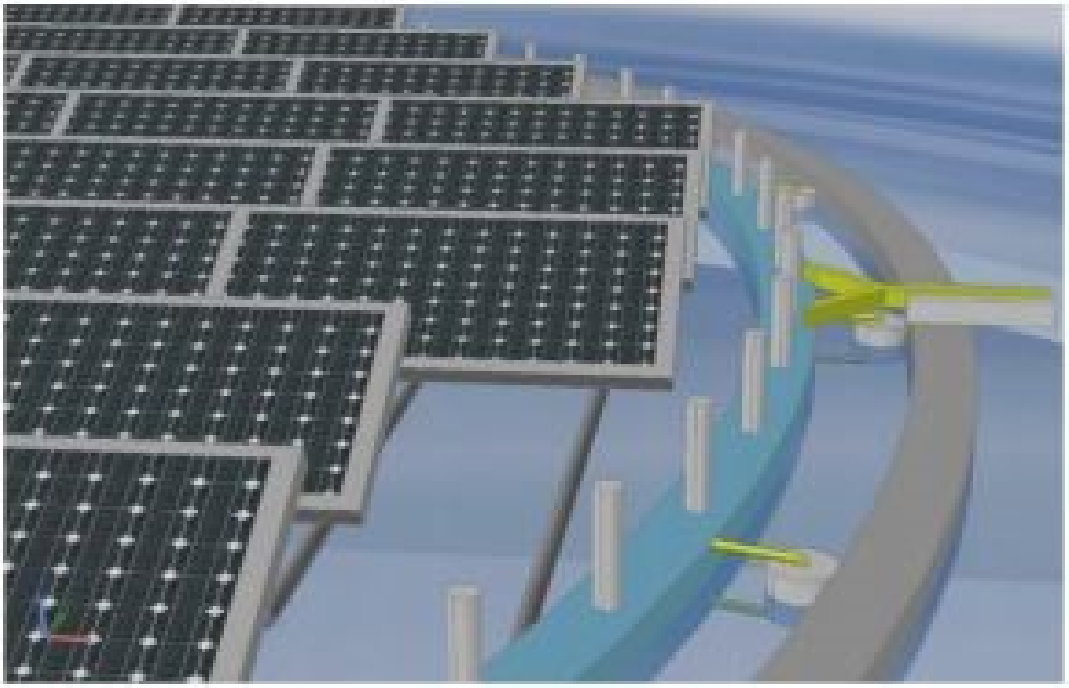

Figure 15 Tracking system with confinement, for a platform of 50 kWp

Sunfloat in [55] proposed the rope system with a partial confinement whose azimutal movement is guaranteed by the winches placed around the structure. Figure 16 shows the described system.

Figure 16 Rope system which allows 2 or 1 axis tracking

A tracker without the confinement structure that can also be installed in deep basins and connected to the ground via three chains forming an equilateral triangle has been

proposed in [56]. This system allows to reduce construction costs and is more functional than other solutions proposed in the past. The movement is guaranteed by the bow thrusters generating the torque that creates the azimuth movement.

Rosa Clot and Tina in [54] propose a HAT (horizontal axis tracker) system that can offer significant advantages especially for low latitudes. As for the medium and high latitudes, one could think of tilting the photovoltaic modules a few degrees. Within the tropical region, the gain in energy harvesting compared to a fixed installation with optimal inclination varies between 21% and 32%. In the temperate region, these values drop to 15% and 25% and the result is worse for high latitudes. The problem that immediately emerges is the shading which for a ground-mounted system can be easily solved by increasing the surface occupied.

In Figure 17 can be seen the proposed structure with the tracking system that acts on a long row of modules (12 m) and the large space between the two rows necessary to avoid shading. Using a “gable” structure, it is possible to create a tracking system with inclination angles that are around 45°.

Some of the previously illustrated solutions have been realized in different parts of the world.

K-water (Korea Water Resources Corporation) in Korea has installed the world's first 100 kW tracking floating photovoltaic system inside a confinement facility [57]. In it there are four 24.8 kW systems, one of which is passive tracking, one automatic and two fixed systems (

Figure 18).

Scienza Industria Technologia (SCINTEC) has designed and built a TFPV at the Cantina Petra in Italy. Furthermore, in 2011, SCINTEC also installed another floating tracking photovoltaic system on Lake Colignola. The feature of this system is the use of mirrors to reflect the solar irradiance on the photovoltaic panels [58].

In this regards, Tina in [59], suggests installing flat reflectors to constitute the so-called FTCC, which manage to increase the annual energy collected by 60-70% compared to fixed systems.

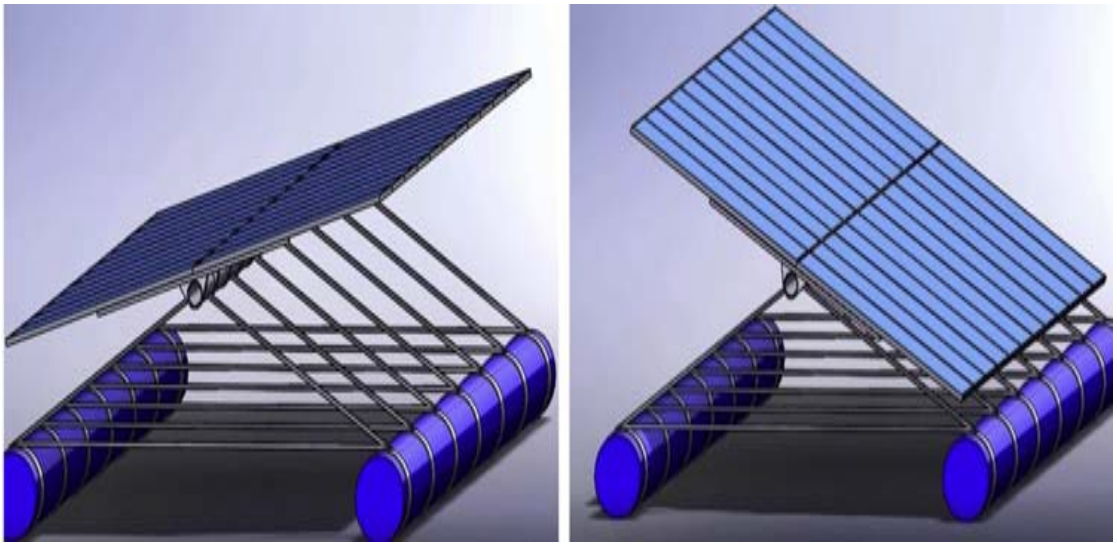

Figure 17 HAT with gable structure

Figure 18 K-water tracking installation

In the academic field, several studies have been conducted on TFPV, but many topics are completely unexplored and a considerable effort is required to fill these gaps. Below is an overview of the works developed to date.

In [58] an algorithm for tracking on FPV systems is proposed, which compensates the azimuth angle error due to the continuous movement of the floating structure for wind and waves, using a GPS receiver and a geomagnetic sensor.

In [29], sensor-based controls are suggested that take two different approaches: one uses shading patterns to find the solar position and optimal orientation, and the other is based on images captured by a wide-angle camera pointing the sky and orient the system, in the direction in which there is more light. With these systems, an accuracy of 0.5 ° is guaranteed in the event of cloudy skies.

Choi [58], proposes the finite element study of the mechanical structure of a 100 kW plant in which it evaluates the impact of the wind and uses different materials for the simulations including, steel, aluminium, polyethylene (PE) and reinforced polymeric plastic with fibers (FRP). For floats that are subject to corrosion, glass fiber reinforced plastic (GFRP) and polyethylene (PE) have been proposed; In the study he also includes the control algorithm of the confined tracker in which there are a passive and an active system.

In [60] a dual axis tracking system with management software in an Arduino environment is proposed. For handling, stepper motors are used.

However, the systems listed above absorb energy for the movement of the tracking mechanisms through actuators. Furthermore, being placed in environments with high humidity, in the long term they could deteriorate more quickly than the components installed on the ground, this would cause a greater frequency of maintenance and therefore higher costs.

The TFPV system proposed in [61], is of the passive type, that is, it uses wave energy to automatically adjust the position of the system, without the aid of mechanical drive components such as motors, which as previously anticipated could cause increase maintenance costs during the useful life cycle of the plant. Although floating-tracking PV systems have higher specific investment costs, the higher electricity production compared to fixed floating PV system make them competitive from a levelized cost of electricity point of view [62].

Figure 19 presents a classification of the tracking photovoltaic systems in which FPVs are classified.

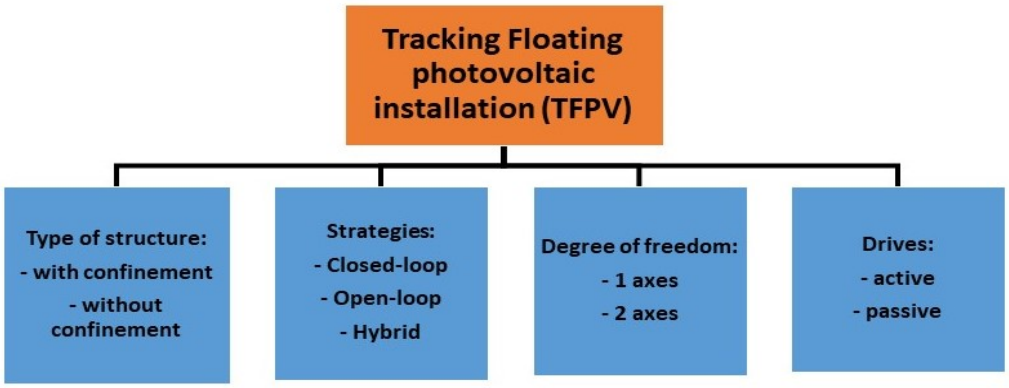

Figure 19 Classification of tracking FPV

2.2.4 Hybridization of FPV

The hybridization is the possibility of integrating the FPV system into the basin of a hydroelectric power plant. A scheme is reported in Figure 20.

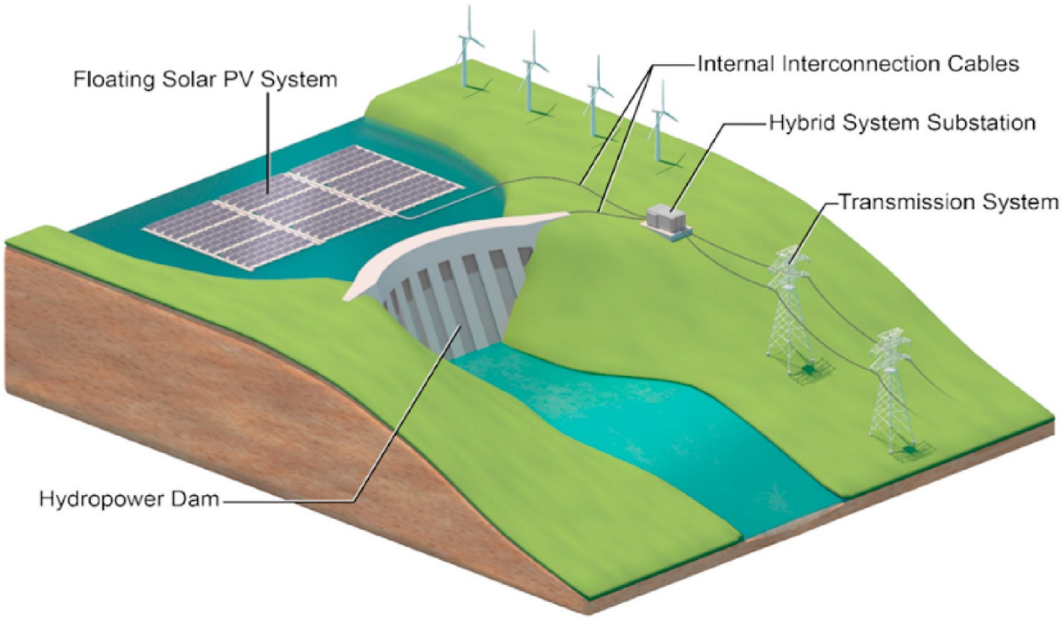

Figure 20 Schematic of a hybrid FPV-hydropower system

Thanks to the advantages deriving from the integration of these two systems, various benefits can be obtained, such as:

- FPV systems compared to GPVs installed in the vicinity of a hydroelectric power plant, are certainly more advantageous in terms of construction as they do not interfere with any surfaces of soil intended for agricultural use or for breeding. The

ground could have an uneven surface and the installation would be more complex while the irreversible uninstallation;

- allows the use of the existing transmission infrastructure, such as transformers and connection to the electricity grid, obtaining cost savings related to the additional infrastructure;
- it is possible to avoid power variations in FPV due to the intermittent solar radiation profile;
- FPV output can compensate power reduction from hydropower plants especially during droughts;
- power output from FPV prevents the consumption of water from hydropower plants which can be otherwise used during peak load conditions.

Hybridization, as suggested in several studies, increases the overall CF of the system [63].

In [64] it is stated that covering the 2.4% of the water basin by FPV increases the energy production of 35.9%, raising the CF value from 3343 to 4450 hours. This result can be extended to other situations and to smaller HPP basins where the CF factor is lower, i.e., around 2000 hours. In this case, the benefits are more important and the increase in energy production can reach 50%.

A study conducted in [65] states that, using a coverage rate of the basin of a hydroelectric power plant of 25%, the FPV system is able to provide 6270 TWh compared to 2510 TWh of hydroelectric power. Moreover, there is an availability of water in more than 6.3% thanks to the lack of evaporation of the basin due to the partial coverage. Assuming an HPP efficiency of 90%, pumping this with 6.3% of water can potentially increase the energy collected by 142.5 TWh.

The global FPV installation due to hybridization FPV-HPP can range from 3.0 TW to 7.6 TW depending on the proposed scenario. This is equivalent to an energy production of 4,251 TWh to 10,616 TWh per year [66].

In a Brazilian scenario, thanks to the synergy between FPV-HPP systems, the energy gain by the hybrid system is 76%, while the capacity factor increases by an average of 17.3% [67].

In [68] a study on the evaluation of energy potential on 22 HPPs was carried out. The HPPs surveyed have significant water storage reservoirs and approximately 28% of total hydropower capacity installed in Brazil 31.5 of 114 MW. Adding 34 GW of floating PV systems on their reservoirs it is possible to have an additional CF of 20% to this installed hydro capacity per year, equivalent to almost 10% of the Brazilian electricity demand in 2018.

2.2.5 Environmental impact

Any newly developed technology can be implemented only if it has a low negative impact on the environment and also it is economical for large scale deployments. In this section, the environmental impacts of FPVs ranging from its commissioning to decommissioning are presented and discussed based on the available literature.

In general, the EIs (Environmental Impact) of both ground-mounted and FPV systems are not nil, as the manufacturing processes of PV modules, inverters, and all the composed components require huge amounts of energy and release harmful substances in the environment [69]. However, during the operating phase, a FPV system shows positive impacts such as being completely silent, allowing for a reduction in the growth of algae in the presence of eutrophication, producing clean electrical energy with no CO2 emission, saving water resources by preventing evaporation, less water requirement for cleaning PV modules [29], saving valuable lands for agriculture, mining, tourism, and other activities due to installing PV panels over water bodies, reducing bird collision with panels compared to the ground-mounted systems [70], and improving the quality of the water of reservoirs [71]. Pimentel Da Silva et al. [72] proposed a multi-criteria modeling approach to assess the extent and importance of the environmental and socio-economic impacts of ground-mounted and floating large-scale PV (LSPV) systems. Liu et al. [73] provided an assessment of both the environmental impacts and synergies between economic benefits and environmental impacts without considering CO2 emissions. The model consisted of the cross-spectrum analysis to evaluate the coherent fluctuation between economic and environmental benefits. An empirical study was conducted by Hass et al. [74] on a demonstration project for the integration of a fishing farm and 10 MW photovoltaics in the Chinese province of Jiangsu. The model was capable of providing the optimal sizing in terms of the interaction between the FPV system and the environment of a

hydroelectric power station. They concluded that the FPV should ideally be sized between 40 and 60% of the lake surface.

2.2.5.1 EIs of plant design and allocation

In the sitting phase, it is necessary to look for potential sites whose impacts on flora, fauna, air, and water are as low as possible, because, in both construction and operating phases, local ecosystems could be altered [75]. Therefore, basins in unprotected areas without particular plants, protected animal species, and environmental restrictions are recommended [76]. The visual impact of ground-mounted PV systems can be high which can be solved through careful design by considering PV panels as architectural elements. As far as floating systems are concerned, bamboo buoyancy systems are proposed in the literature (Figure 21) that minimize both the visual and polluting impact since they are made of natural raw materials with a lifetime of more than 10 years in water [33].

Figure 21 PV modules installed on a floating base made of Bamboo

2.2.5.2 EIs during plant construction

In the implementation phase, the EIs that can occur are of different types and entities. For example, access to the site is a potential impact that can cause deforestation. As for floating systems, this impact could be limited since the allocation of the modules takes place on the surface of the water. The transit of heavy vehicles or boats for the construction and transportation of materials are potential causes of noise and air pollution. Although these items all generated noise, it is at lower levels in comparison

with industrial noise guidelines and occupational noise levels, and therefore it doesn't cause environmental, health, or safety impacts [77]. Also, the impact of noise is truly negligible because the construction phase duration is much shorter than the life cycle (20 years) of the plant. Moreover, both large ground-mounted PV plants and FPV plants are often constructed far from settlements, so the impact of noise affects very few people. Also, the leakage of polluting materials in the water (such as oil, fuel, etc.) of the working machines (for example boats) can be harmful to the lake environment. The positioning of ballasts for anchors on the bottom of the basins certainly causes water mixing and therefore cloudiness which could cause loss of habitat of the fauna in the water [70]. At this stage, noise pollution is also necessary to be considered as an EI. It is mainly linked to the movement of vehicles for the construction of the plant and could harm the fauna in the surrounding environment. The time required for the installation of FPV systems has not yet been fully defined since unlike ground installations, site preparation is eliminated (suppressing vegetation and civil infrastructure). Nonetheless, the FPVinstallation can be complex as some working phases take place in water [70]. Usually, the construction phase for plants on the ground that vary from 1 to 5 MW of capacity lasts up to 100 days, while for plants greater than 25 MW, it lasts more than 210 days [78].

2.2.5.3 EIs during plant operation

A phase that requires more attention, in the case of floating systems, is that of operation since there are no exhaustive studies that quantify/qualify the real impact and causes of the interaction between the surrounding environment and the system. This is also due to the recent birth of this technology, and therefore the absence of long-term data. Conventional ground-mounted PV systems require a quantity of water and other chemicals to clean the modules. It is clear that chemicals are extremely toxic to the environment and could impose many negative impacts on fauna and flora during a long period [79]. The potential contamination of water through these substances can result in the mortality of fishes and other aquatic species or the alteration of the water quality because of the growth of algae and loss of oxygen in the water. In FPVs, it is necessary to limit or even change cleaning methods, not using chemical materials that can contaminate and pollute the reservoir. Additionally, floating systems require less water for cleaning as the system is positioned away from the ground and the effects of dust

carried by the wind are also eliminated [80]. Besides, unlike ground-mounted systems (especially for those in desert environments), water is easily available and in the immediate vicinity. Bird activities and specifically bird droppings may bring some disadvantages, however, no influence has been reported from FPV on bird fauna [80]. In this phase, there could also be the risk of contaminating water with oils, lubricants, fuels, paints, when mechanical devices for maintenance are moved, and with material scraps due to corrosion [81]. During maintenance, it is important to also take into account waste management which mainly consists of following the management plan and guidelines for the replacement and disposal of batteries (if any), panels, and other defective equipment [69]. Partial or total coverage of the water surface reduces algae growth. This positive impact could be useful for lakes where eutrophication problems occur. Eutrophication is the abnormal growth of algae (and other aquatic plants) and is sometimes referred to as "green tide" which can also lead to the establishment of highly anoxic conditions which is the main cause of fish death and foul-smelling emissions [29].

However, it is not recommended to cover the entire surface [74], particularly in lakes with living organisms, to ensure the penetration of sunlight and the production of oxygen through photosynthetic organisms. Reducing oxygenation can even increase GHG emissions from the tank [82]. Hence, installations on natural lakes could create further consequences than artificial water surfaces. The environmental impact deriving from the quality of the water can be resolved by installing systems for monitoring the water state [83]. To mitigate the effect of reducing the penetration of solar radiation in the basin, it is possible to adopt technologies of bifacial semi-transparent PV modules. Some associated risks can also arise from the aquatic animals on the FPV systems. Sometimes animals may vandalize structural components or cables. Barrier methods must be employed during the operating and maintenance (O&M) stages to prevent animal visits. Nonbarrier methods such as laser-beam equipment could also be a practical technique in this way. It is also important to maintain such equipment per the supplier's recommendation. In some cases, it is essential to store anti-venom at the O&M site office and identify the nearest medical center for emergency cases to mitigate snakebite threats. It is important to maintain both the equipment and personnel safety at all times [84]. The floating structures could also reduce the formation of

waves by reducing the effect of wind on the free surface of the water. Other impacts of FPVs on lakes and the aquatic environment may involve the electromagnetic field produced by conductors installed on the bottom or surface of the lake [81]. Most of the floating systems are made of HDPE which are in different shapes and types of floats. In reality, direct contact with water (20% or more according to the proposed technical solution) occurs mainly through HDPE pipes that support galvanized steel structures or through rafts completely built-in HDPE. Galvanized iron (or aluminum) is not in direct contact with water, but for various reasons, including rain or waves, these structures and PV modules can be wetted with water and can release small quantities of materials that can be dissolved in the water.

2.2.5.4 EIs of plant decommissioning

The environmental impact deriving from the decommissioning phase essentially consists in the change of the geomorphology of the lake bottom caused by the removal of the ballast and the anchors of the plant; short-term change in water quality, due to mixing for handling and therefore cloudiness; increase in noise caused by the traffic of vehicles and machinery; recycling and management of waste deriving from the uninstallation process [70]. However, it should be noted that, unlike ground-mounted systems, floating systems, at least as regards the surface of the water, do not require any remediation. This aspect is important because it reduces the impact due to the noise of the vehicles, pollution, and changes in the geomorphology of the soil [27].

2.2.6 Economical aspects

Unlike the ground-mounted PV plants, floating systems are still in the first phase of the learning curve. There are not enough installations to be able to make an accurate analysis of installation, maintenance, and operating costs. The support, mooring, anchoring, and floating systems are constantly changing, improving, and optimizing. Therefore, the assessments could undergo drastic changes, positively, in the near future when the technology of the entire system will be established as well as that of the systems on the ground.

2.2.6.1 Capital expenditure (CAPEX)

To evaluate the implementation costs of a PV system, the actions are required to make the system working.

Below are the components of a FPV system along with some comments on costs [27]:

- Floats: they are generally made of HDPE or glass fiber reinforced plastic (GRP). Concerning the type chosen, the cost can change considerably. These components are not used in ground systems.
- Moorings: the installation of a mooring system can be expensive in deep water or where the change in water level is relatively large. These components are not used in ground systems.
- PV modules: they are the same as those used for ground systems, or with a higher protection index (in this case they could be more expensive) to avoid the penetration of water into them. Cables and connectors: for application in water, special cables should be installed. Even if there is no electrical component under the water, waterproof IP67 junction boxes are recommended which are more expensive.
- Other electrical components, inverters and/or batteries: they are installed on the ground or floating cabins; therefore, they work in normal conditions as in conventional ground systems.

The construction of FPV systems entails different costs as some works are carried out in the water with all their difficulties. In a study by Martins [85], it was reported that labor cost for the ground-mounted system is equal to 40 US$/h, while for the FPVs it is increased as 60 US$/h. These additional costs could be offset by the fact that the system does not use the soil, which leads to overall lower costs. As mentioned above, the water surface is immediately useable without the need for levelling works as in the case of the ground. Besides, the soil resource plays an important role in terms of cost and can be relevant where there is scarcity. In particular, solar radiation measurements, bathymetry and lake bottoms, wind and wave surveys, grid connection studies, possible ship traffic surveys, and environmental impact assessments (EIAs) are considered essential on large lakes and are estimated in the range 20-70 keuro per study [86]. In a study by Galdino and Marta Maria de Almeida Olivieri [82], the installation cost for a 1.2 MWp plant was reported 30% higher than that of a ground-mounted system due to the utilization of a premature technology which has not been fully optimized yet for systems of this size. Teixeira et al. [87] conducted an economic

feasibility study of a hybrid hydro-FPV system in which he declared a 30% increase in costs for the FPV when compared with a ground-mounted system. An estimate made in Ref. [88] states that floating systems with an installed capacity greater than 10 MWp would have a cost similar to ground-mounted installations. The plants described in Ref. [84] with 100 kWp and 500 kWp capacities had a cost of US$ 6.4/Wp and US$ 4.35/Wp respectively. It was claimed that the cost reduction in the second case was due to system optimization. Oliveira-Pinto and Stokkermans [32] indicated that CAPEX for FPV systems is generally 25% higher than ground systems, mainly due to floats, moorings, and anchors. In Ref.[84], it has been stated that the average total investment cost of a FPV system in 2018 ranged between 0.8 US$/Wp and 1.2 US$/Wp, depending on the size and location of the system. It was reported that the CAPEX of large-scale FPV projects (around 50 MWp) is between 0.7 and 0.8 US$/Wp in the third and fourth quarters of 2018, depending on the location and type of installed modules. The CAPEX of a hypothetical 50 MWp FPV installation was calculated and compared with a land-based system (both with fixed inclination) in the same position. For PV modules a cost of US$ 0.25/Wp was considered, while for inverters, a cost of 0.06 US$/Wp for both the ground and floating system was obtained. For assembling systems, a cost of US$ 0.15/Wp for the FPV and US$ 0.10/Wp for the ground system, for the BOS (balance of system) US$ 0.13/Wp and US$ 0.08/Wp for the FPV and the ground system respectively, US$ 0.14/Wp and US$ 0.13/Wp, respectively was considered. These resulted in overall CAPEX of US$ 0.73/Wp for the FPV and US$ 0.62/ Wp for the ground system [84]. Rosa Clot and Tina [89] made a list of the costs for building a FPV plant for various proposed technological solutions. They assumed that the cost relating to the PV modules is 0.25 US$/W, the electrical components including cables and inverters is 0.12 US$/W, the galvanized steel is 2.20 US$/kg, and finally, the cost of the HDPE is 2.40 US$/kg. Starting from this hypothesis, they proposed three types of 1 MW plant that cost respectively: US$ 803,692 the Singapore Solution, US$ 590,556 the Gable “Slender” Solution, and US$ 630,106 Gable2 Solution and compared them with a ground.

2.2.6.2 Operating expense (OPEX)

The costs related to the operational phase are for leasing or renting the space in which the system will be installed, operation and maintenance, and insurance. In the case of

FPV systems, the rent could be less expensive or not present as the water surface cannot be used for other purposes (i.e. agriculture or construction). The O&M costs of a PV system generally consist of the replacement of faulty and malfunctioning devices or objects (inverters, PV modules, electrical and electronic components), and cleaning of PV modules [84]. Generally, for ground-mounted systems, especially in desert areas where there is a presence of dust, the latter component is important and expensive. Besides, the soil may need to be periodically cleaned, as the presence of spontaneous vegetation (shrubs, brushwood, dry material) could reduce the performance of the plants and cause fires in the summer season. Therefore, the conditions in which the FPV systems are operating, in this sense, could be advantageous as there is the availability of large quantities of water near the plant and the absence of growth of wild plant species near the modules. Maintenance costs could be different between the conventional and floating systems since in the latter: Moorings, submarine cables, or floating platforms require different knowledge, tools, and processing times. It may be necessary to act on the moorings in case of a change in the level of the lake beyond the limit concerning the permitted one (a practical example is the maintenance of the floating system installed in the laboratories of the Enel Innovation Lab in Catania (IT) consists of adjusting the length of the moorings in conditions where the level of the basin has fallen beyond the minimum level). There may be a cleaning and cooling system that requires maintenance and cleaning of the filters of the water suction pumps due to the excessive turbidity of the water. Modules may need to be cleaned more frequently due to bird droppings. Checking for any malfunctions or wear of cables submerged in water, specialized personnel, divers, or robots capable of carrying out inspections under the water may be required. Maintenance takes place mainly on the water with vehicles such as boats, which could be among the items of expenditure in the OPEX phase if not already present on site. As for insurance, it depends on many factors but also on the location and weather variables. According to Ref. [84], the annual cost of insurance can vary from 0.25% to 0.5% of CAPEX. Maintenance and operating costs for a conventional utility-scale ground system, declared by NREL in 2018 for the US, was 0.0154 US$/Wp/year. However, 0.009 US$/Wp/year was reported in Lazard and 2.5% of the CAPEX was reported by Fraunhofer. A study on the costs of ground-mounted PV systems, projected up to 2050, stated that OPEX in

Germany in 2019 was 9.2 $/kWp/y [90]. It has also been shown that OPEX will decrease by about 30% and 50% until 2030 and 2050 respectively. In Ref. [91], it has been stated that the plausible values for the OPEX costs for floating installation on dams are two-fold of the OPEX costs on the ground. For FPV systems, most of the maintenance is allocated to inverters which imposed costs ranging from 6.15 to 9.50 US$/kWp. In a study by Martin [85], it was stated that the OPEX costs in the economic evaluation phase for the comparison between the ground-mounted and floating systems are 0.013 US$/ Wp/year and 0.026 US$/Wp/year respectively. This is because the working conditions in the FPV could be more complex than the ground system. Rosa-Clot and Tina [92] stated that the maintenance costs are constant throughout the life cycle and limited for the floating system (with some increases if a localization system is implemented) and on average are higher for a ground system. Regarding the decommissioning, they declared that it is much cheaper for FPV systems since there is no fixed structure, except for the mooring blocks which can be easily moved.

As regards the evaluation of the OPEX, the revenues relating to the water saved due to the reduction in evaporation can be be taken into account. Regarding this question, there will be a dedicated section in which this topic will be deepened and analyzed.

2.2.6.3 Levelized cost of electricity (LCOE)

Numerous researches have been carried out to evaluate the LCOE of a PV system. Several scenarios were often considered, in which the variables involved were parameterized to evaluate their possible variations in the final result. Usually, sensitivity studies are carried out considering the following variables: solar radiation, climatic zone (arid/desert, tropical, temperate), PR (performance ratio), CAPEX, years of operation, system degradation rate, yearly insurance, O&M, and financial leverage. In a study conducted by Barbuscia [86], the following LCOE values for ground-mounted systems were reported: 48 US$/MWh in Peru in early 2016; 36 US$/MWh in Mexico; and 29.9 US$/MWh in Dubai. It was concluded that the costs depend on the installation site where the world average cost amounts are about 67 US$/MWh. A recent study by Vartiainen et al. [86] conducted an assessment of the LCOE for ground-mounted systems according to the WACC5 indicated the development from 2019 to 2050 for six European locations. They studied LCOE with a nominal WACC of 2%, 4%, 7%, and 10%. LCOE with 7% nominal WACC in 2019 ranged from 24

€/MWh in Malaga to 42 €/MWh in Helsinki. In 2030, this range would be 14€ 24 €/MWh and 9€ 15 €/MWh in 2050. It should be noted that the increase in the nominal WACC from 2% to 10% doubles the LCOE. In [93], an LCOE calculation was made considering three geographical areas with three WACC and two PR scenarios (+5% and +10% concerning the evaluation of the natural evaporative cooling of the modules in the water). In a recent study by Oliveira-Pinto and Stokkermans [32], the LCOE concerning the type of used floats, and the location of installation were evaluated. The calculated LCOE was ranged from 50.3 $/MWh for Almeria to 96.2 $/MWh for Barrow Gurney for the floating system and compared with the reference values of the ground-mounted system. The LCOE was reported as 33.1 $/MWh and 59.3 $/MWh for the two mentioned locations. Barbuscia [86] presented a sensitivity analysis of the LCOE as a function of the size of the system and type of the float. The role played by the capacity of the system on the cost of the energy was highlighted, which indicated an almost exponential decreasing trend as the installed power increases, reaching values similar to those of conventional technologies for utility-scale systems. It started from values of about 80 cUSD/kWh for the power of 52 kW up to 12 cUSD/kWh for capacities greater than 2 MW. Sensitivity analysis was also conducted on the choice of mounting structures, among the modular and rigid ones, and it showed a 20% variation in the LCOE for a 5 MW plant. In another study carried out by Rosa-Clot and Tina [89], the LCOE was calculated concerning the location. LCOE for Dubai with different plant configurations were obtained as 36.3 US$/MWh for Fix 20° ground-based unit, 31.8 US$/MWh for Fix 10°+ cooling, 26.5 US$/MWh for Gable 10°+ cooling, 26.9 US$/ MWh for vertical axis tracking tilt 20. Temiz and Javani [94] obtained an LCOE value of 0.6124 US$/kW for a FPV system which produces both electricity and hydrogen. The FPV systems have good prospects for further growth and development which can be seen from the continuous research, development, and deployments listed out in various abovementioned literature. In many cases, the analysis affirms that FPVs are more expensive than conventional ground-mounted systems.

The economic evaluation and therefore the calculation of the LCOE of an FPV system will be developed in the next chapters as they are the crucial topic of this research work.

3 Experimental plants at Enel Inn. Lab–Passo Martino

3.1 Introduction

The experimental monitored plants (Figure 22), intend to explore innovative PV floating components, systems, and plant configurations, to define and validate possible advantageous solutions to be adopted in industrial utility scale plants of EGP.

These plants were monitored during the research period also to validate the models implemented and described in the following chapters. From now on, when we talk about the experimental plant, we refer to the system described below.

Figure 22 Plants monitored by Enel Green Power at the Enel Innovation Hub and Lab in Catania (IT)

Each plant has a different configuration and moreover, is equipped with both monofacial and bifacial modules. One of the FPV plants is also equipped with a hydraulic plant for the active water cooling of the modules.

The plants installed in EGP reservoir were built in July 2019 and June 2020.

3.2 Systems description

The test bench is equipped with various instruments and sensors follow described.

Three different FPV plant solutions have been installed:

- Figure 23a (Modules in landscape position)
- Figure 23b (Modules in landscape position)
- Figure 23c (Modules in portrait position)

Each plant is composed by two subfields, one equipped with monofacial modules and the other one with bifacial.

Totally, seven photovoltaic systems were monitored (see Figure 23 and Figure 24), of which six were installed on the water and one used as a reference, installed on the ground. All the plants examined are south facing, so, the azimuthal orientation of the all PV modules is fixed at 180°.

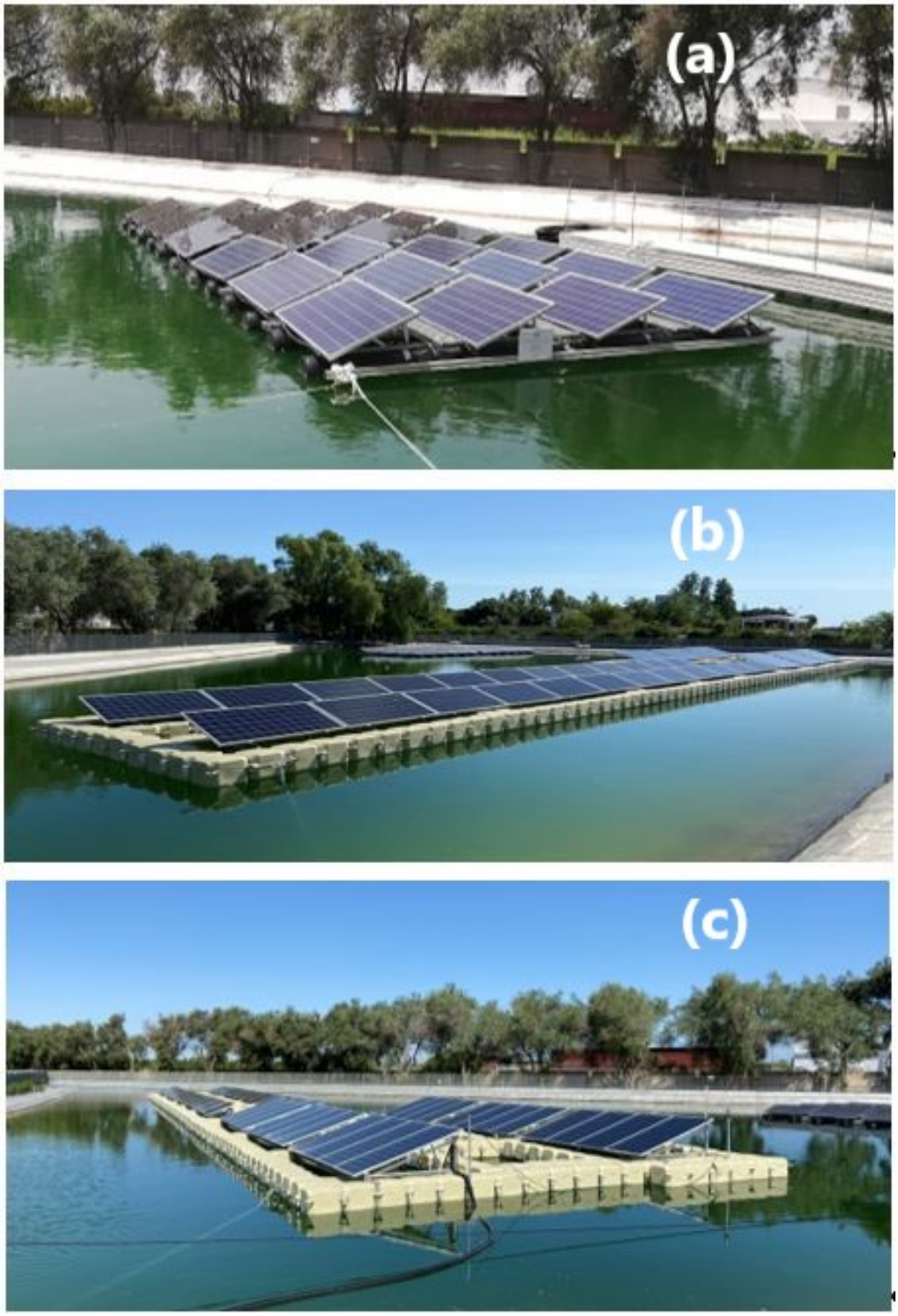

Figure 23. A 6 different solution installed in the lake of EGP

Figure 24 Ground mounted PV plant (GPV)

The characteristics of G/FPV systems analysed are shown in Table 3.

Table 3 Characteristics of the plants

Typology	Ground	Floating					
Plant	Figure 24	Figure 23a		Figure 23b		Figure 23c	
Technology	mono	mono	bifi	mono	bifi	mono	bifi
γ_M [°]	35	20	20	20	20	20	20
d_r [m]	-	1.58	1.58	2.93	2.93	5.36	5,36
$h_{w/g}$ [m]	1	0.4	0.4	0.4	0.4	0.5	0.5
P_m [W]	315	320	345	380	380	380	380
P_{tot} [W]	2205	3840	4140	4560	4560	4560	4560
n_m	7	12	12	12	12	12	12
n_{row}	1	4	4	2	2	2	2
n_{str}	1	2	2	1	1	1	1
Config.	landsc.	landsc.	landsc.	landsc.	landsc.	portr.	portr.

For clarity, the geometrical variables reported in Table 3 are shown in Figure 25.

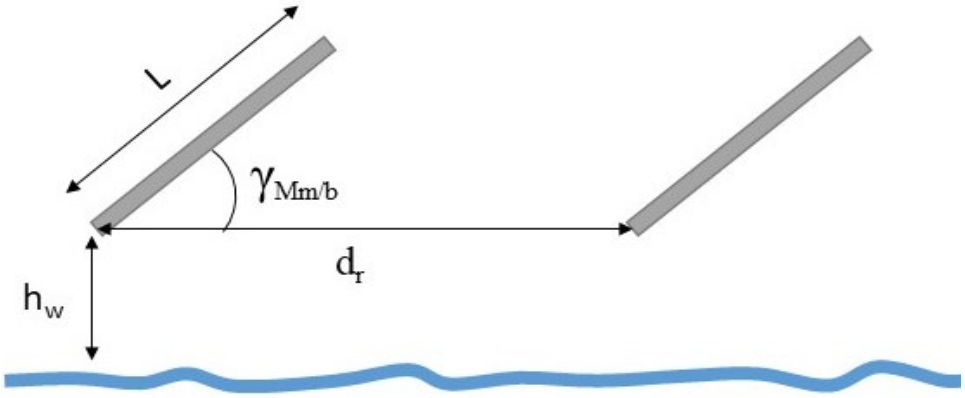

Figure 25 Relevant geometrical variables of the PV systems

The significant environmental variables for the operation of a photovoltaic system were monitored (G_{fr}, G_{bk}, T_a, T_w, u_{10}, RH, T_{nw}) and acquired in part by the local weather station (see Figure 26) and in part by datalogger, whose function is to monitor the quantities in the vicinity of the plants.

Figure 26 Weather station (dot line) and FPV system position (continuous line)

The back-module temperatures (T_{bk}) of each technology were monitored, in order to evaluate their thermal behavior near the water surface or on the ground and also the

electrical quantities ($I_{AC/DC}$, $V_{AC/DC}$, $P_{AC/DC}$) of each system, through measurements carried out by sensors placed on the inverter.

3.2.1 Cooling system

To study the behaviour in the presence of active cooling, a cooling system with electric pump and sprinkler described below was installed in the FPV of Figure 23a.

A 500 W electric pump was used for pumping the water. The pump flow rate ranges from 20 to 70 l/min and its head ranges from 40.3 to 15.9 m, it is single-phase with a nominal voltage of 230V. Figure 27 shows the components of the system in detail, Figure 27a pump, Figure 27b the filters and valve, Figure 27c the sprinkler.

Figure 27 Components of cooling system

For each module, 4 sprinklers are installed, one for each corner (upper-lower right and left), for a total of 48 per plant. Two filters, one for monofacial and one for bifacial modules, were installed upstream of the pump inlet, to clean the water taken from the lake. Furthermore, valves for closing the circuits of the two systems have been inserted to stop the circulation of water.

Figure 28 shows the mono and bifacial modules during the active cooling phase.

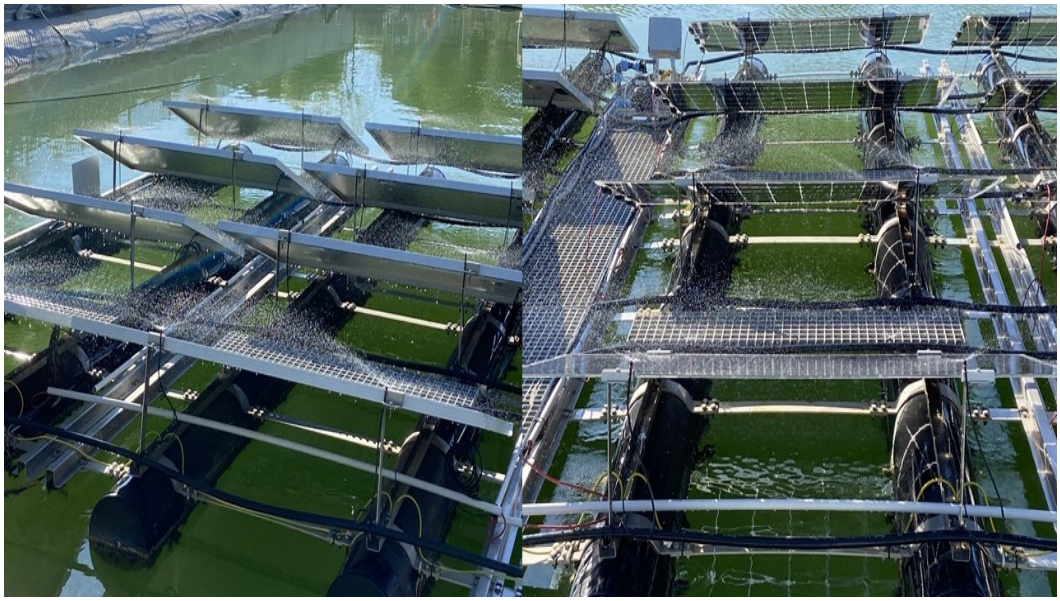

Figure 28 Floating mono-bifacial cooled modules

Figure 29 represents the scheme of the system.

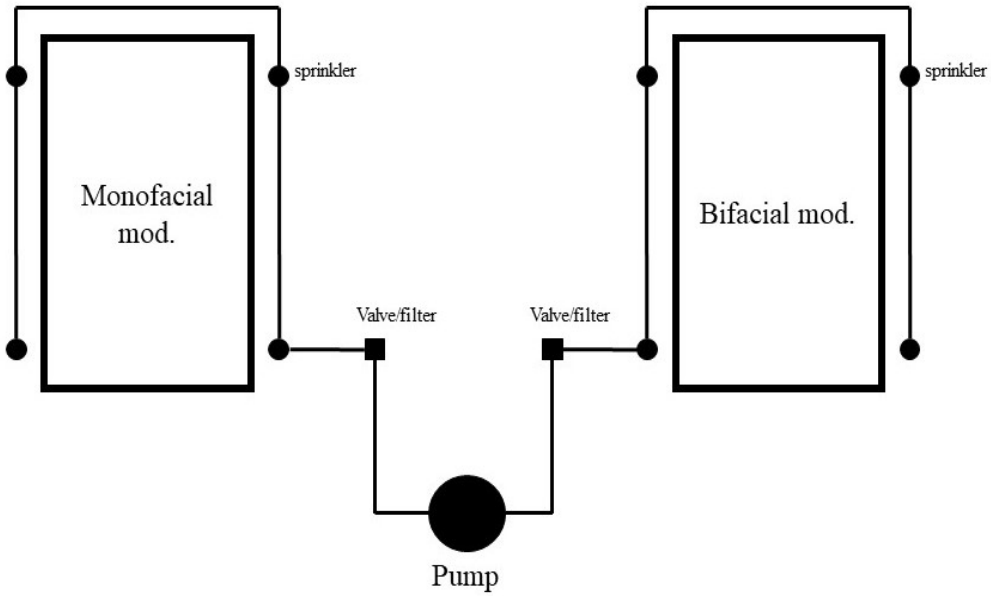

Figure 29 Scheme of cooling system

3.2.2 Measuring instruments

The test bench is equipped with various instruments and sensors, the characteristics of electrical sensors are described in Table 4.

Table 4 Characteristics of electrical sensors

Sensor	Accuracy class	Thermal drift	Response time
Current	AC/DC: 0,2% f.s.	< 150 ppm/K	100 ms (without filter) 600 ms (with filter)
Voltage	0,5% input; 0,1% outputs	+100 ppm/K	1 s from 10 to 90%

The characteristics of the other sensors are shown in the Table 5.

Table 5 Characteristics of the measuring instruments

Solarimeter				
Class	Accuracy 95% confidence level (%)	Spectral field (nm)	Non linearity (1000 W/m^2) (%)	Stability (%)
secondary standard	± 2	285 ÷ 3000	<± 0.2	<± 0.5
Air temperature sensors				
Principle	Type	Measuring range (°C)	Accuracy (°C at 0°C)	Resolution(°C)
Pt100	RTD 4 wires	-50 ÷ 70	± 0.10	0.01
Modules temperature sensors				
Pt100	RTD 4 wires	-50 ÷ 180	± 0.10	0.01
Wind speed sensors				
Principle	Type	Measuring range (m/s)	Accuracy (m/s)	Resolution(m/s)
Optoelectronic disc	standard anemometer	0 ÷ 75	± 0.25	0.06

Figure 30 shows an overview diagram of the test bench.

Through an acquisition system, which can also be managed remotely through access from the web platform, all the data is brought together on a PC and stored in the form of a csv file. It is possible to download the data in processed and unprocessed mode.

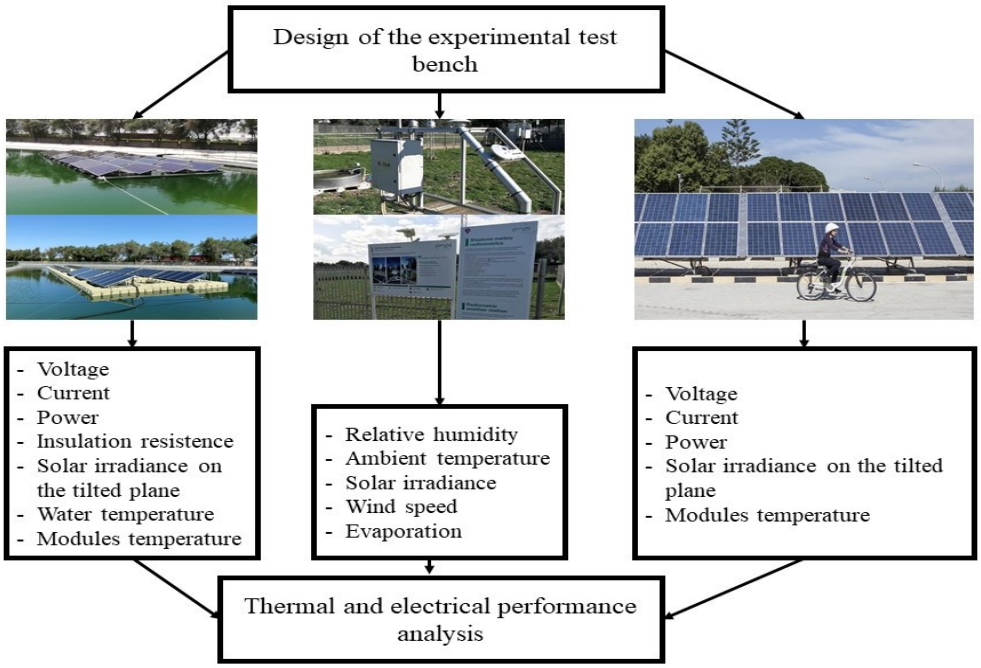

Figure 30 Overview of the proposed test bench

3.2.3 Consideration on installation

The system of Figure 23a is made with galvanized metal carpentry resting on HDPE pipes, for water pipes about 6 meters long (Figure 31). The assembly of the entire system took place partly on land and partly in water. In particular, all the carpentry was mounted on the ground, and with the aid of a mechanical crane was placed in the water. Subsequently the modules were installed with the help of a boat as well as the connection of the moorings. The ballasts, made with prefabricated concrete blocks, were also placed with the help of a crane.

Figure 31 (a) solution (bifacial-monofacial)

The system of Figure 23b-c is modular, made with HDPE floats assembled together with additional plastic components (Figure 32). The support structure is made of aluminium and is very light. The launch took place without the aid of any mechanical crane, simply by sliding the various floats on the dock ramp. The modules were installed on the rafts on the ground before they were launched and a floating platform called "*Caronte*", also made with the modular floats of the FPV system, allowed to move inside the basin, to position the ballast and anchor the plant. *Caronte* remained at the service of the plant and is used for maintenance. According to what was seen during the construction works, all systems are practical and allow flexibility and modularity therefore installation times are fast. To increase the solar radiation reflected on the rear side of the bifacial modules, we are considering inserting reflective surfaces anchored to the aluminium structures that will allow to increase the energy yield.

Figure 32 (b)-(c) solution (bifacial-monofacial)

Another possible solution that is being evaluated is the light-coloured floating hollow spheres placed on the water surface and in correspondence with the bifacial modules inside the confined structure. This solution seems interesting because unlike corrugated sheets it is easier to install and does not completely cover the water surface, therefore it shouldn't reduce much the cooling effect and allows a portion of solar radiation to penetrate and keep the water surface unchanged lake environment.

For the auxiliary components, which are necessary both for operation (mooring, anchoring etc…) and for increasing performance (cooling systems) it is necessary a constant monitoring.

Malfunctioning of these components cause energy losses that result in lower economic revenues.

Regarding the cooling systems, it is necessary not only to monitor the PV plant, but also its components such as pumps, sprinklers, filters. These components should be equipped with sensors capable of providing information about their operating status.

In FPV systems, where active cooling systems are used and water is drawn from the basin, filter monitoring and frequent cleaning are essential for the optimal functioning of the cooling system.

Other components that need to be monitored in FPV systems are the moorings and anchors, which are continuously subjected to mechanical stress. A failure in the

anchoring and mooring system can lead to energy losses as the system could move from the initial position, identified during installation phase in order to optimize the performance of the system. O&M operators suggest installing strain gauges in order to detect the movement of the system's moorings. This can allow to predict malfunctioning and faults of the system.

Moreover, it may be necessary to monitor also the water temperature, the water level of the basin, the relative humidity and the possible presence of waves.

First of all, water temperature monitoring is necessary for estimate the temperature of the photovoltaic modules and environmental conditions.

Moreover, knowing the water level of the basin allows to estimate the reduction of evaporation caused by the partial coverage of the water surface; but also to act on the moorings, modifying their length, in case of too high or low level of the basin which would lead to the destruction of the system.

As for the data acquisition systems, the cables passage in the water could be expensive, therefore, to minimize the installation costs of the monitoring system, a solution suggested in the FPV systems monitored at the 'Enel Innovation Hub and Lab' in Catania (IT) is to install components in water and use the RS-485 data transmission. In this way it is possible to avoid voltage drops, sensor signal losses and large quantities of cables, moreover costs of installation are reduced and it is possible to obtain a much more versatile, flexible and modifiable system. However, it must be taken into account that sensors must be more robust and withstand high humidity rates.

In addition, in FPV systems it is necessary to use suitable adhesives to avoid separation of contact sensors, such as those used for measuring the PV module temperature. That can be due to high humidity rates and/or mechanical stress.

During the monitoring of FPV it was noted that many animal species are attracted to the plant (Figure 35).

Figure 33 Animals and FPV systems in perfect symbiosis

This, on the one hand, is a positive aspect as it demonstrates the low environmental impact, on the other hand it causes frequent fouling of the modules.

In this regard, by way of example, Figure 35 shows a common species of duck with its young that is perfectly integrated and absolutely undisturbed by the FPV system.

4 Evaporation rate models on a water basin with FPV plants

4.1 Introduction

Water is an asset, so it is possible to attribute an economic value to it. In [95] the results of the study show at macro-agricultural irrigation water price of 1.023 yuan/m^3 = 0.13 euro/m^3. Reports from the Arpa [96] of Sicilian region report that the cost of water for irrigation fluctuates between 0.14 euro/m^3 and 0.19 euro / m^3.

If the FPV plant is installed on the water surface of the storage basin of an HPP plant, the water accumulated by the lack of evaporation can be converted into electricity, obtaining further economic revenues from the HPP plant.

Therefore, attributing to the saved water an economic value, it can be deduced that the levelized cost of electricity of the FPV or FPV-HPP, considering also the revenue of the water saved, will decrease from its original value.

As reported in the annual report of the manager of the Italian national energy markets (GME) [96], the sale price of electricity can be fluctuating throughout the year fluctuating in the various months of the year so to attribute a value have to collocate in a situation of intermediate cost.

In this chapter, the methodology adopted for estimating the evaporation reduction in the presence of partial coverage of the water surface through the use of FPV systems in relationship to their features will be illustrated and the results obtained will be presented.

This study will allow to develop models for estimating the performance of FPV systems but also to make technical-economic evaluations of FPV systems.

4.2 Features of FPV

The study of evaporation in presence of floating photovoltaic systems in water requires a preliminary analysis of the different typologies of FPV plants. In this paragraph is take care of giving an overview of the various existing FPV technologies, in order to

appropriately highlight the features that have direct interaction with the water evaporation.

The solar radiation (direct and/or diffuse component) that hits the surface of the water is the main variable that affects the water evaporation; therefore, it is crucial to define how and how much the contribution of solar radiation varies in relation with the typologies of installation. In [27] different installation solutions are referred which are classified as follows:

- **floating systems with floats that cover the entire surface below the module** (Figure 34a). The system consists of modular floating platforms in polyethylene that are anchored to the ground by elastomers. This allows greater flexibility in the event that the variation of the water level is considerable and sudden. The transmission of solar radiation below the platforms is almost zero as they are made so as to completely cover the underlying surface.
- **floating systems with modules anchored to a tubular buoyancy system** (Figure 34b). These systems allow good ventilation of the modules and cooling due to the natural evaporation of the water of the basin. This kind of installation lets the modules to operate at lower temperatures and therefore to increase their efficiency. The transmission of solar radiation through the water surface is reduced, but it is not completely stopped as the photovoltaic modules are suspended and the buoyancy structure occupies only a part of the water surface.
- **canal top solar systems** with structures anchored to the ground that are installed as covers of surfaces or watercourses (Figure 34c). Such installations are mainly implemented on waterways, rivers or canals. In addition to reducing the evaporation of the surface on which they are installed, they allow optimal use of the latter. The transmission of solar radiation depends on the geometric configuration of the system, that is, the distance between the rows and inclination of the modules and also the type of PV module. In fact, if the module is of the glass-glass type with gaps between the cells such as the bifacial, there will be a portion of the radiation that will pass through the module and reach the water surface.

- **flexible floats**, in direct contact with the water, the whole system is integrated into overflow with the pond and with the thin film lamellar, which allows the photovoltaic structure to deform with the wave motion of the water (Figure 34d). Direct contact with water activates the cooling effect without the implementation of pumping systems and self-cleaning. A further advantage is that of implementing the submersion of the modules in the case of waves that cannot be tolerated by the system, this is useful for offshore installations.

Figure 34 shows the different types of FPV installation.

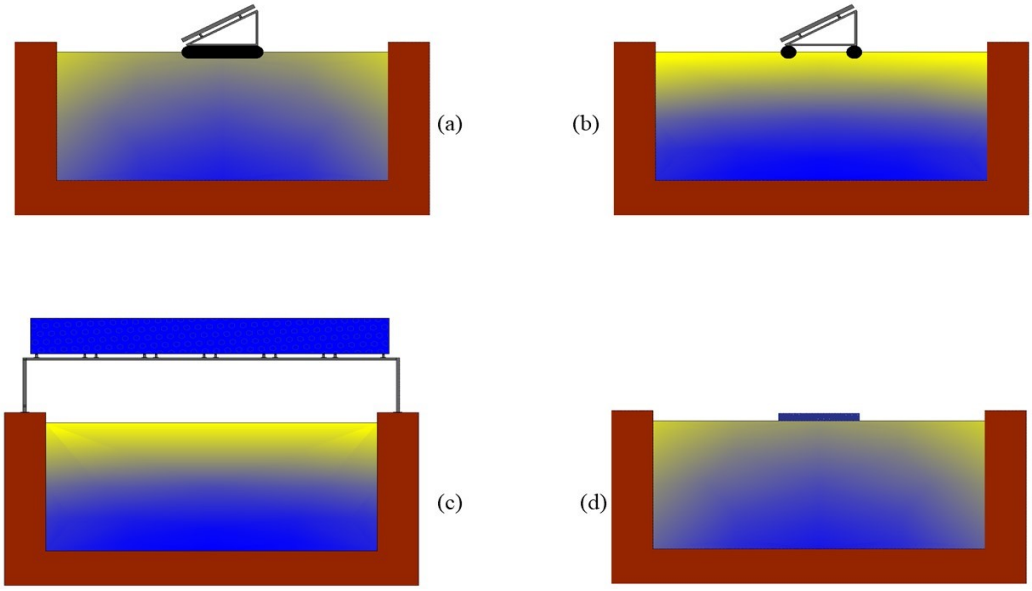

Figure 34 Typologies of FPVs (a) the floats cover entirely the surface below the module, (b) modules anchored to a buoyancy system, (c) canal top solar systems, (d) flexible floats.

4.3 Methodology

The mathematical models used for estimating the evaporation are subdivided into two main groups:

- evaporation models for free water surfaces (EVM_{free});
- evaporation models for water surfaces partially covered by FPVs (EVM_{FPV}).

As regards the (EVM_{free}), 11 different mathematical models will be presented. Among them, six are literature models (see Table 6), three are novel models specifically designed by the DoE method, namely DoE models, and two are derived through the linear regression theory, namely linear regression models (see Table 7) [97].

Table 6 List of examined literature models (EVM_{free})

Literature evaporation models for free water surfaces	***Input variables***	***n. equation***
Penman Monteith $E = \left(\frac{0.404\Delta(Q^* - N) + \gamma \frac{900u_2(e_s - e_a)}{T_a + 273}}{\Delta + \gamma(1 + 0.34u_2)} \right)$	$R_s\ RH\ T_a\ u_2$	**Eq. 5**
Penman-Monteith modified $E = \frac{1}{\lambda} \left(\frac{\Delta_w(Q^* - N) + \frac{86400\rho_a C_a(e_w^* - e_a)}{r_a}}{\Delta_w + \gamma} \right)$	$R_s\ RH\ T_w\ u_2$	**Eq. 6**
Valiantzas $E = 0.051(1-\alpha)R_s\sqrt{T_a + 9.5} - 0.188(T_a + 13)\left(\frac{R_s}{R_a} - 0.194\right)\left(1 - 0.00014(0.7T_{amax} + 0.3T_{amin} + 46)^2\sqrt{\frac{RH}{100}}\right) + 0.049(T_{amax} + 16.3)\left(1 - \frac{RH}{100}\right)(0.62 + 0.53u_2)$	$R_s\ RH\ T_a$ $T_{amin}\ T_{amax}\ u_2$	**Eq. 7**
Rohwer $E = 0.44(1 + 0.27u_{10})(e_s - e_a)$	$R_s\ RH\ T_a\ u_{10}$	**Eq. 8**
Mc Guinness and Bordne $E = (0.082T_a - 0.19)\left(\frac{R_s}{1500}\right)2.54$	$R_s\ T_a$	**Eq. 9**
Hargreaves $E = 0.408 * 0.0025(T_a + 16.8)(T_{amax} - T_{amin})^{0.5}R_a$	$T_a\ \ T_{amin}\ T_{amax}$	**Eq. 10**

EVM_{FPV} are mainly based on EVM_{free} that uses the water temperature as input data. The main difference of these two categories consists in the introduction of the different quantity of radiation that strikes the water surface, which is, in turn, a function of the type of FPVs.

In this contest two main typologies of FPV are defined:

- suspended systems subdivided into two sub-categories: floating systems with modules anchored to tubular buoyancy systems (Figure 34b), canal top solar systems (Figure 34c);
- floating systems subdivided into two sub-categories: floats that cover the entire surface below the module (Figure 34a), flexible floats (Figure 34d).

4.3.1 EVM_{free} based on the DoE and linear regression method

In this paragraph the proposed evaporation models will be presented, which can be used in the case of free water surfaces. These models, unlike those existing in the literature, are easily implemented and very performing.

The three proposed evaporative models $EVM_{freeDoE}$ [97] were derived starting from a vector containing the quantity of evaporated water for each day under examination, calculated with Eq. 5.

Then, the Design of Experiments (DoE) method was applied for calculating for each variable (e.g. solar radiation, humidity, wind velocity, and air temperature) the unknown coefficients "a" that appear in Eq. 11.

$$y = a_0 + \sum_{i=1}^{n} a_i x_i + \sum_{i=1}^{n} a_{ii} x_i^2 + \sum_{\substack{i,j=1 \\ j<i}}^{n} a_{ij} x_{ij} \qquad \textbf{Eq. 11}$$

Also to implement the linear regression models $EVM_{freel.r.}$, [97] a known evaporation vector was used, calculated starting from Eq. 5 (Penman Monteith).

Then, the linear regression method (l. r.) was applied for calculating for each variable (e.g. solar radiation, humidity, wind velocity, and air temperature) the unknown coefficients "a" that appear in Eq. 12.

$$y_i = a_0 + a_1 x_{i1} + \cdots a_p x_{ip} + \varepsilon_i \qquad i=1,\ldots,n \qquad \textbf{Eq. 12}$$

Table 7 Polinomial equations for DoE and Linear regression proposed models

DoE Equation	***Input variable***	***n. equation***
$E = a_0 + a_1 R_s + a_2 T_a + a_3 RH \quad + a_4 u_{10} + a_{12} R_s T_a + a_{13} R_s RH \quad + a_{14} R_s u_{10} + a_{23} T_a RH \quad + a_{24} T_a u_{10} + a_{34} RH \quad u_{10} + a_{11} R_s^2 + a_{22} T_a^2 + a_{33} RH^2 + a_{44} u_{10}^2$	$R_s\ RH\ T_a\ u_{10}$	**Eq. 13**
$E = a_0 + a_1 R_s + a_2 T_a + a_3 u_{10} + a_{12} R_s T_a + a_{13} R_s u_{10} + a_{23} T_a u_{10} + a_{11} R_s^2 + a_{22} T_a^2 + a_{33} u_{10}^2$	$R_s\ T_a\ u_{10}$	**Eq. 14**
$E = a_0 + a_1 R_s + a_2 T_a + a_{12} R_s T_a + a_{11} R_s^2 + a_{22} T_a^2$	$R_s\ T_a$	**Eq. 15**
Linear regression Equation	***Input variable***	***n. equation***
$E = a_0 + a_1 R_s + a_2 T_a + a_3 RH \quad + a_4 u_{10}$	$R_s\ RH\ T_a\ u_{10}$	**Eq. 16**
$E = a_0 + a_1 R_s + a_2 T_a + a_3 T_w + a_4 RH \quad + a_5 u_{10}$	$R_s\ RH\ T_a\ T_w\ u_{10}$	**Eq. 17**

The $EVM_{free\ lin\ reg}$, expressed in Table 7, has the particularity include as input parameter the water temperature T_w.

4.3.2 EVM_{FPV} for covered water surfaces

This section describes the methodology followed for estimating the evaporation reduction due covering of the water surface with floating photovoltaic systems. The 4 different typologies of installations illustrated in Figure 34 will be taken into account.

For each case, a target energy balance equation for the surface of the basin has to be defined as function of the quantities acting in presence of FPV plant. In Figure 35, a representation of the flows of the energy balance.

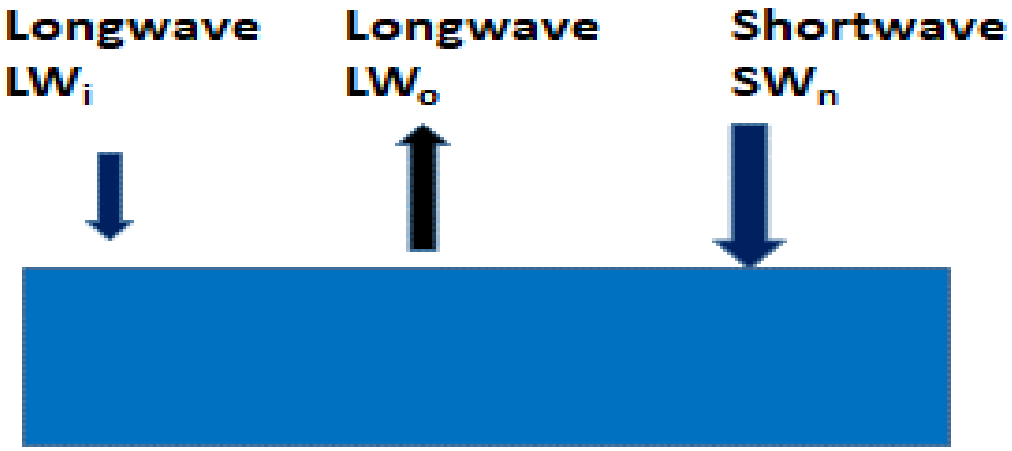

Figure 35 Water surface energy balance

The energy balance equation for free surface can be written as [97]:

$$Q^* = SW_i - SW_o + LW_i - LW_o \quad \textbf{Eq. 18}$$

$$SW_i = R_d + R_b \quad \textbf{Eq. 19}$$

$$SW_o = \alpha(R_d + R_b) \quad \textbf{Eq. 20}$$

$$SW_n = SW_i - SW_o = (1 - \alpha) * (R_d + R_b) \quad \textbf{Eq. 21}$$

$$LW_n = LW_i - LW_o = \sigma\, T_w^4 \left(0.56 - 0.0092\sqrt{e_a}\right)(0.10 + 0.90\, C) \quad \textbf{Eq. 22}$$

Where C is the cloudiness function.

4.3.2.1 Suspended photovoltaic covers

Suspended systems (Figure 34b and c), are not completely in contact with the surface of the water, so they shield the solar radiation but not the diffuse component of the solar radiation, which can reach the water surface beneath the PV module. For the part of the surface of the basin occupied by the suspended system it is assumed that the contribution of the direct radiation is modest since the system faces south and the distance between the rows is reduced. Therefore, only the contribution of diffuse radiation has been taken into account. Consequently, Eq. 21 and Eq. 22 became the following:

$$SW_{nScover} = (1 - \alpha)R_d \quad \textbf{Eq. 23}$$

$$LW_{nScover} = \sigma\, T_w^4 \left(0.56 - 0.0092\sqrt{e_a}\right)(0.10 + 0.90 * 0.3) \quad \textbf{Eq. 24}$$

For this type of FPV, the net contribution of short-wave radiation (SW_n) is only the diffuse component, and the net contribution of the longwave radiation (LW_n) is modified assuming C = 0.3, which correspond to full cloudy condition.

In this way, it is possible to calculate the evaporation rate in the portion of the water basin covered, namely E_{Scover} with a suspended photovoltaic cover using one of the EVM previously described.

Specifically, the term Q^* is calculated through the Eq. 23 and Eq. 24, if the Penman Monteith model (Eq. 5) is adopted for evaluating the evaporation rate, $E_{ScoverPenman}$.

Similarly, E_{Scover} may be calculated using the linear regression model through the following formula:

$$E_{Scoverlin.reg.} = a_0 + 0.2a_1R_s + a_2T_a + a_3RH \quad + a_4u_{10} \quad \textbf{Eq. 25}$$

For taking into account that in the cover part of the water surface only the diffuse component of the solar radiation acts, the coefficient "a_1", which multiplies the solar radiation, is in turn multiplied by a coefficient of 0.2.

The total evaporation rate of the water surface E_{FPVS} is given by the sum of the evaporation on the free water surface and the evaporation on the covered water surface and is calculated by:

$$E_{FPVS} = (1 - x)E_{free} + xE_{Scover} \quad \textbf{Eq. 26}$$

Where, E_{free} is the evaporation on the free water surface, while E_{Scover} is the evaporation on the area covered by photovoltaic modules. The x value is the percentage of water surface covered by the FPV.

4.3.2.2 Floating photovoltaic covers

The floating systems (Figure 34a and d), do not allow that solar radiation hits the water surface where they are installed. Consequently, Eq. 21 and Eq. 22 became the following:

- floats that cover entirely the surface below the module (Figure 34a),

$$SW_{nFcover,a} = 0 \quad \textbf{Eq. 27}$$

$$LW_{nFcover,a} = \sigma\, T_w^4 \left(0.56 - 0.0092\sqrt{e_a}\right)0.10 \quad \textbf{Eq. 28}$$

The net contribution of the shortwave radiation (SW_n) is zero, while the net contribution of the longwave radiation (LW_n) is modified assuming $C = 0$.

- flexible floats (Figure 34d):

$$SW_{nFcover,d} = \alpha_{pv}(R_d + R_b)(1 - \eta_{el})0.4 \quad \textbf{Eq. 29}$$

$$LW_{nFcover,d} = \sigma\, T_w^4 \left(0.56 - 0.0092\sqrt{e_a}\right)0.10 \quad \textbf{Eq. 30}$$

The net contribution of the shortwave radiation (SW_n) is not zero because a portion of the solar radiation incident on the PV module is transferred to the water surface. This portion is calculated considering that only the aliquot of solar radiation absorbed by the solar cell through the coefficient of absorptivity α_{pv}, subtracting the aliquot transformed in electric power through the electrical efficiency η_{el}. And finally considering that only 40% of this reduced solar radiation is effectively transferred to the water surface.

In this way it is possible to calculate the net heat flux Q^* in the portion of the water basin covered, namely Q^*_{Fcover}, for both (a) and (d) systems through the subsequent equation.

$$Q^* = Q^*_{free}(1-x) + Q^*_{Fcover}(x) \quad \textbf{Eq. 31}$$

The above equation indicates that the net energy inlet comes both by the free surface and the covered surface for reason before illustrated.

Finally, the total evaporation for a water surface, where a floating PV system is installed, is calculated by:

$$E_{FPVF,a/d\ Penman} = (1-x)E'_{free} \quad \textbf{Eq. 32}$$

Where E'_{free} is the evaporation rate calculated with an EVM (e.g. Penman Monteith model) with the term Q^* has to be calculated by Eq. 31.

Similarly, the evaporation rate, in the case of partially covered surfaces with floating covers, may be calculated using the linear regression model through the following:

- floats that cover entirely the surface below the module (Figure 34a)

$$E_{Fcover,a\ lin.reg.} = a_0 + (1-x)a_1R_s + a_2T_a + a_3RH \quad + a_4u_{10} \quad \textbf{Eq. 33}$$

- with flexible floats (Figure 34d)

$$E_{Fcover,d\ lin.reg.} = a_0 + (1-0.95x)a_1R_s + a_2T_a + a_3RH \quad + a_4u_{10} \quad \textbf{Eq. 34}$$

The multiplicative coefficient 0.95 in Eq. 34 takes into account the solar radiation transmitted through the photovoltaic modules to the water surface.

For the calculation of total evaporation in the case of the systems of Figure 34a and d the formula used is the following:

$$E_{FPVF,a/d\ lin.reg.} = E_{Fcover\ lin.reg.}\ (1-x) \quad \textbf{Eq. 35}$$

Where $E_{Fcover\ lin.reg}$ is calculated by Eq. 33 for (a) systems and Eq. 34 for (d) systems.

4.3.3 Yield indexes and model comparison

The annual amount of water evaporated is calculated summing the daily evaporation rate by the equation:

$$E_{cum} = \sum_{d=1}^{n} E_d \qquad \textbf{Eq. 36}$$

Thus, it is possible to evaluate the evaporation reduction caused by the partial coverage of the water surface, calculating the difference of the annual evaporation between a free water surface $E_{free\ cum}$ and a partially covered surface $E_{FPV\ cum}$:

$$\Delta E_{FPV} = E_{free\ cum} - E_{FPV\ cum} \qquad \textbf{Eq. 37}$$

To quantify the effect of the FPV in reducing the evaporation, it has been defined the efficiency of the evaporation decrement as:

$$\eta = \frac{\Delta E_{FPV}}{E_{free\ cum}} * 100 \qquad \textbf{Eq. 38}$$

Two different methods for estimating evaporation reduction have been implemented, which have been compared. The first has been implemented starting from the Penman-Monteith equation, the second has been implemented using the linear regression equations, in which some terms are modified.

As regarding the trustworthiness of the proposed EVM_{free} models, the comparison between the measurements made with an evaporimeter and predictions of the models has been evaluated as follows:

$$\Delta E_{cum} = E_{cum\ measured} - E_{cum\ models} \qquad \textbf{Eq. 39}$$

Finally, the comparison between the two methods that can be used for estimating the evaporation reduction (Penman-Monteith and linear regression), were implemented using following formula:

$$\varepsilon_{FPV\ cum} = \frac{E_{FPV\ \ Penman\ cum} - E_{FPV\ lin.reg.cum}}{E_{FPV\ Penman\ cum}} * 100 \qquad \textbf{Eq. 40}$$

4.4 Test validation of EVM

A practical application has been conducted with the aim to evaluate the accuracy of the results carried out by the proposed evaporation models. With this aim, experimental observations on weather climate (ambient temperatures, solar radiation,

wind velocity, humidity) as well the measure of the evaporation rate were used. These data have been collected by the climate station described in Chapter 3.

To validate the models, statistical indices reported in 'Appendix A: Statistical evaluation indexes' were calculated, in particular the MBE PE RMSE and R^2.

As case study the Lentini Lake, located at lat. 37°19′22.8″N and long 14°57′00″E, water body altitude 18 m a.s.l., depth of water Z=10 m, lake water body area, A=12 km^2, was chosen to compare the results of the proposed EVMs with experimental observations. The waters of this reservoir are intended for industrial use and irrigation of neighbouring municipalities. Figure 36 shows the Lentini lake.

Figure 36 Biviere Lake in Lentini (CT) Italy

The volume of water in the basin is (12 10^6 m^2) (10 m) = 120 10^6 m^3. The volume evaporated for free water surface in a year is (1.743 m) (12 10^6 m^2) = 20.92 10^6 m^3 that, it is 17.43% of the water contained in the basin for a height of the basin equal to Z = 10 m. This amount of water, if saved, can be used for irrigation or for energy production purposes if the floating plant is installed in the storage basin of a hydroelectric plant.

4.4.1 Numerical models for evaluation of the evaporation rate of free water surfaces

In this section will be explicitly stated the equations that define the EVM obtained by the DoE and the linear regression method.

4.4.1.1 Data and measurements

The characteristics of the weather station are described in Chapter 3 where the class "A" evaporimeter and the pyranometers for measuring solar radiation were installed.

The meteorological data measured by the weather station during the period going from 10/04/2018 to 30/05/2018 are reported as a function of time, in Figure 37.

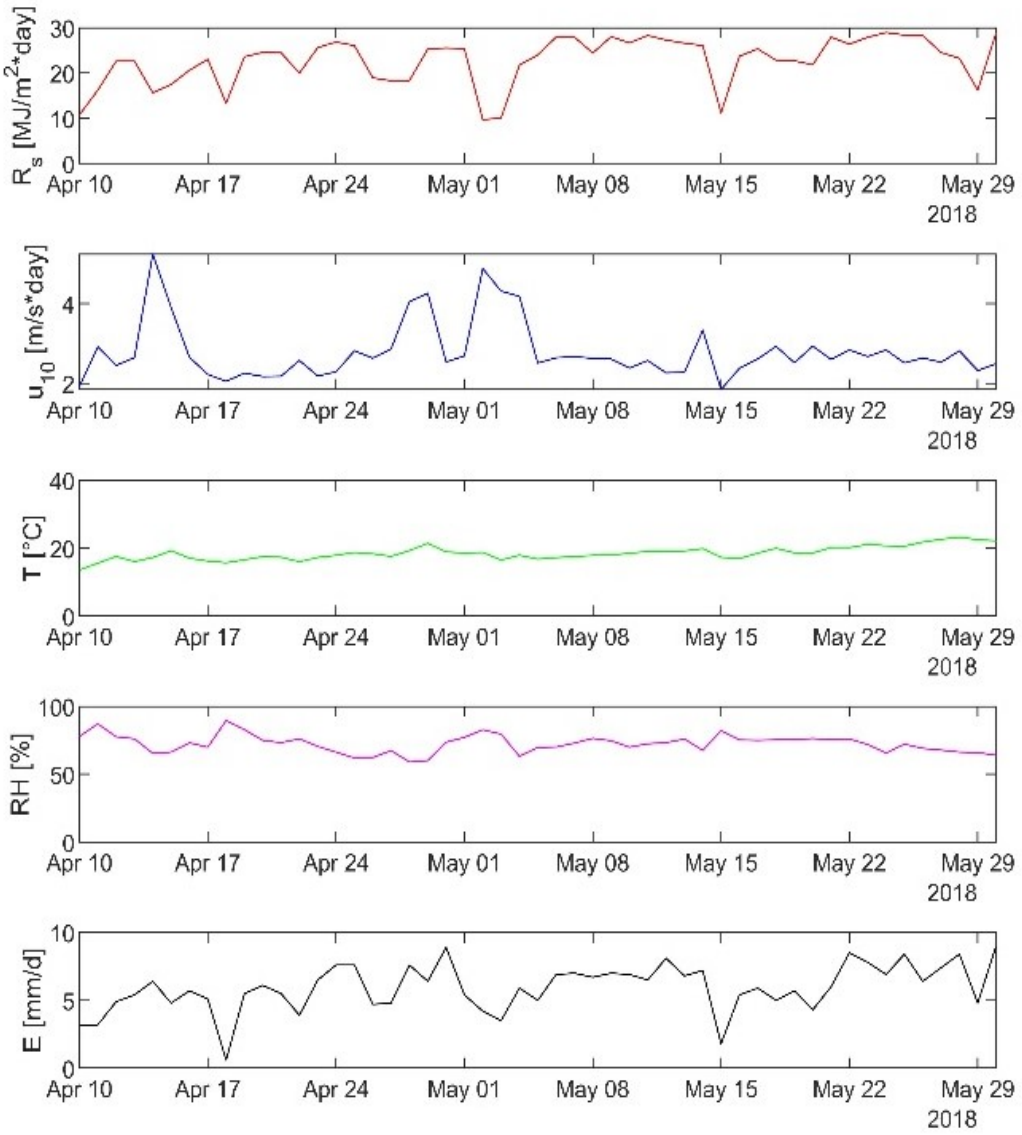

Figure 37 Monitored variables for 51 days at Passo Martino Lake (CT)

The water vapour absorb radiation in the longwave part of the spectrum. Such effect is taken into account because of the evaporation models use the solar irradiation measured close to the water basin, so considering the actual fraction of water vapour.

4.4.1.2 DoE and linear regression evaporation models

Using the weather data previously mentioned it is possible to calculate the daily evaporation rate for a water basin. Subsequently, it was possible to determine the unknown coefficients necessary for obtaining the $EVM_{free\ DoE}$ as well the $EVM_{free\ lin.reg.}$

Eq. 41 to Eq. 45, represent the models obtained through the DoE method and the linear regression theory.

Table 8 Proposed Evaporation Model for free water basins

Models	***Input variable and method***	***n. eq.***
$E = 0.2389 + 0.0133R_s + 0.0077T + 0.1589T_w - 0.0325RH + 0.2302u_{10}$	$R_s\ T\ T_w\ RH\ u_{10}$ (lin.reg. 5)	**Eq. 41**
$E_{l.r.\ 4} = 2.421 + 0.012R_s + 0.159T - 0.056RH + 0.122u_{10}$	$R_s\ T\ RH\ u_{10}$ (lin.reg. 4)	**Eq. 42**
$E = -0.307 - 0.0486R_s + 0.177T + 0.0119RH + 1.00781u_{10} + 0.00163R_sT + 0.00098R_sRH - 0.00601R_su_{10} - 0.00244T\ RH + 0.0153T\ u_{10} - 0.0115RH\ u_{10} + 0.0045R_s^2 + 0.00248T^2 - 0.0109u_{10}^2$	$R_s\ RH\ T\ u_{10}$ (DoE 4)	**Eq. 43**
$E = 1.802 + 0.047R_s - 0.133T - 0.146u_{10} + 0.028R_sT + 0.012R_su_{10} + 0.013T\ u_{10} + 0.003R_s^2 + +0.006T^2 + 0.001u_{10}^2$	$R_s\ T\ u_{10}$ (DoE 3)	**Eq. 44**
$E = 1.505 + 0.052R_s - 0.080T + 0.002R_sT + 0.003R_s^2 + 0.006T^2$	$R_s\ T$ (DoE 2)	**Eq. 45**

The polynomial models listed above, determine the evaporation rate using the actual weather data for a given site. Note that both the DoE equations and the linear regression equations were obtained starting from the results carried out by the Penman-Monteith model.

It is fundamental to underline as the proposed EVMs require as input to calculate the daily evaporation rate just usually known weather data.

4.4.1.3 Comparison of the proposed EVMs with the Penman-Monteith model

For both DoE and linear regression models, the statistical indices have been calculated and reported in

Table 9.

Furthermore, the evaporation trends during the period under examination were represented, and compared with the reference model, in Figure 38.

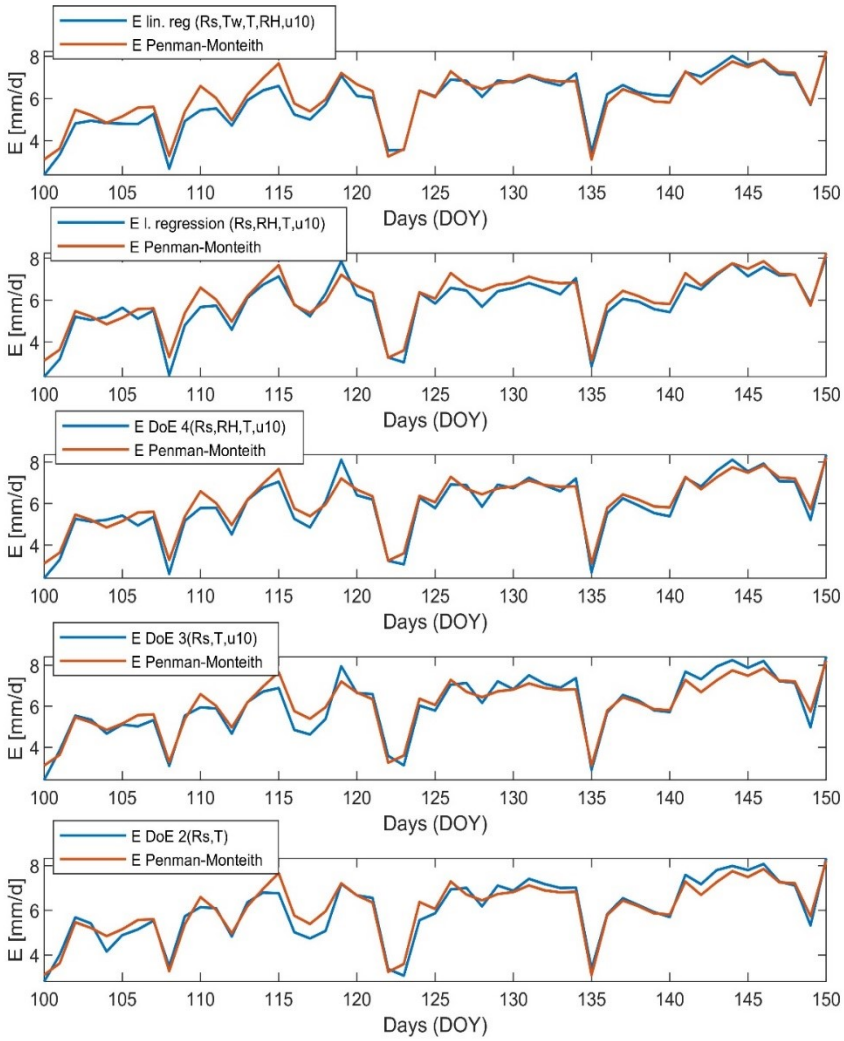

Figure 38 Comparison among reference model (Penman-Monteith) and proposed models

Table 9 Comparison among reference model (Penman-Monteith) and proposed models

	Linear Regression Eq. 41	***Linear Regression*** Eq. 42	***Design of Experiments 4*** Eq. 43	***Design of Experiments 3*** Eq. 44	***Design of Experiments*** Eq. 45
MBE (mm d^{-1})	-0.16	-0.25	-0.03	-0.04	-0.16
PE (%)	2.68	4.12	0.56	0.66	2.65
RMSE (mm d^{-1})	0.39	0.40	0.37	0.41	0.41
R^2	0.97	0.97	0.98	0.97	0.96

From the critical analysis of the statistical values calculated for the proposed models, the linear regression model with five variables and the DoE model with 4 variables are the ones the best performing.

From the *MBE* sign, we understand how the models understate evaporation.

4.4.1.4 Comparison between models and measures

In Figure 39 a graphic comparison is proposed among the models existing in the literature and the measurements taken by the aforementioned evaporimeter.

For each literature model, the statistical indices have been calculated and reported in Table 10.

Table 10 Statistical comparison between reference measures and literature models

	Eq. 5	Eq. 6	Eq. 7	Eq. 8	Eq. 9	Eq. 10
MBE (mm d^{-1})	0.12	-0.22	-0.17	-0.67	-0.10	0.21
PE (%)	2.18	3.94	3.03	11.44	1.92	3.37
RMSE (mm d^{-1})	0.94	1.13	1.01	1.56	1.06	1.22
R^2	0.85	0.79	0.83	0.64	0.81	0.74

The statistical comparison between the evaporation data measured with an evaporimeter and those calculated with the models shows a good correlation. This is shown by the values of R^2 obtained. In fact, as can be seen from Table 10, a correlation of 0.85 was obtained for the Penman model.

A necessary observation concerns the fact that from the value of the *MBE* obtained for the Rhower model, it can be deduced that the latter considerably underestimates the evaporation with respect to the measurements.

Another important consideration concerns the fact that the Penman-Monteith model, as many literature studies also confirm, is the most performing.

Figure 40 shows the comparison among the proposed EVM and the measurements taken by the aforementioned evaporimeter.

Table 11 shows the values statistical indices calculated for each proposed model.

Table 11 Statistical comparison between reference measures and proposed models

	Linear Regression Eq. 41	***Linear Regression*** Eq. 42	***Design of Experiments 4*** Eq. 43	***Design of Experiments 3*** Eq. 44	***Design of Experiments*** Eq. 45
MBE ($mm\ d^{-1}$)	-0.03	-0.12	-0.03	0.09	0.10
PE (%)	0.56	2.07	0.53	1.50	1.61
RMSE ($mm\ d^{-1}$)	0.98	0.92	0.89	0.97	1.02
R^2	0.82	0.85	0.86	0.83	0.81

From a critical analysis of the calculated statistical indices, it can be deduced that the four-variable DoE model is the best. From the sign of the *MBE* we can say that the Eq. 41 and Eq. 42 of linear regression and the Eq. 43 DoE, understate the evaporation to the measured values. DoE models with 2 and 3 variables then Eq. 44 and Eq. 45 overstate the evaporation to the measured values. The correlation coefficients obtained show that the proposed models have excellent performances. In fact, the best model has a correlation coefficient of 0.86.

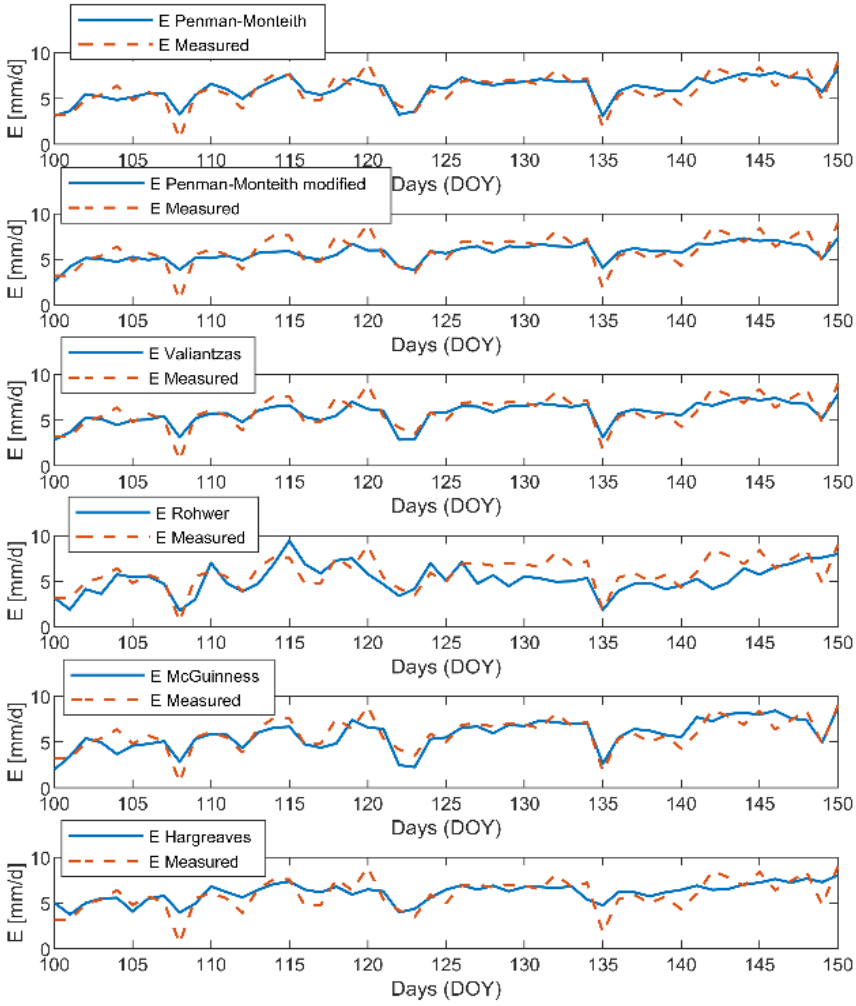

Figure 39 Graphical comparison between literature models and measurements

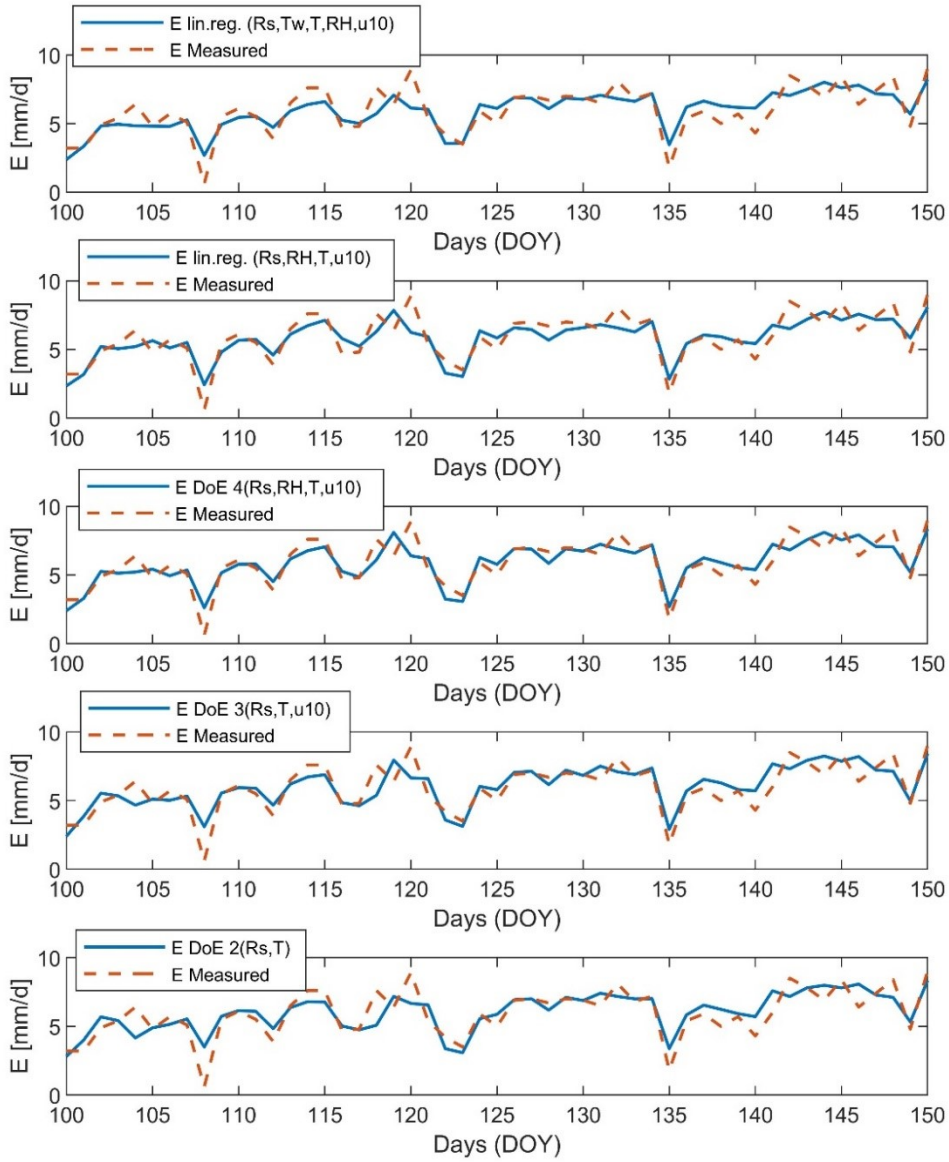

Figure 40 Graphical comparison between proposed models and measurements

4.4.1.5 Comparison of cumulated evaporation

This section compares the cumulative evaporation calculated for all the models with that one coming from the observations.

The graphic comparison of the E_{cum} in the time interval considered is reported in Figure 41. In particular, the one calculated with the models (of literature and proposed) is compared with that of the observations.

A numerical comparison of the cumulated evaporation calculated by the models and measured in the observations was also carried out. The calculated values are shown in Table 12.

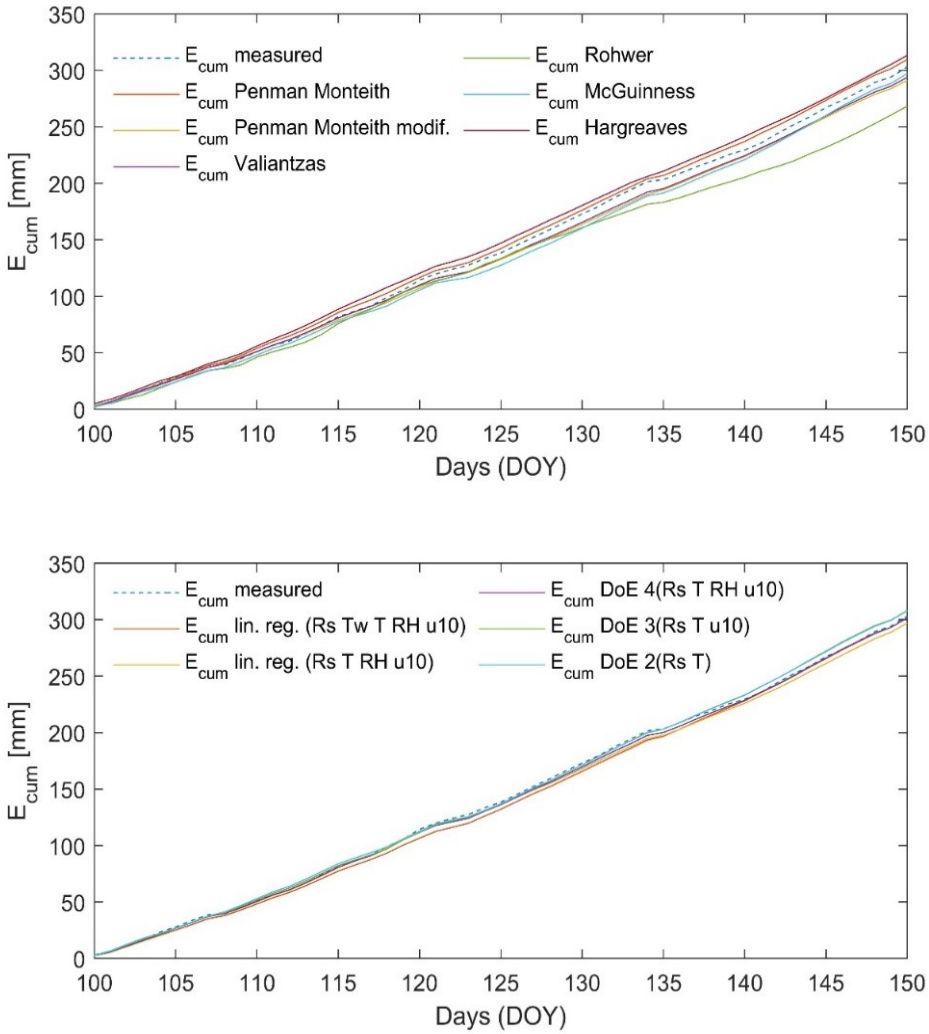

Figure 41 Cumulated Evaporation

Comparing the evaporation models and that measured by the evaporimeter was obtained by ΔE_{cum}, in which the observed evaporation was taken as a reference. In addition, the percentage difference was also calculated ($\Delta E_{cum}\,\%$).

The cumulative evaporation analysis shows that using even the worst of models, we obtain acceptable data, so if a long-term analysis is performed, we can serenely use all the models examined, while if the analysis to be performed it is short term or even for

a single day, to obtain valid results, it is advisable to use more complex models like that of Penman-Monteith.

Table 12 Numerical comparison of cumulated evaporation

Measures/models	E_{cum} *(mm)*	ΔE_{cum} *(mm)*	ΔE_{cum} *(%)*
Measures	303.21	0.00	0.00
Penman Monteith	309.82	-6.62	-2.18
Penman Monteith-modif.	291.24	11.96	3.94
Valiantzas	293.99	9.21	3.04
Rohwer	268.49	34.71	11.45
Mc Guinness Bordne	297.35	5.85	1.93
Hargreaves	313.39	-10.19	-3.36
Linear Regression 5	301.49	1.71	0.56
Linear Regression 4	297.05	6.15	2.03
Design of Experiment 4	301.59	1.61	0.53
Design of Experiment 3	307.76	-4.56	-1.50
Design of Experiment 2	308.09	-4.89	-1.61

From the ΔE_{cum} % results, the DoE 4 model is the most performing in terms of cumulative evaporation. This confirms once again the robustness of the proposed models.

4.4.2 Evaporation proposed models for partially covered surfaces

As previously mentioned, the proposed evaporation models developed for partially covered surfaces by FPV are tested on the water basin of the “Biviere di Lentini”.

4.4.2.1 Data and measurements

The results were obtained from measurements of the quantities (relative humidity, solar radiation, wind velocity, ambient temperatures) in input to the model, obtained from the PVGIS.

Figure 42 and Figure 43 show the one-year weather data in Lentini.

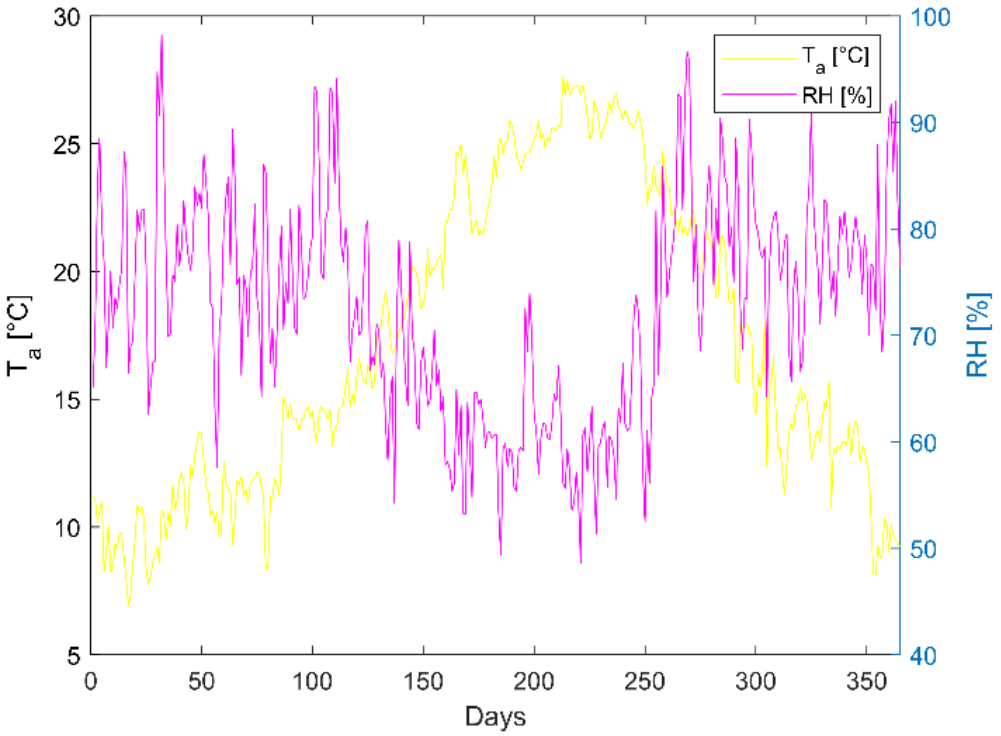

Figure 42 RH and ambient temperature in Lentini (CT)

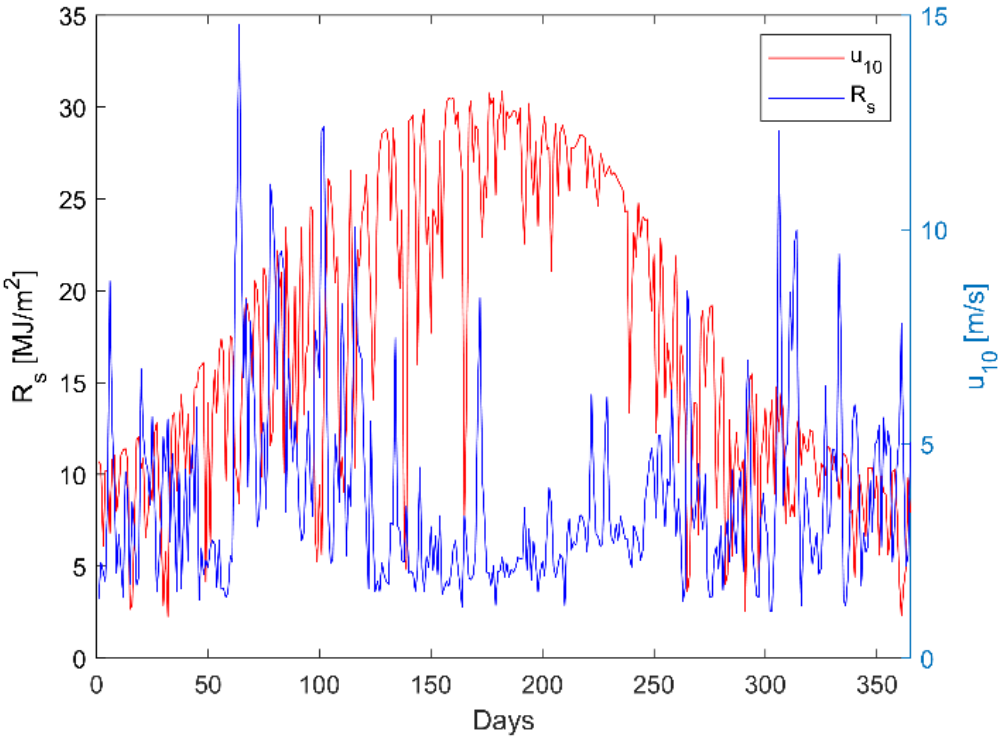

Figure 43 Solar radiation and wind speed in Lentini (CT).

4.4.2.2 Suspended systems

For this type of installation, the evaporation was calculated by the proposed EVM model as a function of the percentage of covered water surface (CWS). These models take into account the reduction of the solar energy incident on the water surface. In Figure 44 the daily evaporation rate, as well as the cumulative evaporation curves, are depicted:

- for the case of the free water basin, calculated with the Penman method ($E_{free\ Penman}$; $E_{free\ cum\ Penman}$) and with the linear regression method ($E_{free\ lin.reg.}$; $E_{free\ cum\ lin.reg.}$);
- for the 50% of the water basin covered by FPVs, ($E_{FPVS,Penman\ (50\%)}$; $E_{FPVS,cum\ Penman\ (50\%)}$) and ($E_{FPVS,lin.reg.\ (50\%)}$; $E_{FPVS,cum\ lin.reg.\ (50\%)}$).

It can be observed that between the two cases there is a difference in the cumulated evaporation of about 500 mm, this result is confirmed by both two models adopted. As regards the daily evaporation once again relevant differences emerge among the values calculated with the two models. However, since these differences are both positive and negative the cumulate evaporation is very similar along all the periods of the year. Table 13 shows the main parameters which characterize the evaporation of the investigated basin as function of the percentage of water surface covered by suspended FPV calculated by the Penman and the linear regression method.

Table 13 Yearly Water evaporation for suspended FPV

Percentage of covering [%]	0 (free surface)	10	30	50	70	100
$E_{FPVS\ cum\ Penman}$ *[mm y^{-1}]*	1742	1638	1429	1221	1013	701
$E_{FPVS\ cum\ lin.reg.}$ *[mm y^{-1}]*	1743	1644	1446	1248	1051	754
$\varepsilon_{FPV\ cum}$ *[%]*	-	-0.39	-1.17	-2.22	-3.69	-7.55
$\Delta E_{FPVS\ cum\ Penman}$ *[mm y^{-1}]*	-	104	312	520	728	1041
$\Delta E_{FPVS\ cum\ lin\ reg.}$ *[mm y^{-1}]*	-	99	297	494	692	989
η *[%]*	-	6	18	30	42	60

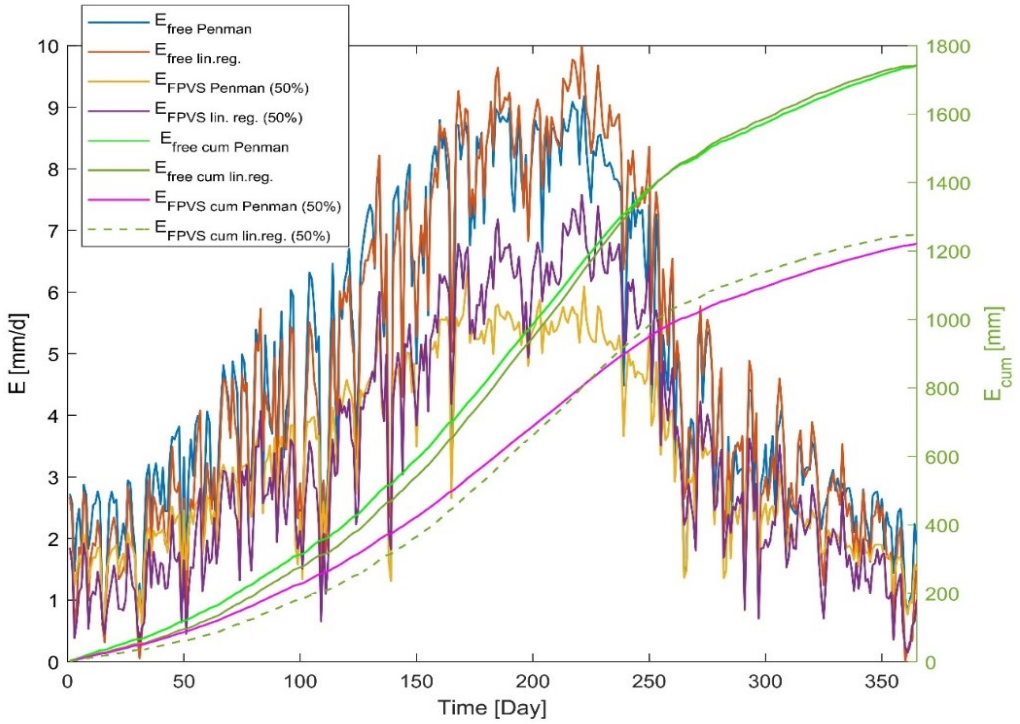

Figure 44 Daily and cumulated evaporation for free and 50% of CWS by suspended FPVs.

Negative values of the parameters ε_{FPVcum} indicate that the $E_{FPVS\ cum\ lin.reg.}$ is higher than $E_{FPVS\ cum\ Penman}$. Thus, a FPV that covers just 30% of the investigated water basin attains a decrease of the evaporation rate of about 18%.

4.4.2.3 Floats that cover the entire surface below the module (Figure 34a)

As previously described FPV installed in floating manner (see Figure 34a) causes different interactions on the water basin.

Daily and cumulative evaporation are calculated with the Penman-Monteith and linear regression models using the equation defined in the previous paragraphs.

In Figure 45 the daily evaporation rate, as well as the cumulative evaporation curves, are depicted:

- for the case of the free water basin, calculated once again with the Penman method ($E_{free\ Penman}$; $E_{free\ cum\ Penman}$) and with the linear regression method ($E_{free\ lin.regr}$; $E_{free\ cum\ lin.regr.}$);
- for the 50% of the water basin covered by FPVFa, ($E_{FPVF,a,Penman\ (50\%)}$; $E_{FPVF,a,cum\ Penman(50\%)}$) and ($E_{FPVF,a\ lin.reg.(50\%)}$; $E_{FPVF,a\ cum\ lin.reg.(50\%)}$).

It can be observed that between the two cases there is a difference in the cumulated evaporation of about 1300 mm, this result is confirmed by both two models adopted.

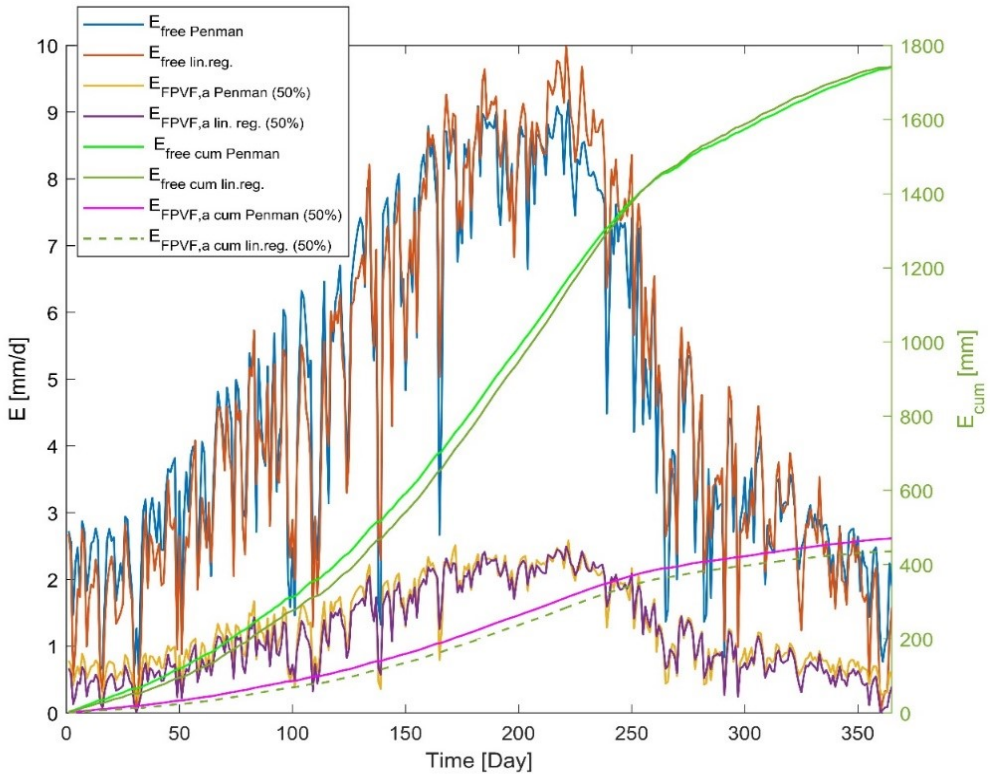

Figure 45 Daily and cumulated evaporation for free and 50% of CWS by floating FPVF $_a$.

As regards the daily evaporation very modest differences emerge among the values calculated with the two models. Table 14 shows the main parameters which characterize the evaporation of the investigated basin as a function of the percentage of WSC by floating FPVFa calculated by the Penman and the linear regression method.

Table 14 Yearly Water evaporation for FPVF $_a$

Percentage of covering [%]	0 (free surface)	10	30	50	70	100
$E_{FPVF,a\ cum\ Penman}$ *[mm y^{-1}]*	1742	1423	883	471	186	0
$E_{FPVF,a\ cum\ lin.reg.}$ *[mm y^{-1}]*	1743	1412	854	436	171	0
$\varepsilon_{FPV\ cum}$ *[%]*	-	0.82	3.30	7.45	8.29	-
$\Delta E_{FPVF,a\ cum\ Penman}$ *[mm y^{-1}]*	-	318	859	1271	1555	1742
$\Delta E_{FPVF,a\ cum\ lin\ reg.}$ *[mm y^{-1}]*	-	331	889	1307	1572	1743
η *[%]*	-	18	49	73	89	100

Thus, a FPV that covers just 30% of the investigated water basin allows reducing its evaporation of about 50%. It is evident as this kind of installation provides a higher reduction of the evaporation in comparison with the installation of FPV with suspended PV modules.

4.4.2.4 Flexible floats (Figure 34d), in direct contact with the water

Daily and cumulative evaporation are calculated with the Penman-Monteith and linear regression models using the equation defined in the previous paragraphs.

In Figure 46 the daily evaporation rate, as well as the cumulative evaporation curves, are depicted:

- for the case of the free water basin, calculated once again with the Penman method ($E_{freePenman}$; $E_{free\ cum\ Penman}$) and with the linear regression method ($E_{free\ lin.regr}$; $E_{free\ cum\ lin.regr.}$);
- for the 50% of the water basin covered by FPV_F, ($E_{FPVF,d\ Penman(50\%)}$; $E_{FPVF,d\ cum\ Penman(50\%)}$) and ($E_{FPVF,d\ lin.reg.(50\%)}$; $E_{FPVF,d\ cum\ lin.reg.(50\%)}$).

It can be observed that between the two cases there is a difference in the cumulated evaporation of about 1100 mm, this result is confirmed by both two models adopted.

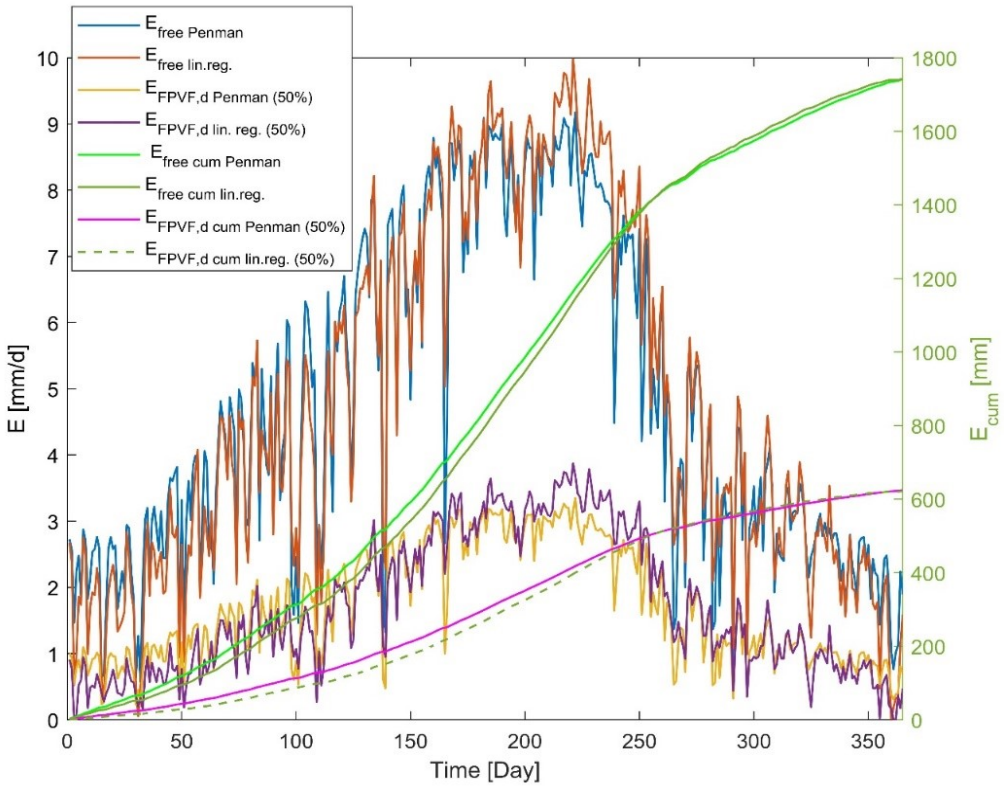

Figure 46 Daily and cumulated evaporation for free and 50% of CWS by floating $FPVF_d$.

As regards the daily evaporation once again some differences emerge among the values calculated with the two models. However, since these differences are both positive and negative the cumulate evaporation is very similar along all the periods of the year. Table 15 shows the main parameters which characterize the evaporation of the investigated basin as function of the percentage of water surface covered by floating FPV type 1d, calculated by the Penman and the linear regression method.

Thus, a FPV that covers just 30% of the investigated water basin allows reducing its evaporation of about 42%. It is evident as this kind of installation provides a higher reduction of the evaporation in comparison with the installation of FPV with suspended PV modules and a little bit lower than the $FPVF_a$ installation.

Table 15 Yearly Water evaporation for floating FPVF $_d$

Percentage of covering [%]	0 (free surface)	10	30	50	70	100
$E_{FPVF,d\ cum\ Penman}$ $[mm\ y^{-1}]$	1742	1479	1012	624	315	0
$E_{FPVF,d\ cum\ lin.reg.}$ $[mm\ y^{-1}]$	1743	1478	1010	621	313	0
$\varepsilon_{FPV\ cum}$ $[\%]$	-	0.01	0.18	0.40	0.57	-
$\Delta E_{FPVF,d\ cum\ Penman}$ $[mm\ y^{-1}]$	-	263	730	1118	1427	1742
$\Delta E_{FPVF,d\ cum\ lin\ reg.}$ $[mm\ y^{-1}]$	-	264	733	1121	1430	1743
η $[\%]$	-	15	42	64	82	100

4.5 Conclusions

One of the main advantages of using the proposed numerical models is their very simple implementation and that they need just a few usually known environmental variables; i.e. solar radiation, humidity, air temperature, water temperature, wind velocity. Therefore, in function of the most diffuse typologies of FPV three further numerical models EVM_{FVP} are developed, which allow estimating the evaporation rate in water basin partially covered by FPV. These models start by the energy balance on the water surface considering the effects due to the different typology of FPV installation, suspended or floating.

The results of the developed analysis show the quantity of evaporated water depends not only on the percentage of WSC but also on the characteristics of floating systems.

Indeed, installing the FPV on the 30% of the basin area, suspended systems achieve a reduction of the evaporation rate of about 18%, systems that cover entirely the surface below the modules achieve a reduction of 49%, and flexible modules in direct contact with water achieve a reduction of 42%. Obviously increasing the water surface occupied by FPV the reduction of the evaporation rate increase (e.g. covering 50 % of the surface the decrease of the evaporation rate are, 30-73-64% respectively).

It has been shown that floating systems compared to suspended systems have a higher yield in terms of evaporation reduction. The floating systems that cover the entire surface below the modules are the most efficient, followed by the flexible floats

systems which have a lower efficiency since a part of the heat produced by the photovoltaic modules is exchanged with water.

Through this study it is possible to estimate the reduction of evaporation in the presence of FPV systems on water basins and therefore consequently:

- the increase in energy collected by FPV modules due to evaporative cooling
- the revenues in economic terms of non-evaporated water that can be used for other purposes such as: Energy production from HPP plants and rrigation and civil use.

Chapter 6 will deal with the study on the effect of evaporation in the energy collected and in Chapter 9 an economic analysis will be developed that takes into account the revenues deriving from the lack of evaporation.

5 Thermal models for evaluating the performances of monofacial and bifacial PV modules

5.1 Introduction

This chapter has the objective to describe mono-dimensional multilayer mathematical model apt to estimate the temperature of photovoltaic (PV) cells for both monofacial and bifacial PV modules. A dynamic three-layer model (3L-NM) will be developed, in which the contribution of solar radiation that hits the back of the PV module is included. The model is constituted by energy balance equations, one for each layer of the PV module. The input data of the proposed model are the environmental weather conditions as well as the withdrawal electrical power. The outputs are the average temperature of each layer, so it is possible to determine the PV cell temperatures that typically cannot be directly measured.

This study allows to establish the basis for the realization of models for the estimation of energy performances in the case of photovoltaic modules installed in water environment (FPV).

5.2 Methodology

The schemes of a monofacial and bifacial module, as well as the heat fluxes incoming and outgoing, are depicted in Figure 47.

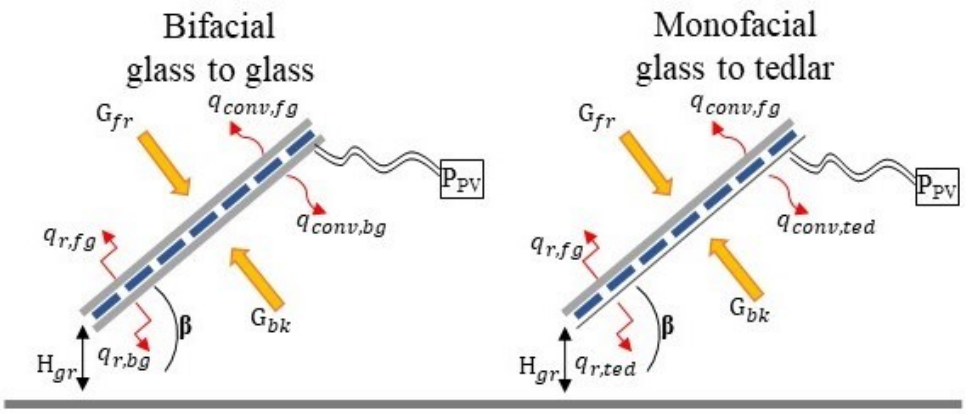

Figure 47 Schematic representation of the mono and bifacial modules

The terms q_{conv} and q_r are referred to the heat fluxes on both sides of the PV module, described by the subscripts "$_{fg}$", "$_{bg}$"/"$_{ted}$", due to the convection and radiation phenomena respectively. G_{fr} and G_{bk} represent the solar irradiance that hit the module on the front and the backside respectively. It is important to highlight that the term G_{bk} is a function of the view factor of the back surface to the skydome, which in turn a function of the height from the ground H_{gr} and the angle of tilt of the module. The "Bifaciality Factor" (BF) is used for characterizing the performances of the "Bifacial modules.

5.2.1 Mathematical Model of PV cell temperatures

In this study, the model proposed by King [98], which is a single point model and the model developed by TamizhMani [99], which is a linear regression model, were assumed as reference for comparing the results carried out through the proposed model.

TamizhMani's model was chosen because it is based on a methodology analogous with that one used for a novel linear regression model presented in this chapter.

5.2.2 Model description

The numerical multi-layer model 3L-NM presented in this chapter is characterized by the introduction of supplementary terms in the set of equations of the thermal energy balance, respect to multi-layer models developed by the literature.

Figure 48 shows the three layers discretization scheme of the PV modules, monofacial (a) and bifacial (b) implemented in the model.

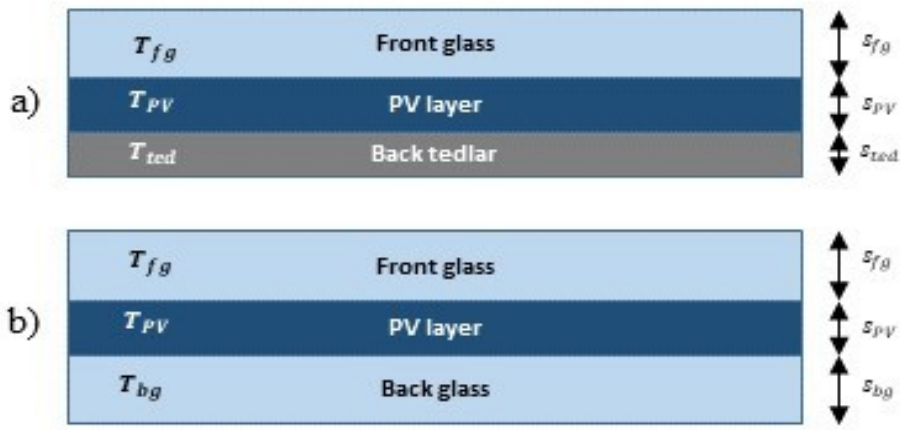

Figure 48 PV module layers: a) monofacial; b) bifacial.

The energy balance equation of each layer is defined taking into account the thermal fluxes due to radiation, convection, and conduction, as well as the energy converted by the PV cell. In particular, the radiative heat fluxes between front glass (fg) and back tedlar (ted) for a monofacial module, or the back glass (bg) for bifacial module surfaces with the sky (T_{sky}) and the ground (T_{ground}) are embedded. Convective heat fluxes are calculated by the Newton equation and the temperature of the surrounding environment (T_a). Specifically, the convective coefficients were calculated taking into account the possible different fluid dynamic conditions (e.g. natural, forced or mixed convection). Thus, the convective coefficients are defined in function on either the characteristic length of the PV module, temperature gradient and wind speed.

Figure 49 shows the thermal equivalent electrical circuit for a three-layer ground-mounted PV module, where the thermal fluxes and the unknown temperatures in a PV module are highlighted. The complexity of the thermal equivalent electrical circuit is a function of the number of considered layers. It is worth noticing that the voltage source T_{sky} is a controlled voltage source as it depends on the ambient temperature T_a, whereas the conductance related to the radiative heat exchange is indicated as a nonlinear element. A common simplifying hypothesis allows us to turn them into linear elements. The bifaciality of the PV cells is included in the numerical model taking into account the front and back solar radiation conversion in electricity. In the

follows section these terms are made explicit in the differential energy balance equations.

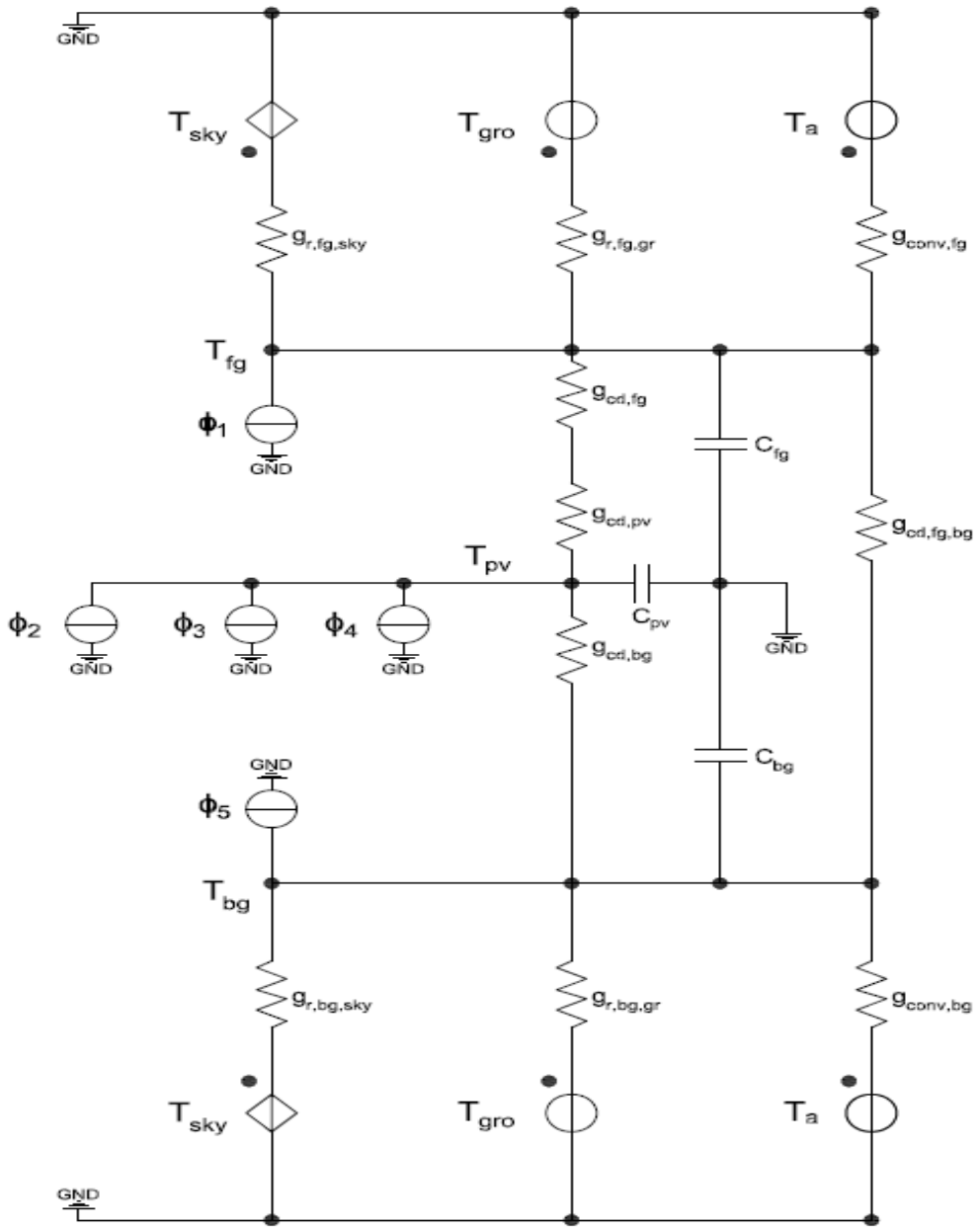

Figure 49 Equivalent thermal circuit for multilayer proposed model

5.2.3 Energy balance equations

The common hypothesis of the models are:

- The heat loss from the border of the photovoltaic module are neglected (one-dimensional model);

- All of the properties of the thermal material are considered homogeneous and independent by temperature;
- The part of solar radiation that is not converted into electrical energy is absorbed by the PV cells as thermal energy;
- The ambient temperature is postulated as equal on both sides of the module.

Each layer of the PV module is schematized as a homogenous slab, thus in the layers that contain both PV cell and glass fiber or tedlar (see Figure 48), the thermal properties of such layers are defined taking into account the percentage area of PV cell and fiberglass. Field measurements have proved that it is a sufficient representation of the actual thermal behaviour of a semi-transparent PV panel [100].

The proposed numerical model is one-dimensional, i.e. made of a serial assembling of one-dimensional layers. The energy balance equations are defined in the middle of each layer. Consequently, three independent Eq. 46 Eq. 54 Eq. 61 are derived, which allow calculating the three unknowns temperatures, i.e: T_{fg}= central point of the front glass; T_{pv} = PV cell layer; $T_{bg/ted}$ = surface of the back glass/tedlar (mono facial/bifacial module) [18];

- FRONT GLASS

The energy balance equation for the front layer is:

$$C_{fg}\frac{dT_{fg}}{dt} = (\dot{q}_{r,fg-sky} + \dot{q}_{r,fg-gr} + \dot{q}_{conv,fg} + \dot{q}_{cd,fg-pv} + \dot{q}_{cd,fg-bg/ted} + \Phi_1) \quad \textbf{Eq. 46}$$

The expressions for each term of the upper surface are shown below.

$$C_{fg} = \rho_{fg} A_{fg} s_{fg} c_{fg} \quad \textbf{Eq. 47}$$

$$\dot{q}_{r,fg-sky} = A_{fg} h_{r,fg-sky}(T_{sky} - T_{fg}) \quad \textbf{Eq. 48}$$

$$\dot{q}_{r,fg-gr} = A_{fg} h_{r,fg-gr}(T_{gr} - T_{fg}) \quad \textbf{Eq. 49}$$

$$\dot{q}_{conv,fg} = A_{fg} h_{conv,fg}(T_{fg} - T_a) \quad \textbf{Eq. 50}$$

$$\dot{q}_{cd,fg-pv} = A_{pv}\frac{1}{r_{cd,fg}+r_{cd,pv}}(T_{fg} - T_{pv}) \quad \textbf{Eq. 51}$$

$$\dot{q}_{cd,fg-bg/ted} = (A_{fg} - A_{pv})\frac{1}{r_{cd,bg/ted}+r_{cd,fg}}(T_{fg} - T_{bg/ted}) \quad \textbf{Eq. 52}$$

$$\Phi_1 = \alpha_{fg} G_{fr} A_{fg} \quad \textbf{Eq. 53}$$

- PV LAYER

The energy balance equation for the PV layer is:

$$C_{pv}\frac{dT_{pv}}{dt} = (\dot{q}_{cd,pv-fg} + \dot{q}_{cd,pv-bg/ted} + \Phi_2 + \Phi_3 + \Phi_4{}^*) \quad \textbf{Eq. 54}$$

* only for the bifacial module.

The expressions for each term of the central surface are shown below.

$$C_{pv} = \rho_{pv}A_{pv}s_{pv}c_{pv} \quad \textbf{Eq. 55}$$

$$\dot{q}_{cd,fg-pv} = A_{pv}\frac{1}{r_{cd,fg} + r_{cd,pv}}(T_{fg} - T_{pv}) \quad \textbf{Eq. 56}$$

$$\dot{q}_{cd,bg/ted-pv} = A_{pv}\frac{1}{r_{cd,bg/ted} + r_{cd,pv}}(T_{pv} - T_{bg/ted}) \quad \textbf{Eq. 57}$$

$$\Phi_2 = \left(\tau_{fg}\alpha_{pv} - \eta_{b/m-fr}\right)G_{fr}A_{pv} \quad \textbf{Eq. 58}$$

$$\Phi_3 = \alpha_{eva}\tau_{fg}G_{fr}A_{pv} \quad \textbf{Eq. 59}$$

$$\Phi_4 = \left(\tau_{bg}\alpha_{pv} - \eta_{b-bk}\right)G_{bk}A_{pv} \quad \textbf{Eq. 60}$$

- BACK GLASS OR TEDLAR (BIFACIAL/MONOFACIAL)

The energy balance equation for the back layer is

$$\boldsymbol{C_{bg/ted}\frac{dT_{bg/ted}}{dt} = (\dot{q}_{cd,bg/ted-pv} + \dot{q}_{r,bg/ted-gr} + \dot{q}_{r,bg/ted-sky} + \dot{q}_{conv,bg/ted} + \dot{q}_{cd,bg/ted-fg} + \Phi_5)} \quad \textbf{Eq. 61}$$

The expressions for each term for the back surface are shown below.

$$C_{bg} = \rho_{bg}A_{bg}s_{bg}c_{bg} \quad \textbf{Eq. 62}$$

$$C_{ted} = \rho_{ted}A_{ted}s_{ted}c_{ted} \quad \textbf{Eq. 63}$$

$$\dot{q}_{cd,bg/ted-pv} = A_{pv}\frac{1}{r_{cd,bg/ted} + r_{cd,pv}}(T_{pv} - T_{bg/ted)} \quad \textbf{Eq. 64}$$

$$\dot{q}_{r,bg/ted-gr} = A_{bg/ted}h_{r,bg/ted-gr}(T_{bg/ted} - T_{gr)} \quad \textbf{Eq. 65}$$

$$\dot{q}_{r,bg/ted-sky} = A_{bg/ted}h_{r,bg/ted-sky}(T_{bg/ted} - T_{sky)} \quad \textbf{Eq. 66}$$

$$\dot{q}_{conv,bg/ted} = A_{bg/ted}h_{conv,bg/ted}(T_{bg/ted} - T_{a)} \quad \textbf{Eq. 67}$$

$$\dot{q}_{cd,fg-bg/ted} = (A_{fg} - A_{pv})\frac{1}{r_{cd,bg/ted} + r_{cd,fg}}(T_{fg} - T_{bg/ted)} \quad \textbf{Eq. 68}$$

$$\Phi_5 = \alpha_{bg/ted}G_{bk}A_{bg/ted} \quad \textbf{Eq. 69}$$

If the solar irradiance (G_{bk}) data on the back of the module are not available, they could be determined following the procedure reported in [101] in which a model is

implemented that obtains radiation on the back from direct and diffuse radiation with an average error of 1.86%.

The conductive resistances of three above mentioned layers are:

$$r_{cd,fg} = \frac{s_{fg}}{2\lambda_{fg}} \quad r_{cd,bg} = \frac{s_{bg}}{2\lambda_{bg}} \quad r_{cd,ted} = \frac{s_{ted}}{2\lambda_{ted}} \quad r_{cd,pv} = \frac{s_{pv}}{2\lambda_{pv}} \qquad \textbf{Eq. 70}$$

The radiative coefficients are:

$$h_{r,fg-sky} = \sigma\varepsilon_{fg}F_{fg-sky}(T_{sky} + T_{fg})(T_{sky}^2 + T_{fg}^2) \qquad \textbf{Eq. 71}$$

$$h_{r,fg-gr} = \sigma\varepsilon_{fg}F_{fg-gr}(T_{gr} + T_{fg})(T_{gr}^2 + T_{fg}^2) \qquad \textbf{Eq. 72}$$

$$h_{r,bg/ted-sky} = \sigma\varepsilon_{bg/ted}F_{bg/ted-sky}(T_{sky} + T_{bg/ted})(T_{sky}^2 + T_{bg/ted}^2) \qquad \textbf{Eq. 73}$$

$$h_{r,bg/ted-gr} = \sigma\varepsilon_{bg/ted}F_{bg/ted-gr}(T_{gr} + T_{bg/ted})(T_{gr}^2 + T_{bg/ted}^2) \qquad \textbf{Eq. 74}$$

The sky temperature has been calculated through the Brunt's equation [102] and T_{gr} has been assumed equal to T_a.

Convective coefficients:

$$h_{conv} = \frac{\lambda Nu}{L_c} \qquad \textbf{Eq. 75}$$

The convective coefficients for both forced or free convection flows are calculated as a function of the Nusselt number (Nu), which in turn is calculated as a function of Reynolds (forced convection), or Grashof (free convection), and Prandtl number. The front glass coefficient of convection is calculated using the relations presented in [103] [104] for forced or free convection respectively. The convection is classified as forced if $Gr/Re^2 << 1$, while as free convection if $Gr/Re^2 >> 1$.

$$h_{conv,fg,forced} = 5.7w + 11.4 \qquad \textbf{Eq. 76}$$

$$h_{conv,fg,free} = \frac{\lambda_{air}Nu_{free,fg}}{L_c} \qquad \textbf{Eq. 77}$$

$$Nu_{free,fg} = 0.14\left[(GrPr)^{\frac{1}{3}} - (Gr_{cr} - Pr)^{\frac{1}{3}}\right] + 0.56(GrPr\cos\beta)^{\frac{1}{4}} \qquad \textbf{Eq. 78}$$

When the ratio of Gr/Re^2 does not verify anybody of the previous conditions the convection is classified as mixed. Then, the coefficient of convection is calculated as [105].

$$h_{mix} = (h_{forced}^3 + h_{free}^3)^{1/3} \qquad \textbf{Eq. 79}$$

The back glass/tedlar coefficient of convection is calculated using the relations reported in [106]:

$$h_{conv,bg/ted,free} = \frac{Nu_{free,bg/ted}\lambda_{air}}{L_c} \quad \textbf{Eq. 80}$$

$$h_{conv,bg/ted,forced} = 5.7w \quad \textbf{Eq. 81}$$

$$Nu_{free,bg/ted} = \left[0.825 + \frac{0.387Ra^{\frac{1}{6}}}{\left[1+\left(\frac{0.492}{Pr}\right)^{\frac{9}{16}}\right]^{\frac{8}{27}}}\right]^2 \quad \textbf{Eq. 82}$$

The characteristic length that appears in the previous equations has been calculated as follows:

$$L_c = \frac{4A_{fg}}{p} \quad \textbf{Eq. 83}$$

All the physical characteristics of the ambient air have been calculated considering the so-called film temperature (T_f)

$$T_f = \frac{T_a + T_{fg/bg/ted}}{2} \quad \textbf{Eq. 84}$$

5.3 Experimental results

The weather data (i.e. solar radiation, wind speed, and air temperature) used in input and for the validation of the numerical model data were derived from the observations of two weather stations. The characteristics of meteorological stations are reported in 'Chapter 3'. For monofacial module, the temperatures of the front, rear and central layers were monitored, as well as the solar irradiance on the front and back surfaces. For the bifacial module, the temperature on the rear surface and the solar radiation on the front and back surfaces were monitored. Meteorological data and module temperatures were acquired with a time step of 10 seconds. The black circles in Figure 50 indicate the positioning of the temperature sensors for mono and bifacial modules. The characteristics of the used sensors are shown in Chapter 3.

Figure 50 Graphic representation of temperature sensor positioning

Figure 51 and Figure 52 show the measured meteorological data used for modeling the thermal behavior of the monofacial and bifacial module respectively.

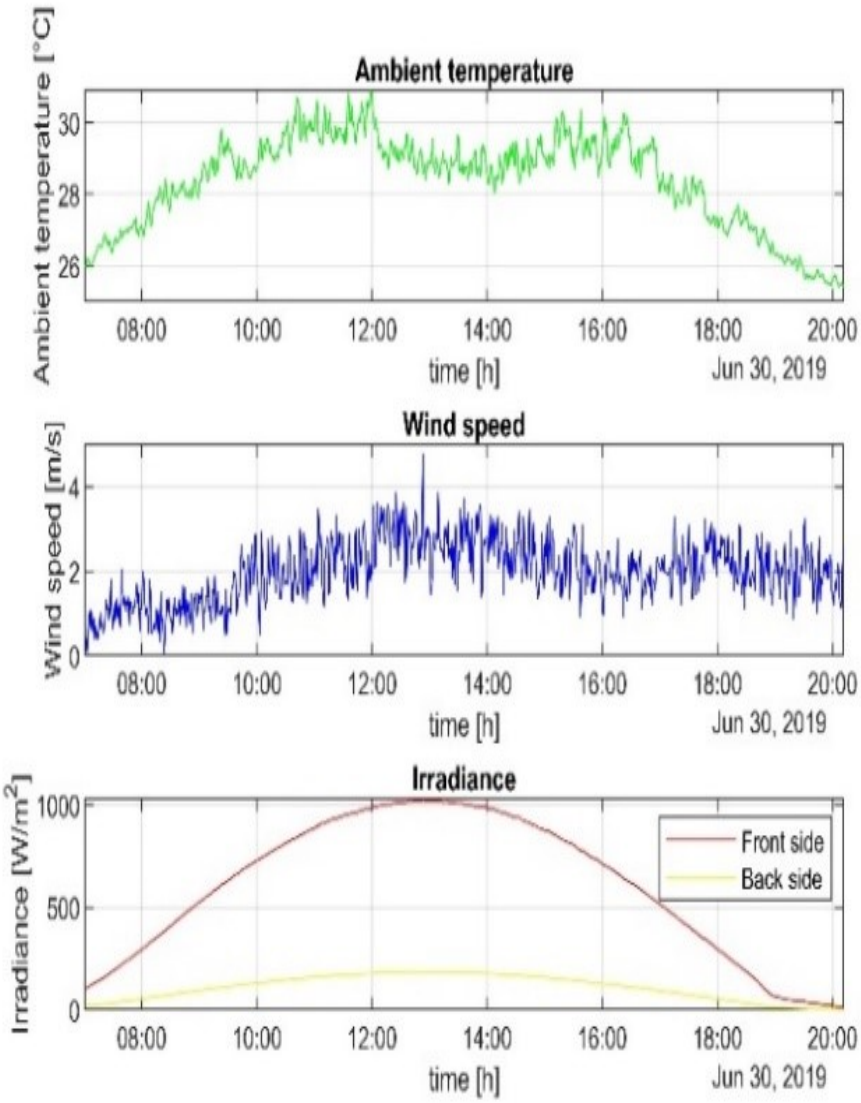

Figure 51 Experimental data used for monofacial module

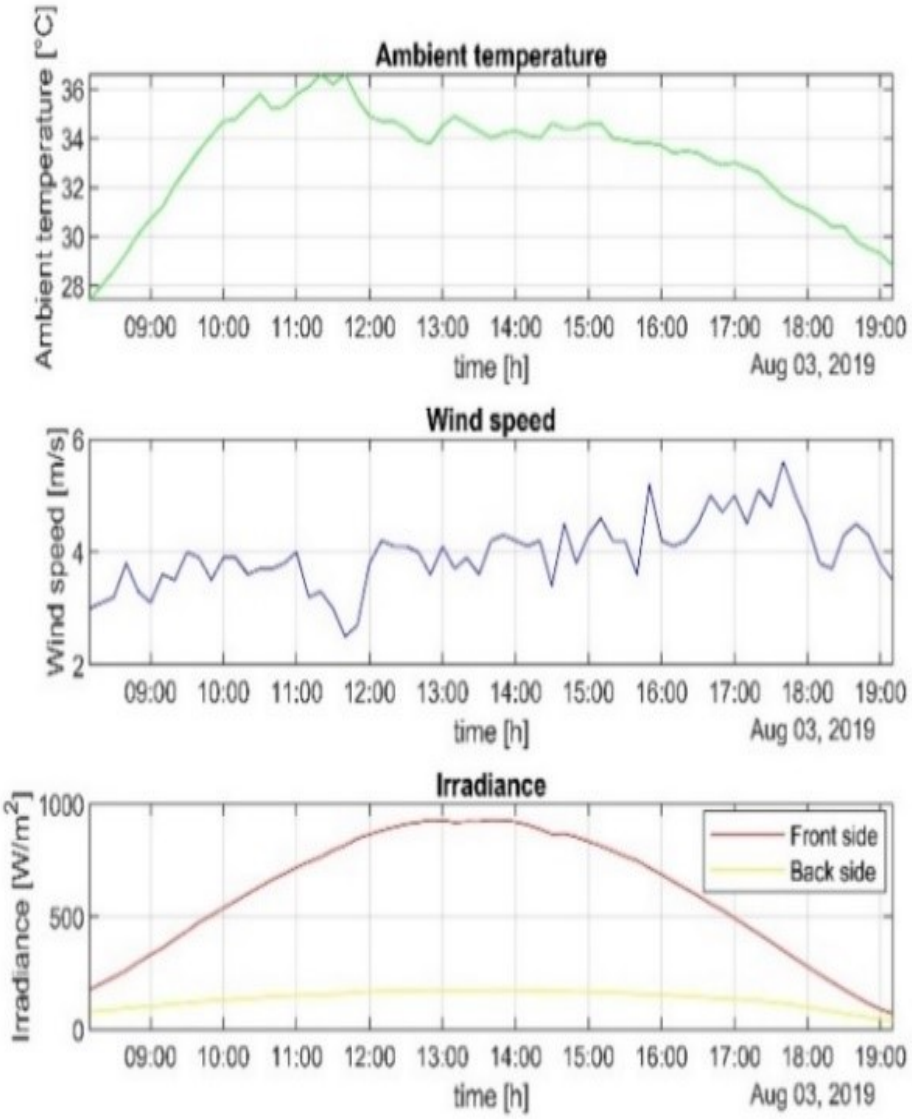

Figure 52 Experimental data used for bifacial module

The characteristics of the modeled monofocial and bifacial modules are shown in Chapter 3.

5.3.1 Comparison of measured and calculated data for monofacial module

To validate the model, the calculated and the measured temperatures of each layer were compared. Figure 53 Figure 54 Figure 55 demonstrates the measured and calculated temperatures of each layer (i.e. front glass, PV cell and tedlar) as well as the difference between these temperatures, for the monofacial module.

Table 16 reports the values of the statistical indexes, which allows evaluating the effectiveness of the proposed model.

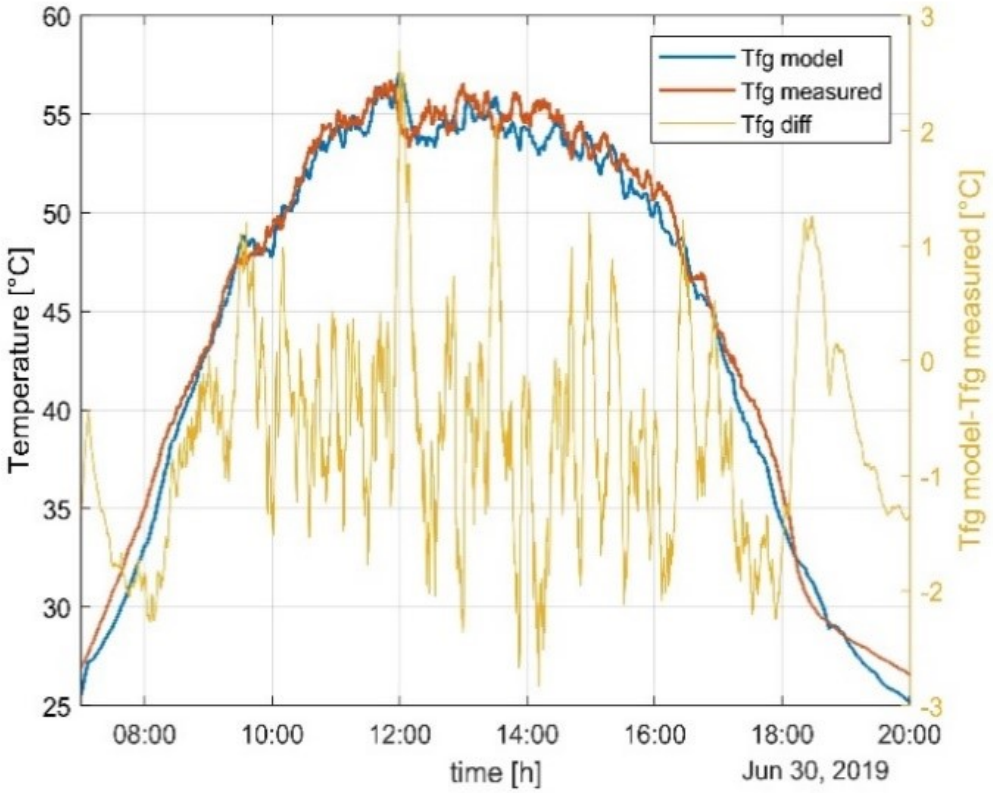

Figure 53 Front glass temperature modeled vs measured (m-module)

Table 16 Statistical evaluation for monofacial module

	Front glass	**PV cell**	**Back Tedlar**
MBE (°C)	0.668	0.421	-0.340
RMSE (°C)	1.130	1.153	1.048
PE (%)	1.498	0.881	0.718
R^2	0.992	0.993	0.992

It is possible to observe that the modeled temperature of the cell gives rise to a better correlation with the measurements. Otherwise, the temperature of the front surface gives rise to the worst reliability as emerges by the values of MBE, RMSE, PE. Globally, it is possible to highlight a very good fit between the measured and calculated data.

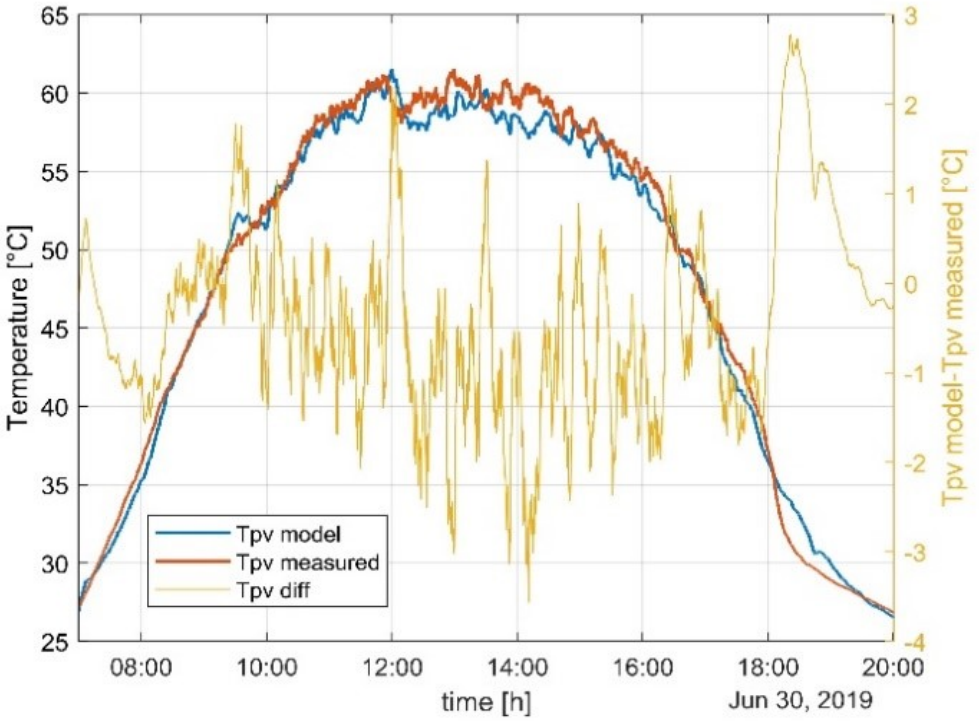

Figure 54 PV cells temperature modeled vs measured (m-module)

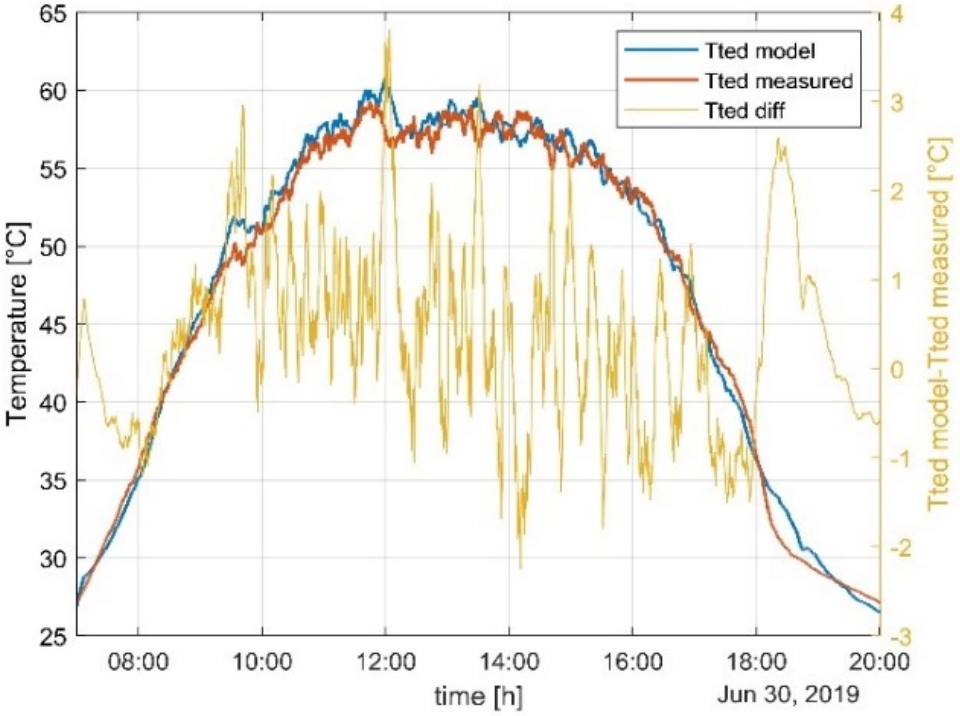

Figure 55 Back tedlar temperature modeled vs measured (m-module)

5.3.2 Comparison of measured and calculated data for bifacial module

Figure 56 shows the predicted temperatures of each layer of the bifacial module (i.e. front glass, PV cells, rear glass).

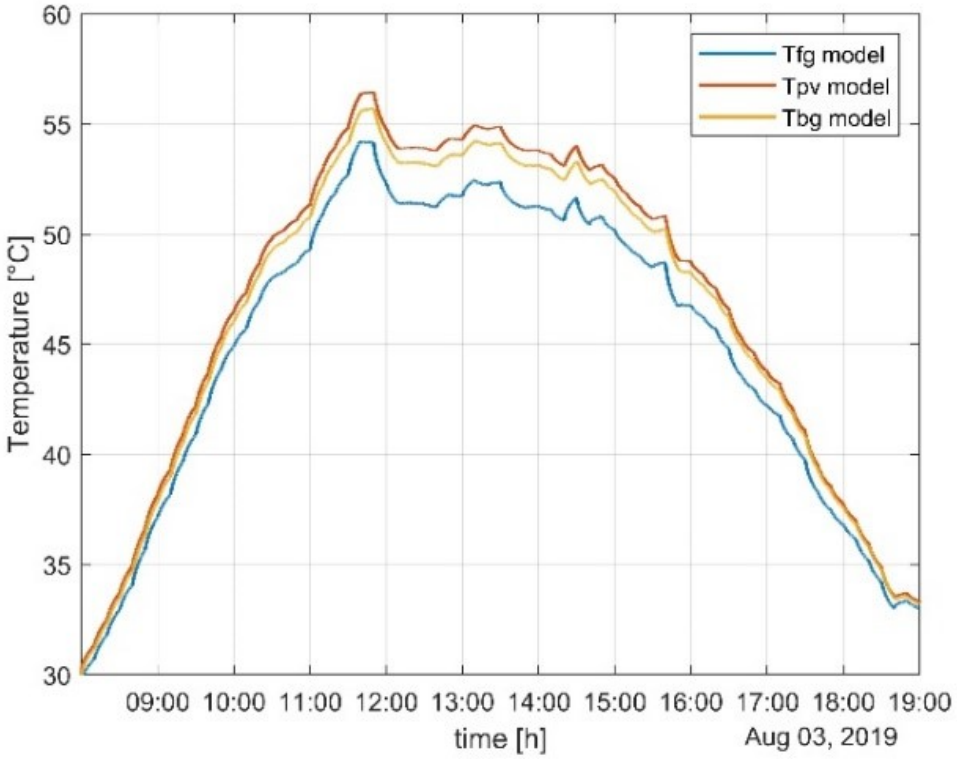

Figure 56 Modeled temperatures of the layers (b-module)

It can be noted that the temperature of the back glass module is very close to the cell temperature, while T_{fg} is at least 2°C less than T_{PV}. Figure 57 shows the measured and predicted temperatures of the rear glass as well as the difference between these temperatures, for bifacial module.

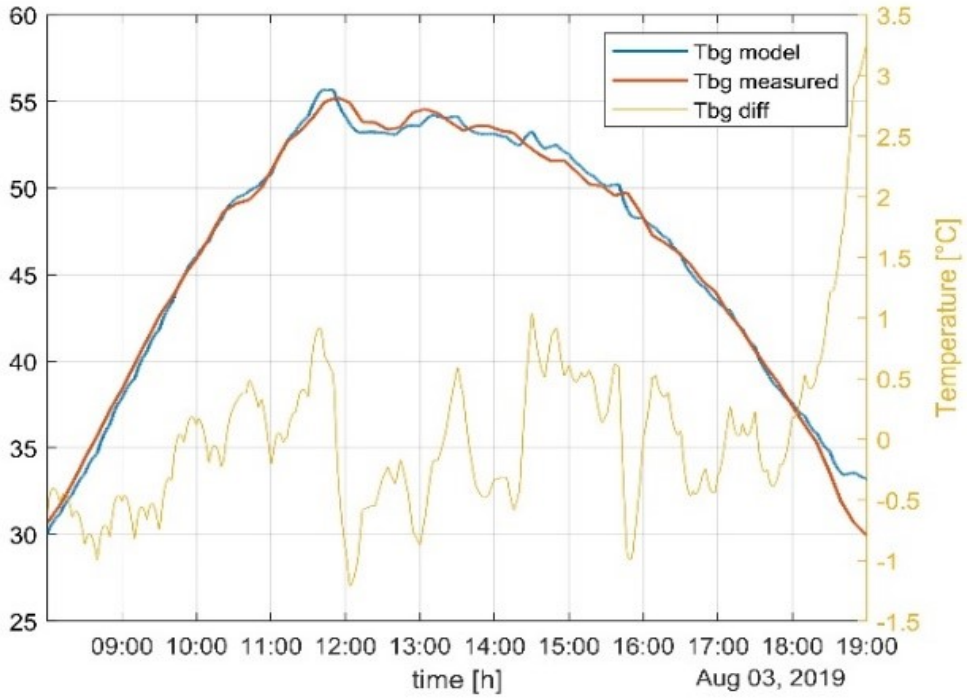

Figure 57 Back-glass temperature modeled vs measured (b-module)

Table 17 shows the statistical indices, which are useful for evaluating the reliability of the numerical model.

Table 17 Statistical evaluation for bifacial module

Layer	MBE (°C)	RMSE (°C)	PE (%)	R^2
Backglass	-0.071	0.773	0.161	0.990

It is possible to observe a very performing results in terms of MBE, RMSE, PE. Considering that the simulations have shown that T_{bg} and T_{PV} have very similar values, it is possible to predict with very good accuracy the cell temperature for a bifacial module.

5.3.3 Effect of solar radiation on the back of the module

One of the characteristics of the proposed model is of taking into account, in the thermal balance of the PV module, of the contribution of the solar radiation that hit the back surface G_{bk}. So it is of interest to evaluate the contribution of G_{bk} on the cell temperature considering different operative conditions (i.e. varying the intensity of the solar irradiance G_{fr} and the wind speed). These analyses were conducted at a constant ambient temperature of 20 °C, and varying: G_{fr} from 200 to 1000 W/m^2; three different

wind velocity, representative of low, medium and high wind speed; three values of G_{bk} expressed as a percentage of G_{fr}. Table 18 summarized the different scenarios simulated. The case G_{bk}=0 does not take into account the solar radiation on the back of the module. Figure 58 depicts the variation of T_{pv}, as well as the difference (T_{pv} (G_{bk} ≠0) – T_{pv} (G_{bk} =0) , versus the G_{fr} radiation for the different percentages of G_{bk} and u=3.0 m/s, for a bifacial module.

Table 18 Simulated scenario

Wind speed	G_{bk}			
u = 0.5 m/s	0	$0.05G_{fr}$	$0.10G_{fr}$	$0.20G_{fr}$
u = 3.0 m/s	0	$0.05G_{fr}$	$0.10G_{fr}$	$0.20G_{fr}$
u = 10.0 m/s	0	$0.05G_{fr}$	$0.10G_{fr}$	$0.20G_{fr}$

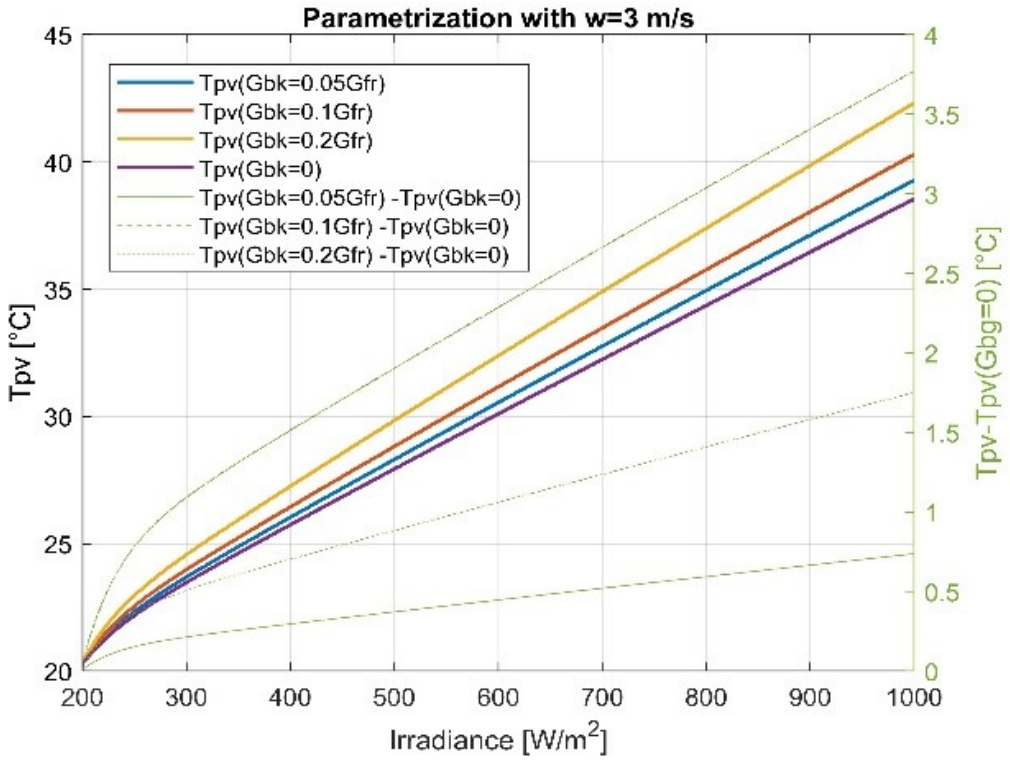

Figure 58 Tpv vs Irradiance (G_{fr}) at u=3 m/s

Table 19 summarizes the values of T_{PV} for a solar irradiance of 500 and 1000 W/m^2.

Table 19 Cell temperature for bifacial module

G_{fr}=1000 [W/m^2]					
u (m/s)	Temp. (°C)	G_{bk}			
		0	0.05G_{fr}	0.1G_{fr}	0.2G_{fr}
u =0.5	T_{pv}	45.4	46.6	47.9	50.7
	T_{pv}-T_{pv}(G_{bk}=0)	0.0	1.2	2.5	5.2
u =3	T_{pv}	38.5	39.3	40.3	42.3
	T_{pv}-T_{pv}(G_{bk}=0)	0.0	0.7	1.7	3.8
u =10	T_{pv}	31.2	31.6	32.2	33.4
	T_{pv}-T_{pv}(G_{bk}=0)	0.0	0.4	1.0	2.2
G_{fr}=500 [W/m^2]					
u =0.5	T_{pv}	30.9	31.5	32.2	33.6
	T_{pv}-T_{pv}(G_{bk}=0)	0.0	0.6	1.3	2.7
u =3	T_{pv}	28.1	28.4	28.9	30.0
	T_{pv}-T_{pv}(G_{bk}=0)	0.0	0.4	0.9	1.9
u =10	T_{pv}	25.0	25.2	25.5	26.1
	T_{pv}-T_{pv}(G_{bk}=0)	0.0	0.2	0.5	1.1

It is quite evident that the effect of G_{bk} is most important when G_{fr} has the highest values and the wind velocity is the lowest. The difference of T_{PV} can reach about 5.2°C when the wind speed is 0.5 m/s and 2.2°C when the wind speed is 10.0 m/s for the case of 1000 W/m^2 and 2.7°C when the wind speed is 0.5 m/s, and of 1.1°C when the wind speed is 10.0 m/s for the case of 500 W/m^2 at G_{bk}=0.2 G_{fr}.

Figure 59 depicts the variation of T_{pv}, as well as the difference (T_{pv} (Gbk ≠0) – T_{pv} (G_{bk} =0) , versus the G_{fr} radiation for the different percentages of G_{bk} and u=3.0 m/s, for a monofacial module.

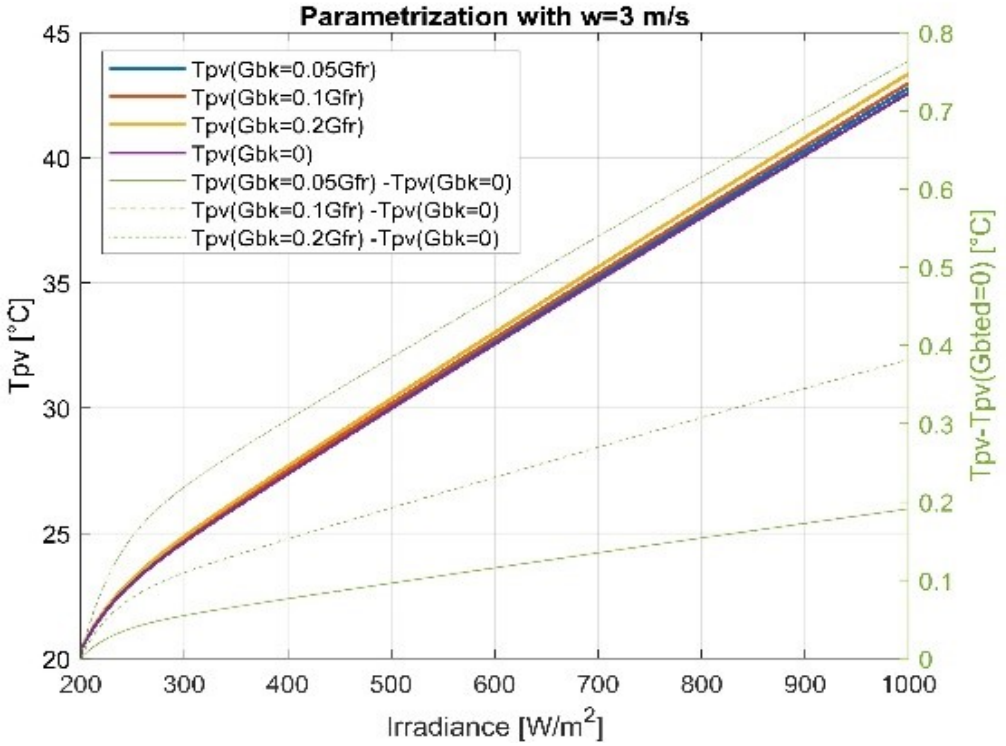

Figure 59 Tpv vs Irradiance at u =3 m/s

Table 20 summarizes the values of T_{PV} for a solar irradiance of 500 and 1000 W/m^2.

Table 20 Cell temperature for monofacial module

G_{fr}=1000 [W/m^2]					
u (m/s)	Temp. (°C)	G_{bk}			
		0	0.05G_{fr}	0.1G_{fr}	0.2G_{fr}
u =0.5	T_{pv}	51.0	51.3	51.5	52.0
	T_{pv}-T_{pv}(G_{bk}=0)	0.0	0.3	0.5	1.0
u =3	T_{pv}	42.6	42.8	43.0	43.3
	T_{pv}-T_{pv}(G_{bk}=0)	0.0	0.2	0.4	0.8
u =10	T_{pv}	33.6	33.7	33.8	34.1
	T_{pv}-T_{pv}(G_{bk}=0)	0.0	0.1	0.2	0.5
G_{fr}=500 [W/m^2]					
u =0.5	T_{pv}	33.8	34.0	34.1	34.4
	T_{pv}-T_{pv}(G_{bk}=0)	0.0	0.1	0.3	0.5
u =3	T_{pv}	30.1	30.2	30.3	30.5
	T_{pv}-T_{pv}(G_{bk}=0)	0.0	0.1	0.2	0.4
u =10	T_{pv}	26.2	26.3	26.3	26.4
	T_{pv}-T_{pv}(G_{bk}=0)	0.0	0.1	0.1	0.2

For the monofacial module the difference of T_{PV} can reach about 1.0 °C when the wind speed is 0.5 m/s and of 0.5°C when the wind speed is 10.0 m/s for the case of 1000 W/m^2 and 0.5°C when the wind speed is 0.5 m/s, and 0.2°C when the wind speed is 10.0 m/s for the case of 500 W/m^2 at G_{bk}=0.2 G_{fr}. The results obtained indicate that the effect of the rear radiation has a greater impact on the bifacial glass-glass module. This derives from two main phenomena: one that concerns the term of conversion of solar radiation into energy, which is present only in the bifacial, and the other regards the physical properties of the the modules. In fact, the monofacial module consists of tedlar, a reflective and insulating material, the bifacial is made of glass, a material with thermal conductivity higher than that of the tedlar. In addition, the glass-glass module is semi-transparent while the tedlar glass module is opaque and therefore does not allow solar radiation to pass through the module, where there is no cell.

The results are in line with [107] where it is demonstated that the bifacial modules have lower cell temperature than monofacial. Moreover, it is apparent that, given the same operating conditions, (e.g. T_a=20° C; G_{fr}=1000 W/m^2; G_{bk}=0.2G_{fr}; wind speed u=3 m/s), there is a cell temperature difference between a bifacial and a monofacial module ($T_{PV(monofacial)}$-$T_{PV(bifacial)}$) equal to 1.0°C. Such parametric analysis has been further extended with the aim to investigate the temperature variation of the monofacial and bifacial modules in the transition from the open circuit (o.c.) to maximum power point (m.p.p.). Table 21 and Table 22 summarizes the values of T_{pv} for a solar irradiance of 800 W/m^2 and an ambient temperature of 20° C, for the bifacial and mofocial module respecitevly.

Table 21 Bifacial Cells temperature at o. c. and m.p.p.

Wind velocity m/s	T_{PV} (°C)	G_{bk}			
		0	$0.05G_{fr}$	$0.1G_{fr}$	$0.2G_{fr}$
u =0.5	$T_{PV\ (o.c.)}$	43.1	44.3	45.5	48.0
	$T_{PV\ (m.p.p.)}$	39.7	40.7	41.8	44.0
	$T_{PV\ (o.c.)} - T_{PV\ (m.p.p.)}$	3.4	3.6	3.7	4.0
u =3.0	$T_{PV\ (o.c.)}$	36.9	37.7	38.6	40.5
	$T_{PV\ (m.p.p.)}$	34.3	35.0	35.8	37.4
	$T_{PV\ (o.c.)} - T_{PV\ (m.p.p.)}$	2.6	2.7	2.8	3.1
u =10.0	$T_{PV\ (o.c.)}$	30.3	30.8	31.3	32.5
	$T_{PV\ (m.p.p.)}$	28.7	29.0	29.5	30.5
	$T_{PV\ (o.c.)} - T_{PV\ (m.p.p.)}$	1.6	1.7	1.8	1.9

Table 22 Monofacial cells temperature at o. c. and m.p.p.

Wind velocity m/s	T_{PV} (°C)	G_{bk}			
		0	$0.05G_{fr}$	$0.1G_{fr}$	$0.2G_{fr}$
u =0.5	$T_{PV\ (o.c.)}$	46.3	46.5	46.7	47.1
	$T_{PV\ (m.p.p.)}$	44.3	44.5	44.7	45.2
	$T_{PV\ (o.c.)} - T_{PV\ (m.p.p.)}$	2.0	2.0	2.0	2.0
u =3.0	$T_{PV\ (o.c.)}$	39.2	39.4	39.5	39.8
	$T_{PV\ (m.p.p.)}$	37.7	37.8	38.0	38.3
	$T_{PV\ (o.c.)} - T_{PV\ (m.p.p.)}$	1.6	1.6	1.6	1.6
u =10.0	$T_{PV\ (o.c.)}$	31.7	31.8	31.9	32.1
	$T_{PV\ (m.p.p.)}$	30.7	30.8	30.9	31.0
	$T_{PV\ (o.c.)} - T_{PV\ (m.p.p.)}$	1.0	1.0	1.0	1.1

In the case of a bifacial model, an increase in the temperature is obtained from load to open circuit, which is greater than in the case of a monofacial module. Furthermore, it can be noted that, as the radiation on the back changes, the variations of T_{pv} in the monofacial module are not very sensitive. This outcome is coherent with the fact that in the balance equation of the bifacial model there is a term that takes into account the energy production on the back, which strongly depends on the irradiance on the back, while the monofacial module obviously does not have this term. The radiation on the back of the monofacial module affect the temperature of the cell only through the flow Φ_5.

5.3.4 Models used to assess the performance of PV plants

Starting from the results of 3L-NM for a bifacial module, a regression model (l.r.3) has been developed, which allows calculating in very simple manner the cell temperature as a function of the environmental variables, i.e. solar radiation (W/m^2) ambient temperature (°C) and wind speed (m/s).

The developed regression model (l.r.3) is described by the following equations.

$$T_{pv} = -22.1499 + 0.0300G_{fr} + 1.9839T_a - 0.0142w \quad \textbf{Eq. 85}$$

The adoption of the l.r.3 model could be convenient for calculating the cell temperatures for the glass-glass bifacial module. Thus, it is interesting to compare the results of this regression model with the results of other numerical models proposed in the literature. In particular, the comparison of the l.r.3 model versus the King, TamizhMani and 3L/NM models is proposed. Figure 60 shows the T_{pv} calculated through the above-mentioned models, the measured on the back of the module T_{bg} and the temperature differences between the temperatures calculated with different models and the temperature measured on the back surface (T_{pv} -T_{bg}), under the same weather conditions. As regards the King model for the coefficients "a" and "b " the values of -3.47 -0.0594 were assumed.

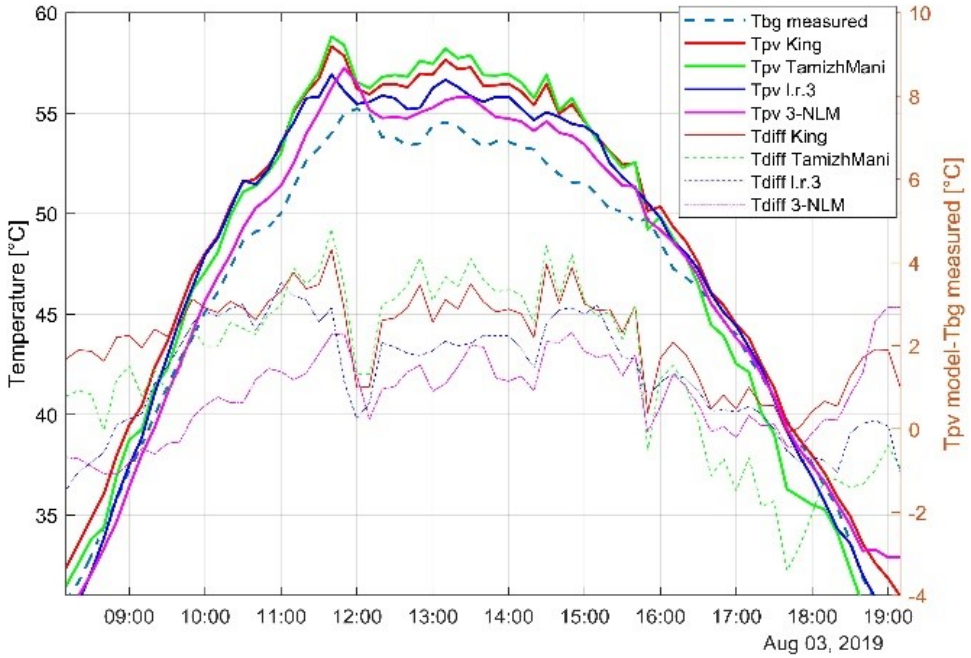

Figure 60 Comparison of TPV derived by different models

From this analysis, it can be observed that the results of the different models are very similar. However, the model 3L-NM as well the l.r.3 give rise to differences between the cell and the back surface temperature smaller than the other models. This result is in line with the thermal behavior of the bifacial cells because the absorbed solar radiation on the backside is partly converted into power so reducing the differences of temperature between the cell and the back surface. This result further confirms the fundamental importance to consider the effect of solar radiation on the back of the module, especially for the bifacial cells.

5.4 Conclusions

The results highlight the very good reliability of the proposed multi-layer model. In fact, from the statistical analysis, correlation values of 0.993 and 0.990 were obtained, PE values equal to 0.718 % and 0.161 % respectively for the monofacial and bifacial module. The sensitivity study shows that the solar radiation on the backside of the module has a greater impact on the bifacial module, so it has absolutely to be taken into account in the implementation of thermal models for bifacial modules, as well in the case of monofacial module for obtaining more performing model. When the contribution of back radiation is included in a numerical model, temperature differences up to 5.2°C for the bifacial and 1.0°C for the monofacial module at 1000 W/m^2 were observed. From the comparison between the existing models in the literature and those proposed, it is possible to highlight that the proposed models give rise to differences between the cell and the back surface temperature smaller than the other models. This result is in line with the thermal behavior of the bifacial cells because the absorbed solar radiation on the backside is partly converted into power so reducing the differences of temperature between the cell and the back surface.

This preliminary study on the thermal behavior of mono and bifacial modules will be used in the following chapters to implement the energy performance models of FPV systems, in which the interactions between the system and the surrounding environment (water) will be considered.

6 Energy performance models for FPV systems

6.1 Introduction

The objective of this chapter is to create a performance models of bifacial and monofacial PV modules installed on water surfaces considering active and passive water cooling techniques. The PV modules installed on water surface experience lower PV cell temperatures due to the cooling effect related with the favourable microclimate, in which they operate, and the large availability of water for cooling systems. As regards the first point, in the calculations of the energy balance used to estimate the temperature of the modules, the effects of the interaction between the FPV and the surrounding environment were taken into account. Furthermore, the case in which a layer of water flows over the modules (active cooling with water veil) was simulated, and the performance under these conditions was evaluated.

The numerical models implemented in this chapter are based on methodology adopted in the previous chapter but with some modifications that have allowed to evaluate the effect of natural and forced cooling of the FPV modules.

This study will make it possible to make technical-economic evaluations in the following chapters, considering the increase in energy due to cooling effect. Therefore, it will be possible to compare in economic terms, a GPV with a FPV system with active and passive water cooling techniques.

6.2 Methodology

To get a clear view of the implemented models, Figure 61 and Figure 62 is a representation of the cases, monofacial-bifacial:

- floating with passive cooling;
- floating with active cooling.

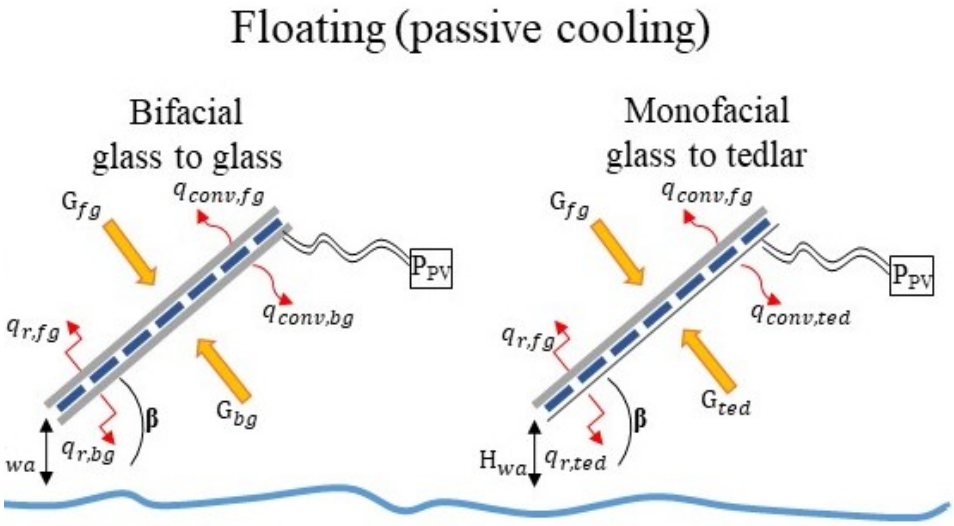

Figure 61 Graphic schematization of the passive cooling case.

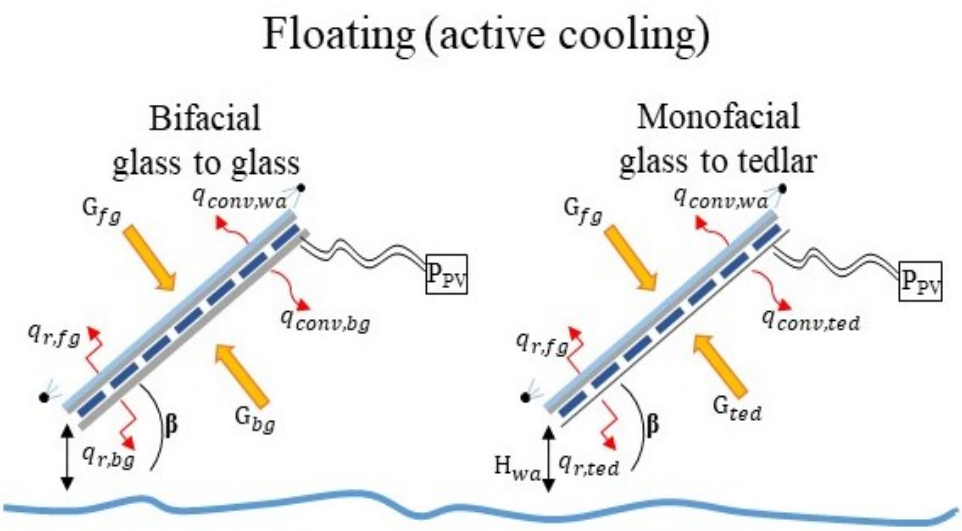

Figure 62 Graphic schematization of the active cooling case.

A model for each type of installation has been developed in particular floating mono-bifacial, active and passive cooled and a rooftop mono-bifacial system is utilised as a reference. In the following paragraphs, the energy balance equations for each model and the evaluation of the different effects in the various installation cases are shown.

The methodology adopted for the implementation of this model is the same as the one adopted for the multilayer model developed in [18], but with some changes reported below.

The implemented rooftop-model consists of three differential equations, one for each layer of the module, in which the convective, radiative and conductive effects are

considered. The air between the roof and the modules was considered quiet with zero speed. The methodology and equations used in this case are not reported as they can be consulted in chapter "Thermal models for evaluating the performances of monofacial and bifacial PV modules".

6.2.1 Floating modules with passive cooling

The modules installed on the water (Figure 61) enjoy natural cooling due to the favorable microclimate conditions. In the proximity of the body of water, the evaporative effect is generated which allows a further heat exchange of the module with the surrounding environment. To take these effects into account, the equation of evaporation *E* have been implemented in the energy balance.

E, is the Penman-Monteith [108] model that evaluates the evaporation of a body of water, starting from the temperature, wind speed, solar radiation and relative humidity data of the location in question. The evaluation of *E* was carried out according to the methodology implemented in chapter "Evaporation rate models on a water basin with FPV plants".

So, for monofacial and bifacial modules, cooling due to water evaporation is considered by subtracting the heat due to evaporation on the rear surface.

The adoption of this methodology to take into account the effect of evaporation on the cooling of the module was suggested in [45].

To obtain the equivalent of water evaporated into energy, the Eq. 86 was used, where 28.4 is the evaporated water-energy conversion coefficient:

$$\dot{q}_{ev,bg/ted} = 28.4 * E * A_{bg/ted} \quad \textbf{Eq. 86}$$

In the Penman-Monteith equation, radiation expressed in MJ m^{-2} is converted to equivalent evaporation in mm by using a conversion factor equal to the inverse of the latent heat of vaporization ($1/\lambda = 0.408$), so equivalent evaporation [mm] = 0.408 * Radiation [MJ m^{-2}]. By making the appropriate substitutions and conversions, obtain the coefficient 28.4, as reported in ref. [109].

For the calculation of the radiative heat exchanges between the module and the water, a model is used which, starting from the air temperature, provides the temperature of the body of water [110]. The Eq. 87 describes the model.

$$T_w = 5 + 0.75T_a$$ **Eq. 87**

Another hypothesis concerns the microclimate conditions that are created in the environment surrounding the front and back of the modules. In fact, relative humidity must be taken into consideration. Therefore, it is appropriate to consider for the convective motions on the back of the module, the apparent air temperature [111] as follows:

$$T_{ap} = T_{db} + 0.33e_a - 0.7u - 4$$ **Eq. 88**

Where T_{ap} is apparent temperature (°C), T_{db} is dry bulb temperature (°C), u is the wind speed at 10 m height (m/s) and e_a is the vapour pressure of air (hPa).

The energy balance equations for the FPV system, in which heat exchanges with water and the surrounding environment are taken into account, become the following [112]:

$$C_{fg}\frac{dT_{fgfl}}{dt} = (\dot{q}_{r,fg-sky} + \dot{q}_{r,fg-wa} + \dot{q}_{conv,fg} - \dot{q}_{cd,fg-pv} + \dot{q}_{cd,fg-bg/ted} + \Phi_1)$$ **Eq. 89**

$$C_{pv}\frac{dT_{pvfl}}{dt} = (\dot{q}_{cd,fg-pv} - \dot{q}_{cd,bg/ted-pv} + \Phi_2 + \Phi_3 + \Phi_4{}^*)$$ **Eq. 90**

$$C_{\frac{bg}{ted}}\frac{dT_{bg/tedfl}}{dt} = (\dot{q}_{cd,pv-\frac{bg}{ted}} - \dot{q}_{r,-\frac{bg}{ted}-wa} - \dot{q}_{r,\frac{bg}{ted}-sky} - \dot{q}_{conv,\frac{bg}{ted}} - \dot{q}_{cd,fg-\frac{bg}{ted}} + \Phi_5 - \dot{q}_{ev,bg/ted})$$ **Eq. 91**

*only for bifacial modules.

Where in the front glass:

$$\dot{q}_{r,fg-sky} = A_{fg}h_{r,fg-sky}(T_{sky} - T_{fg})$$ **Eq. 92**

$$\dot{q}_{r,fg-w} = A_{fg}h_{r,fg-wa}(T_{wa} - T_{fg})$$ **Eq. 93**

$$\dot{q}_{conv,fg} = A_{fg}h_{conv,fg}(T_{fg} - T_a)$$ **Eq. 94**

$$\dot{q}_{cd,fg-pv} = A_{pv}\frac{1}{r_{cd,fg}+r_{cd,pv}}(T_{fg} - T_{pv})$$ **Eq. 95**

$$\dot{q}_{cd,fg-bg/ted} = (A_{fg} - A_{pv})\frac{1}{r_{cd,bg/ted}+r_{cd,fg}}(T_{fg} - T_{bg/ted})$$ **Eq. 96**

Where in the pv layer:

$$\dot{q}_{cd,fg-pv} = A_{pv}\frac{1}{r_{cd,fg} + r_{cd,pv}}(T_{fg} - T_{pv})$$ **Eq. 97**

$$\dot{q}_{cd,bg/ted-pv} = A_{pv}\frac{1}{r_{cd,bg/ted} + r_{cd,pv}}(T_{pv} - T_{bg/ted})$$ **Eq. 98**

Where in the back glass (for bifacial) or tedlar (for monofacial):

$$\dot{q}_{cd,bg/ted-pv} = A_{pv} \frac{1}{r_{cd,\frac{bg}{ted}} + r_{cd,pv}} (T_{pv} - T_{bg/ted})$$ **Eq. 99**

$$\dot{q}_{r,bg/ted-wa} = A_{\frac{bg}{ted}} h_{r,\frac{bg}{ted}-wa} (T_{\frac{bg}{ted}} - T_{wa})$$ **Eq. 100**

$$\dot{q}_{r,bg/ted-sky} = A_{\frac{bg}{ted}} h_{r,\frac{bg}{ted}-sky} (T_{\frac{bg}{ted}} - T_{sky})$$ **Eq. 101**

$$\dot{q}_{conv,bg/ted} = A_{\frac{bg}{ted}} h_{conv,\frac{bg}{ted}} (T_{\frac{bg}{ted}} - T_{ap})$$ **Eq. 102**

$$\dot{q}_{cd,fg-bg/ted} = (A_{fg} - A_{pv}) \frac{1}{r_{cd,\frac{bg}{ted}} + r_{cd,fg}} (T_{fg} - T_{bg/ted})$$ **Eq. 103**

6.2.2 Floating modules with active cooling

In this circumstances (Figure 62), a layer of water flows on the front surface of the module, which is made up of glass. The basic assumptions are the same as for the FPV photovoltaic module without water flow, the only difference is in the front layer of glass, where the water flows. Being a one-dimensional model (not variable with the length/width of the module), it is assumed that the water temperature T_{wa} is in the center of gravity of the module. The equations of the energy balance in the cell layer and in the back layer remain the same as those considered for the FPV system with passive cooling, the only equation that changes is that of the first layer or the front glass in contact with water. The equation described above is shown below [112].

$$C_{fg\,fl} \frac{dT_{fg}}{dt} = (\dot{q}_{r,fg-sky} + \dot{q}_{r,fg-wa} + \dot{q}_{conv,wa} - \dot{q}_{cd,fg-pv} + \dot{q}_{cd,fg-bg/ted} + \Phi_1)$$ **Eq. 104**

Where, all terms remain the same as the FPV with passive cooling, except for the following term, which was implemented as described below:

$$\dot{q}_{conv,wa} = A_{wa} h_{conv,wa} (T_w - T_{fg})$$ **Eq. 105**

$$h_{conv,wa} = \frac{\lambda_{wa} Nu}{L_c}$$ **Eq. 106**

Where:

$$L_c = \frac{4A_{fg}}{p}$$ **Eq. 107**

The coefficient $h_{conv,wa}$ is evaluated after computing the Nusselt number Nu, which has been considered fixed for a laminar flow and equal to Nu=3.608 [113].

The Reynolds number is:

$$Re = \frac{u_{wa}\, L_c}{v_{wa}} \qquad \textbf{Eq. 108}$$

Where:

$$u_{wa} = \dot{v}\, L_{pan} s_{wa} \qquad \textbf{Eq. 109}$$

u_w is the mean velocity of water (m s^{-1}), $\dot{v}$ is the volume flow rate of water (l h^{-1}), and v_{wa} is the kinematic viscosity of water.

For the calculation of $h_{conv,w}$ has been used the table proposed in [114] which for completeness it is reported below.

Table 23 Water parameter used in the thermal model

T_w (K)	$\lambda_w(\frac{W}{mK})$	v_w(m^2 s^-1)	*Re*
288	0.5892	1.157 10^-6	13.64
293	0.5984	1.006 10^-6	15.69
313	0.6305	0.658 10^-6	23.98
333	0.6543	0.475 10^-6	33.22

Using the interpolation, intermediate values have been obtained at the tabulated values of Table 23.

6.2.3 Models comparison

To evaluate the effect of cell cooling on power and efficiency, a comparison is made between the results deriving from the different models implemented. This comparison is made on the basis of the following formulas.

The efficiency is calculated by Eq. 2 Eq. 3 and the increase/decrease in efficiency is calculated by Eq. 110.

$$\Delta_\eta = 100 \frac{\eta_{b/m-fl}}{\eta_{b/m-gr}} \qquad \textbf{Eq. 110}$$

The power produced by the front of bifacial and monofacial rooftop module is:

$$P_{pvm/b,fr} = P_{mpp} \frac{G_{fr}}{G_{STC}} \left[1 + \beta\left(T_{pv} - T_{STC)}\right)\right] \qquad \textbf{Eq. 111}$$

For the bifacial rooftop module, the contribution of power produced from the back was also considered as follow.

$$P_{pvb,bk} = BF\, P_{mpp} \frac{G_{bk}}{G_{STC}} \left[1 + \beta\left(T_{pv} - T_{STC)}\right)\right] \qquad \textbf{Eq. 112}$$

To evaluate the temperature difference from the floating (with active and passive cooling) respect to rooftop, the Eq. 113 is calculated for both the monofacial and bifacial module.

$$T_{diff}\% = 100\frac{T_{bg/ted\,rt} - T_{bg/ted\,fl}}{T_{bg/ted\,rt}} \quad \textbf{Eq. 113}$$

The equivalent hours $Y_{m/b}$, in kWh/kW, is evaluated it is the sum of hourly average power values under the hypothesis that the system works at maximum power point, mpp, then it is normalized respect with peak power, in kW. The subscripts *m* and *b* indicate, respectively, the monofacial system and the bifacial one:

$$Y_m = \sum_{t=0}^{n} \frac{P_{mpp,m}(t)\Delta t}{P_{mpp,m}} = \frac{Y'_m}{P_{mpp,m}} \quad \textbf{Eq. 114}$$

$$Y_b = \sum_{t=0}^{n} \frac{P_{mpp,b(t)\Delta t}}{P_{mpp,\mathrm{b}}} = \frac{Y'_b}{P_{mpp,b}} \quad \textbf{Eq. 115}$$

It is worth noticing that Y'_b is normalized respect with the front side module power $P_{mpp,b}$

The bifacial gain BG, in %, is defined in Eq. 1.

BG is used to evaluate the energy gain of a bifacial system compared to the monofacial.

The comparison of the performance between the rooftop and floating systems is important for evaluating the actual increase in energy produced by FPV. To evaluate this increase, is calculated the floating gain (FG).

FG, in %, is defined in Eq. 116.

$$FG = 100\frac{Y_{fl} - Y_{rt}}{Y_{rt}} \quad \textbf{Eq. 116}$$

FG is used to compare the producibility of a floating system compared to a rooftop system. The rooftop system is taken as a reference.

6.3 Test of models

The validation tests were performed by comparing the experimental data with the numerical values of the models. Therefore, the data from Enel's experimental plant described in Chapter 3 were used.

Ambient temperature, solar irradiance, wind speed, relative humidity (T_a, G_{fr}, G_{bk}, u, RH) are the input of the models used to simulate the systems. These data were collected by the meteorological station run by Enel Green Power described in Chapter 3.

In Figure 63 it are shows the values of global horizontal irradiance [W/m^2], wind speed [m/s] at 10 meters in height, ambient temperature [°C], relative humidity [%] in the period between 03/08/19 to 05/08/19 (case of passive cooling).

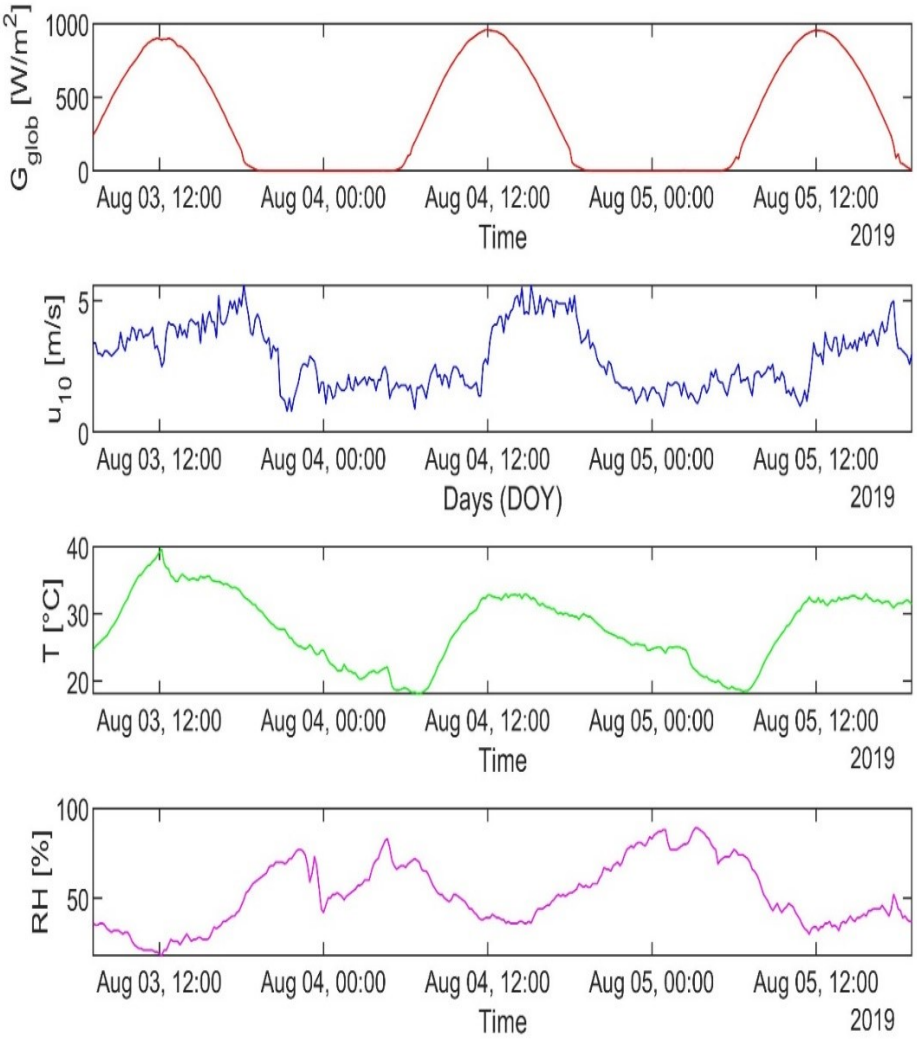

Figure 63 Weather data from 03/08/19 to 05/08/19

In Figure 64 it are shows the values of global horizontal irradiance [W/m^2], wind speed [m/s] at 10 meters in height, ambient temperature [°C], relative humidity [%] in the

period of 30/07/19 when the active cooling with pumping system was activated. All data are sampled at 10 second intervals and averaged at 10 minute intervals.

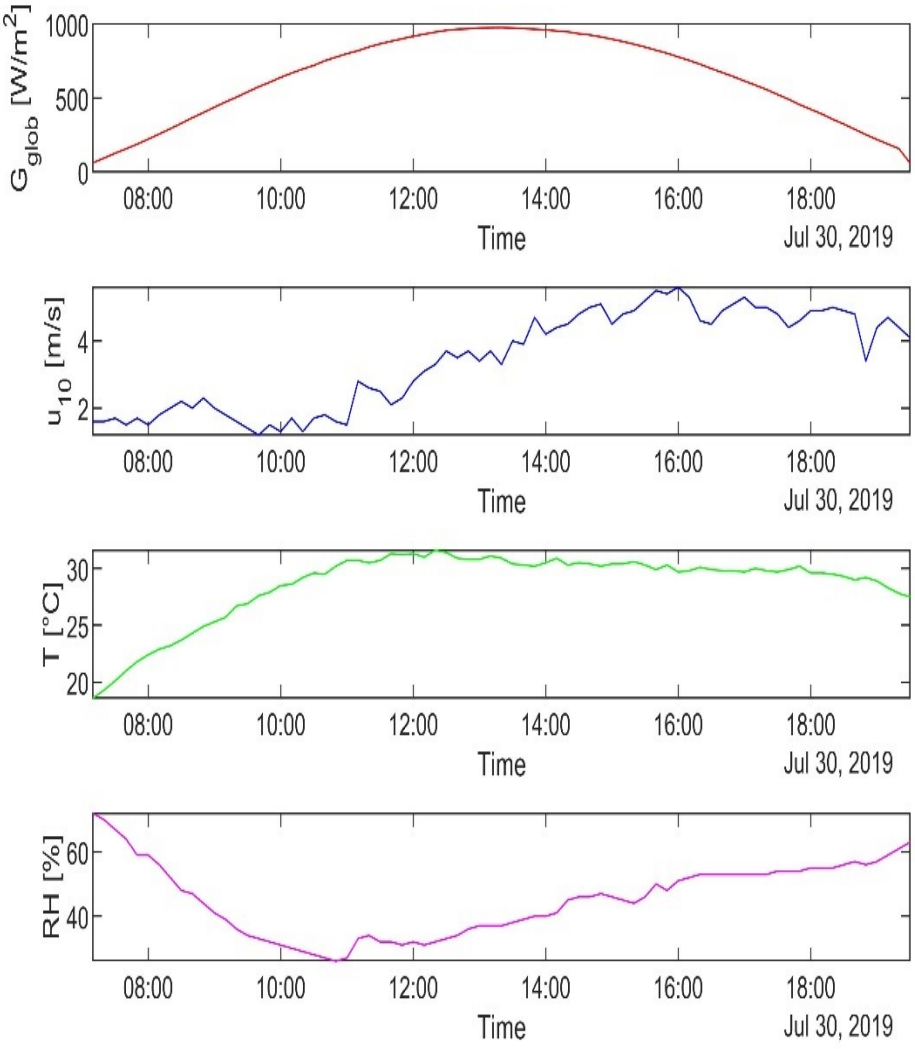

Figure 64 Weather data of 30/07/19

In this paragraph the results obtained on the basis of the methodology adopted will be shown. In particular, the temperatures obtained from the models and those measured, the power/energy produced by the systems divided by type of installation, the energy gain of the mono and bifacial floating system due to natural/forced cooling and finally the efficiencies will be shown.

6.3.1 Temperature models comparison

To validate the models, the temperatures measured on the rear surface of the module with those calculated by the models were compared, therefore for the monofacial and bifacial modules installed on water. Below are the temperature trends in the various cases. For the case of rooftop systems, not having an experimental system with the same configurations as the floating system, only the simulated temperatures and power are reported. The latter data are reliable as the model for has been previously validated with experimental data in [18].

6.3.1.1 Floating bifacial modules with passive cooling vs rooftop

The measured temperature values for the bifacial system installed above water were compared with the values calculated by the model. Furthermore, the modelled temperatures of the two systems (floating case and rooftop case) are compared to evaluate the differences.

The Figure 65 shows the temperatures of the bifacial module on the rooftop calculated with the model and the temperatures of FPV system calculated with the model and compared with the measurements.

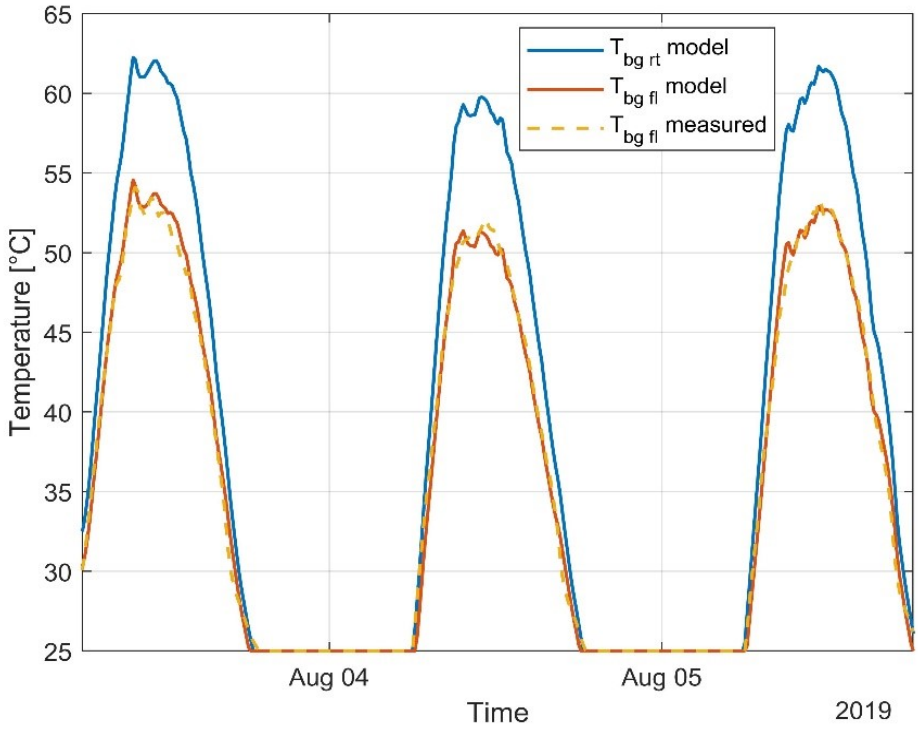

Figure 65 Simulated and measured back surface temperature of bifacial rooftop/floating module

The maximum temperature difference, in percentage, between the bifacial rooftop system compared to the bifacial floating system is higher than 14%. The average temperature difference in percentage is equal to 10.86%.

The difference in temperatures between the two systems is due to the cooling effect due to the favourable microclimate conditions that are created near the floating modules.

6.3.1.2 Floating monofacial modules with passive cooling vs rooftop

Figure 66 shows the temperatures of the monofacial rooftop module calculated with the model and the temperatures of FPV system calculated with the model and compared with the measurements.

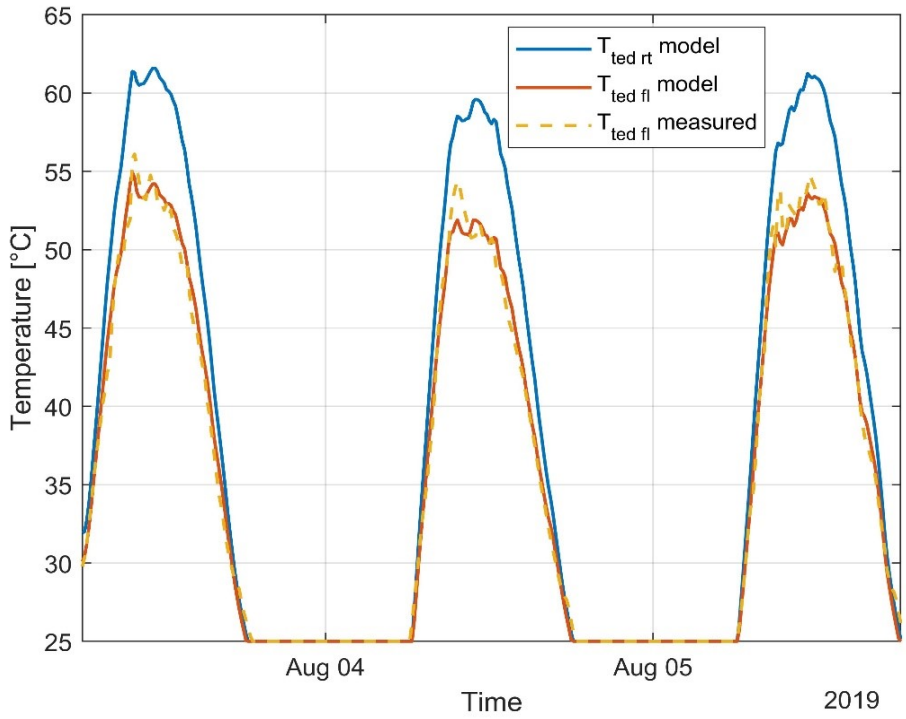

Figure 66 Simulated and measured back surface temperature of monofacial rooftop/floating module

The maximum temperature difference between the monofacial rooftop system compared to the monofacial floating system is greater than 13%. The average temperature difference is equal to 9.0%.

The difference in temperatures between the two systems is due to the cooling effect due to the favorable microclimate conditions that are created near the floating modules.

6.3.1.3 Floating bifacial modules with active cooling vs rooftop

The measured temperature values for the bifacial system installed above water with water active cooling turned on, were compared with the values calculated by the model. Subsequently, the modelled temperatures of the two systems (floating case and rooftop case) are compared to evaluate the differences.

Figure 67 shows the temperatures of the bifacial module on the rooftop calculated with the model, on the water calculated with the model and compared with the measurements.

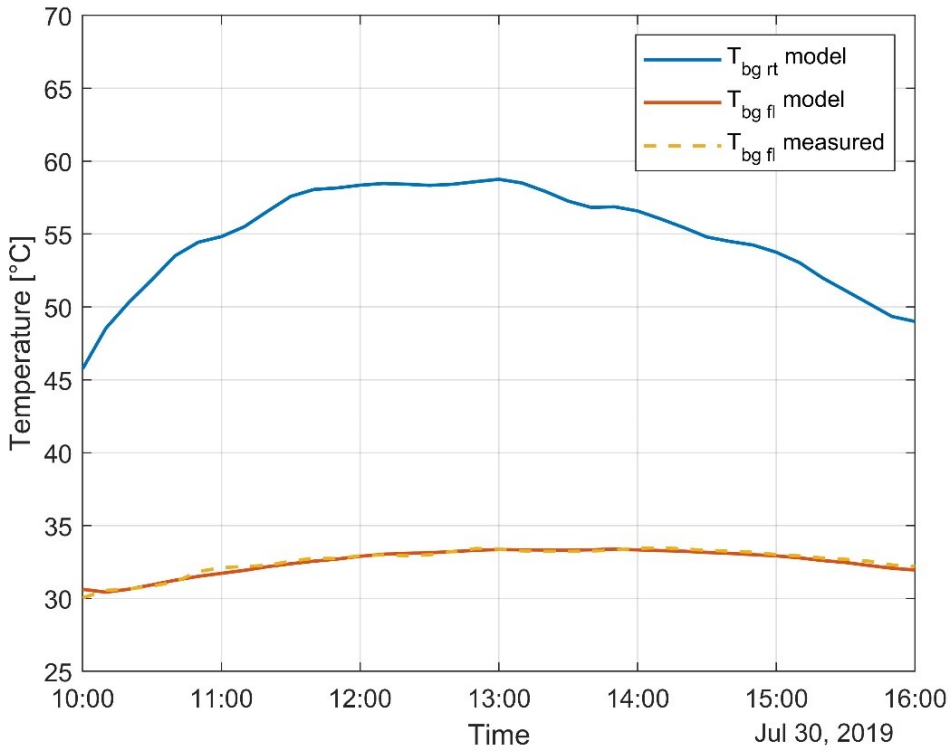

Figure 67 Simulated and measured back surface temperature of bifacial rooftop/floating module

The maximum temperature difference, in percentage, between the bifacial rooftop system compared to the bifacial floating system with active cooling is higher then 44%. The average temperature difference in percentage is equal to 40.58%.

The difference in temperatures between the two systems is due to the cooling effect due to the water veil that laps the floating modules.

6.3.1.4 Floating monofacial modules with active cooling vs rooftop

Figure 68 shows the temperatures of the monofacial rooftop module calculated with the model, on the water calculated with the model and compared with the measurements.

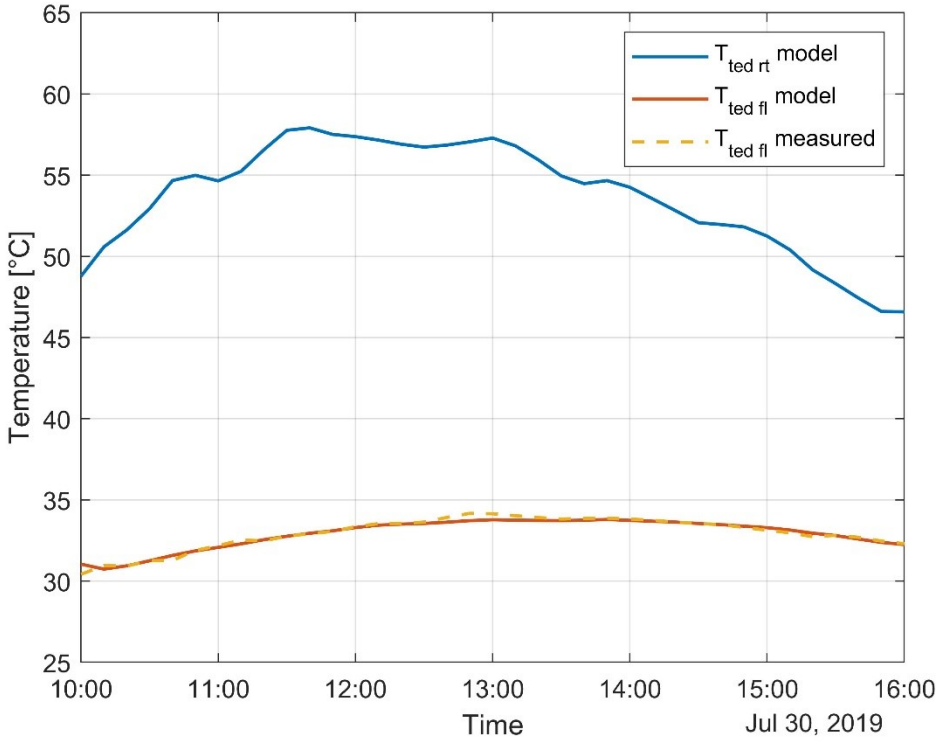

Figure 68 Simulated and measured back surface temperature of monofacial rooftop/floating module

The maximum temperature difference between the monofacial rooftop system compared to the monofacial floating system with active water cooling is greater than 43%. The average temperature difference is equal to 38.46%.

6.3.1.5 Thermal behaviour of modules

The monofacial module on the roof is a few tenths of a degree colder than the bifacial module on the roof. This behaviour is due to the fact that the monofacial does not receive radiation on the back as it is completely opaque while the bifacial has a filling factor of 90% which allows a portion of solar radiation to go beyond the module to be reflected by the roof and hit it on the back again. Part of this radiation is converted into energy, the remainder is converted into heat.

This does not happen for the temperatures of the floating system where the temperature of the bifacial is lower than the monofacial. In this case, both the bifacial and

monofacial receive radiation on the back. The rear glass of the bifacial exchanges heat more effectively than the tedlar, but the most important reduction effect of the temperature is due to the fact that the bifacial has a filling factor of about 90% (i.e. only 90% of the total surface of the module is opaque and covered by the cells, the remaining 10% is transparent and made of glass), which means that 10% of the glass-glass surface is let through by solar radiation and does not accumulate energy. This does not happen in the monofacial module as it is completely opaque and therefore thermal energy is accumulated in the spaces between the cells.

All this translates into a different percentage difference between the mono-bifacial temperatures of the rooftop system compared to those of the floating system. This difference for the passive cooling is equal to 1.86%. This difference for the active cooling is equal to 2.12%.

To evaluate the effect of the input variables to the models, a parametric study is conducted. The absolute temperature and the temperature difference between the model of rooftop system and the model of FPV system are calculated.

The values are obtained by setting:

- T_a=20°C
- T_w=15° C
- G_{bk}= 0.05G_{fr}.

Figure 69 shows the absolute temperature trends of the bifacial modules and the temperature differences between the two models (rooftop and FPV) as a function of solar irradiance and for three different wind speed values in the case of passive cooling.

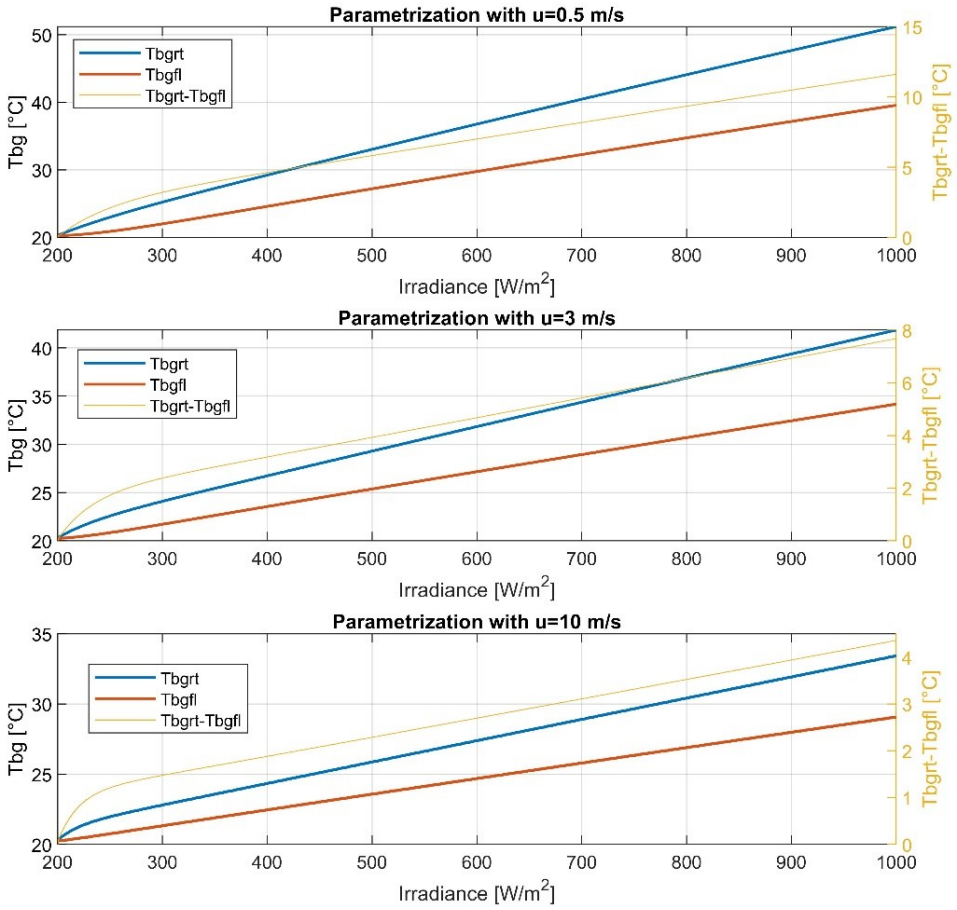

Figure 69 Bifacial absolute modules temperature and difference in temperature of rooftop and FPV systems for passive cooling

Figure 70 shows the absolute temperature trends of the monofacial modules and the temperature differences between the two models (rooftop and FPV) as a function of solar irradiance and for three different wind speed values in the case of passive cooling.

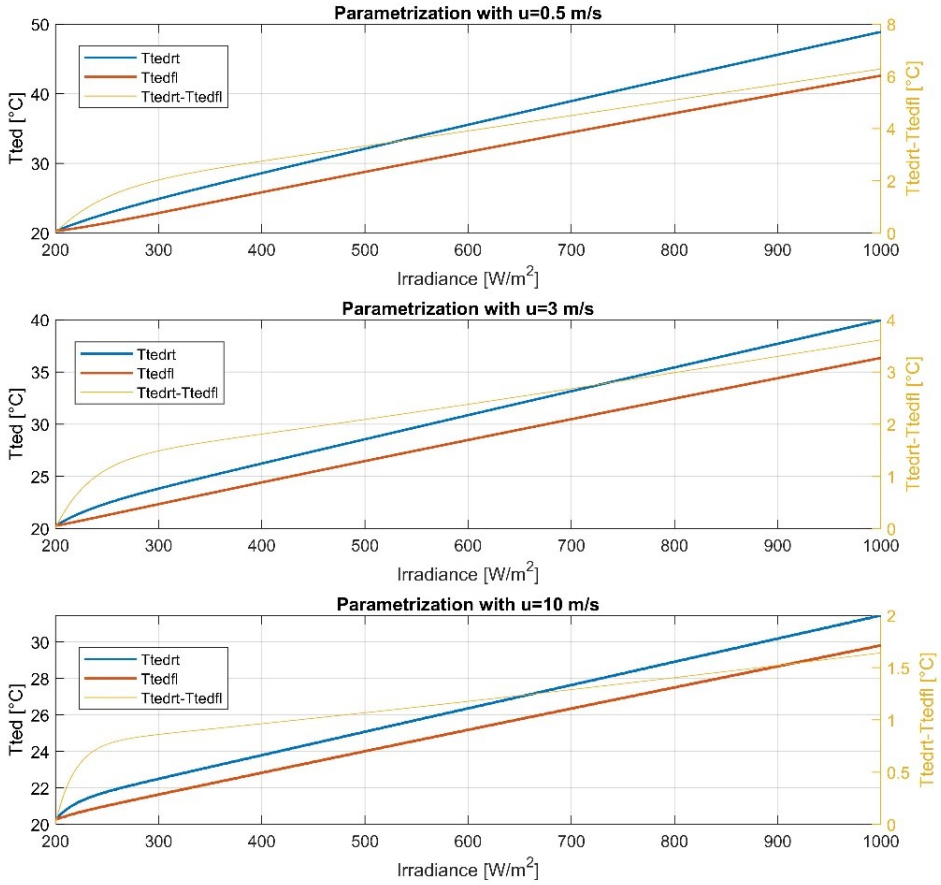

Figure 70 Monofacial absolute modules temperature and difference in temperature of rooftop and FPV systems for passive cooling

Figure 71 shows the absolute temperature trends of the bifacial modules and the temperature differences between the two models (rooftop and FPV) as a function of solar irradiance and for three different wind speed values in the case of active cooling.

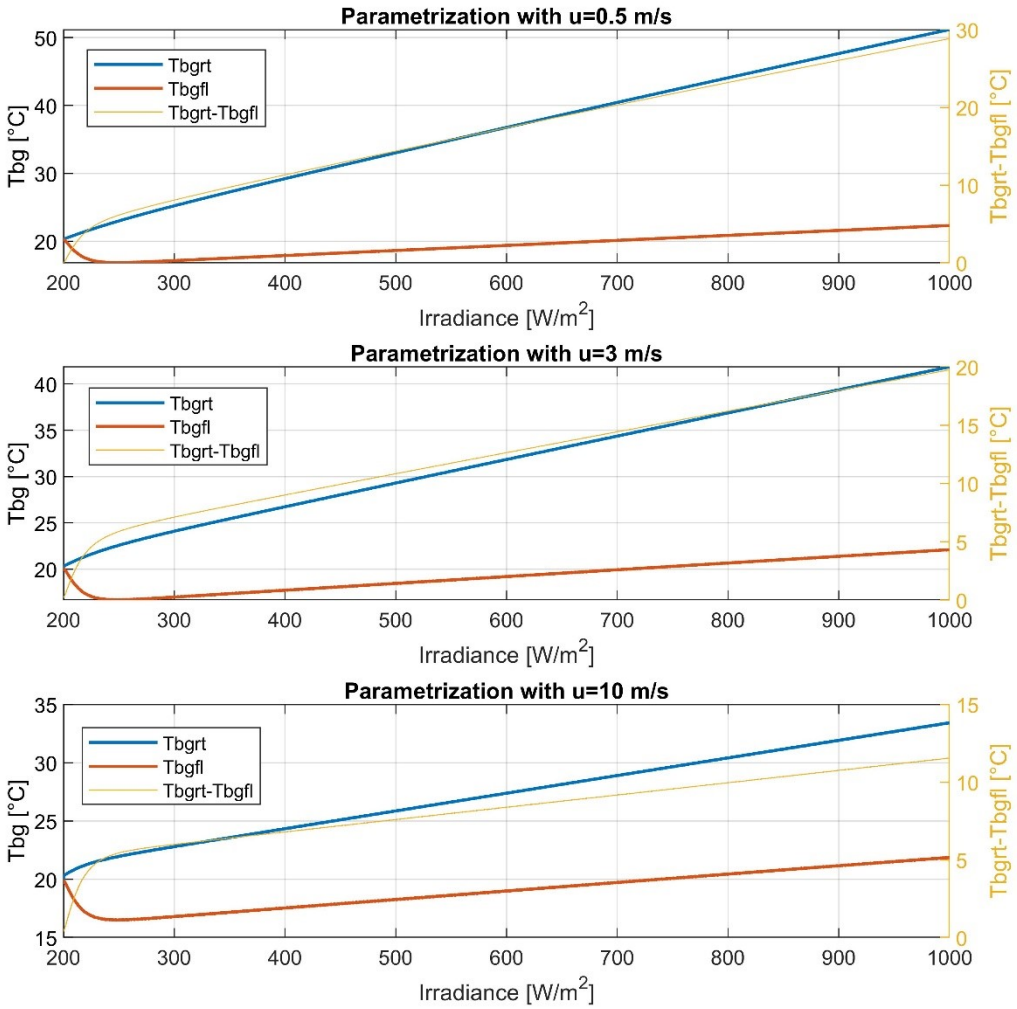

Figure 71 Bifacial absolute modules temperature and difference in temperature of rooftop and FPV systems for active cooling

Figure 72 shows the absolute temperature trends of the monofacial modules and the temperature differences between the two models (rooftop and FPV) as a function of solar irradiance and for three different wind speed values in the case of active cooling.

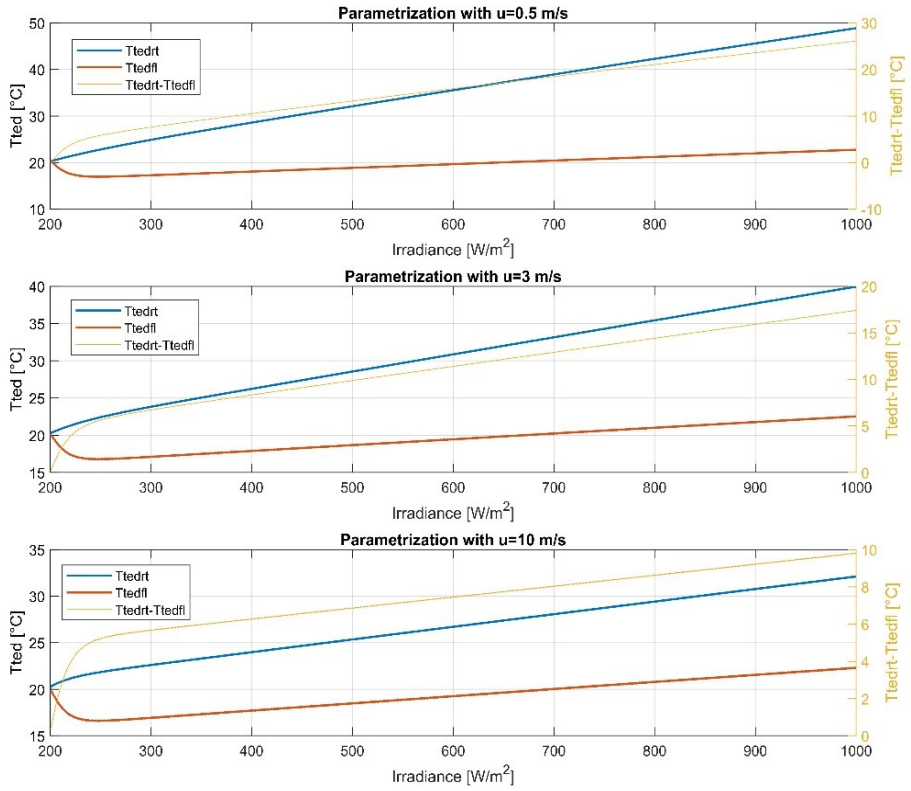

Figure 72 Monofacial absolute modules temperature and difference in temperature of rooftop and FPV systems for active cooling

6.3.1.6 Statistical analysis

To validate the models, statistical indices reported in 'Appendix A: Statistical evaluation indexes' were calculated, in particular the MAE RMSE and R^2. The results for the 4 cases of the floating system, obtained from the comparison between the measured values and those calculated by the models are shown in Table 24.

Table 24 Statistical indexes of floating temperature models

Type of cooling	Modules	Statistical indexes		
		MAE[°C]	RMSE [°C]	R^2
passive	Bifacial	0.034	0.675	0.998
	Monofacial	0.058	0.792	0.997
active	Bifacial	0.100	0.197	0.981
	Monofacial	0.065	0.203	0.979

From the statistical analysis showed in Table 24 it is evident that the implemented model, in all cases, provides an excellent correlation. For the passive cooling, the lowest MAE and RMSE are for the bifacial system and are equal to 0.034 °C and 0.675 °C respectively.

For the active cooling, the lowest MAE is calculated for the monofacial system and is equal to 0.065 °C and the lowest RMSE is 0.197.

6.3.2 Performances comparison

In this section, energy performances of FPV systems, are shown. To evaluate the energy gain due to natural cooling and active cooling of installation of the modules on the water, the equivalent hours (Y) of each system were calculated with equations reported in Eq. 114 and Eq. 115, the energy gain of bifacial modules with Eq. 1 and the energy gain of floating modules with Eq. 117. It is important to underline that the power values of the floating system are measured while those of the ideal rooftop system are estimated using Eq. 2 Eq. 3 Eq. 4.

To compare the performance of the floating system with respect to the one on the rooftop, the *FG* index is calculated for the monofacial and bifacial modules. Furthermore, the gain deriving from the bifacial compared to the monofacial of the floating system is evaluated.

The energy yield of the mono/bifacial floating system with active cooling is assessed, net of pump consumption, which is equal to 250 Wh per system (mono and bifacial). The pump is turned on from 10 am to 4 pm.

In this case is necessary to evaluate the energy yield moment by moment as in some hours of the day, it may not be convenient to switch on the pump as the cooling effect cannot compensate the pump consumption.

Figure 73 shows the BG_{fl} and *FG* of mono and bifacial FPV system for the monitoring hours, i.e. from 10 am to 4 pm in the case of active cooling. It is easy to see how the effect of the gain is reduced closer and closer to sunrise and sunset.

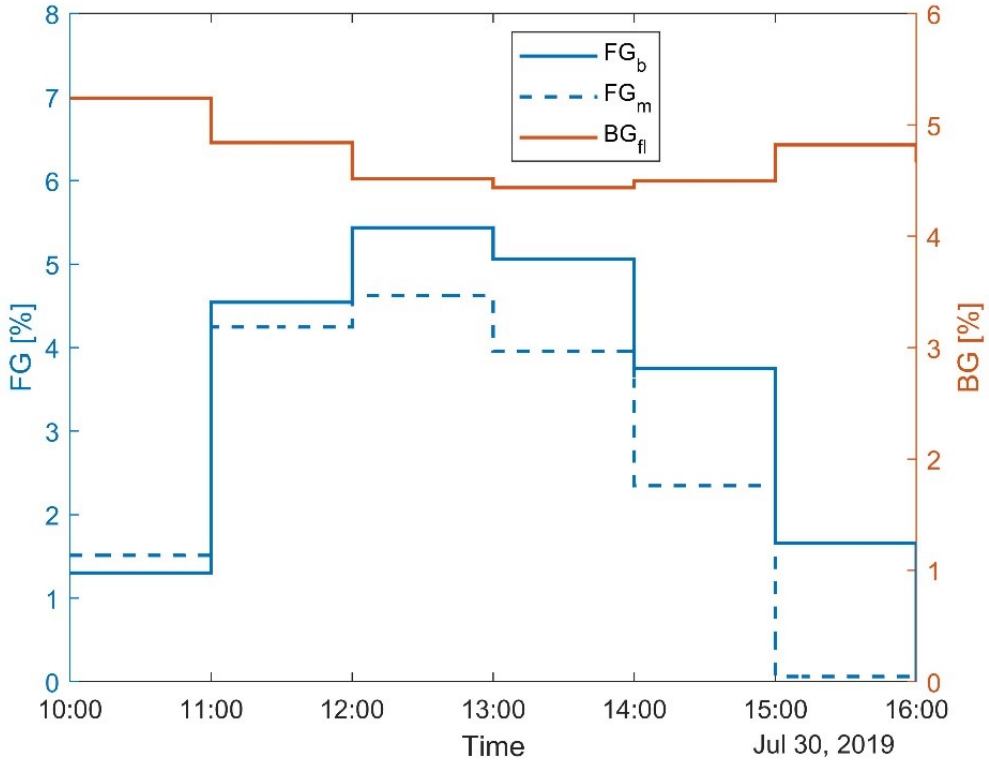

Figure 73 BG and FG for FPV mono and bifacial cooled systems

In Figure 73 can be see how at 10 am the *FG* is minimal and at 4 pm the monofacial is approaching a zero gain while the bifacial continues to have positive gain, and then in the next hour it too goes to a negative gain. At that point it will no longer be convenient to activate the active cooling system.

The maximum values of *FG* are obtained from 12 am to 13 am and are equal to 5.43% and 4.62% respectively for the mono and bifacial FPV.

The BG_{fl} trend is minimal and equal to 4.44% in the hours in which the solar height is maximum, since at that point the radiation reflected by the water is minimal. BG_{fl} is maximum and equal to 5.24% (see right axis) at 10 am.

Table 25 shows the values of *FG* and *BG* of the entire period under examination obtained in the various cases studied, therefore: passive cooling; active cooling without considering the pump consumption; active cooling considering the pump consumption.

Table 25 Performances indexes for mono and bifacial modules with active and passive cooling

	Passive cooling	Active cooling	
Energy of pumping	-	not considering energy consumption	considering energy consumption
FG_b [%]	3.0	9.7	3.8
FG_m [%]	2.6	9.5	3.0
BG_{fl} [%]	3.8	4.0	4.7
BG_{fl}+FG_m [%]	6.4	13.5	7.7
$\Delta\eta_b$ [%]	103.8	109.6	104.2
$\Delta\eta_m$ [%]	103.5	109.4	103.7

It should be noted that the (ideal) rooftop system does not take into account the losses due to dirt, losses of conductors and reciprocal shading of the rows, therefore these results are indicative of a marked improvement in the performance of modules installed in the water.

6.4 Conclusions

A bifacial gain *BG* of 5.24% was detected. An increase in the collected energy *FG* of 3% and 2.6% respectively for the bifacial and monofacial systems was calculated, with a maximum achievable for the bifacial floating compared to the monofacial on the rooftop equal to 6.4% in the case of passive cooling. Annual studies show an increase in performance that goes over 7%.

An increase in the collected energy *FG* of 9.7% and 9.5% respectively for the bifacial and monofacial systems was calculated, with a maximum achievable for the bifacial floating compared to the monofacial on the rooftop equal to 13.5% in the case of active cooling. This results are in line with the studies of literature.

Thanks to these models, it will be possible to attribute to FPV systems the increase in energy yield due to the type of cooling technique adopted.

Then, the results obtained in this study will be used for the economic evaluation of FPV systems to take into account the effect of natural and forced cooling with water.

7 Adaptation of PV simulation software to FPV systems

7.1 Introduction

The purpose of this chapter is to implement a methodology that allows to adapt the simulation software of the classic PV systems installed on the ground to FPV systems in order to evaluate their performance in the long-term period. In this regard, starting from some considerations on thermal models, on the geometry of the system and on the microclimatic conditions in which an FPV system operates, the main commercial software PVsyst and SAM of NREL have been adapted for use. Using the experimental data of a plant installed at the "Enel Innovation Lab" of Catania (IT) (see Chapter 3 for the description of the plant), adequate heat transfer coefficients of the most commonly thermal models were calculated by the two software, which allowed to take into account the thermal effects for this type of installations. The simulated data for a GPV system are compared, by means of performance indices, with the data of an FPV system. In addition, the models of the monofacial modules are compared with the bifacial ones. Albedo is a sensitive factor mainly for bifacial modules, therefore it has been considered as a parameter in the various proposed solutions. Since the analysis of photovoltaic systems is strongly site-dependent, the study was developed for two locations, characterized by different components of diffuse solar radiation and albedo, in particular at high latitudes (Frankfurt, DE) and at intermediate latitudes (Catania, IT).

This is a preliminary study to the next chapter which will allow to carry out long-term simulations on the energy performance of FPV systems in order to evaluate both the energy increase due to passive cooling and the competitiveness in economic terms compared to a GPV system.

7.2 Preliminary information

The PV floating system analysed consists of two floating PV fields, one made of monofacial modules and the other made of bifacial modules. The PV systems studied

in this chapter are realized at the experimental site of the Enel Innovation Lab (Enel Green Power) in Catania (Italy). (See Chapter 3 for the description of the plant.

The system simulations are developed by two software tools, hereinafter referred to as csw1 and csw2, while data processing was performed in the MATLAB environment.

The energy performances could change if the geometric variables, such as tilt and the azimuth angles, change during the passage of the waves under the floating structure.

As for azimuth angle, thanks to the use of effective mooring solutions, for instance by elastic mooring systems [115] the effect on production in relation to the change of orientation of a few degrees is negligible.

The effect on tilt of the passage of a wave is reported in Figure 74, at the beginning the pontoon is in a horizontal condition and the angle of incidence between the normal to the module and the solar beam is θ_0, subsequently, at the wave passage, the pontoon tilts and the angle of incidence becomes $\theta_0 + \theta_{waves}$, in the next phase it tilts an angle opposite to the previous one and the angle of incidence is $\theta_0 - \theta_{waves}$ and finally in the last phase it returns to the state of quiet with angle of incidence θ_0.

Under the assumption that the PV system is working at maximum power point, as a first approximation, the PV power is, proportional to the irradiance, so there is linear dependency between Power and irradiance.

Under this assumption the global effect of the variation of the tilt angle on the energy production is nil.

On the other hand, the impact of the variation of the temperature due to the variation of irradiance can be neglected due to the thermal inertia of the PV module and the frequency of the wave phenomenon.

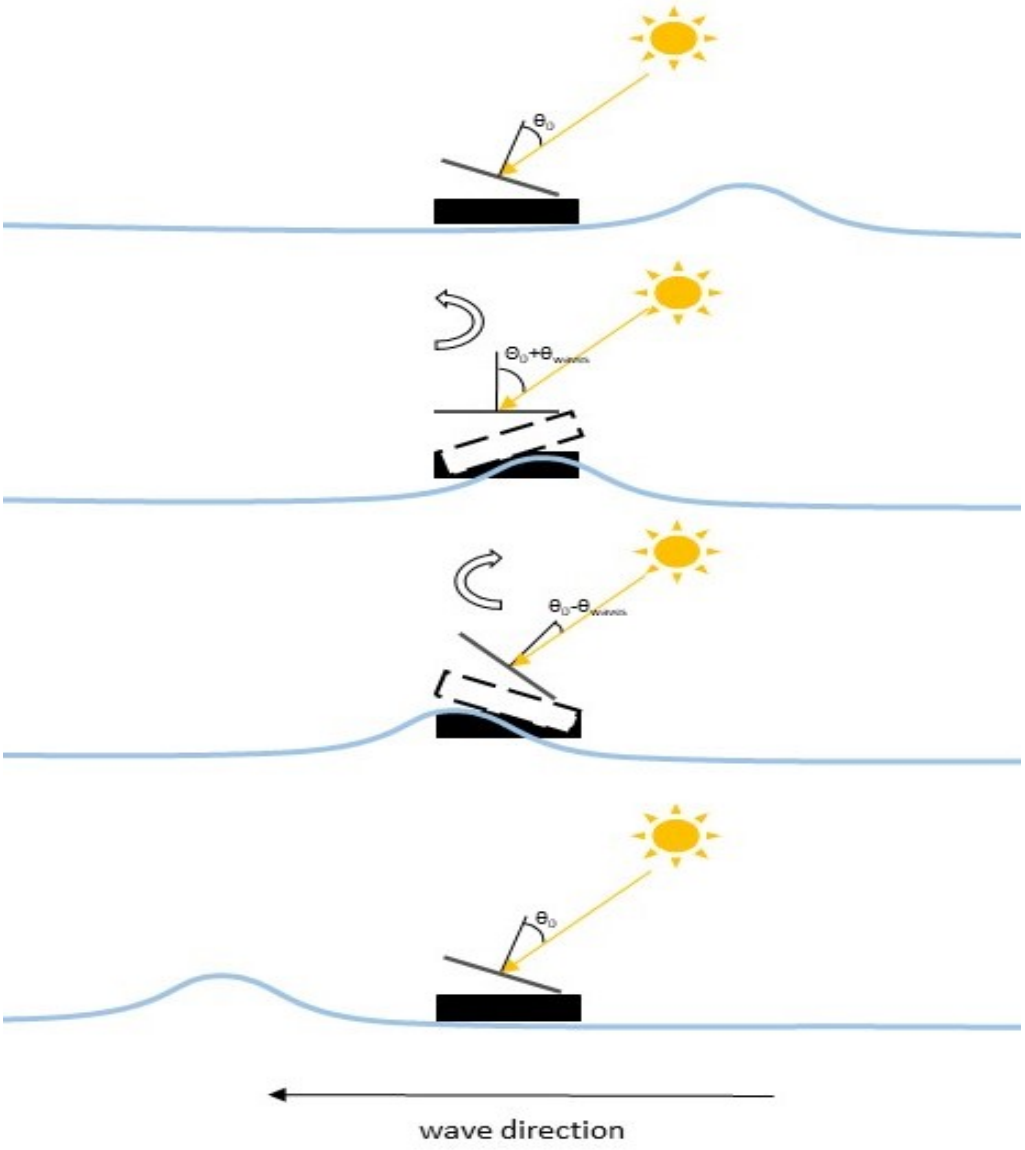

Figure 74 Effect of the waves on the pontoon.

The impact of tilt variation is also dependent on the type of floating structure [116], since in case of rigid floating platforms the waves affect the orientation of the whole PV system, whereas in case of no rigid floating systems some PV modules can undergo to a local angle variation. In this case a mismatch of irradiance among modules that belong to the same string can determine losses [117].

In the final analysis it is important to emphasize that usually floating photovoltaics are designed for water basins where there are favourable climatic conditions (low wind

and waves). Whereas for offshore applications, both from the point of view of the high demanding mechanical design of the structures and of duration of the components (reduced due to the salty ambient), it may not be convenient [84]. Moreover, in the latter case, appropriate simulation models may be needed for performance evaluation [118].

7.3 Models comparison

A performance comparison between mono- and bifacial systems is critical due to both different definitions of rated power and converted solar energy quantities.

In this chapter, first, the yearly energy yield Y', in kWh, is evaluated then it is normalized with respect to peak power, in kW. The calculation equations of this index are shown in Eq. 114 and Eq. 115.

The bifacial gain, BG (in %), defined in Eq. 1 is used to evaluate the energy gain of a bifacial system compared to a monofacial system.

The comparison of the performance between the ground and floating systems is important for evaluating the actual increase in energy produced. To evaluate this increase, it is calculated the floating gain (FG) of Eq. 116.

The ground system is taken as a reference, in which the heat exchange coefficients of the thermal models are those usually used for free mounted systems with air circulation and are compared with the floating systems whose heat exchange coefficients of the thermal models are those obtained for the floating experimental plant installed at the "Enel Innovation Lab" of Enel Green Power in Catania (IT).

7.4 Software adaptation and PV technology comparison

This section will describe the methodology adopted to adapt software to simulation for monofacial and bifacial FPV systems.

The models of the mono and bifacial systems will be compared, and an optimization of the producibility with respect to the geometric variables of the photovoltaic system will be carried out.

The used software programs for simulations are: PVsyst (csw1) and SAM (csw2), which are commercial software specialized for sizing and analysis of PV systems. The programs have been chosen as are more common on the market. Furthermore, among the software tools on the market, used for calculating the performance of the PV systems, these give the possibility of simulating also bifacial PV systems.

The simulations were carried out by changing the three geometrical parameters of the PV systems, graphically described in Figure 25. Specifically, the pitch, d_r, is normalized with respect to the length of the module, L (the dimension of the PV module perpendicular to the row direction) and tilt $\gamma_{Mm/b}$ of modules; for bifacial systems, the height from the surface of the water, h_w, is also considered.

7.4.1 Calibration of models

To adapt the software models to the floating applications, the experimental data were compared with the models of the two software programs, csw1 and csw2, where the following geometric configuration was considered: $d_r/L=1.55$, $\gamma_{Mm/b}=20°$ and $h_w=0.4$ m. The heat exchange coefficients of the models, which minimized the error with respect to the measured data, both in terms of temperature and estimated power, were obtained.

PV module temperature, current, voltage and DC and AC power produced by the two systems were measured as well as the environmental variables. Specifically, ambient temperature, diffuse and global solar irradiance, and wind speed are the inputs of the software used to simulate the systems. These data were collected by the meteorological station run by Enel Green Power. It is positioned (37° 24'41.4 "N 15° 02'38.4" E, IT) near the perimeter of the reservoir where the floating photovoltaic system is installed (for more detail see Chapter 3).

Two clear-sky days (13 and 14 July 2019) and two cloudy days (15 and 16 July 2019) were chosen to test the software. The environmental data are measured every minute, but considering the hourly analysis performed by the software tools, the measured data are hourly averaged. The measured meteorological variables and their hourly averaged values are shown in Figure 75.

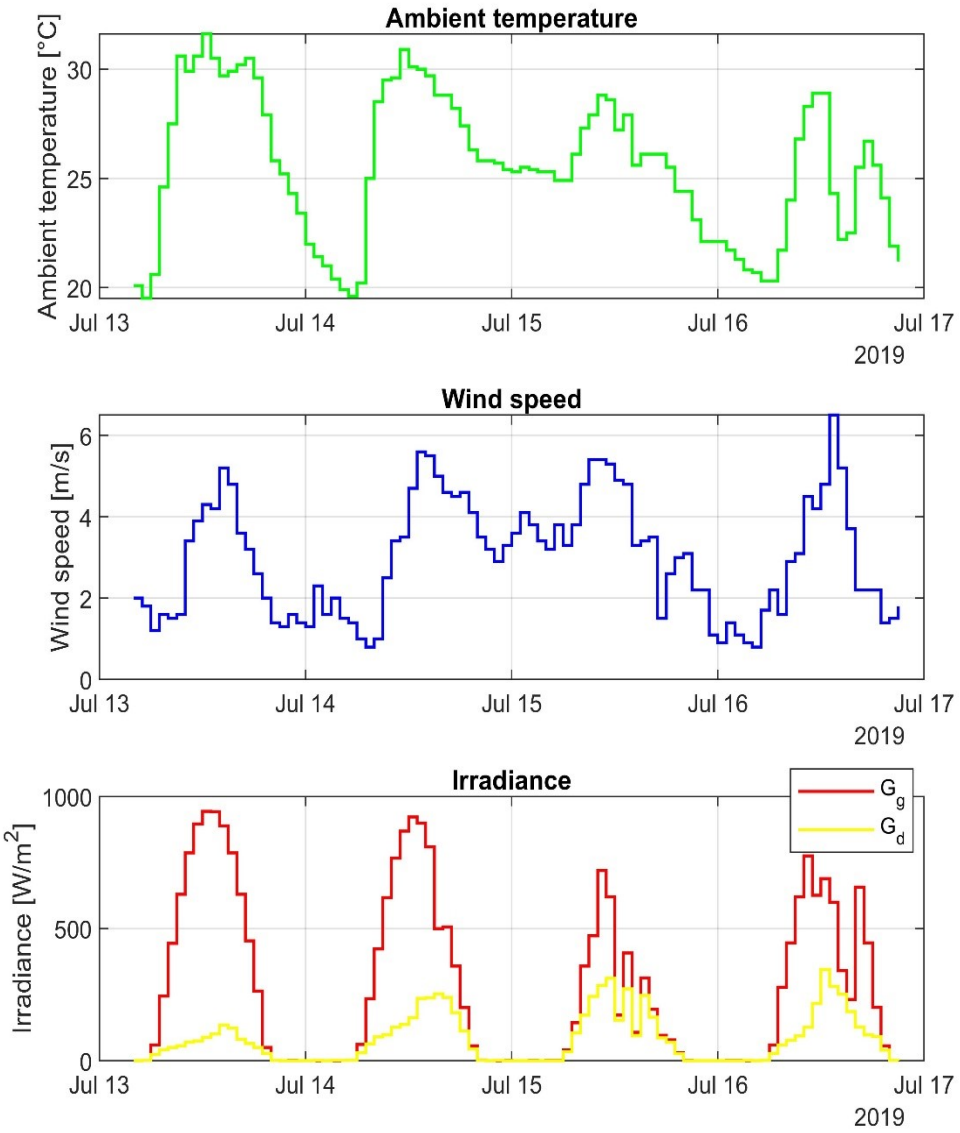

Figure 75 Weather data from 13 to 16 July 2019

7.4.1.1 Thermal models validation

In this paragraph, the temperature of the back of both the mono- and bifacial modules measured in the experimental system are compared with the cell temperature calculated by the two software packages csw1 and csw2. The cell temperature of csw1 is calculated using Eq. 117 [16], while the cell temperature calculated by csw2 is carried out using Eq. 118 and Eq. 119 [98].

$$T_{pv} = T + \frac{\alpha\, G_T(1-\eta_{ref})}{U_0 + U_1 u_v} \qquad \textbf{Eq. 117}$$

where U_0 and U_1 depend on the type of installation.

$$T_{pv} = T_m + \frac{G_T}{1000}\Delta T_{pv-bk} \quad \textbf{Eq. 118}$$

where T_m of Eq. 118 and Eq. 119 depends on the different solar array structures and mounting.

$$T_m = G_T e^{a+bu_v} + T \quad \textbf{Eq. 119}$$

In order to make the models usable in the case of floating systems, an optimization algorithm has been developed whose purpose is to obtain the heat transfer coefficients of equations Eq. 117 and Eq. 118 starting from the temperature values measured in the real system installed on the lake of Enel Green Power (Enel Innovation Lab of Catania (IT)).

For the optimization of the coefficients, the MATLAB function 'fmincon' was used, the operative variables (U_0, U_1, a and b) are forced to vary between lower and upper limits to maintain their physical values and, the optimization function was the minimization of the RMSE between the measurements and the numerical results [119].

To clarify what is described, an algorithm flow chart is shown in Figure 76.

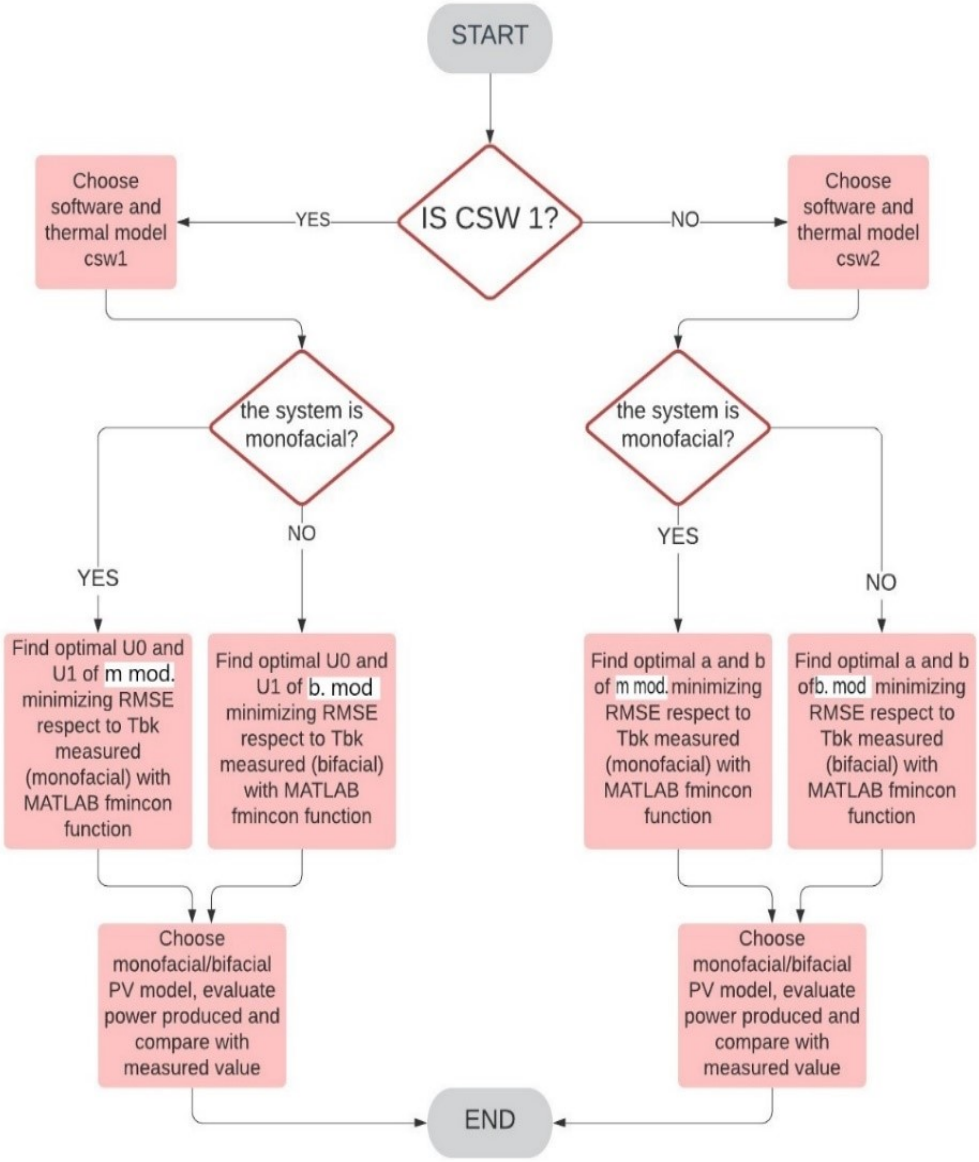

Figure 76 Flow chart for the optimization of the heat transfer coefficients of the temperature models of the software csw1 and csw2

The csw1 software optimization algorithm has been set up as follows:

$$U_{0min} \leq U_0 \leq U_{0max} \quad \textbf{Eq. 120}$$

$$U_{1min} \leq U_1 \leq U_{1max} \quad \textbf{Eq. 121}$$

$$obj = \min\left(RMSE(T_{pv}, T_{bk\,measured})\right) \quad \textbf{Eq. 122}$$

Where $U_{0min} = 10, U_{0max} = 40, U_{1min} = 1,\ U_{1max} = 2$

The csw2 software optimization algorithm has been set up as follows:

$$a_{min} \leq a \leq a_{max} \quad \textbf{Eq. 123}$$

$$b_{min} \leq b \leq b_{max} \quad \textbf{Eq. 124}$$

$$obj = \min\left(RMSE(T_{pv}, T_{bk\,measured})\right)$$ **Eq. 125**

Where $a_{min} = -4$, $a_{max} = -3$, $b_{min} = -0.08$, $b_{max} = -0.05$

Monofacial PV plant results:

For the model of the csw 1 software, U_0 =31.92 and U_1 =1.5 have been obtained with optimization. For the model of the software csw2, a=-3.743 and b=-0.0746 have been obtained with optimization. These coefficients have made it possible to adapt the thermal models of monofacial modules of commercial software to floating systems.

Figure 77 shows the plot of the measured back-surface PV module temperature on a string of the monofacial system (solid line) and the plots of the temperature calculated by csw1 and csw2 (dashed lines).

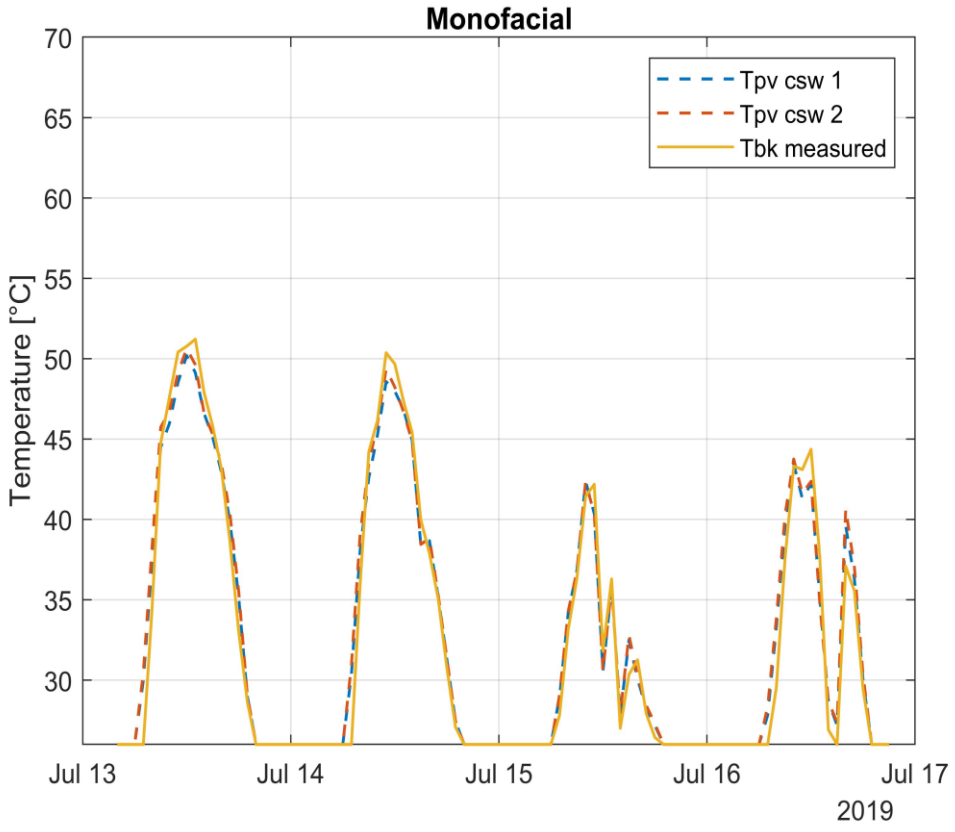

Figure 77 Monofacial temperature comparison measure vs csw1 and csw2

Bifacial PV plant results:

For the model of the csw1 software, U_0 =35.22 and U_1 =1.5 have been obtained with optimization. For the model of the software csw2, a=-3.876 and b=-0.0738 have been obtained with optimization. These coefficients have made it possible to adapt the thermal models of bifacial modules of commercial software to floating systems.

Figure 78 shows the plot of the measured back-surface PV module temperature on a string of the bifacial system (solid line) and the plots of the temperature calculated by csw1 and csw2 (dashed lines).

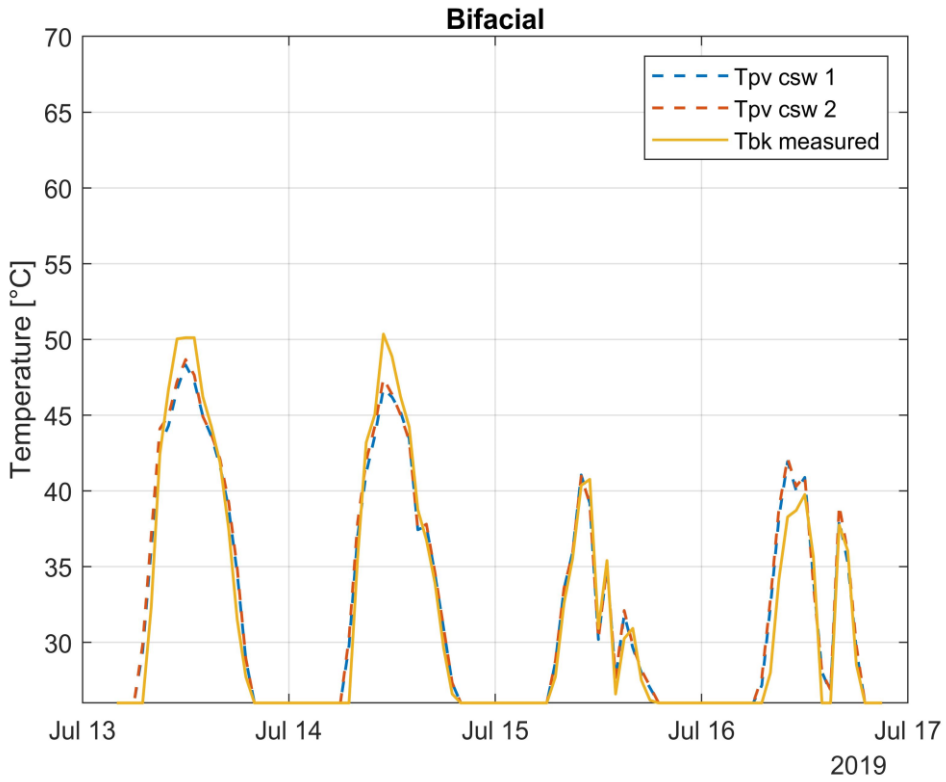

Figure 78 Bifacial temperature comparison measure vs csw1 and csw2

Table 26 shows the statistical indices for mono- and bifacial PV module temperatures calculated by the csw1 and csw2 software tools considering the measurements as a reference.

Table 26 Statistical indices of mono- and bifacial PV module temperatures calculated by the models implemented in csw1 and csw2.

System	csw	MAE[°C]	RMSE [°C]	PE [%]	R^2
monofacial	1	0.77	1.27	0.43	0.98
	2	0.83	1.41	1.01	0.97
bifacial	1	0.89	1.46	0.60	0.97
	2	0.94	1.55	1.10	0.96

In the case of the monofacial and bifacial system, both models are performing. In fact, the correlation coefficients are between 0.98 and 0.97 for csw1 and 0.97 and 0.96 for csw2. The MAE is between 0.77 and 0.94 [°C], RMSE is between 1.27 and 1.55 [°C].

Furthermore, the percentage error values range from a minimum of 0.43% to a maximum of 1.10 %.

The back-surface temperature is a good approximation of the actual cell temperature, and studies have shown that solar cells typically run 3 °C warmer than back-surface temperatures for glass–glass laminate constructions [98].

7.4.1.2 Power comparison

In this paragraph, the power measured in the experimental systems of both mono- and bifacial modules are compared with the power calculated by csw1 and csw2. From the analysis of the electrical behaviour of the two strings of each system, it has been noted that they show the same behaviour in terms of power production, so for the sake of simplicity, the power of a single string for each system is reported. The comparison power was the upstream of the inverter (DC).

Monofacial PV plant results

Figure 79 shows the plot of the measured power on a string of the monofacial system (solid line) and the plots of the power calculated by csw1 and csw2 (dashed lines). It is worth noticing that during clear days the software csw2 underestimates the power. On cloudy days both software obtains results very close to the measured values.

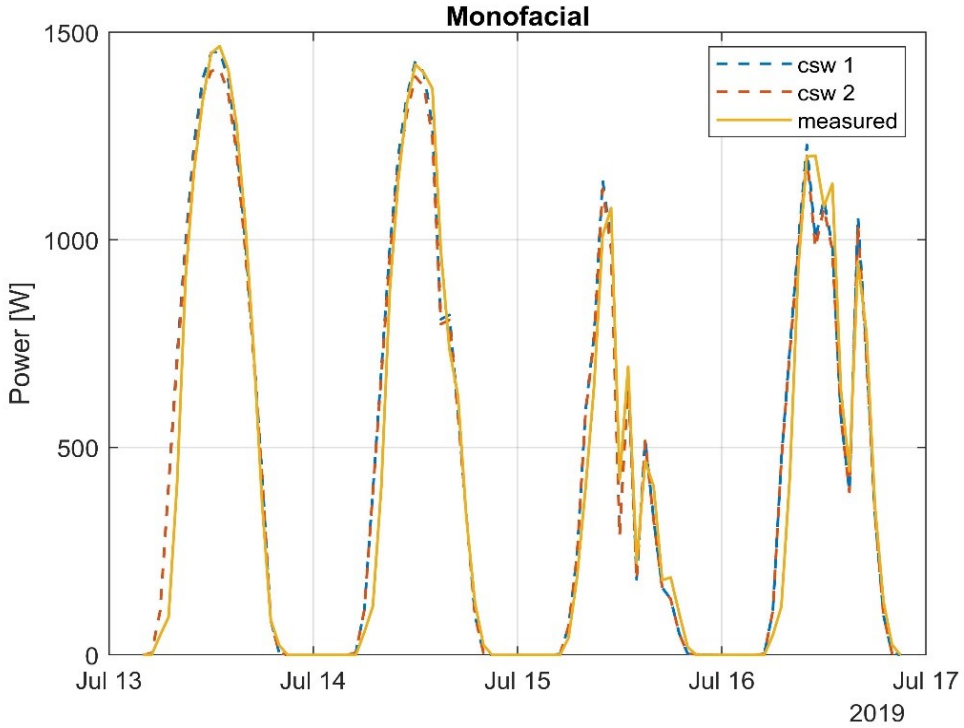

Figure 79 Monofacial power comparison measure vs csw1 and csw2

Bifacial PV plant results

Figure 80 shows the plot of the measured power on a string of the bifacial system (solid line) and the plots of the power calculated by csw1 and csw2 (dashed lines). It is worth noting that during clear days, csw1 overestimates the power. On cloudy days, the calculated values of both software obtain results very close to the measured values.

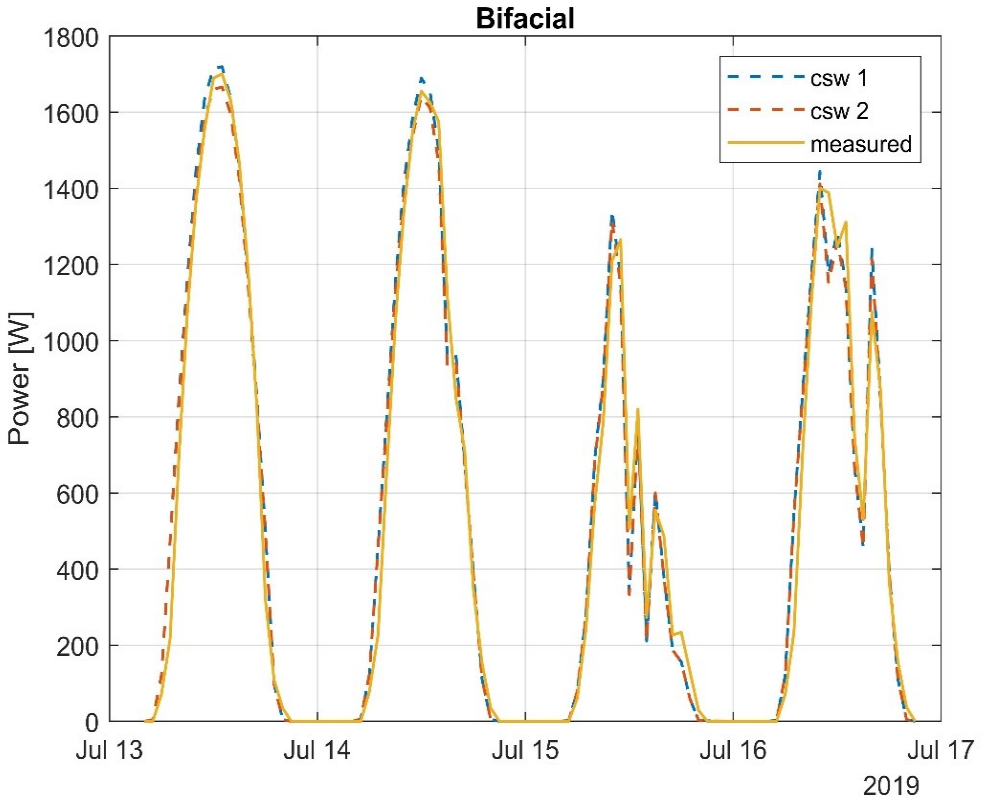

Figure 80 Bifacial power comparison measure vs csw1 and csw2

Table 27shows the statistical indices for the power calculated for the csw1 and csw2 software tools and taking the measurements as a reference.

Table 27 Statistical indices of the power of mono- and bifacial PV modules calculated by the models implemented in csw1 and csw2.

System	csw	MAE [W]	RMSE [W]	PE [%]	R^2
monofacial	1	54.84	98.14	4.71	0.97
	2	55.03	96.98	2.71	0.97
bifacial	1	54.71	86.23	3.23	0.98
	2	51.97	83.86	1.14	0.98

From the statistical analysis it can be seen that the two software, both in the case of monofacial and bifacial systems, are very performing. In fact, the correlation coefficients are between 0.97 and 0.98 for csw1 and csw2. The MAE is between 51.97 and 55.03 [W], RMSE is between 83.86 and 98.14 [W]. Furthermore, the percentage error values range from a minimum of 1.14% to a maximum of 4.71%.

7.4.2 Energy performance analysis and models comparison

This section will report the energy performance obtained from the simulations carried out using the methodology described above. The results will be shown for a common

geometric installation configuration, in which the angle of inclination has been optimized in relation to the distance between the rows (see Figure 25). The energy gains from bifaciality and natural cooling will be shown through the BG and FG indices respectively. The albedo is considered a parameter.

The model of the PV system is bi-dimensional, and it has been assumed that the shed layout is made of 40 rows. The electrical losses due to near shading are taken into account in the evaluation of Y, considering 3 bypass diodes in each PV module.

For the bifacial model, mismatch losses on the back of the module equal 2.5% and losses due to the shading of the structures equal 2.5% were considered. Furthermore, a 10% shed transparent fraction was considered.

The values of $Y_{m/b\text{-}gr}$ are calculated using the heat exchange coefficients of the thermal models for installations of free mounted modules with air circulation, while the values of $Y_{m/b\text{-}fl}$ are calculated using the coefficients obtained starting from the methodology adopted in previous paragraph.

The data acquisition and processing algorithm used for the geometric optimization of the system in the two case studies examined is shown in Figure 81.

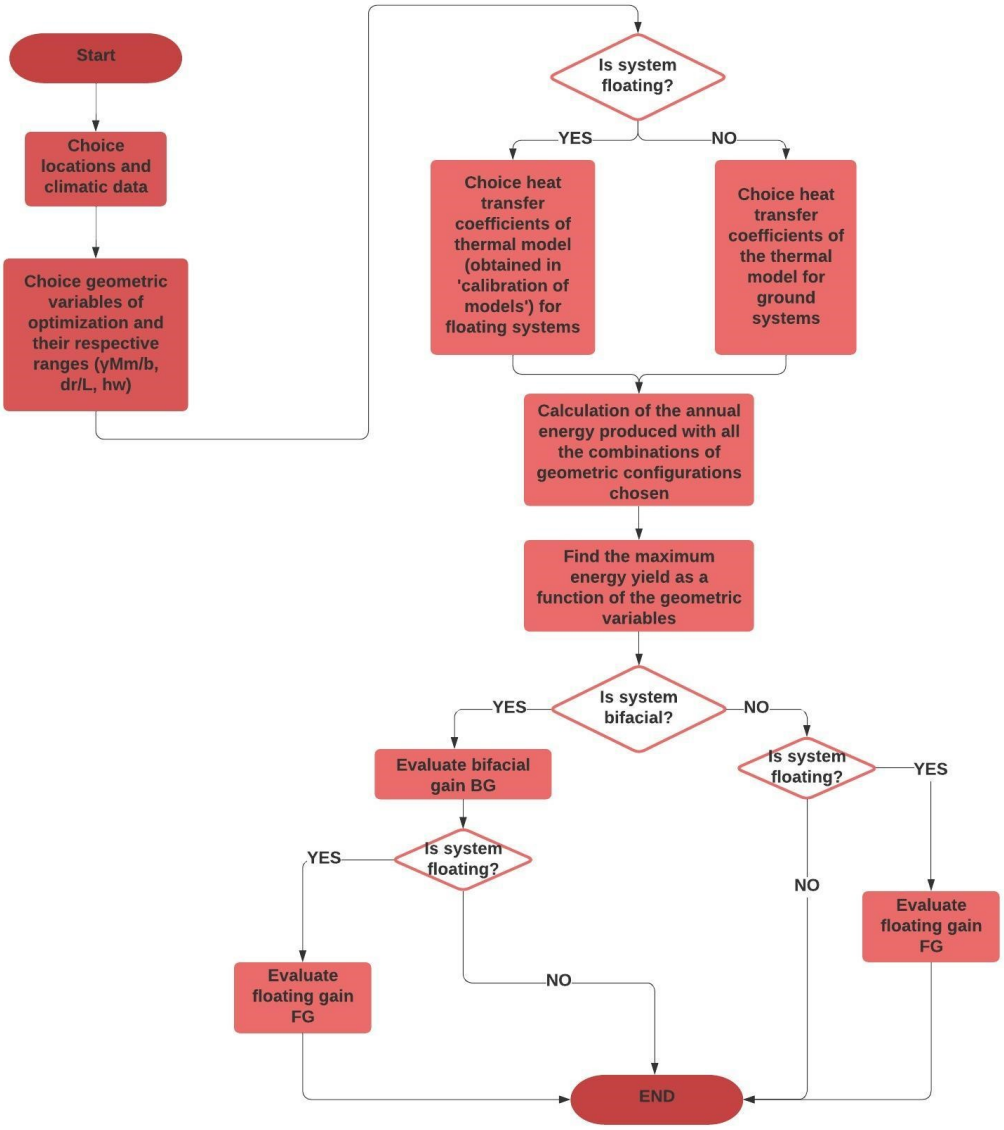

Figure 81 Algorithm of geometrical optimization

7.4.2.1 Catania

Monofacial technology: Table 28 shows the results obtained in terms of equivalent hours Y of operation of the plant in one year and natural cooling FG of the modules.

Table 28 Performances of monofacial system (Catania)

d_r/L	γ_{Mm}	a (%)								
		20	10	5	20	10	5	20	10	5
		$Y_{m\text{-}gr}$			$Y_{m\text{-}fl}$			FG (%)		
1.55	20	1655	1654	1654	1737	1737	1737	4.7	4.8	4.8

From the results, there is no ΔY_m when the albedo varies (moving horizontally in Table 28). This finding demonstrates the fact that monofacial systems, if the albedo variability is relatively small, are not very sensitive to this parameter.

The energy gain of a floating system (FG) compared to a ground system varies from 4.7 to 4.8%.

Bifacial technology: Table 29 shows the results obtained in terms of equivalent hours Y of operation of the plant in one year and natural cooling FG of the modules in the case of h_w = 0 m.

Table 29 Performances of bifacial system with h_w = 0 m

d_r/L	γ_{Mb}	a (%)								
		20	10	5	20	10	5	20	10	5
		$Y_{b\text{-}gr}$			$Y_{b\text{-}fl}$			FG (%)		
1.55	20	1759	1724	1706	1888	1849	1830	7.3	7.3	7.3

The bifacial module, as can be seen from Table 29 is more sensitive to albedo, therefore when estimating the energy performance it is important to know in advance the reflection coefficient of the ground or water. The FG of the floating system for the bifacial module with an albedo of 5% shown in Table 29 is 7.3%. The results for h_w=0.9 m are shown in Table 30.

Table 30 Performances of bifacial system with h_w = 0.9 m

d_r/L	γ_{Mb}	a (%)								
		20	10	5	20	10	5	20	10	5
		$Y_{b\text{-}gr}$			$Y_{b\text{-}fl}$			FG (%)		
1.55	20	1790	1739	1713	1921	1866	1838	7.3	7.3	7.3

Table 30 shows that for h_w=0.9 m, the variation of Y in function to albedo become more significant.

Bifacial gain: The energy gains (Eq. 1) of the bifacial system compared to the monofacial have been calculated, taking as a reference the monofacial at the different albedo and the different heights.

Table 31 shows BG at h_w=0 m.

Table 31 Bifacial gains for h_w=0 m

d_r/L	γ_{Mb}	γ_{Mm}	a (%)		
			20	10	5
			BG_{fl}		
1.55	20	20	8.6	6.4	5.3

Table 31 shows that at h_w=0 m, for an albedo of 5%, the BG is equal to 5.3%.

Table 32 shows BG at h_w=0.9 m.

Table 32 Bifacial gains for h_w=0.9 m

d_r/L	γ_{Mb}	γ_{Mm}	a (%)		
			20	10	5
			BG_{fl}		
1.55	20	20	10.6	7.4	5.8

Table 32 shows that at h_w= 0.9, for an albedo equal to 5%, the BG is equal to 5.8.

7.4.2.2 Frankfurt

Monofacial technology: Table 33 shows the results obtained in terms of equivalent hours Y of operation of the plant in one year and natural cooling FG of the modules.

Table 33 Performances of monofacial system

d_r/L	γ_{Mm}	a (%)								
		20	10	5	20	10	5	20	10	5
		$Y_{m\text{-}gr}$			$Y_{m\text{-}fl}$			FG (%)		
1.55	20	964	963	963	997	996	996	3.4	3.4	3.4

Similar considerations made regarding the Catania case can be made here. The energy gain of a floating system (FG) compared to a ground system is 3.4% that is lower than Catania due to different climatic conditions.

Bifacial technology: Table 34 shows the results obtained in terms of equivalent hours Y of operation of the plant in one year and natural cooling FG for the bifacial modules installed at h_w = 0 m.

Table 34 Performances of bifacial system with h_w = 0 m

d_r/L	γ_{Mb}	a (%)								
		20	10	5	20	10	5	20	10	5
		$Y_{b\text{-}gr}$			$Y_{b\text{-}fl}$			FG (%)		
1.55	20	1033	1010	998	1090	1066	1053	5.5	5.5	5.6

By comparing the Y values as a function of the albedo in Table 33 and Table 34, it is noted that the bifacial system is much more sensitive to albedo parameter than the monofacial.

The energy gain (FG) of the floating system compared to the ground system varies from 5.5 to 5.6%.

Table 35 shows the results obtained in terms of equivalent hours of operation Y of the plant in one year and natural cooling FG for the bifacial modules installed at h_w = 0.9 m.

Table 35 Performances of bifacial system with h_w = 0.9 m

d_r/L	γ_{Mb}	a (%)								
		20	10	5	20	10	5	20	10	5
		$Y_{b\text{-}gr}$			$Y_{b\text{-}fl}$			FG (%)		
1.55	20	1051	1019	1003	1093	1065	1051	5.6	5.5	5.5

Similar considerations made regarding the Catania case can be made here. Moving horizontally in Table 35, there is considerable energy variation, perhaps because for places at high latitudes, the albedo is more important since the back of the module works mainly with diffuse radiation, which surely has a higher percentage in Frankfurt than in Catania. Therefore, knowing a priori the reflection coefficient of water and its variations throughout the year leads to minimizing the error in estimating the performance of a bifacial system.

The energy gain of the floating system (FG) compared to the ground system varies from 5.6 to 5.5%.

Bifacial gain: Table 36 shows the results obtained of BG in one year at h_w = 0 m.

Table 36 Bifacial gain for h_w = 0 m

d_r/L	γ_{Mb}	γ_{Mm}	a (%)		
			20	10	5
			BG_{fl}		
1.55	20	20	9.4	7.0	5.7

As the results show, for the same system with the same peak power with optimal configuration, the BG is more sensitive to the albedo in Frankfurt than in Catania. This is because the back of the module works more with reflected and diffuse radiation. The BG with h_w = 0 m reaches up to 9.4%.

Table 37 shows the results obtained of BG in one-year with h_w = 0.9 m.

Table 37 Bifacial gain for $h_w = 0.9$ m

d_r/L	γ_{Mb}	γ_{Mm}	a (%)		
			20	10	5
			BG_{fl}		
1.55	20	20	11.3	7.9	6.2

The BG with $h_w = 0.9$ m reaches up to 11%. The results highlight the fact that in the presence of more diffuse radiation, bifacial systems increase their energy yield.

7.5 Conclusions

It was shown that with the studied configurations, it is possible to obtain energy gains with bifacial modules, which reach up to 11% compared to monofacial configurations. Furthermore, for the two studied sites (Catania and Frankfurt), it was noted that in Frankfurt, where the diffusion factor is greater than in Catania, there is a greater bifacial gain. Monofacial systems, unlike bifacial systems, have a lower sensitivity to albedo.

For the analysed configurations, the trend of the BG as a function of h_w is exponential and then saturated at 0.9 m.

Furthermore, if the pitch is increased up to 2.5 m, the saturation point of h_w will move to 1.5 m, and a BG up to 15% can be obtained with such configurations.

Using the heat transfer coefficients for thermal models obtained from the experimental data of the floating plant installed in Catania, has been obtained a gain of floating systems (FG) between 3.4 and 5.6% for Frankfurt and between 4.7 and 7.3% for Catania.

For more details on the optimization of the geometry of an FPV system in relation to energy performance, please refer to ref. [119]

Thanks to this study, in the next chapter it will be possible to carry out long-term simulations for different types of plants (mono or bifacial, fixed and tracking) which will allow to estimate the performance of a floating or ground system in relation to the geometric configuration adopted. Furthermore, it will be possible to evaluate, in relation to performance, the economic competitiveness of an FPV system compared to a GPV.

8 Energy performance analysis of different FPV design solutions

8.1 Introduction

The purpose of this chapter is to evaluate the energy performance on an annual basis of a fixed G/FPV system, with vertical, horizontal or two-axis tracking, with mono or bifacial modules. The values obtained will be used for the economic calculations of the various plant solutions considered which will be addressed in the following chapters. The simulated data for FPV systems will be compared with those of a GPV system through performance indexes in order to evaluate the benefits in terms of performance of these solutions. The energy performance analysis will be performed in relation to the geometric variables of the plant. Since the analysis of photovoltaic systems is highly site-dependent, the study was developed for two locations, characterized by different components of diffuse solar radiation, in particular at high latitudes and intermediate latitudes.

8.2 Methodology

In this paragraph, the methodology that leads to the results obtained regarding the different cases examined will be illustrated.

The performance study of a floating system has been developed for two basins: one at high latitudes (Aar Dam, DE) and one with intermediate latitudes (Anapo, IT). Weather data are taken from the Meteonorm database, with a one-hour step for the entire year. During the simulations, the albedo is assumed constant and equal to 5%, since in most cases, FPV systems are installed at sites where the presence of waves is limited. It is clear that when there is a noticeable rippling of the surface of the water, the phenomenon of the diffusion of the reflected radiation is generated; therefore, considering a constant albedo is no longer possible [119]. These two sites were chosen to evaluate the behaviour of the bifacial modules at different latitudes, where the percentage of diffuse horizontal irradiance with respect to the global horizontal irradiance is different and the impact of natural cooling of FPV is different due to climatic conditions.

The PV floating/ground systems analysed consists of two PV fields, one made of monofacial modules and the other made of bifacial modules. The system simulations are developed by PVsyst software tools, while data processing was performed in the MATLAB environment.

Each field, whose rated power is 16.32 kW for the mono and bifacial system, has 48 modules, divided into 4 strings that are connected to a multi-string inverter equipped with separate MPP trackers. The modules are Jinkosolar Si-mono JKM340M-60H-V (monofacial) and JKM340M-60H-BDVP (bifacial). The inverter is SMA SunnyBoy 9.0 kW 9000TLUS-12.

The model of the PV system is bi-dimensional, the effect of shading was considered linear, therefore without evaluating the electrical effect. For the bifacial model, mismatch losses on the back of the module equal 2.5% and losses due to the shading of the structures equal 2.5% were considered. Furthermore, a 10% shed transparent fraction was considered.

8.2.1 Configurations analysed

This work analyzes the performance of floating and ground photovoltaic systems, with tracker or fixed. Specifically, the following configurations will be analysed (on ground and floating):

- FXPVm Fixed PV Monofacial
- FXPVb Fixed PV Bifacial
- FXGPVm Fixed Gable PV Monofacial
- HATPVm Horizontal Axes Tracker PV Monofacial
- HATPVb Horizontal Axes Tracker PV Bifacial
- VATPVm Vertical Axes Tracker PV Monofacial
- 2AXTPVm Dual Axis Tracker PV Monofacial

The simulations were carried out by varying three geometric parameters of the photovoltaic systems, namely tilt angle ($\gamma_{Mm/b}$ (°)), distance between the rows d_r normalised respect to length of modules L and azimuth angle Φ (the value of 0 correspond to axes parallel to N-S and 90 parallel to E-W). The representation of the variables is reported on Figure 25.

Table 38 shows the lower and upper limits of the variables.

Table 38. Geometrical variables of the PV systems

Variable	Min. value	Max. value
2AXTPV		
$\gamma_{Mm/b}$ (°)	0-50	
d_r/L	1.2	3.0
Φ(°)	±120	
HATPV		
$\gamma_{Mm/b}$ (°)	-30/-35/-40/-45/-50	30/35/40/45/50
d_r/L	1.2	3.0
Φ(°)	0	90
VATPV		
$\gamma_{Mm/b}$ (°)	20	30
d_r/L	1.2	3.0
Φ (°)	-120	120
FXPV		
$\gamma_{Mm/b}$ (°)	20	30
d_r/L	1.2	3.0
Φ(°)	0	0
FXGPV		
γ_{Mm} (°)	10	10
d_r/L	-	-
Φ(°)	90	-90

8.2.2 Thermal losses

In PVsyst the Faiman [16] model of Eq. 117 is used to estimate the temperature of PV. The quantity U_0 and U_1 for the FPV are chosen respectively as follow [119]:

- 35.22 W/m^2 K and 1.5 W/m^3 s K for bifacial
- 31.92 W/m^2 K and 1.5 W/m^3 s K for monofacial

The ground system is taken as a reference, in which the heat exchange coefficients of the thermal models are those usually used for free mounted systems with air circulation and are compared with the floating systems whose heat exchange coefficients of the thermal models are those obtained for the floating experimental plant installed at the "Enel Innovation Lab" of Enel Green Power in Catania (IT) [119].

8.2.3 Comparison indices

The yearly energy yield Y', BG, FG, are evaluated as reported in Eq. 114 and Eq. 115, Eq. 1 and Eq. 117 respectively.

To compare the gable systems (FXFGPV or FXGGPV) with the fixed systems (FXPV) can be use the GG which is calculated with the following equation:

$$GG = 100\frac{Y_{\mathrm{FXFG}m} - Y_{FXFm}}{Y_{FXFm}}$$ **Eq. 126**

This index makes it possible to evaluate the gain or losses deriving from the gable installation compared to the classic fixed system oriented to the south.

To compare the tracking systems (TPV) with the fixed systems (FXPV) can be use the TG which is calculated with the following equation:

$$TG = 100\frac{Y_{TFm/b} - Y_{FXFm/b}}{Y_{FXFm/b}}$$ **Eq. 127**

TG is calculated comparing the same module technology (monofacial tracking with monofacial fixed or bifacial tracking with bifacial fixed).

From the combination of the performance indices listed above, the following indices can be obtained:

TBG which is the energy gain of the bifacial tracking system compared to the fixed system, calculated only for the floating system.

$$TBG = 100\frac{Y_{TFb} - Y_{FXFm}}{Y_{FXFm}}$$ **Eq. 128**

TFG which is the energy gain of the floating tracking system compared to the fixed ground system monofacial and bifacial.

$$TFG = 100\frac{Y_{TFm/b} - Y_{FXGm/b}}{Y_{FXGm/b}}$$ **Eq. 129**

TBFG which is the energy gain of the floating bifacial tracking system compared to the fixed ground system.

$$TBFG = 100\frac{Y_{TFb} - Y_{FXGm}}{Y_{FXGm}}$$ **Eq. 130**

All the indices are in percentage (%).

8.3 Results

In this sub-paragraph the results obtained in terms of energy yield of each analyzed system will be reported for two different locations, Anapo Dam (IT) and Aar Dam (DE).

8.3.1 Anapo Dam

This paragraph shows the results in terms of energy performance, obtained for the Anapo locality with coordinates 37.11° N, 15.13° E.

In the Anapo Dam is installed an HPP power plant, is in Sicily, in southern Italy just over 10 km north-west of the city of Syracuse.

It consists of two artificial basins:

- a lower artificial basin with an area of 0.46 km^2 and a volume of 7 million m^3.
- an upper artificial basin with an area of 0.36 km^2 and a volume of 5 million m^3. It is located at a maximum distance of 1 km on the mountain that forms the north (left) side of the Anapo Valley.

With an altitude difference of 312 meters between the reservoirs, the plant allows water equivalent to 4 million kWh of electricity to be stored.

The power station is equipped with four reversible hydraulic units with a capacity of 125 MW in turbine mode (generates energy) and 145 MW in pump mode (consumes energy).

8.3.1.1 Fixed systems

Table 39 shows the Y values (equivalent operating hours) of fixed ground and floating systems analysed. These values will serve as a reference for comparing the energy yield of mono and bifacial tracking systems and monofacial gable systems.

Table 39 $Y_{m/b}$ for fixed F/GPV systems

System	$\gamma_{Mm/b}$ [°]	Technology	d_r/L		
			1.2	2.1	3.0
			Y [h]		
FXGPV	20	m	1617.5	1722.7	1726.3
		b	1635.8	1757.0	1764.5
	25	m	1601.3	1736.6	1743.5
		b	1621.6	1774.3	1786.4
	30	m	1578.1	1737.4	1748.2
		b	1601.5	1779.4	1796.9
FXFPV	20	m	1690.5	1803.0	1806.9
		b	1714.4	1844.2	1852.1
	25	m	1673.2	1818.5	1825.8
		b	1699.1	1863.2	1876.0
	30	m	1648.2	1819.6	1831.0
		b	1677.1	1868.8	1887.4

Table 40 shows BG values for FPV fixed systems. BG values are obtained by comparing the same bifacial with monofacial configurations (for example 30 ° bifacial FXPV vs 30 ° monofacial FXPV).

Table 40 BG for fixed system

System	γ_{Mb} [°]	d_r/L		
		1.2	2.1	3.0
		BG [%]		
FXFPV	20	1.4	2.3	2.5
	25	1.5	2.5	2.8
	30	1.8	2.7	3.1

The highest BG for the fixed system is 3.1%.

Table 41 shows FG values for fixed systems that allow to evaluate the increase in performance due to the natural cooling of the modules of the FPV compared to the GPV, in various configurations for mono and bifacial modules.

Table 41 FG for fixed system

System	$\gamma_{Mm/b}$ [°]	Technology	d_r/L		
			1.2	2.1	3.0
			FG [%]		
FXFPV	20	m	4.5	4.7	4.7
		b	4.8	5.0	5.0
	25	m	4.5	4.7	4.7
		b	4.8	5.0	5.0
	30	m	4.4	4.7	4.7
		b	4.7	5.0	5.0

The highest FG for the fixed system is obtained for the tilt $\gamma_{Mm/b}$=30° and dr/L=3.0 configuration and is equal to 5%.

8.3.1.2 Gable systems

As discussed in the introductory part of this thesis work, gable solutions provide various advantages in terms of material savings and therefore CAPEX against of small energy losses that are dependent on latitude.

Table 42 shows the Y values, the gain/losses due to the system solution and the gain due to the cooling of the modules

Table 42 Ym, GGL and FG for gable solution

System	γ_{Mm} [°]	Technology	d_r/L=1.2		
			Y	GGL [%]	FG [%]
FXGGPV	10	m	1527.2	-5.6	-
FXGFPV	10	m	1591.6	-5.9	4.2

The gable solution, if compared with a classic ground system, for the considered latitude, loses 5.6% in the case of a ground system and 5.9% in the case of an FPV system. FG is equal to 4.2%

8.3.1.3 Horizontal single-axis tracking system E-W

Table 43 shows the Y (equivalent operating hours) of each type of system analysed.

Table 43 $Y_{m/b}$ for Horizontal single-axis tracking E-W F/GPV systems

System	$\gamma_{Mm/b}$ [°]	Technology	d_r/L		
			1.2	2.1	3
			Y [h]		
TGPV	±30	m	1653.2	1811.3	1821.2
		b	1673.9	1851.3	1866.6
	±40	m	1648.3	1833.8	1852.9
		b	1672.5	1876.5	1901.6
	±50	m	1643.4	1839.2	1866.0
		b	1671.0	1885.2	1918.5
TFPV	±30	m	1727.9	1897.5	1908.0
		b	1754.4	1945.3	1961.3
	±40	m	1722.9	1922.6	1942.6
		b	1752.9	1973.1	1999.4
	±50	m	1717.7	1928.9	1957.2
		b	1751.2	1982.8	2018.0

The Figure 82 is shown to illustrate the behavior of the various systems as the geometric quantities vary.

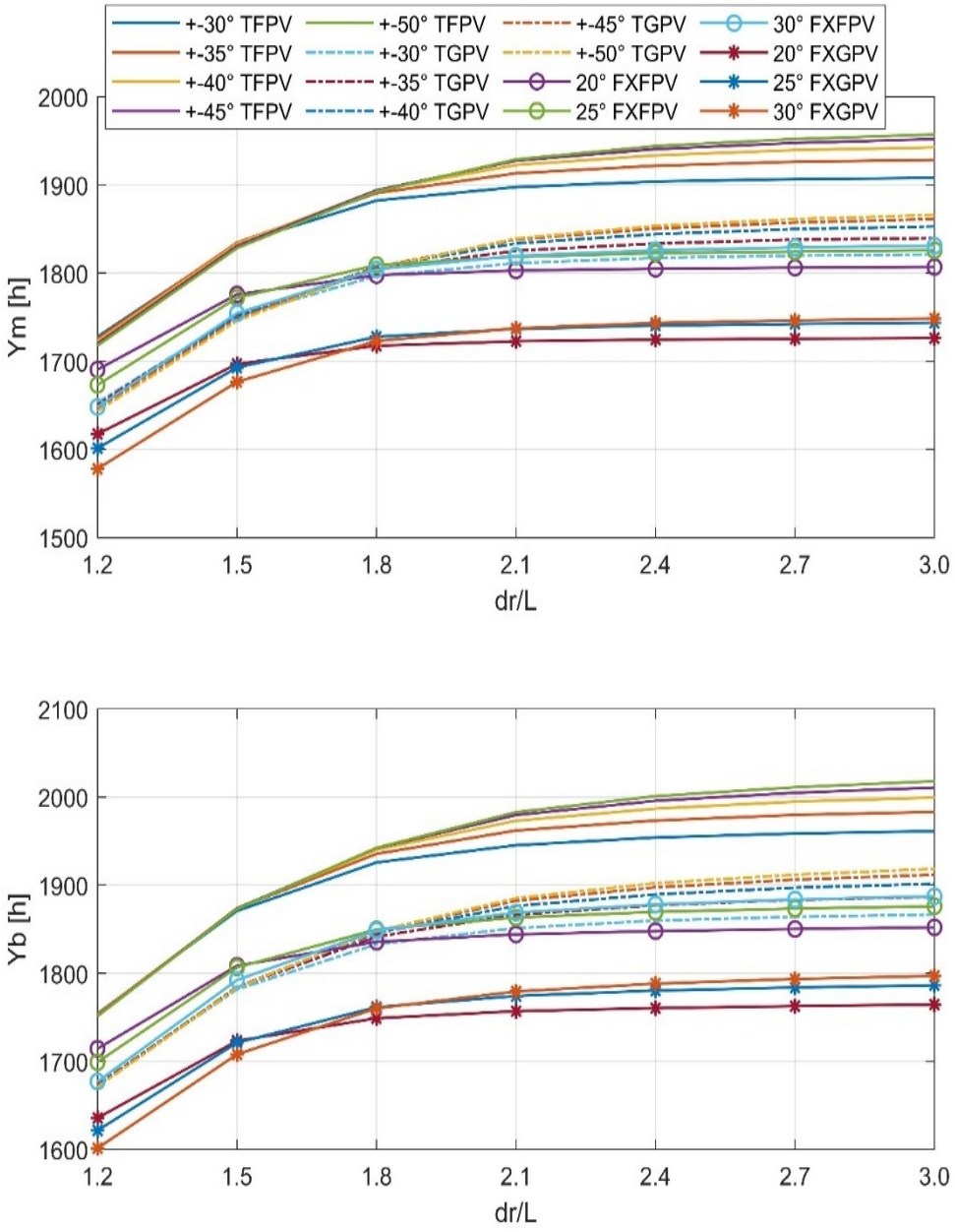

Figure 82 Trend of $Y_{m/b}$ for Horizontal single-axis tracking E-W and fixed F/GPV systems

What can be seen from Figure 82 is that the values of Y of systems with trackers, from d_r/L =1.2 up to d_r/L = 1.8, have minimal differences between them, while in fixed systems the difference is more marked. For values of d_r/L> 1.8 the curves of the fixed systems begin to saturate while those of the tracking systems, in particular those with greater inclination angles (for example ±50), saturate at about d_r/L =2.7. This behaviour is due to the fact that in the case of tracking systems, there is a need, under the same climatic conditions, to increase the distance between the rows due to the mutual shading between the modules.

The analysis of this behaviour, in addition to evaluating the energy aspect, is important for the purpose of economic evaluations since, for ground-based systems, the increase in interdistance involves greater costs relative to the cost of the land per unit of occupied surface, while for floating systems, the increase in the interdistance and therefore the occupied water surface, involves costs related to the construction and installation of the rafts and all the components connected to them that could cause the CAPEX and OPEX to rise so much to make them less advantageous while producing more energy.

Please refer to the following chapters for economic evaluations.

Table 44 shows BG values for FPV tracking systems. BG values are obtained by comparing the same bifacial with monofacial configurations (for example ±50 bifacial TPV system vs ±50 monofacial TPV).

Table 44 BG for Horizontal single-axis tracking E-W system

System	**γ_{Mb} [°]**	**d_r/L**		
		1.2	**2.1**	**3.0**
		BG [%]		
TFPV	±30	1.5	2.5	2.8
	±40	1.7	2.6	2.9
	±50	2.0	2.8	3.1

The maximum values of BG = 3.1% is obtained in the case of configuration ± 50° TPV for d_r/L =3.0.

Table 45 shows FG values for tracking systems that allow to evaluate the increase in performance due to the natural cooling of the modules of the FPV compared to the GPV, in various configurations for mono and bifacial modules.

Table 45 FG for Horizontal single-axis tracking E-W system

System	**$\gamma_{Mm/b}$ [°]**	**Technology**	**d_r/L**		
			1.2	**2.1**	**3.0**
			FG [%]		
TFPV	±30	m	4.5	4.8	4.8
		b	4.8	5.1	5.1
	±40	m	4.5	4.8	4.8
		b	4.8	5.1	5.1
	±50	m	4.5	4.9	4.9
		b	4.8	5.2	5.2

The FG values range from 4.5% to 5.2%.

Table 46 shows TG values for mono and bifacial FPV systems. Specifically, tracking systems are compared with fixed in different geometric configurations. The TG is calculated in function to the interdistance.

The highest TG value is obtained for the ±50 vs 20° combination and is equal to 9.0%.

Table 46 $TG_{m/b}$ for Horizontal single-axis tracking system E-W

System comparison		**Technology**	**d_r/L**		
TFPV	**FXFPV**		**1.2**	**2.1**	**3**
$\gamma_{Mm/b}$ [°]			**TG [%]**		
±30	20	m	2.2	5.2	5.6
		b	2.3	5.5	5.9
	25	m	3.3	4.3	4.5
		b	3.2	4.4	4.5
	30	m	4.8	4.3	4.2
		b	4.6	4.1	3.9
±40	20	m	1.9	6.6	7.5
		b	2.2	7.0	8.0
	25	m	3.0	5.7	6.4
		b	3.2	5.9	6.6
	30	m	4.5	5.7	6.1
		b	4.5	5.6	5.9
±50	20	m	1.6	7.0	8.3
		b	2.1	7.5	9.0
	25	m	2.7	6.1	7.2
		b	3.1	6.4	7.6
	30	m	4.2	6.0	6.9
		b	4.4	6.1	6.9

Table 47 shows the TBG values which take into account the effect of energy gain due to tracking and bifaciality only for the FPV. Then systems with bifacial trackers are compared with fixed monofacial. The TBG is calculated in function to the distance of rows.

Table 47 TBG for Horizontal single-axis tracking FPV system E-W

System comparison		d_r/L		
$TFPV_b$	**$FXFPV_m$**	**1.2**	**2.1**	**3**
$\gamma_{Mm/b}$ [°]		TBG [%]		
±30	20	3.8	7.9	8.5
	25	4.8	7.0	7.4
	30	6.4	6.9	7.1
±40	20	3.7	9.4	10.7
	25	4.8	8.5	9.5
	30	6.4	8.4	9.2
±50	20	3.6	10.0	11.7
	25	4.7	9.0	10.5
	30	6.3	9.0	10.2

The maximum TBG=11.7% is obtained for combination of ±50° $TFPV_b$ and 20° $FXFPV_m$

Table 48 shows the TFG values which take into account the effect of the energy gain due to the tracking and natural cooling of the floating system compared to the mono and bifacial fixed ground system.

Table 48 TFG for Horizontal single-axis tracking monofacial FPV system E-W

System comparison		Technology	d_r/L		
TFPV	**FXFPV**		**1.2**	**2.1**	**3**
$\gamma_{Mm/b}$ [°]			**TFG [%]**		
±30	20	m	6.8	10.2	10.5
		b	7.2	10.7	11.2
	25	m	7.9	9.3	9.4
		b	8.2	9.6	9.8
	30	m	9.5	9.2	9.1
		b	9.5	9.3	9.1
±40	20	m	6.5	11.6	12.5
		b	7.2	12.3	13.3
	25	m	7.6	10.7	11.4
		b	8.1	11.2	11.9
	30	m	9.2	10.7	11.1
		b	9.5	10.9	11.3
±50	20	m	6.2	12.0	13.4
		b	7.1	12.9	14.4
	25	m	7.3	11.1	12.3
		b	8.0	11.8	13.0
	30	m	8.8	11.0	12.0
		b	9.4	11.4	12.3

The maximum and minimum values that can be obtained are, TFGm = 6.2% and 13.4% (monofacial) and TFGb = 7.1% and 14.4 (bifacial).

Table 49 shows TBFG values of TFPV which take into account the effect of energy gain due to tracking, natural cooling and the bifaciality. So, the comparison is between floating bifacial tracker and fixed monofacial ground.

Table 49 TBFG for Horizontal single-axis tracking FPV system E-W

System comparison		d_r/L		
$TFPV_b$	$FXGPV_m$	1.33	2.33	3.33
$\gamma_{Mm/b}$ [°]		TBFG [%]		
±30	20	8.5	12.9	13.6
	25	9.6	12.0	12.5
	30	11.2	12.0	12.2
±40	20	8.4	14.5	15.8
	25	9.5	13.6	14.7
	30	11.1	13.6	14.4
±50	20	8.3	15.1	16.9
	25	9.4	14.2	15.7
	30	11.0	14.1	15.4

The maximum and minimum values that can be obtained from comparison of TFPVb and FXGPVm are, TBFG = 8.3% and 16.9%.

It can therefore be concluded that a bifacial E-W floating horizontal axis tracking system can increase the yield compared to a fixed ground system by 16.9%.

8.3.1.4 Horizontal single-axis tracking FPV system N-S

Table 50 shows the Y values (equivalent operating hours) of each type of system analysed.

Table 50 $Y_{m/b}$ for Horizontal single-axis tracking N-S F/GPV systems

System	$\gamma_{Mm/b}$ [°]	Technology	d_r/L		
			1.2	2.1	3
			Y [h]		
TGPV	±30	m	1693.0	1925.5	1969.5
		b	1712.6	1963.7	2014.0
	±40	m	1689.9	1952.9	2019.4
		b	1713.4	1994.1	2067.3
	±50	m	1685.8	1960.0	2040.4
		b	1713.1	2005.1	2092.8
TFPV	±30	m	1769.5	2018.3	2064.2
		b	1795.0	2064.6	2117.2
	±40	m	1766.3	2048.8	2118.6
		b	1795.8	2098.2	2175.6
	±50	m	1762.0	2056.9	2141.9
		b	1795.5	2110.5	2203.5

Figure 83 is shown to illustrate the behavior of the various systems as the geometric quantities vary.

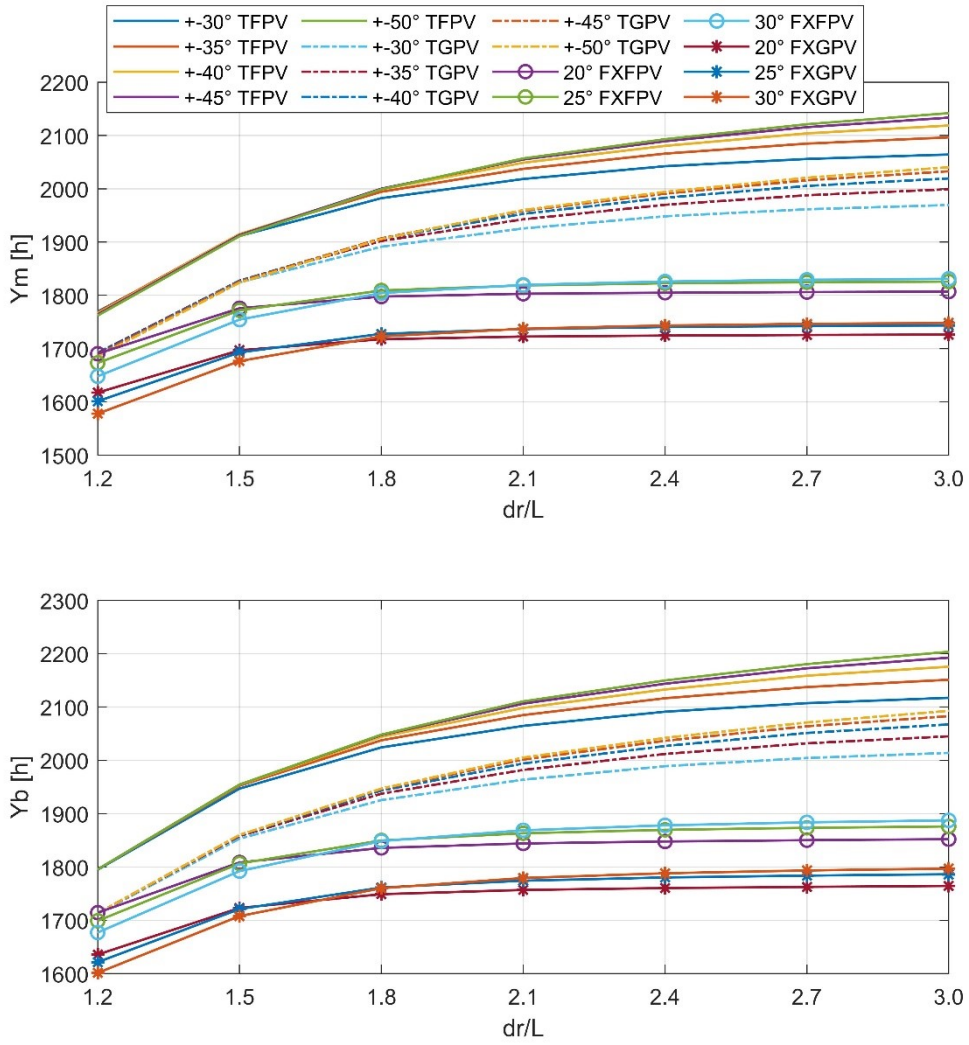

Figure 83 Trend of $Y_{m/b}$ for Horizontal single-axis tracking N-S and fixed F/GPV systems

Also in this case as in the case of the E-W trackers, the same considerations can be made for Y trend.

Between the E-W and N-S systems with the same interdistance, a greater slope of the curve is noted in the N-S. Therefore, to obtain the same performance between the two systems, the E-W system must necessarily have a greater interdistance than the N-S system.

This behavior translates into a higher cost of the E-W system compared to the N-S since, with the same installed power, the E-W must occupy a greater surface area to have the same performance as the N-S (therefore higher costs due to components such as floats, structures, moorings and anchors).

Please refer to the following chapters for economic evaluations.

Table 51 shows BG values for FPV tracking systems N-S. BG values are obtained by comparing the same bifacial with monofacial configurations (for example ±50 bifacial TPV system vs ±50 monofacial TPV).

Table 51 BG for Horizontal single-axis tracking N-S system

System	γ_{Mb} [°]	d_r/L		
		1.2	2.1	3.0
		BG [%]		
TFPV	±30	1.4	2.3	2.6
	±40	1.7	2.4	2.7
	±50	1.9	2.6	2.9

The maximum values of BG = 2.9% are obtained in the case of configuration ± 50° TPV for d_r/L=3.0.

Table 52 shows FG values for tracking systems that allow to evaluate the increase in performance due to the natural cooling of the modules of the FPV compared to the GPV, in various configurations for mono and bifacial modules.

Table 52 FG for Horizontal single-axis tracking N-S system

System	$\gamma_{Mm/b}$ [°]	Technology	d_r/L		
			1.2	2.1	3.0
			FG [%]		
TFPV	±30	m	4.5	4.8	4.8
		b	4.8	5.1	5.1
	±40	m	4.5	4.9	4.9
		b	4.8	5.2	5.2
	±50	m	4.5	4.9	5.0
		b	4.8	5.3	5.3

The FG values range from 4.5% to 5.3%.

Table 53 shows TG values for mono and bifacial FPV systems. Specifically, tracking systems are compared with fixed in different geometric configurations. The TG is calculated in function to the interdistance.

The highest TG value is obtained for the ±50 vs 20° combination and is equal to 19.0%.

Table 53 $TG_{m/b}$ for Horizontal single-axis tracking system N-S

System comparison		Technology	d_r/L		
TFPV	**FXFPV**		**1.2**	**2.1**	**3**
$\gamma_{Mm/b}$ [°]			**TG [%]**		
±30	20	m	4.7	11.9	14.2
		b	4.7	12.0	14.3
	25	m	5.8	11.0	13.1
		b	5.6	10.8	12.9
	30	m	7.4	10.9	12.7
		b	7.0	10.5	12.2
±40	20	m	4.5	13.6	17.3
		b	4.7	13.8	17.5
	25	m	5.6	12.7	16.0
		b	5.7	12.6	16.0
	30	m	7.2	12.6	15.7
		b	7.1	12.3	15.3
±50	20	m	4.2	14.1	18.5
		b	4.7	14.4	19.0
	25	m	5.3	13.1	17.3
		b	5.7	13.3	17.5
	30	m	6.9	13.0	17.0
		b	7.1	12.9	16.7

Compared to the E-W, the N-S one with the same geometric configurations is much more performing. This can be seen by comparing the two tables of TG for the E-W and N-S system.

Table 54 shows the TBG values which take into account the effect of energy gain due to tracking and bifaciality only for the FPV. Then systems with bifacial trackers are compared with fixed monofacial. The TBG is calculated in function to the distance.

Table 54 TBG for Horizontal single-axis tracking FPV system N-S

System comparison		d_r/L		
$TFPV_b$	**$FXFPV_m$**	**1.2**	**2.1**	**3.0**
$\gamma_{Mm/b}$ [°]		**TBG [%]**		
±30	20	6.2	14.5	17.2
	25	7.3	13.5	16.0
	30	8.9	13.5	15.6
±40	20	6.2	16.4	20.4
	25	7.3	15.4	19.2
	30	9.0	15.3	18.8
±50	20	6.2	17.1	21.9
	25	7.3	16.1	20.7
	30	8.9	16.0	20.3

The maximum TBG=21.9% is obtained for combination of ±50° $TFPV_b$ and 20° $FXFPV_m$.

Compared to the E-W configuration, the N-S with the same geometric configurations has a higher TBG. This is shown by comparing two TBG tables for E-W and N-S system.

Table 55 shows the TFG values which take into account the effect of the energy gain due to the tracking and natural cooling of the floating system compared to the mono and bifacial fixed ground system.

Table 55 TFG for Horizontal single-axis tracking monofacial FPV system N-S

System comparison		**Technology**	**d_r/L**		
TFPV	**FXFPV**		**1.2**	**2.1**	**3.0**
$\gamma_{Mm/b}$ [°]			**TFG [%]**		
±30	20	m	9.4	17.2	19.6
		b	9.7	17.5	20.0
	25	m	10.5	16.2	18.4
		b	10.7	16.4	18.5
	30	m	12.1	16.2	18.1
		b	12.1	16.0	17.8
±40	20	m	9.2	18.9	22.7
		b	9.8	19.4	23.3
	25	m	10.3	18.0	21.5
		b	10.7	18.3	21.8
	30	m	11.9	17.9	21.2
		b	12.1	17.9	21.1
±50	20	m	8.9	19.4	24.1
		b	9.8	20.1	24.9
	25	m	10.0	18.4	22.8
		b	10.7	19.0	23.3
	30	m	11.7	18.4	22.5
		b	12.1	18.6	22.6

The maximum and minimum values that can be obtained are, TFGm = 8.9% and 24.1% (monofacial) and TFGb = 9.7% and 24.9 (bifacial).

Table 56 shows TBFG values of TFPV which take into account the effect of energy gain due to tracking, natural cooling and the bifaciality. So the comparison is between floating bifacial tracker and fixed monofacial ground.

Table 56 TBFG for Horizontal single-axis tracking FPV system N-S

System comparison		d_r/L		
$TFPV_b$	$FXGPV_m$	1.2	2.1	3
$\gamma_{Mm/b}$ [°]		TBFG [%]		
±30	20	11.0	19.8	22.6
	25	12.1	18.9	21.4
	30	13.7	18.8	21.1
±40	20	11.0	21.8	26.0
	25	12.1	20.8	24.8
	30	13.8	20.8	24.4
±50	20	11.0	22.5	27.6
	25	12.1	21.5	26.4
	30	13.8	21.5	26.0

The maximum and minimum values that can be obtained from comparison of TFPVb and FXGPVm are, TBFG = 11.0% and 27.6%.

It can therefore be concluded that a bifacial N-S floating horizontal axis tracking system can increase the yield compared to a fixed ground system by 27.6%

8.3.1.5 Vertical single-axis tracking system

For this type of TFPV, simulations were carried out only for the monofacial system as the software does not allow to simulate bifacial modules with a vertical tracker.

Table 57 shows the energy collected values Y, normalized respect to the peak power of the system, for the configuration with vertical tracker and fixed on ground and on water, with monofacial modules.

Table 57 $Y_{m/b}$ for Vertical single-axis tracking and fixed F/GPV system

System	Φ [°]	$\gamma_{Mm/b}$ [°]	d_r/L		
			1.2	2.1	3.0
			Y [h]		
TGPV	±120	20	1802.3	1993.9	2019.2
		25	1823.8	2065.1	2093.4
		30	1839.0	2108.8	2152.5
TFPV	±120	20	1888.3	2094.2	2120.7
		25	1911.6	2172.2	2201.8
		30	1927.9	2220.6	2266.9

Figure 84 is shown to illustrate the behavior of the various systems as the geometric quantities vary.

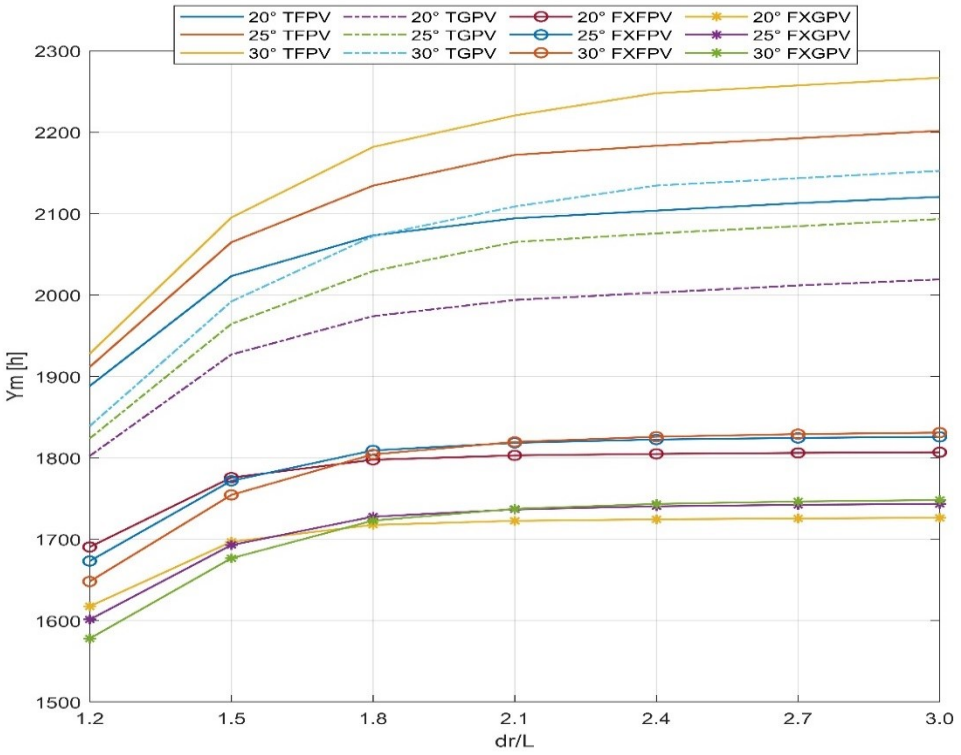

Figure 84 Trend of $Y_{m/b}$ for Vertical single-axis tracking and fixed F/GPV system

What can be seen from Figure 84 is that the curves of the tracker systems in this case have an important offset between them, which means that in addition to the distance, the tilt also plays an important role even for small pitch values. This offset becomes larger as the pitch increases. The behavior as a function of the distance is almost similar to the cases examined above, ie the curves of the tracking system saturate with higher pitches than the fixed system. This behavior is due to the fact that in the case of tracking systems, there is a need, under the same climatic conditions, to increase the distance between the rows due to the mutual shading between the modules.

Table 58 shows the FG values for vertical tracking systems that allow to evaluate the increase in performance of FPV systems due to natural cooling thanks to the favourable microclimate in which they operate.

Table 58 FG for Vertical single-axis tracking system

System Comparison		Φ [°]	$\gamma_{Mm/b}$ [°]	d_r/L		
				1.2	2.1	3.0
				FG [%]		
TFPV	TGPV	±120	20	4.8	5.0	5.0
			25	4.8	5.2	5.2
			30	4.8	5.3	5.3

FG values range from 4.8% to 5.3%.

Table 59 TG for Vertical single-axis tracking system

System comparison		d_r/L		
TFPV	FXFPV	1.2	2.1	3.0
γ_{Mm} [°]		TG [%]		
20	20	11.7	16.2	17.4
	25	12.9	15.2	16.2
	30	14.6	15.1	15.8
25	20	13.1	20.5	21.9
	25	14.2	19.5	20.6
	30	16.0	19.4	20.2
30	20	14.0	23.2	25.5
	25	15.2	22.1	24.2
	30	17.0	22.0	23.8

The maximum TG values are obtained for the TFPV configuration with 30 ° tilt and d_r/L = 3.0 compared with a fixed system with 20 ° tilt and dr / L = 20 ° and is 25.5%.

The Table 60 shows the TFG values which take into account the effect of the energy gain due to the tracking and natural cooling of the floating system compared to the monofacial ground system.

Table 60 TFG for Vertical single-axis tracking monofacial FPV system

System comparison		d_r/L		
TFPV	**FXGPV**	**1.2**	**2.1**	**3.0**
γ_{Mm} [°]		**TFG [%]**		
20	20	16.7	21.6	22.8
	25	17.9	20.6	21.6
	30	19.7	20.5	21.3
25	20	18.2	26.1	27.5
	25	19.4	25.1	26.3
	30	21.1	25.0	25.9
30	20	19.2	28.9	31.3
	25	20.4	27.9	30.0
	30	22.2	27.8	29.7

The maximum and minimum values obtainable are, TFGm=16.7% and 31.3% (monofacial) respectively with 20 ° TPV configuration compared with 20 ° tilt FXGPV and 30 ° TPV compared with 20 ° tilt FXGPV.

The TFG values for the vertical tracker are higher than horizontal N-S and E-W.

From what can be seen from the energy yield data, the vertical axis system is more efficient than horizontal axis system. It is to be understood, what is the difference in cost of this system compared to the previous ones. The previous ones are made with rafts with a gable structure, this one with a vertical axis can be of a different type, that is, a carousel, with or without a confinement structure. The cost therefore depends on the type of raft considered.

8.3.1.6 Dual axis tracking system

For this type of TFPV, simulations were carried out only for the monofacial system as the software does not allow to simulate bifacial modules with a 2 axes tracker.

Table 61 shows the energy collected values Y, normalized respect to the peak power of the system, for the configuration with 2 axes tracker in Anapo Dam.

Table 61 $Y_{m/b}$ for Dual-axis tracking F/GPV system

System	Φ [°]	$\gamma_{Mm/b}$ [°]	d_r/L		
			1.2	2.1	3.0
			Y [h]		
TGPV	±120	0-50	1969.4	2380.5	2407.2
TFPV	±120	0-50	2060.2	2515.1	2544.7

Between the values of Y obtained for dr/ L= 1.2 and the subsequent ones, there is a considerable difference in terms of collected energy, this means that for the same installed power, compared to other technologies, it requires a greater installation surface.

Table 62 shows the FG values obtained for the two-axis system. The FG is the gain resulting from the natural cooling of the modules installed on water.

Table 62 FG for Dual-axis tracking system

System	**Φ [°]**	**γ_{Mm} [°]**	**d_r/L**		
			1.2	**2.1**	**3.0**
			FG		
TFPV	±120	0-50	4.6	5.7	5.7

For the analyzed configurations the FG values oscillate between 4.6% and 5.7.

Table 63 shows the gain of the tracking effect.

Table 63 TG for Dual axis tracking system

System comparison		**d_r/L**		
TFPV	**FXFPV**	**1.2**	**2.1**	**3.0**
Φ=±120 γ_{Mm}=0-50	γ_{Mm} [°]	TG [%]		
	20	21.9	39.5	40.8
	25	23.1	38.3	39.4
	30	25.0	38.2	39.0

With the effect of dual tracking alone, without considering the effect of cooling, the energy collected could increase up to almost 41%.

Table 64 shows the gain due to cooling and tracking, then comparing fixed system on ground with the tracking system on water.

Table 64 TFG for Dual axis tracking system

System comparison		**d_r/L**		
TFPV	**FXGPV**	**1.33**	**2.33**	**3.33**
Φ=±120 γ_{Mm}=0-50	γ_{Mm} [°]	TFG [%]		
	20	27.4	46.0	47.4
	25	28.7	44.8	46.0
	30	30.6	44.8	45.6

Thanks to the dual effect of cooling and tracking, up to about 47% more energy can be collected.

8.3.2 Aar Dam

This paragraph shows the results in terms of energy performance, obtained for the Aar Dam locality with coordinates 50.69 ° N, 8.45 ° E.

The Aar Dam and its reservoir, the Aartalsee, lie in the upper Aar valley in the German state of Hesse. Both are in the municipalities of Bischoffen and Hohenahr in the county of Lahn-Dill-Kreis and about 15 km northwest of the town of Gießen in Hesse

The dam is primarily used for flood protection for the Aar and Dill. In Winter the reservoir is filled to a capacity of 1.33 million m³; in summer this rises to 1.84 million m³. Other uses are: raising low water levels, electricity generation, fishing and recreation. As a result, the dam and reservoir also contribute economically to the region. By integrating an FPV system to the HPP plant, the energy produced on site can be increased.

8.3.2.1 Fixed systems

Table 65 shows the Y values (equivalent operating hours) of fixed ground and floating systems analysed. These values will will be a reference for comparing the energy yield of mono and bifacial tracking systems and monofacial gable systems.

Table 65 $Y_{m/b}$ for fixed F/GPV systems

System	$\gamma_{Mm/b}$ [°]	Technology	d_r/L		
			1.2	2.1	3.0
			Y [h]		
FXGPV	20	m	887.4	957.8	964.0
		b	900.9	981.1	990.2
	25	m	873.0	960.8	972.0
		b	889.0	987.6	1002.6
	30	m	855.6	956.5	973.0
		b	875.2	987.9	1009.0
FXFPV	20	m	915.7	989.6	996.0
		b	931.7	1016.1	1025.5
	25	m	901.0	993.5	1005.1
		b	919.5	1023.6	1039.1
	30	m	883.1	989.6	1006.7
		b	905.3	1024.4	1046.3

Table 66 shows BG values for FPV tracking systems. BG values are obtained by comparing the same bifacial with monofacial configurations (for example 30 ° bifacial FXPV vs 30 ° monofacial FXPV).

Table 66 BG for fixed system

System	γ_{Mb} [°]	d_r/L		
		1.2	**2.1**	**3.0**
		BG [%]		
FXFPV	20	1.8	2.7	3.0
	25	2.1	3.0	3.4
	30	2.5	3.5	3.9

The highest BG for the fixed system is 3.9%.

The BG values of Aar Dam (Germany) are greater than those of Anapo Dam (Italy). This is due to the greater contribution given by the diffuse component of solar radiation. In fact, if we look at the solar radiation data for the two locations, the diffusion factor is greater in Aar Dam than in Anapo Dam.

Table 67 shows FG values for fixed and tracking systems that allow to evaluate the increase in performance due to the natural cooling of the modules of the FPV compared to the GPV, in various configurations for mono and bifacial modules.

Table 67 FG for fixed system

System	$\gamma_{Mm/b}$ [°]	Technology	d_r/L		
			1.2	**2.1**	**3.0**
			FG [%]		
FXFPV	20	m	3.2	3.3	3.3
		b	3.4	3.6	3.6
	25	m	3.2	3.4	3.4
		b	3.4	3.6	3.6
	30	m	3.2	3.5	3.5
		b	3.4	3.7	3.7

The highest FG for the fixed system is obtained for the tilt $\gamma_{Mm/b}$=30° and dr/L=5 configuration and is 3.7%.

The cooling effect in Aar Dam is reduced compared to Anapo Dam as the average monthly temperatures but also the solar radiation is lower in Aar.

8.3.2.2 Gable systems

As discussed in the introductory part of this thesis work, gable solutions provide various advantages in terms of material savings and therefore CAPEX at the expense of small energy losses that are dependent on latitude.

Table 68 shows the energy yield values, the losses due to the system solution and the gain due to the cooling of the modules

Table 68 Ym, GGL and FG for gable solution

System	γ_{Mm} [°]	Technology	$d_r/L=1.2$		
			Y	GGL [%]	FG [%]
FXGGPV	10	m	857.9	-3.3	-
FXGFPV	10	m	878.1	-4.1	2.4

The gable solution, if compared with a classic system, for the considered latitude, loses 3.3% in the case of a ground system and 4.1% in the case of an FPV system.

FG is equal to 2.4%

8.3.2.3 Horizontal single-axis tracking system E-W

Table 69 shows the Y (equivalent operating hours) of each type of system analysed.

Table 69 $Y_{m/b}$ for Horizontal single-axis tracking E-W F/GPV systems

System	$\gamma_{Mm/b}$ [°]	Technology	d_r/L		
			1.2	2.1	3
			Y [h]		
TGPV	±30	m	892.4	994.2	1010.8
		b	910.5	1024.3	1044.9
	±40	m	879.7	994.2	1019.4
		b	902.5	1029.0	1058.8
	±50	m	870.4	988.6	1018.6
		b	897.4	1028.1	1063.1
TFPV	±30	m	920.8	1028.1	1045.4
		b	941.6	1061.7	1083.1
	±40	m	907.8	1028.9	1055.1
		b	933.4	1067.3	1098.3
	±50	m	898.3	1023.3	1054.7
		b	928.2	1066.5	1103.1

The Figure 85 is shown to illustrate the behavior of the various systems as the geometric quantities vary.

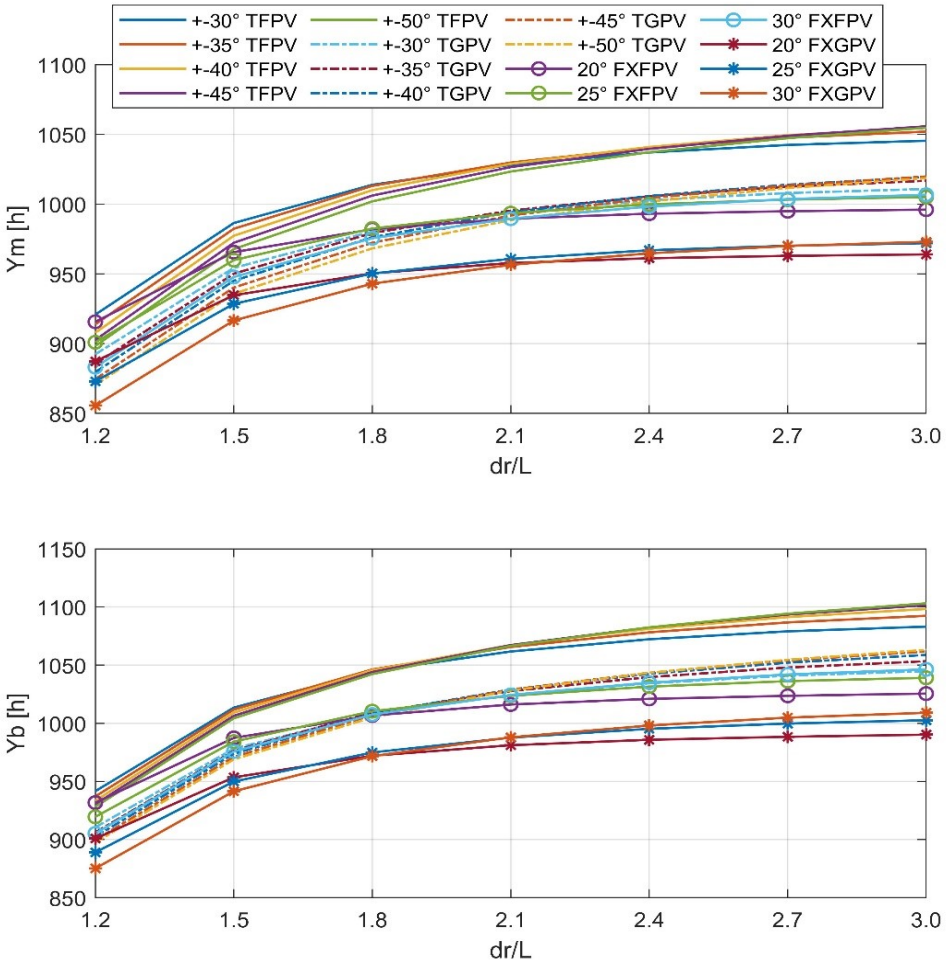

Figure 85 Trend of $Y_{m/b}$ for Horizontal single-axis tracking E-W and fixed F/GPV systems

For the location examined, can be see how there is an inversion of the energy yield trend as the interdistance increases for the trackers (for monofacial at dr / L =2.4 and for bifacial at dr / L =1.9). Therefore, at low pitch values it is convenient to use trackers with small tilt and vice versa. Since we are in a high latitude situation, the shading effect is accentuated compared to low latitudes.

Table 70 shows BG values for FPV tracking systems. BG values are obtained by comparing the same bifacial with monofacial configurations (for example ±50 bifacial TPV system vs ±50 monofacial TPV).

Table 70 BG for Horizontal single-axis tracking E-W system

System	γ_{Mb} [°]	d_r/L		
		1.2	**2.1**	**3.0**
		BG [%]		
TFPV	±30	2.3	3.3	3.6
	±40	2.8	3.7	4.1
	±50	3.3	4.2	4.6

The maximum values of BG = 4.6% is obtained in the case of configuration ± 50° TPV.

Table 71 shows FG values tracking systems that allow to evaluate the increase in performance due to the natural cooling of the modules of the FPV compared to the GPV, in various configurations for mono and bifacial modules.

Table 71 FG for Horizontal single-axis tracking E-W system

System	$\gamma_{Mm/b}$ [°]	Technology	d_r/L		
			1.2	**2.1**	**3.0**
			FG [%]		
TFPV	±30	m	3.2	3.4	3.4
		b	3.4	3.7	3.7
	±40	m	3.2	3.5	3.5
		b	3.4	3.7	3.7
	±50	m	3.2	3.5	3.5
		b	3.4	3.7	3.8

The FG values range from 3.2% to 3.8%.

Table 72 shows TG values for mono and bifacial FPV systems. Specifically, tracking systems are compared with fixed in different geometric configurations. The TG is calculated in function to the interdistance.

For dr/L= 1.2 in some cases the fixed system is more convenient than the tracking system, again for the reasons listed in the previous cases analyzed.

The highest TG value is obtained for the ±50 vs 20° combination and is equal to 7.6%.

Table 72 $TG_{m/b}$ for Horizontal single-axis tracking system E-W

System comparison		Technology	d_r/L		
TFPV	**FXFPV**		**1.2**	**2.1**	**3**
$\gamma_{Mm/b}$ [°]			**TG [%]**		
±30	20	m	0.6	3.9	5.0
		b	1.1	4.5	5.6
	25	m	2.2	3.5	4.0
		b	2.4	3.7	4.2
	30	m	4.3	3.9	3.8
		b	4.0	3.6	3.5
±40	20	m	-0.9	4.0	5.9
		b	0.2	5.0	7.1
	25	m	0.8	3.6	5.0
		b	1.5	4.3	5.7
	30	m	2.8	4.0	4.8
		b	3.1	4.2	5.0
±50	20	m	-1.9	3.4	5.9
		b	-0.4	5.0	7.6
	25	m	-0.3	3.0	4.9
		b	0.9	4.2	6.2
	30	m	1.7	3.4	4.8
		b	2.5	4.1	5.4

Table 73 shows the TBG values which take into account the effect of energy gain due to tracking and bifaciality only for the FPV. Then systems with bifacial trackers are compared with fixed monofacial. The TBG is calculated in function to the distance.

Table 73 TBG for Horizontal single-axis tracking FPV system E-W

System comparison		d_r/L		
$TFPV_b$	**$FXFPV_m$**	**1.2**	**2.1**	**3.0**
$\gamma_{Mm/b}$ [°]		**TBG [%]**		
±30	20	2.8	7.3	8.7
	25	4.5	6.9	7.8
	30	6.6	7.3	7.6
±40	20	1.9	7.9	10.3
	25	3.6	7.4	9.3
	30	5.7	7.9	9.1
±50	20	1.4	7.8	10.8
	25	3.0	7.4	9.8
	30	5.1	7.8	9.6

The maximum TBG=10.8% is obtained for combination of ±50° $TFPV_b$ and 20° $FXFPV_m$

Table 74 shows the TFG values which take into account the effect of the energy gain due to the tracking and natural cooling of the floating system compared to the mono and bifacial fixed ground system.

Table 74 TFG for Horizontal single-axis tracking monofacial FPV system E-W

System comparison		Technology	d_r/L		
TFPV	**FXFPV**		**1.2**	**2.1**	**3.0**
$\gamma_{Mm/b}$ [°]			TFG [%]		
±30	20	m	3.8	7.3	8.4
		b	4.5	8.2	9.4
	25	m	5.5	7.0	7.6
		b	5.9	7.5	8.0
	30	m	7.6	7.5	7.4
		b	7.6	7.5	7.3
±40	20	m	2.3	7.4	9.5
		b	3.6	8.8	10.9
	25	m	4.0	7.1	8.5
		b	5.0	8.1	9.5
	30	m	6.1	7.6	8.4
		b	6.7	8.0	8.8
±50	20	m	1.2	6.8	9.4
		b	3.0	8.7	11.4
	25	m	2.9	6.5	8.5
		b	4.4	8.0	10.0
	30	m	5.0	7.0	8.4
		b	6.1	8.0	9.3

The maximum and minimum values that can be obtained are, TFGm = 1.2% and 9.4% (monofacial) and TFGb = 3% and 11.4 (bifacial).

Table 75 shows TBFG values of TFPV which take into account the effect of energy gain due to tracking, natural cooling and the bifaciality. So the comparison is between floating bifacial tracker and fixed monofacial ground.

Table 75 TBFG for Horizontal single-axis tracking FPV system E-W

System comparison		d_r/L		
$TFPV_b$	$FXGPV_m$	1.2	2.1	3.0
$\gamma_{Mm/b}$ [°]		TBFG [%]		
±30	20	6.1	10.9	12.4
	25	7.9	10.5	11.4
	30	10.0	11.0	11.3
±40	20	5.2	11.4	13.9
	25	6.9	11.1	13.0
	30	9.1	11.6	12.9
±50	20	4.6	11.4	14.4
	25	6.3	11.0	13.5
	30	8.5	11.5	13.4

The maximum and minimum values that can be obtained from comparison of TFPVb and FXGPVm are, TBFG = 4.6% and 14.4%.

It can therefore be concluded that in Aar Dam a bifacial E-W floating horizontal axis tracking system can increase the yield compared to a fixed ground system by 14.4%.

8.3.2.4 Horizontal single-axis tracking FPV system N-S

Table 76 shows the Y values (equivalent operating hours) of each type of system analysed.

Table 76 $Y_{m/b}$ for Horizontal single-axis tracking N-S F/GPV systems

System	$\gamma_{Mm/b}$ [°]	Technology	d_r/L		
			1.2	2.1	3.0
			Y [h]		
TGPV	±30	m	905.3	1047.2	1077.9
		b	922.1	1075.2	1110.3
	±40	m	893.3	1052.0	1096.5
		b	914.8	1084.8	1134.1
	±50	m	883.5	1047.2	1100.8
		b	909.6	1085.2	1144.2
TFPV	±30	m	933.5	1083.1	1115.0
		b	952.9	1114.8	1151.2
	±40	m	921.2	1089.0	1135.6
		b	945.3	1125.7	1177.3
	±50	m	911.2	1084.4	1140.8
		b	940.1	1126.5	1188.5

Figure 86 is shown to illustrate the behavior of the various systems as the geometric quantities vary.

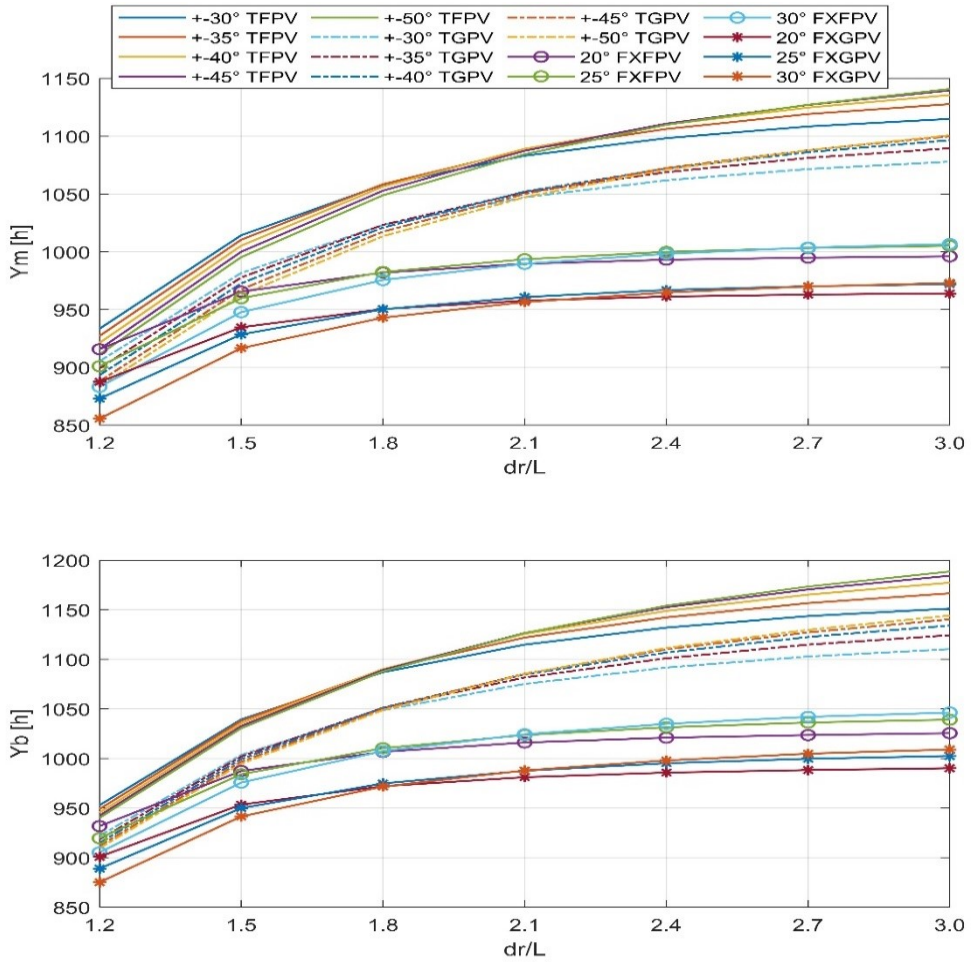

Figure 86 Trend of $Y_{m/b}$ for Horizontal single-axis tracking N-S and fixed F/GPV systems

Also in this case, as in the case of the E-W trackers, the same considerations can be made for Y trend.

Between the E-W and N-S systems with the same interdistance, a greater slope of the curve is noted in the N-S. Therefore, to obtain the same performance between the two systems, the E-W system must necessarily have a greater interdistance than the N-S system

This behavior translates into a higher cost of the E-W system compared to the N-S since, with the same installed power, the E-W must occupy a greater surface area to have the same performance as the N-S (therefore higher costs due to components such as floats, structures, moorings and anchors).

Please refer to the following chapters for economic evaluations.

Table 77 shows BG values for FPV tracking systems N-S. BG values are obtained by comparing the same bifacial with monofacial configurations (for example ±50 bifacial TPV system vs ±50 monofacial TPV).

Table 77 BG for Horizontal single-axis tracking N-S system

System	γ_{Mb} [°]	d_r/L		
		1.2	**2.1**	**3.0**
		BG [%]		
TFPV	±30	2.1	2.9	3.3
	±40	2.6	3.4	3.7
	±50	3.2	3.9	4.2

The maximum values of BG = 4.2% are obtained in the case of configuration ± 50° TPV.

Table 78 shows FG values for fixed and tracking systems that allow to evaluate the increase in performance due to the natural cooling of the modules of the FPV compared to the GPV, in various configurations for mono and bifacial modules.

Table 78 FG for Horizontal single-axis tracking N-S system

System	$\gamma_{Mm/b}$ [°]	Technology	d_r/L		
			1.2	**2.1**	**3.0**
			FG [%]		
TFPV	±30	m	3.2	3.3	3.3
		b	3.4	3.6	3.6
	±40	m	3.2	3.4	3.4
		b	3.4	3.6	3.6
	±50	m	3.2	3.5	3.5
		b	3.4	3.7	3.7

The FG values range from 3.2% to 3.7%.

Table 79 shows TG values for mono and bifacial FPV systems. Specifically, tracking systems are compared with fixed in different geometric configurations. The TG is calculated in function to the interdistance.

The highest TG value is obtained for the ±50 vs 20° combination and is equal to 15.9%.

Table 79 $TG_{m/b}$ for Horizontal single-axis tracking system N-S

System comparison		Technology	d_r/L		
TFPV	**FXFPV**		**1.2**	**2.1**	**3.0**
$\gamma_{Mm/b}$ [°]			**TG [%]**		
±30	20	m	1.9	9.4	11.9
		b	2.3	9.7	12.3
	25	m	3.6	9.0	10.9
		b	3.6	8.9	10.8
	30	m	5.7	9.4	10.8
		b	5.3	8.8	10.0
±40	20	m	0.6	10.0	14.0
		b	1.5	10.8	14.8
	25	m	2.2	9.6	13.0
		b	2.8	10.0	13.3
	30	m	4.3	10.0	12.8
		b	4.4	9.9	12.5
±50	20	m	-0.5	9.6	14.5
		b	0.9	10.9	15.9
	25	m	1.1	9.2	13.5
		b	2.2	10.1	14.4
	30	m	3.2	9.6	13.3
		b	3.8	10.0	13.6

Compared to the E-W, the N-S one with the same geometric configurations is much more performing. This can be seen by comparing the two tables of TG for the E-W and N-S system.

Table 80 shows the TBG values which take into account the effect of energy gain due to tracking and bifaciality only for the FPV. Then systems with bifacial trackers are compared with fixed monofacial. The TBG is calculated in function to the distance.

Table 80 TBG for Horizontal single-axis tracking FPV system N-S

System comparison		d_r/L		
$TFPV_b$	**$FXFPV_m$**	**1.2**	**2.1**	**3.0**
$\gamma_{Mm/b}$ [°]		**TBG [%]**		
±30	20	4.1	12.7	15.6
	25	5.8	12.2	14.5
	30	7.9	12.7	14.4
±40	20	3.2	13.8	18.2
	25	4.9	13.3	17.1
	30	7.0	13.8	17.0
±50	20	2.7	13.8	19.3
	25	4.3	13.4	18.3
	30	6.4	13.8	18.1

The maximum TBG=19.3% are obtained for combination of ±50° $TFPV_b$ and 20° $FXFPV_m$.

Compared to the E-W, N-S with the same geometric configurations has a higher TBG. This is shown by comparing TBG tables for the E-W and N-S system.

Table 81 shows the TFG values which take into account the effect of the energy gain due to the tracking and natural cooling of the floating system compared to the mono and bifacial fixed ground system.

Table 81 TFG for Horizontal single-axis tracking monofacial FPV system N-S

System comparison		**Technology**	**d_r/L**		
TFPV	**FXFPV**		**1.2**	**2.1**	**3.0**
$\gamma_{Mm/b}$ [°]			**TFG [%]**		
±30	20	m	5.2	13.1	15.7
		b	5.8	13.6	16.3
	25	m	6.9	12.7	14.7
		b	7.2	12.9	14.8
	30	m	9.1	13.2	14.6
		b	8.9	12.8	14.1
±40	20	m	3.8	13.7	17.8
		b	4.9	14.7	18.9
	25	m	5.5	13.3	16.8
		b	6.3	14.0	17.4
	30	m	7.7	13.9	16.7
		b	8.0	13.9	16.7
±50	20	m	2.7	13.2	18.3
		b	4.4	14.8	20.0
	25	m	4.4	12.9	17.4
		b	5.7	14.1	18.5
	30	m	6.5	13.4	17.2
		b	7.4	14.0	17.8

The maximum and minimum values that can be obtained are, TFGm = 2.7% and 18.3% (monofacial) and TFGb = 4.4% and 20.0% (bifacial).

Table 82 shows TBFG values of TFPV which take into account the effect of energy gain due to tracking, natural cooling and the bifaciality. So the comparison is between floating bifacial tracker and fixed monofacial ground.

Table 82 TBFG for Horizontal single-axis tracking FPV system N-S

System comparison		d_r/L		
$TFPV_b$	**$FXGPV_m$**	**1.2**	**2.1**	**3.0**
$\gamma_{Mm/b}$ [°]		**TBFG [%]**		
±30	20	7.4	16.4	19.4
	25	9.2	16.0	18.4
	30	11.4	16.6	18.3
±40	20	6.5	17.5	22.1
	25	8.3	17.2	21.1
	30	10.5	17.7	21.0
±50	20	5.9	17.6	23.3
	25	7.7	17.2	22.3
	30	9.9	17.8	22.2

The maximum and minimum values that can be obtained from comparison of TFPVb and FXGPVm are, TBFG = 5.9% and 23.3%.

It can therefore be concluded that a bifacial N-S floating horizontal axis tracking system can increase the yield compared to a fixed ground system by 23.3%.

8.3.2.5 Vertical single-axis tracking system

For this type of TFPV, simulations were carried out only for the monofacial system as the software does not allow to simulate bifacial modules with a vertical tracker.

Table 83 shows the energy collected values Y, normalized respect to the peak power of the system, for the configuration with vertical tracker on ground and on water, with monofacial modules.

Table 83 $Y_{m/b}$ for Vertical single-axis tracking and fixed F/GPV system

System	**Φ [°]**	**$\gamma_{Mm/b}$ [°]**	d_r/L		
			1.2	**2.1**	**3.0**
			Y [h]		
TGPV	±120	20	983.2	1100.6	1120.3
		25	989.0	1135.2	1157.6
		30	991.8	1153.7	1186.0
TFPV	±120	20	1015.9	1140.1	1160.6
		25	1022.4	1177.8	1201.1
		30	1025.6	1198.5	1232.3

Figure 87 is shown to illustrate the behavior of the various systems as the geometric quantities vary.

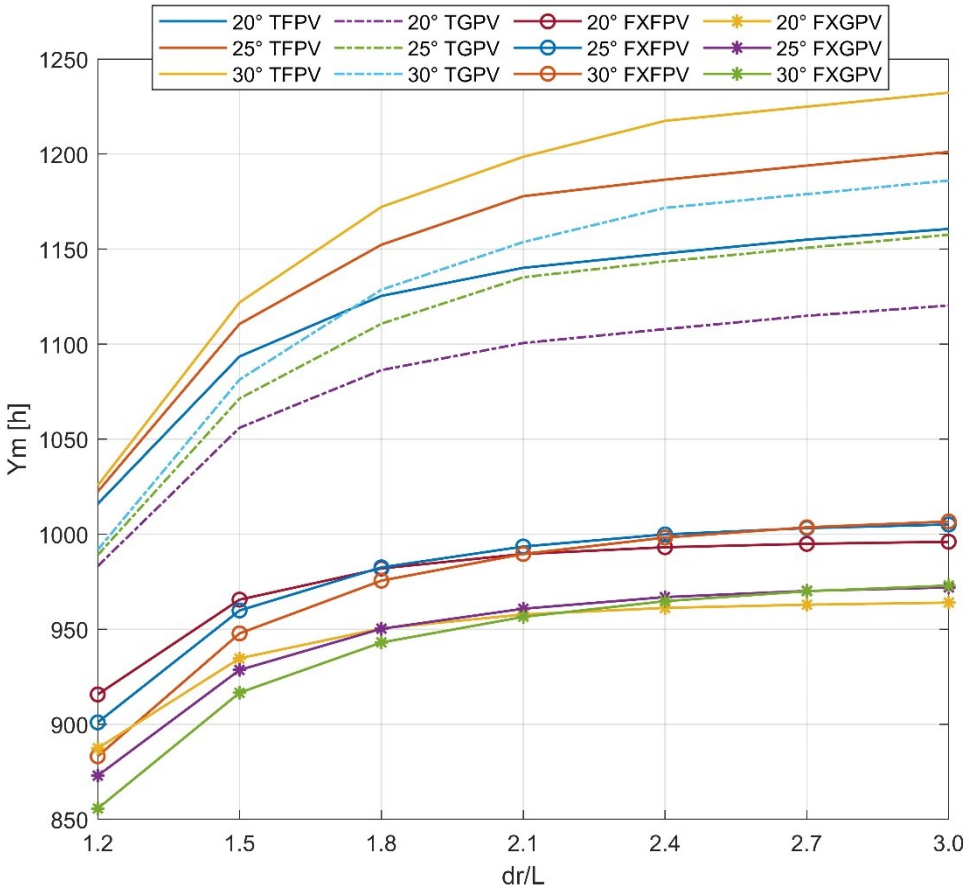

Figure 87 Trend of $Y_{m/b}$ for Vertical single-axis tracking and fixed F/GPV system

What can be seen from Figure 87is that the curves of the tracker systems in this case have an important offset between them, which means that in addition to the distance, the tilt also plays an important role even for small pitch values. This offset becomes larger as the pitch increases. The behavior as a function of the distance is almost similar to the cases examined above, ie the curves of the tracking system saturate with higher pitches than the fixed system. This behavior is due to the fact that in the case of tracking systems, there is a need, under the same climatic conditions, to increase the distance between the rows due to the mutual shading between the modules.

Table 84 shows the FG values for vertical tracking systems that allow you to evaluate the increase in performance of FPV systems due to natural cooling thanks to the favourable microclimate in which they operate.

Table 84 FG for Vertical single-axis tracking system

System Comparison		Φ [°]	$\gamma_{Mm/b}$ [°]	d_r/L		
				1.2	2.1	3.0
				FG [%]		
TFPV	TGPV	±120	20	3.3	3.6	3.6
			25	3.4	3.8	3.8
			30	3.4	3.9	3.9

FG values range from 3.3% to 3.9%.

Table 85 shows the TG values which take into account the effect of the energy gain due to the tracking of the floating system compared to the fixed floating system.

Table 85 TG for Vertical single-axis tracking system

System comparison		d_r/L		
TFPV	FXFPV	1.2	2.1	3.0
γ_{Mm} [°]		TG [%]		
20	20	10.9	15.2	16.5
	25	12.8	14.8	15.5
	30	15.0	15.2	15.3
25	20	11.7	19.0	20.6
	25	13.5	18.6	19.5
	30	15.8	19.0	19.3
30	20	12.0	21.1	23.7
	25	13.8	20.6	22.6
	30	16.1	21.1	22.4

The maximum TG values are obtained for the configuration with 30 ° tilt and dr / L = 3.0 compared with a fixed system with 20 ° tilt and dr / L = 20 ° and is equivalent to 23.7%.

Table 86 shows the TFG values which take into account the effect of the energy gain due to the tracking and natural cooling of the floating system compared to the monofacial ground system.

Table 86 TFG for Vertical single-axis tracking monofacial FPV system

System comparison		d_r/L		
TFPV	**FXGPV**	**1.2**	**2.1**	**3.0**
γ_{Mm} [°]		**TFG [%]**		
20	20	14.5	19.0	20.4
	25	16.4	18.7	19.4
	30	18.7	19.2	19.3
25	20	15.2	23.0	24.6
	25	17.1	22.6	23.6
	30	19.5	23.1	23.4
30	20	15.6	25.1	27.8
	25	17.5	24.7	26.8
	30	19.9	25.3	26.7

The maximum and minimum values obtainable are, TFGm=14.5% and 27.8%.

The TFG values for the vertical tracker are higher than horizontal N-S and E-W.

From what can be seen from the energy yield data, the vertical axis system is more efficient than horizontal axis system. It is to be understood, what is the difference in cost of this system compared to the previous ones. The previous ones are made with rafts with a gable structure, this one with a vertical axis can be of a different type, that is, a carousel, with or without a confinement structure. The cost therefore depends on the type of raft considered.

8.3.2.6 Dual axis tracking system

For this type of TFPV, simulations were carried out only for the monofacial system as the software does not allow to simulate bifacial modules with a 2 axes tracker.

Table 87 shows the energy collected values Y, normalized respect to the peak power of the system, for the configuration with 2 axes tracker in Aar Dam.

Table 87 $Y_{m/b}$ for Dual-axis tracking F/GPV system

System	**Φ [°]**	**$\gamma_{Mm/b}$ [°]**	d_r/L		
			1.2	**2.1**	**3.0**
			Y [h]		
TGPV	±120	0-50	1058.0	1291.0	1316.1
TFPV	±120	0-50	1095.2	1346.9	1373.7

Between the values of Y obtained for dr/ L= 1.2 and the subsequent ones, there is a considerable difference in terms of collected energy, this means that for the same installed power, compared to other technologies, it requires a greater installation surface.

Table 88 shows the FG values obtained for the two-axis system. The FG is the gain resulting from the natural cooling of the modules installed on water.

Table 88 FG for Dual axis tracking system

System	**Φ [°]**	**γ_{Mm} [°]**	**d_r/L**		
			1.2	**2.1**	**3.0**
			FG		
TFPV	±120	0-50	3.5	4.3	4.4

For the analyzed configurations the FG values oscillate between 3.5 and 4.4.

Table 89 shows the gain of the tracking effect.

Table 89 TG for Dual axis tracking system

System comparison		d_r/L		
TFPV	FXFPV	1.33	2.33	3.33
Φ=±120 γ_{Mm}=0-50	γ_{Mm} [°]	TG [%]		
	20	19.6	36.1	37.9
	25	21.6	35.6	36.7
	30	24.0	36.1	36.5

With the effect of dual tracking alone, without considering the effect of cooling, the energy collected could increase up to almost 38%.

Table 90 shows the gain due to cooling and tracking, then comparing fixed system on ground with the tracking system on water.

Table 90 TFG for Dual axis tracking system

System comparison		d_r/L		
TFPV	FXGPV	1.33	2.33	3.33
Φ=±120 γ_{Mm}=0-50	γ_{Mm} [°]	TFG [%]		
	20	23.4	40.6	42.5
	25	25.5	40.2	41.3
	30	28.0	40.8	41.2

Thanks to the dual effect of cooling and tracking, up to about 43% more energy can be collected.

8.4 Conclusions

This study made it possible to estimate the energy collected on an annual basis for each system, that is, fixed, with double or single axis tracking, with single or double-sided modules. The values obtained will be used in the next chapter for the evaluation of the economic competitiveness of FPV systems compared to classical fixed ground systems.

The maximum energy performance that can be obtained with the analyzed configurations is shown below.

As for the gain due to the bifaciality of the systems with bifacial modules, it can be stated that for the analyzed configurations, with an albedo of 5%, a gain greater than 3% can be obtained for Anapo Dam in Sicily and greater than 4% for Aar in Germany.

As for the gain due to the natural cooling of the modules, it can be stated that for the analyzed configurations, a gain of more than 5% can be obtained for Anapo Dam in Sicily and greater than 4% for Aare in Germany.

For Anapo Dam site, following maximum values were obtained in terms of increased energy (due to cooling, tracking and only for bPV, bifaciality) collected by an TFPV system compared to a fixed GPV system:

1. Horizontal axis tracker E-W:
    A. monofacial TFGm =13.4%;
    B. bifacial TBFG = 16.9%;
2. Horizontal axis tracker N-S:
    A. monofacial TFGm =24.1%;
    B. bifacial TBFG =27.6%;
3. Vertical axis tracker:
    A. monofacial TFGm =31.3%;
4. Dual axis tracker:

B. monofacial TFGm =47.4%;

For Aar Dam site, following maximum values were obtained in terms of increased energy (due to cooling, tracking and only for bPV, bifaciality) collected by an TFPV system compared to a fixed GPV system:

1. Horizontal axis tracker E-W:
   C. monofacial TFGm =9.4%;
   D. bifacial TBFG =14.4%;
2. Horizontal axis tracker N-S:
   C. monofacial TFGm =18.3%;
   D. bifacial TBFG =23.3%;
3. Vertical axis tracker:
   C. monofacial TFGm =27.8%;
4. Dual axis tracker:
   D. monofacial TFGm =42.5%;

9 Economic analysis of FPV plants

9.1 Introduction

Unlike the ground-mounted PV plants, floating systems are still in the first phase of the learning curve. There are not enough installations to be able to make an analysis of installation, maintenance, and operating costs that can be generalized. In fact, supports, mooring, anchoring, and floating systems are constantly improved and optimized. Therefore, in the near future, the economic assessment could undergo drastic changes, in the reduction direction, and it would reach a reference value when the technology of the entire system will be standardized as well as the one of the PV ground systems.

In this chapter, the comparative economic analysis among different PV plant solutions is based on the evaluation of three metrics, that is: the capital cost (CAPEX), the cost of operation and maintenance (OPEX) and the levelized cost of the electricity (LCOE).

The relevant point in the proposed economic model of the FPV systems is to consider the revenues deriving from the economic valorisation of the yearly volume of water available for other uses due to the reduction of evaporation caused by the partial covering of the water area. Furthermore, the LCOE cost is calculated considering the increase in energy yield due to active cooling with water.

Due to the uncertainty about the capital cost of FPVs a sensitivity analysis of the LCOE is carried out.

9.2 Methodology

To face the cost problem, it is necessary to provide the calculation models of LCOE with the equivalent hours of operation Y [h]; a geometric configuration will then be chosen for each type of system (fixed or tracking with mono and bifacial modules).

The list of the plants examined, and the related nomenclature is the following:

- FXGPVm Fixed Ground PV Monofacial
- FXFPVm Fixed Floating PV Monofacial
- FXFPVb Fixed Floating PV Bifacial

- FXGFPVm Fixed Gable Floating PV Monofacial
- HATFPVm Horizontal Axes Tracker Floating PV Monofacial
- HATFPVb Horizontal Axes Tracker Floating PV Bifacial
- VATFPVm Vertical Axes Tracker Floating PV Monofacial
- 2AXTFPVm 2 Axis Tracker Floating PV Monofacial

In the economic evaluation, the following will be taken into account:

- revenues from water saved due to partial coverage of the basin.
- the increase in energy due to the passive and active cooling of the modules.
- the increase in OPEX costs due to the operation and maintenance of the cooling system.
- the increase in CAPEX for the installation of the cooling system.

The energy production considered refers to the geometric configuration of each system shown in Table 91.

Table 91. Geometrical variables of the PV systems analysed

FXPV	
$\gamma_{Mm/b}$ (°)	25
d_r/L	2.1
Φ(°)	0
FXGFPVm	
γ_{Mm} (°)	10
d_r/L	-
Φ(°)	±90
HATPV	
$\gamma_{Mm/b}$ (°)	±50
d_r/L	2.1
Φ(°)	0-90
VATPV	
$\gamma_{Mm/b}$ (°)	25
d_r/L	2.1
Φ (°)	±120
2AXTPV	
$\gamma_{Mm/b}$ (°)	0-50
d_r/L	2.1
Φ(°)	±120

9.2.1 CAPEX

In this study the CAPEX values of the different plant solutions will be considered, obtained from economic offers of company and methodology for distribution of costs adopted in [89].

The evaluation of the CAPEX refers to the system solutions with the configuration shown in Table 91.

In the cost analysis, an increase in CAPEX for the cooling system will be considered based on the data provided by the companies that have built the active water-cooling systems with electric pumps, for the experimental plants monitored at the Enel Innovation Lab laboratories (see Chapter 3).

For innovative FPV solutions, a reduction of CAPEX could be obtained by increasing the size of the plant for scale economy and, mainly, for the technological improvement passing from prototypes to utility-scale plants, therefore a sensitivity analysis will be carried out for this parameter.

The fixed GPV system will be chosen as a reference to compare the cost differences compared to the FPVs studied.

For the reference GPV, it was decided not to reduce the CAPEX, because these effects are expected to be very modest compared to innovative solutions; at most there could be a reduction in costs due to scale effect.

9.2.2 OPEX

As regards the evaluation of OPEX, a scenario will be considered in which the OPEX increase for the operation and maintenance of the cooling system, and two scenarios in which the revenues deriving from non-evaporated water are also considered, in particular:

- REV_{IRR} water sold for irrigation.
- REV_{HPP} water fed into the turbine of a hydroelectric power plant.

For the reduction of evaporation, reference is made to the values obtained from the models implemented in Chapter 4.

The volume of water saved due to the lack of evaporation due to the partial coverage of the surface was calculated as follows:

$$Vol = \eta_{cover}\, E_{free}\, S$$ **Eq. 131**

Where:

- η_{cover} is the efficiency of the covering with FPV;
- E_{free} is evaporation of free water surfaces [m];
- S is the surface covered by the FPV system [m^2].

9.2.2.1 Revenues

In this paragraph, the methodology adopted for the calculation of revenues deriving from non-evaporated water will be described.

Revenues, Rev_{IRR} [$], from the sale of saved water are calculated as follows:

$$Rev_{IRR} = Vol * c_{w-irr}$$ **Eq. 132**

Where:

- c_{w-irr} is the cost of water for irrigation [$/$m^3$];
- Vol [m^3] is the volume of the water non-evaporated.

Revenues, Rev_{HPP} [$], deriving from the water fed into the turbine for the production of electricity from the HPP plant are calculated as follows:

$$Rev_{HPP} = EE * c_{el.en}$$ **Eq. 133**

Where:

- $c_{el.en}$ is the cost [$/kWh] of the electricity sold;
- EE [kWh] is the energy produced by HPP.

The power produced by the hydroelectric power plant P_{HPP} [kW] is calculated as follows:

$$P_{HPP} = 9.81 * Q * h * \eta$$ **Eq. 134**

Where Q is the flow rate of the turbine in [m^3/s], h is the head in [m] and η is the efficiency of the turbine.

The energy EE [kWh] produced by the turbine is calculated as follows:

$$EE_{HPP} = P_{HPP} * t$$ **Eq. 135**

Where t, is the time spent by the turbine to convert the amount of non-evaporated water into electrical energy.

With the method described above the OPEX, expressed in [$/kW], of each plant are calculated in the case of revenues obtained from the water sold for irrigation, as follows:

$$OPEX_{TOT\ IRR} = OPEX_{BASE} + OPEX_{COOL} - Rev_{IRR} \quad \textbf{Eq. 136}$$

Where $OPEX_{BASE}$ is the OPEX value provided by the system manufacturer, $OPEX_{COOL}$ are the costs related to the operation and maintenance of the active cooling system, and as described above, Rev_{IRR} are the revenues from the sale of non-evaporated water.

With the method described above, the OPEX of each plant are calculated in the case of revenues due to water converted into electricity by the HPP plant, as follows:

$$OPEX_{TOT\ HPP} = OPEX_{BASE} + OPEX_{COOL} - Rev_{HPP} \quad \textbf{Eq. 137}$$

The $OPEX_{COOL}$ value are obtained as follows:

$$OPEX_{COOL} = OPEX_{COOL\ MAINT} + (P_{w\ pump} * Price_{el} * t_{wpump}) \quad \textbf{Eq. 138}$$

Where $P_{w\ pump}$ is the power of the pump, $Price_{el}$ is the price per kWh of the electricity absorbed by the pump, $t_{w\ pump}$ is the operating time of the pump and $OPEX_{COOL\ MAINT}$ is the OPEX due to maintenance of cooling system.

From the experience acquired during the monitoring of the cooling system of the FPV experimental plant of the ENEL Innovation Hub and Lab, it can be assumed that the pump can be activated on average for 3.5 hours per day for the hottest six months of the year. As it is necessary to clean the filters and sprinklers of the cooling system due to the excessive turbidity of the water, it will be considered a cost for maintenance.

As for the revenues for irrigation, they are a function of the selling price of water, so a sensitivity analysis of the revenues will be carried out in relation to the unit cost of water.

As for the revenues from the sale of energy, they depend on the electricity market and vary from day to day and month to month. Furthermore, since the energy produced depends on other variables such as the prevalence of the HPP plant that changes from

plant to plant, it is necessary to make a sensitivity analysis of the revenues according to the prevalence but also the cost of selling electricity.

9.2.3 LCOE

Starting from the hypotheses of costs and producibility of the plants, the LCOE will be calculated for each technology (mono, bifacial, fixed and tracking). Through a sensitivity analysis, the competitiveness of FPV systems with respect to ground-based reference systems will be assessed, evaluating the benefits due to the reduction of evaporation and the increase in energy yield.

The LCOE calculations are based on the model presented by NREL in [120].

The calculation formula is as follows:

$$LCOE = \frac{sum\ of\ costs\ over\ lifetime}{sum\ of\ electrical\ energy\ produced\ over\ lifetime} = \frac{\sum_{t=1}^{n} \frac{CAPEX_t + OPEX_t}{(1+r)^t}}{\sum_{t=1}^{n} \frac{E_t}{(1+r)^t}} \quad \textbf{Eq. 139}$$

Where:

- $\boldsymbol{CAPEX_t}$ [$/kW] is investment expenditures in the year t
- $\boldsymbol{OPEX_t}$ [$/kW] is operations and maintenance expenditures in the year t
- $\boldsymbol{E_t}$ [kWh] is electrical energy generated in the year t
- $\boldsymbol{r}$ is discount rate
- $\boldsymbol{n}$ is expected lifetime of system or power station

The LCOE of each plant will be calculated in absolute value but also the LCOE differences between the innovative FPV solutions and the GPV reference solution.

To evaluate the competitiveness of the various systems examined with respect to the fixed monofacial ground reference system, a sensitivity analysis of the LCOE will be carried out as a function of the CAPEX variation for the different solutions and scenarios considering:

- reduction from 0 to 30% of the CAPEX in active cooling conditions of the modules;
- reduction from 0 to 30% of the CAPEX in conditions of active cooling of the modules and revenues deriving from the sale of additional energy produced with the saved non-evaporated water;

- reduction from 0 to 30% of the CAPEX in conditions of active cooling of the modules and revenues from the sale of non-evaporated water (for irrigation).

The ΔLCOE will be calculated as follows:

$$\Delta LCOE = 100\frac{LCOE_{FPV} - LCOE_{FXGPVm}}{LCOE_{FXGPVm}} \quad \textbf{Eq. 140}$$

A positive ΔLCOE value indicates that the FPV system is not competitive respect to reference system and vice versa.

9.3 Results

This paragraph will show the results obtained in terms of LCOE for the various plant solutions studied but it is necessary to first report the following assumptions:

- The values of equivalent hours Y considered in the LCOE calculations for each single technology are shown Table 92 e and have been calculated in Chapter 8 for the Anapo Dam location.
- The used CAPEX values are shown in Table 93.
- The used OPEX values are Table 95.
- The cost of the active water cooling system is $CAPEX_{COOL}$ = 20 $/kW.
- Discount rate r = 3%
- Plant life n = 30 years
- The increase in energy due to active cooling is 9.5% for monofacial and 9.7% for bifacial modules consistently as reported in Chapter 6
- The annual evaporation for free water surface for Sicily is E_{free} = 1742 mm. This value is coherent with results of Chapter 4.
- The percentage of water surface covered by the modules is x = 50% so the coverage efficiency considering the type d floats (Figure 34d) is 73%. This value is coherent with results of Chapter 4.
- The surface area occupied by 1MW of plant is equal to 10000 m^2.

- The annual evaporation of water surface covered by d system of Figure 34 is E_{FPVd} = 470.34 mm. The water saved is 1271.66 mm. These value are coherent with results of Chapter 4.
- The efficiency of the HPP plant is equal to $\eta = 0.9$
- The head of the HPP plant is equal to h = 500 m
- The selling price of water for irrigation is 0.15 $/m^3$ [96]
- The selling price of the electricity produced by the HPP plant is 90 $/MWh [121].
- The LCOE sensitivity analysis takes into account a CAPEX variation ranging from 0 to 30%.

Below is the summary of Y for different power plant in Anapo Dam (Sicily).

Table 92 Y value for different power plant in Anapo Dam (Sicily)

PV systems	**Y** [h]
FXGPVm	1736.6
FXFPVm	1818.5
FXFPVb	1863.2
FXGFPVm	1591.6
HATFPVm (E-W)	1928.9
HATFPVb (E-W)	1982.8
HATFPVm (N-S)	2056.9
HATFPVb (N-S)	2110.5
VATFPVm	2172.2
2AXTFPVm	2515.1

9.3.1 CAPEX

Below is the summary Table 93 of CAPEX costs per kW in relation to the plant solution for a 1 MW FPV power plant in Anapo Dam (Sicily). The third column shows the CAPEX increased by the cost of the cooling system.

Table 93 CAPEX for different FPV plants for a peak power of 1 MW

	CAPEX ($/kW)	**CAPEX+CAPEX$_{COOL}$** ($/kW)
FXGPVm	899.6	-
FXFPVm	984.0	1004.0
FXFPVb	1012.2	1032.2
FXGFPVm	934.8	954.8
HATFPVm (E-W)	1230.0	1250.0
HATFPVb (E-W)	1266.9	1286.9
HATFPVm (N-S)	1230.0	1250.0
HATFPVb (N-S)	1266.9	1286.9
VATFPVm	1394.3	1414.3
2AXTFPVm	1935.7	1955.7

The data reported in Table 93 were obtained using the methodology previously described.

9.3.2 OPEX

Based on the above methodology and assumptions, the revenues from the sale of water for irrigation and the sale of electricity produced by the HPP plant where the FPV system could be installed were obtained.

As for the revenues from irrigation, they are a function of the selling price of water. According to the assumptions, a sensitivity analysis of the revenues can be carried out in relation to the cost of water sold for irrigation.

The Table 94 shows revenue of irrigation in relation to price of water.

Table 94 Revenue of irrigation in relation to price of water

$Price_{wIRR}$ ($/m^3)	0.05	0.15	0.25
Rev_{IRR} ($/kWp)	0.63	1.90	3.17

In an intermediate condition, in which the cost of water is 0.15 $/m^3, there are revenues equal to Rev_{IRR} = 1.90 $/kWp/y.

As for the revenues from the sale of energy, they depend on the electricity market and vary from day to day and month to month. Furthermore, since the energy produced

depends on other variables such as the head of the HPP plant which changes from plant to plant, a sensitivity analysis of the revenues was made based on the head but also on the cost of selling electricity.

Figure 88 shows the revenues in relation to the head h for the different electricity costs $Price_{el}$.

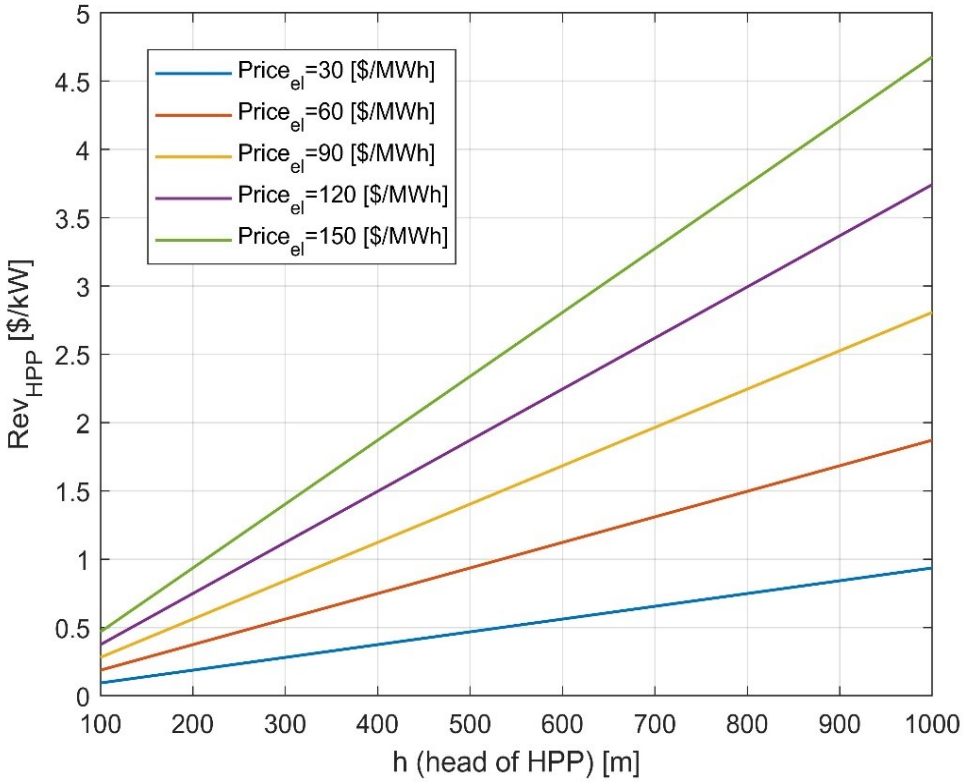

Figure 88 Revenues in relation to h for the different electricity costs

Putting in an intermediate situation, that is $Price_{el}$ = 90 $/MWh and h = 500 m, can be obtain revenues equal to Rev_{HPP} = 1.40 $/kW.

Table 95 shows the base and total OPEX values, ie considering the OPEX of the cooling system and the revenues in the two scenarios studied: water sold for irrigation and water sold in the form of energy produced by the HPP plant. Note that these values are calculated on the basis of the following revenues:

- Rev_{IRR} = 1.90 $ / kW.
- Rev_{HPP} = 1.40 $ / kW.

Assuming that the pump can be activated for an average of 3.5 hours per day for six months of the year, the $OPEX_{COOL}$ value can be obtained as follows.

Pump operation equal to: $t_{w\ pump} = 30\ (\text{days})\ \ 3.5\ (\text{hours per day})\ \ 6\ (\text{months}) = 630\ \text{h}$.

Taking as an example the cooling system of the FPV plant of the Enel Innovation Lab in Passo Martino (CT) mentioned above, it can be said that it is sufficient to use a pump with an absorption of 0.25 kWh for a 5 kWp FPV system. This translates into an energy consumption of 0.05 kWh/kWp FPV installed.

Assuming a cost of electricity equal to $Price_{el}$=0.09$/kWh and a cost for maintenance of 1.8 $/kW so: $OPEX_{COOL} = (630\ h\ \ 0.05\frac{kW}{kWp}0.09\frac{\$}{kWh}) + 1.8\ \frac{\$}{kW} = 4.63\ \$/kWp$ is obtained. Therefore, $OPEX_{COOL}$= 4.63 $/kWp.

Below is the summary Table 95 of OPEX in relation to the plant solution.

Table 95 OPEX of FPV plants

PV systems	**OPEX** ($/kW)	**OPEX+ $OPEX_{COOL}$** ($/kW)	**$OPEX_{TOT\ IRR}$** ($/kW)	**$OPEX_{TOT\ HPP}$** ($/kW)
FXGPVm	51.64	-	-	-
FXFPVm	51.64	56.27	54.36	54.86
FXFPVb	52.15	56.78	54.88	55.38
FXGFPVm	51.64	56.27	54.36	54.86
HATFPVm (E-W)	56.80	61.43	59.52	60.03
HATFPVb (E-W)	57.32	61.95	60.04	60.54
HATFPVm (N-S)	56.80	61.43	59.52	60.03
HATFPVb (N-S)	57.32	61.95	60.04	60.54
VATFPVm	59.38	64.01	62.10	62.61
2AXTFPVm	61.96	66.59	64.69	65.19

The installation of the cooling system increases OPEX costs but at the same time, when activated, increases the performance of the modules, and reduces the effect of degradation and therefore increases the useful life of the system.

9.3.3 LCOE

Table 96 shows the LCOE values calculated on the basis of the previous hypotheses.

Table 96 LCOE of F/GPV plants

(cent$/kWh)	**$LCOE_{BASE}$**	**$LCOE_{COOL}$**	**$LCOE_{COOL+RevHPP}$**	**$LCOE_{COOL+RevIRR}$**
FXGPVm	5.62	-	-	-
FXFPVm	**5.60**	**5.40**	**5.33**	**5.30**
FXFPVb	**5.57**	**5.36**	**5.30**	**5.27**
FXGFPVm	6.24	6.02	5.94	5.91
HATFPVm (E-W)	6.20	5.93	5.86	5.84
HATFPVb (E-W)	6.15	5.87	5.80	5.78
HATFPVm (N-S)	5.81	**5.56**	**5.50**	**5.47**
HATFPVb (N-S)	5.78	**5.51**	**5.45**	**5.43**
VATFPVm	6.01	5.72	5.67	5.64
2AXTFPVm	6.39	6.04	5.99	5.97

While considering the effect of cooling and the revenues deriving from the two scenarios considered, some of the systems analysed have a higher LCOE than the reference system on the ground, but this should not discourage since, as previously mentioned, the FPV systems are of new technology. and in the future there will be a drastic reduction in costs in particular for innovative solutions such as tracking systems.

Under this premise, it is worth seeing what happens when CAPEX are reduced. For this, a sensitivity analysis of the LCOE will be developed below.

9.3.3.1 Sensitivity of LCOE

Since, as already mentioned above, with the improvement of the FPV technology in the future a reduction of costs is foreseen, in this paragraph a sensitivity analysis of the LCOE will be carried out in function to the reduction of the CAPEX.

Figure 89 shows the percentage values of LCOE reduction of the various FPV systems compared to the reference system.

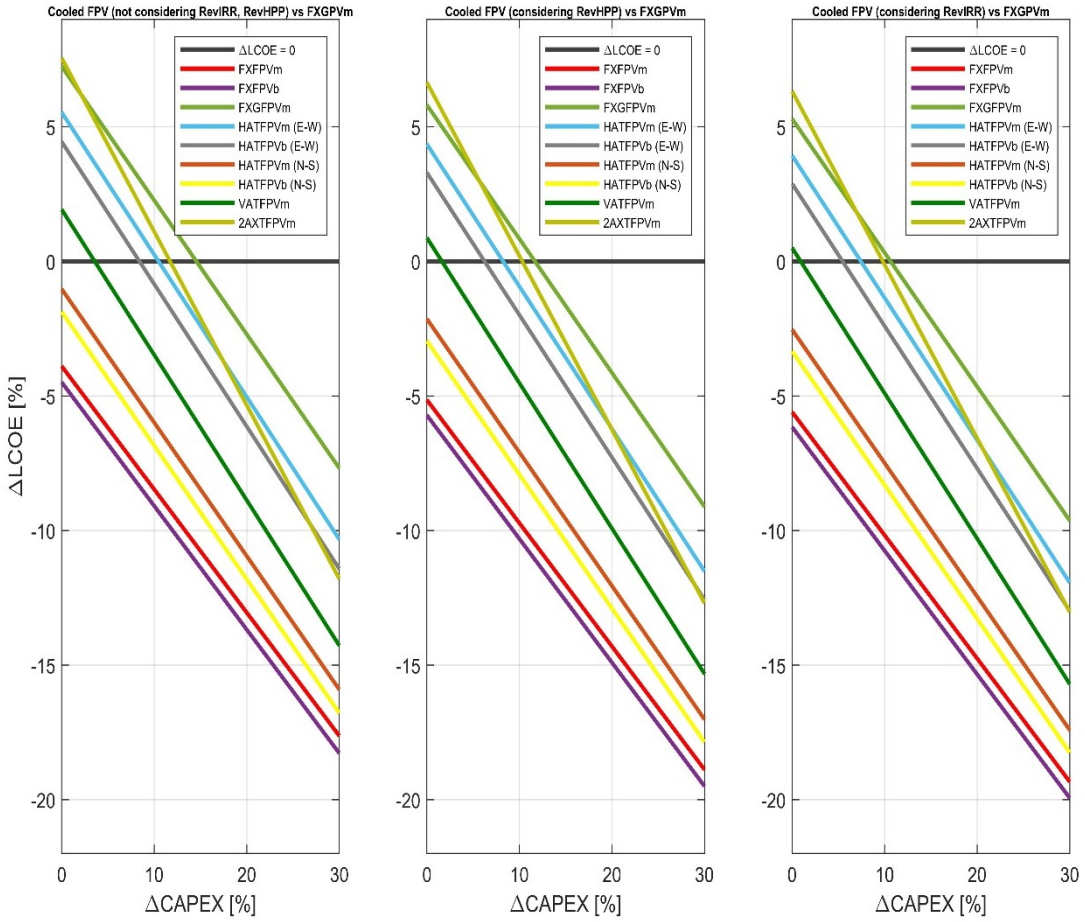

Figure 89 ΔLCOE in function to ΔCAPEX

Table 97 shows the ΔCAPEX(ΔLCOE = 0) for three scenarios analysed, starting from which the FPV system becomes competitive in terms of LCOE with respect to the reference system FXFPVm.

Table 97 ΔCAPEX (ΔLCOE = 0) values for three scenarios analysed

	ΔCAPEX(ΔLCOE=0)		
Scenario	**Cooling**	**Cooling and Rev_{HPP}**	**Cooling and Rev_{IRR}**
FXFPVm	0	0	0
FXFPVb	0	0	0
FXGFPVm	14.5	12	10.5
HATFPVm (E-W)	10.5	8	7
HATFPVb (E-W)	8	6	5
HATFPVm (N-S)	0	0	0
HATFPVb (N-S)	0	0	0
VATFPVm	3.5	2	1
2AXTFPVm	12	10.5	10

Table 98 shows the minimum and maximum ΔLCOE values obtainable by comparing the ground system with the FPV system considering the following scenarios:

- increase in energy yield due to the active cooling of the modules
- increase in energy yield due to the active cooling of the modules and revenues from the sale of additional energy produced with the saved non-evaporated water.
- increase in energy yield due to the active cooling of the modules and revenues from the sale of non-evaporated water (for irrigation).

Table 98 Minimum/maximum ΔLCOE for different FPV

Scenario	Cooling		Cooling and Rev_{HPP}		Cooling and Rev_{IRR}	
	ΔLCOE					
PV systems	**min**	**max**	**min**	**max**	**min**	**max**
FXFPVm	-17.6	-3.9	-18.9	-5.1	-19.3	-5.6
FXFPVb	-18.3	-4.5	-19.5	-5.7	-19.9	-6.2
FXGFPVm	-7.7	7.2	-9.1	5.8	-9.6	5.3
HATFPVm (E-W)	-10.3	5.5	-11.5	4.4	-11.9	3.9
HATFPVb (E-W)	-11.4	4.5	-12.6	3.3	-13.0	2.9
HATFPVm (N-S)	-15.9	-1.0	-17.0	-2.1	-17.4	-2.5
HATFPVb (N-S)	-16.8	-1.9	-17.9	-2.9	-18.2	-3.3
VATFPVm	-14.3	1.9	-15.3	0.9	-15.7	0.5
2AXTFPVm	-11.8	7.6	-12.7	6.7	-13.0	6.3

It can be concluded by stating that the most competitive system in terms of the lowest achievable LCOE value is FXFPVb in which, by reducing the CAPEX of 30%, a reduction in LCOE is obtained compared to the reference which is equal to -19.9%.

This means that the cost of electricity produced by the FXFPVb system, if the CAPEX were to be reduced by 30% in the future, will cost 19.9% less than the FXGPVm system for the reasons that are reiterated below.

There is an increase in performance due to active and passive cooling and revenues from non-evaporated water obtained due to the coverage of the FPV system.

9.4 Conclusions

With non-evaporated water that can be sold for irrigation or in the form of electricity produced by the HPP plant, it is possible to obtain revenues greater than 3 $/kWp in the first case and greater than 4 $/kWp in the second case.

Considering only the effect of cooling without revenues, FXFPVm/b, HATFPVm/b (N-S) systems are competitive without any reduction in CAPEX. FXGFPVm becomes competitive starting from a reduction in CAPEX equal to 14.5%, HATFPVm (E-W) 10.5%, and HATFPVb (E-W) 8%. The VATFPVm system becomes competitive starting from a CAPEX reduction equal to 3.5% and 2AXTFPVm 12%.

Considering the effect of cooling and revenues Rev_{HPP}, FXFPVm/b, HATFPVm/b (N-S) systems are competitive without any reduction in CAPEX. FXGFPVm becomes competitive starting from a reduction in CAPEX equal to 12%, HATFPVm (E-W) 8% and HATFPVb (E-W) 6%. The VATFPVm system becomes competitive starting from a CAPEX reduction equal to 2% and 2AXTFPVm 10.5%.

Considering the effect of cooling and revenues Rev_{IRR}, FXFPVm/b, HATFPVm/b (N-S) systems are competitive without any reduction in CAPEX. FXGFPVm becomes competitive starting from a reduction in CAPEX equal to 10.5%, HATFPVm (E-W) 7% and HATFPVb (E-W) 5%. The VATFPVm system becomes competitive starting from a CAPEX reduction equal to 1% and 2AXTFPVm 10%.

It can be concluded by stating that the most competitive system in terms of the lowest achievable LCOE value is FXFPVb in which, by reducing the CAPEX of 30%, a reduction in LCOE is obtained compared to the reference which is equal to -19.9%.

This means that the cost of electricity produced by the FXFPVb system, if the CAPEX were to be reduced by 30% in the future, will cost 19.9% less than the FXGPVm system for the reasons that are reiterated below.

There is an increase in performance due to active and passive cooling and revenues from non-evaporated water obtained due to the coverage of the FPV system.

10 Conclusions and prospects

10.1 Conclusions

In the context of the study of the integration of FPV systems in water basins, numerical models have been developed that allow to estimate the evaporation rate in relation to the characteristics of the floating systems and the occupied water surface.

The results of the analysis show that the amount of evaporated water depends not only on the percentage of CWS but also on the characteristics of the floating systems.

By installing the FPV on 30% of the basin area, the suspended systems obtain a water saving of about 18%, the systems that completely cover the surface below the modules obtain a saving of 49%, flexible panels in direct contact with water obtain a saving of 42%. Obviously, by increasing the surface of the water occupied by the FPV, the reduction in the evaporation rate increases (eg by covering 50% of the surface, the water saving is respectively 30-73-64%).

It has been shown that floating systems in direct contact with water compared to suspended systems have a higher yield in terms of evaporation reduction. Floating systems that cover the entire surface below the modules are the most efficient, followed by flexible floating systems which have a lower efficiency as part of the heat produced by the photovoltaic modules is exchanged with water.

Thanks to the effect of evaporation and the favourable microclimatic conditions, the PV modules installed on the water surface experience lower PV cell temperatures than classic ground systems.

To evaluate the effect of passive or active cooling with a water veil, models for estimating the energy performance of monofacial and bifacial modules have been implemented. In the energy balances, for the case of passive cooling, the effect due to evaporation is taken into account, and the convective effect on the back considering not the ambient temperature, but the apparent temperature which takes into account the relative humidity under the modules and near the water surface. Furthermore, the water surface temperature is taken into account for the calculation of the radiative contribution.

For the case of active cooling, in addition to the effects mentioned above, the convective effect due to the film of water flowing over the modules is also evaluated.

Result shows a gain due to bifaciality, BG, of 5.24%. An increase in the collected energy FG of 3% and 2.6% is calculated for the bifacial and monofacial systems respectively, with a maximum obtainable for the FPV bifacial compared to the monofacial GPV equal to 6.4% in the case of passive cooling.

An increase in the energy collected FG of 9.7% and 9.5% is calculated respectively for the bifacial and monofacial technology, with a maximum obtainable for bifacial floating compared to the monofacial GPV equal to 13.5% in the case of active cooling. This study made it possible to extend the analysis in long term period by comparing the data obtained from the experiments with the models of commercial software for estimating the performance of PV systems.

In this regard, a methodology is implemented that made it possible to adapt the simulation software of classic ground-mounted PV to FPV systems in order to evaluate their performance in the long term.

In this phase it was possible to analyze the behavior of monofacial and bifacial FPV systems as the geometry changes and evaluate both the energy increase due to passive cooling, and the energy increase due to bifaciality.

For the monofacial module, the following heat exchange coefficients were obtained: U_0=31.92 and U_1=1.5, a =-3.743 and b =-0.0746.

For the bifacial module, the following heat exchange coefficients were obtained: U_0 = 35.22 and U_1=1.5, a=-3.876 and b=-0.0738.

For the various analysed plant solutions, depending on the latitude, a gain due to the bifaciality that varies from 4 to 5% for an albedo of 5% can be obtained. If the albedo is increased, for example with reflective surfaces, gains greater than e 13% can be obtained.

As for the gain due to the natural cooling of the modules, it can be stated that for the analysed configurations, a gain of more than 5% can be obtained. Depending on the module technology and climatic conditions, this gain can be greater than 7%.

As regards the tracking systems, depending on the type adopted, the following energy gains can be obtained for intermediate latitudes: 16.9% (Horizontal axis tracker EW),

27.6% (Horizontal axis tracker NS), 31.3% (Vertical axis tracker) and 47.4% (Dual axis tracker).

With non-evaporated water that can be sold for irrigation or in the form of electricity produced by the HPP plant, it is possible to obtain revenues greater than 3 $/kWp in the first case and greater than 4 $/kWp in the second case.

Considering only the effect of cooling without revenues, FXFPVm/b, HATFPVm/b (N-S) systems are competitive without any reduction in CAPEX. FXGFPVm becomes competitive starting from a reduction in CAPEX equal to 14.5%, HATFPVm (E-W) 10.5%, and HATFPVb (E-W) 8%. The VATFPVm system becomes competitive starting from a CAPEX reduction equal to 3.5% and 2AXTFPVm 12%.

Considering the effect of cooling and revenues Rev_{HPP}, FXFPVm/b HATFPVm/b (N-S) systems are competitive without any reduction in CAPEX. FXGFPVm becomes competitive starting from a reduction in CAPEX equal to 12%, HATFPVm (E-W) 8% and HATFPVb (E-W) 6%. The VATFPVm system becomes competitive starting from a CAPEX reduction equal to 2% and 2AXTFPVm 10.5%.

Considering the effect of cooling and revenues Rev_{IRR}, FXFPVm/b HATFPVm/b (N-S) systems are competitive without any reduction in CAPEX. FXGFPVm becomes competitive starting from a reduction in CAPEX equal to 10.5%, HATFPVm (E-W) 7% and HATFPVb (E-W) 5%. The VATFPVm system becomes competitive starting from a CAPEX reduction equal to 1% and 2AXTFPVm 10%.

It can be concluded by stating that the most competitive system in terms of the lowest achievable LCOE value is FXFPVb in which, by reducing the CAPEX of 30%, a reduction in LCOE is obtained compared to the reference which is equal to -19.9%.

This means that the cost of electricity produced by the FXFPVb system, if the CAPEX were to be reduced by 30% in the future, will cost 19.9% less than the FXGPVm system for the reasons that are reiterated below.

There is an increase in performance due to active and passive cooling and revenues from non-evaporated water obtained due to the coverage of the FPV system.

10.2 Recommendations for future works

To increase the solar radiation reflected on the rear side of the bifacial modules, currently low due to the low albedo of the water, it is advisable to investigate economic and effective solutions that increase water reflection and at the same time do not cancel the cooling effect due to evaporation.

In this regard, the insertion of reflective surfaces anchored to the aluminum structures or light-colored floating hollow spheres placed on the surface of the water and in correspondence with the double-sided modules within the confined structure is being evaluated. These solutions seem feasible but must be tested in order to verify their real effectiveness.

As previously stated, the integration of floating photovoltaic plants (FPV) with hydroelectric plants represents a very effective example for increasing the utilization factor of the integrated hybrid system compared to the values of the individual plants and therefore their overall profitability.

In fact, FPV systems have a potential advantage if installed on storage basins of hydroelectric plants to exploit the residual capacity of pre-existing electrical systems by exploiting the complementarity of energy sources and the programmability of hydroelectric power plants with water basins.

The optimal coupling of these two systems will have to take into account various aspects influenced by the presence of the floating system, including:

- interference from a structural point of view since the anchoring, mooring, and floating systems must be designed to take into account existing structures;
- maximizing both the energy produced and the power fed into the network to which the hybrid system is connected;
- the environmental impact, as the FPV system mustn't cause damage to the surrounding environment and fauna;

In this regard, research must make a further effort to try to solve the problem of the optimal sizing of an FPV system in order to maximize the profitability of the hybrid system, in which the intrinsic characteristics of the HPP system are taken into account, i.e. the nominal power of the transformer, the transport capacity of the interconnection

to the network, the volume of water stored during the year, usable water surface, restrictions on the use of water for agricultural and / or civil uses.

Bibliography

[1] BP, “BP Energy Outlook 2019 edition,” 2019.

[2] “International Renewable Energy Agency, Renewable Capacity Statistics 2020.”

[3] Solar Power Europe, “Global Market Outlook For Solar Power / 2019 - 2023.” 2020.

[4] S. Ong, C. Campbell, P. Denholm, R. Margolis, and G. Heath, “Land-Use Requirements for Solar Power Plants in the United States,” 2013.

[5] W. Lytle *et al.*, “Conceptual Design and Rationale for a New Agrivoltaics Concept: Pasture-Raised Rabbits and Solar Farming,” *J. Clean. Prod.*, 2021, doi: 10.1016/j.jclepro.2020.124476.

[6] “https://www.solarplaza.com/channels/top-10s/11761/top-70-floating-solar-pv-plants/.” .

[7] “http://www.jinkosolar.com/en/site/newsdetail/1452.”

[8] T. S. Liang *et al.*, “A review of crystalline silicon bifacial photovoltaic performance characterisation and simulation,” *Energy and Environmental Science*. 2019, doi: 10.1039/c8ee02184h.

[9] “VDMA. International Technology Roadmap for Photovoltaic (ITRPV). Available: <https://itrpv.vdma.org/en/>; 2020.,” 2020.

[10] W. Gu, T. Ma, S. Ahmed, Y. Zhang, and J. Peng, “A comprehensive review and outlook of bifacial photovoltaic (bPV) technology,” *Energy Convers. Manag.*, vol. 223, no. July, p. 113283, 2020, doi: 10.1016/j.enconman.2020.113283.

[11] R. Guerrero-Lemus, R. Vega, T. Kim, A. Kimm, and L. E. Shephard, “Bifacial solar photovoltaics - A technology review,” *Renewable and Sustainable Energy Reviews*. 2016, doi: 10.1016/j.rser.2016.03.041.

[12] “Where Sun Meets Water,” *Where Sun Meets Water*, 2019, doi: 10.1596/32804.

[13] C. W. Hansen *et al.*, “Analysis of irradiance models for bifacial PV modules,” 2016, doi: 10.1109/PVSC.2016.7749564.

[14] C. Coskun, U. Toygar, O. Sarpdag, and Z. Oktay, “Sensitivity analysis of implicit correlations for photovoltaic module temperature: A review,” *Journal of Cleaner Production*. 2017, doi: 10.1016/j.jclepro.2017.07.080.

[15] E. Skoplaki and J. A. Palyvos, “Operating temperature of photovoltaic modules: A survey of pertinent correlations,” *Renew. Energy*, 2009, doi: 10.1016/j.renene.2008.04.009.

[16] D. Faiman, “Assessing the outdoor operating temperature of photovoltaic modules,” *Prog. Photovoltaics Res. Appl.*, 2008, doi: 10.1002/pip.813.

[17] U. A. Yusufoglu, T. M. Pletzer, L. J. Koduvelikulathu, C. Comparotto, R. Kopecek, and H. Kurz, “Analysis of the annual performance of bifacial modules and optimization methods,” *IEEE J. Photovoltaics*, 2015, doi: 10.1109/JPHOTOV.2014.2364406.

[18] G. M. Tina, F. B. Scavo, and A. Gagliano, “Multilayer Thermal Model for Evaluating the Performances of Monofacial and Bifacial Photovoltaic Modules,” *IEEE J. Photovoltaics*, 2020, doi: 10.1109/JPHOTOV.2020.2982117.

[19] B. G. Bhang, W. Lee, G. G. Kim, J. H. Choi, S. Y. Park, and H. K. Ahn, “Power Performance of Bifacial c-Si PV Modules with Different Shading Ratios,” *IEEE J. Photovoltaics*, 2019, doi: 10.1109/JPHOTOV.2019.2928461.

[20] L. Prat *et al.*, “Performance analysis of bifacial silicon solar cells in a space environment,” *Sol. Cells*, 1990, doi: 10.1016/0379-6787(90)90003-N.

[21] I. Shoukry, J. Libal, R. Kopecek, E. Wefringhaus, and J. Werner, “Modelling of Bifacial Gain for Stand-alone and in-field Installed Bifacial PV Modules,” 2016, doi: 10.1016/j.egypro.2016.07.025.

[22] A. Schmid, “Realistic Yield Expectations for Bifacial PV Systems – an Assessment of Announced, Predicted and Observed Benefits.” .

[23] C. D. Rodríguez-Gallegos *et al.*, “Global Techno-Economic Performance of Bifacial and Tracking Photovoltaic Systems,” *Joule*, 2020, doi: 10.1016/j.joule.2020.05.005.

[24] A. Hasan and I. Dincer, “A new performance assessment methodology of bifacial photovoltaic solar panels for offshore applications,” *Energy Convers.*

Manag., 2020, doi: 10.1016/j.enconman.2020.112972.

[25] A. G. Giuseppe Marco Tina, Fausto Bontempo Scavo, Stefano Aneli, "A novel building ventilated façade with integrated bifacial photovoltaic modules: analysis of the electrical and thermal performances."

[26] S. Guo, T. M. Walsh, and M. Peters, "Vertically mounted bifacial photovoltaic modules: A global analysis," *Energy*, vol. 61, pp. 447–454, 2013, doi: 10.1016/j.energy.2013.08.040.

[27] A. Sahu, N. Yadav, and K. Sudhakar, "Floating photovoltaic power plant: A review," *Renewable and Sustainable Energy Reviews*. 2016, doi: 10.1016/j.rser.2016.08.051.

[28] C. Ferrer-Gisbert, J. J. Ferrán-Gozálvez, M. Redón-Santafé, P. Ferrer-Gisbert, F. J. Sánchez-Romero, and J. B. Torregrosa-Soler, "A new photovoltaic floating cover system for water reservoirs," *Renew. Energy*, 2013, doi: 10.1016/j.renene.2013.04.007.

[29] R. Cazzaniga, M. Cicu, M. Rosa-Clot, P. Rosa-Clot, G. M. Tina, and C. Ventura, "Floating photovoltaic plants: Performance analysis and design solutions," *Renew. Sustain. Energy Rev.*, vol. 81, no. May 2017, pp. 1730–1741, 2018, doi: 10.1016/j.rser.2017.05.269.

[30] K. Trapani and D. L. Millar, "The thin film flexible floating PV (T3F-PV) array: The concept and development of the prototype," *Renew. Energy*, 2014, doi: 10.1016/j.renene.2014.05.007.

[31] S. Kajari-Schröder, I. Kunze, U. Eitner, and M. Köntges, "Spatial and directional distribution of cracks in silicon PV modules after uniform mechanical loads," 2011, doi: 10.1109/PVSC.2011.6186082.

[32] S. Oliveira-Pinto and J. Stokkermans, "Assessment of the potential of different floating solar technologies – Overview and analysis of different case studies," *Energy Convers. Manag.*, 2020, doi: 10.1016/j.enconman.2020.112747.

[33] M. Rosa-Clot and G. M. Tina, "Floating Plants and Environmental Aspects," in *Submerged and Floating Photovoltaic Systems*, 2018.

[34] S. N. Fausto Bontempo Scavo, Giuseppe Marco Tina, Hrvoje Dedić-Jandrek, "Selection and comprehensive analysis of water based cooled floating

photovoltaic power plant," *Renew. Energy*, vol. Under Revi.

[35] S. Nižetić, E. Giama, and A. M. Papadopoulos, "Comprehensive analysis and general economic-environmental evaluation of cooling techniques for photovoltaic panels, Part II: Active cooling techniques," *Energy Convers. Manag.*, vol. 155, no. July 2017, pp. 301–323, 2018, doi: 10.1016/j.enconman.2017.10.071.

[36] A. E. Kabeel, M. Abdelgaied, R. Sathyamurthy, and A. Kabeel, "A comprehensive review of technologies used to improve the performance of PV systems in a view of cooling mediums, reflectors design, spectrum splitting, and economic analysis," *Environ. Sci. Pollut. Res.*, 2020, doi: 10.1007/s11356-020-11008-3.

[37] S. Abdul Hamid, M. Yusof Othman, K. Sopian, and S. H. Zaidi, "An overview of photovoltaic thermal combination (PV/T combi) technology," *Renewable and Sustainable Energy Reviews*. 2014, doi: 10.1016/j.rser.2014.05.083.

[38] S. Nižetić, D. Čoko, A. Yadav, and F. Grubišić-Čabo, "Water spray cooling technique applied on a photovoltaic panel: The performance response," *Energy Convers. Manag.*, 2016, doi: 10.1016/j.enconman.2015.10.079.

[39] S. Mehrotra, P. Rawat, M. Debbarma, K. Sudhakar, E. Centre, and M. Pradesh, "Performance of a Solar Panel With Water Immersion," *Int. J. Sci. Technol.*, 2014.

[40] M. R. Clot, P. Rosa-Clot, and G. M. Tina, "Submerged PV Solar Panel for Swimming Pools: SP3," 2017, doi: 10.1016/j.egypro.2017.09.565.

[41] K. Trapani and M. Redõn Santafé, "A review of floating photovoltaic installations: 2007-2013," *Progress in Photovoltaics: Research and Applications*. 2015, doi: 10.1002/pip.2466.

[42] M. Rosa-Clot, P. Rosa-Clot, G. M. Tina, and P. F. Scandura, "Submerged photovoltaic solar panel: SP2," *Renew. Energy*, vol. 35, no. 8, pp. 1862–1865, 2010, doi: 10.1016/j.renene.2009.10.023.

[43] S. Wu and C. Xiong, "Passive cooling technology for photovoltaic panels for domestic houses," *Int. J. Low-Carbon Technol.*, 2014, doi: 10.1093/ijlct/ctu013.

[44] M. Lucas, F. J. Aguilar, J. Ruiz, C. G. Cutillas, A. S. Kaiser, and P. G. Vicente, “Photovoltaic Evaporative Chimney as a new alternative to enhance solar cooling,” *Renew. Energy*, vol. 111, pp. 26–37, 2017, doi: 10.1016/j.renene.2017.03.087.

[45] E. Drabiniok and A. Neyer, “Bionic micro porous evaporation foil for photovoltaic cell cooling,” *Microelectron. Eng.*, vol. 119, pp. 65–69, 2014, doi: 10.1016/j.mee.2014.02.013.

[46] E. Drabiniok and A. Neyer, “Evaporation Cooling Using a Bionic Micro Porous Evaporation System,” *Heat Transf. Eng.*, 2019, doi: 10.1080/01457632.2018.1457249.

[47] B. Sutanto and Y. S. Indartono, “Computational fluid dynamic (CFD) modelling of floating photovoltaic cooling system with loop thermosiphon,” 2019, doi: 10.1063/1.5086558.

[48] A. H. Alami, “Microstructural, optical and thermal characterization of synthetic clay as a passive cooling medium,” *Energy Convers. Manag.*, vol. 88, pp. 442–446, 2014, doi: 10.1016/j.enconman.2014.08.053.

[49] A. H. Alami, “Synthetic clay as an alternative backing material for passive temperature control of photovoltaic cells,” *Energy*, 2016, doi: 10.1016/j.energy.2015.05.029.

[50] Y. K. Choi, W. S. Choi, and J. H. Lee, “Empirical research on the efficiency of floating PV systems,” *Sci. Adv. Mater.*, 2016, doi: 10.1166/sam.2016.2529.

[51] L. Liu, Q. Wang, H. Lin, H. Li, Q. Sun, and R. Wennersten, “Power Generation Efficiency and Prospects of Floating Photovoltaic Systems,” 2017, doi: 10.1016/j.egypro.2017.03.483.

[52] W. C. L. Kamuyu, J. R. Lim, C. S. Won, and H. K. Ahn, “Prediction model of photovoltaic module temperature for power performance of floating PVs,” *Energies*, 2018, doi: 10.3390/en11020447.

[53] S. Seme, B. Štumberger, M. Hadžiselimović, and K. Sredenšek, “Solar Photovoltaic Tracking Systems for Electricity Generation: A Review,” *Energies*, vol. 13, no. 16, p. 4224, 2020, doi: 10.3390/en13164224.

[54] M. Rosa-Clot and G. M. Tina, “Tracking Systems,” in *Floating PV Plants*,

2020.

[55] “Floating Solar, [Online]. Available: https://floatingsolar.nl/.”

[56] *Floating PV Plants*. 2020.

[57] S. H. Kim, S. J. Yoon, W. Choi, and K. B. Choi, “Application of floating photovoltaic energy generation systems in South Korea,” *Sustain.*, vol. 8, no. 12, pp. 1–9, 2016, doi: 10.3390/su8121333.

[58] Y. K. Choi and Y. G. Lee, “A study on development of rotary structure for tracking-type floating photovoltaic system,” *Int. J. Precis. Eng. Manuf.*, vol. 15, no. 11, pp. 2453–2460, 2014, doi: 10.1007/s12541-014-0613-5.

[59] G. M. Tina and M. Rosa-Clot, “Electrical Behavior and Optimization of Panels and Reflector of a Photovoltaic Floating Plant,” *26th Eur. Photovolt. Sol. Energy Conf. Exhib.*, no. June 2020, pp. 4371–4375, 2011, doi: 10.4229/26thEUPVSEC2011-5BV.2.54.

[60] J. M. Wang and C. L. Lu, “Design and implementation of a sun tracker with a dual-axis single motor for an optical sensor-based photovoltaic system,” *Sensors (Switzerland)*, 2013, doi: 10.3390/s130303157.

[61] R. Xu, C. Liu, H. Liu, Z. Sun, T. L. Lam, and H. Qian, “Design and optimization of a wave driven solar tracker for floating photovoltaic plants,” *IEEE/ASME Int. Conf. Adv. Intell. Mechatronics, AIM*, vol. 2019-July, pp. 1293–1298, 2019, doi: 10.1109/AIM.2019.8868847.

[62] P. E. Campana, L. Wästhage, W. Nookuea, Y. Tan, and J. Yan, “Optimization and assessment of floating and floating-tracking PV systems integrated in on- and off-grid hybrid energy systems,” *Sol. Energy*, vol. 177, no. December 2018, pp. 782–795, 2019, doi: 10.1016/j.solener.2018.11.045.

[63] H. Rauf, M. S. Gull, and N. Arshad, “Integrating floating solar PV with hydroelectric power plant: Analysis of Ghazi barotha reservoir in Pakistan,” *Energy Procedia*, vol. 158, pp. 816–821, 2019, doi: 10.1016/j.egypro.2019.01.214.

[64] R. Cazzaniga, M. Rosa-Clot, P. Rosa-Clot, and G. M. Tina, “Integration of PV floating with hydroelectric power plants,” *Heliyon*, vol. 5, no. 6, p. e01918, 2019, doi: 10.1016/j.heliyon.2019.e01918.

[65] J. Farfan and C. Breyer, “Combining floating solar photovoltaic power plants and hydropower reservoirs: A virtual battery of great global potential,” *Energy Procedia*, vol. 155, pp. 403–411, 2018, doi: 10.1016/j.egypro.2018.11.038.

[66] N. Lee *et al.*, “Hybrid floating solar photovoltaics-hydropower systems: Benefits and global assessment of technical potential,” *Renew. Energy*, vol. 162, pp. 1415–1427, 2020, doi: 10.1016/j.renene.2020.08.080.

[67] N. M. Silvério, R. M. Barros, G. L. Tiago Filho, M. Redón-Santafé, I. F. S. dos Santos, and V. E. de M. Valério, “Use of floating PV plants for coordinated operation with hydropower plants: Case study of the hydroelectric plants of the São Francisco River basin,” *Energy Convers. Manag.*, vol. 171, no. May, pp. 339–349, 2018, doi: 10.1016/j.enconman.2018.05.095.

[68] J. A. Maués, “Floating solar PV-hydroelectric power plants in Brazil: Energy storage solution with great application potential,” *Int. J. Energy Prod. Manag.*, vol. 4, no. 1, pp. 40–52, 2019, doi: 10.2495/EQ-V4-N1-40-52.

[69] M. M. Aman *et al.*, “A review of Safety, Health and Environmental (SHE) issues of solar energy system,” *Renewable and Sustainable Energy Reviews*. 2015, doi: 10.1016/j.rser.2014.08.086.

[70] G. D. Pimentel Da Silva and D. A. C. Branco, “Is floating photovoltaic better than conventional photovoltaic? Assessing environmental impacts,” *Impact Assess. Proj. Apprais.*, 2018, doi: 10.1080/14615517.2018.1477498.

[71] S. El Baradei and M. Al Sadeq, “Effect of solar canals on evaporation, water quality, and power production: An optimization study,” *Water (Switzerland)*, 2020, doi: 10.3390/W12082103.

[72] G. D. Pimentel Da Silva, A. Magrini, and D. A. C. Branco, “A multicriteria proposal for large-scale solar photovoltaic impact assessment,” *Impact Assess. Proj. Apprais.*, 2020, doi: 10.1080/14615517.2019.1604938.

[73] D. Liu, C. Li, M. Sun, and W. Zeng, “Assessment model of economic and environmental synergies for water surface photovoltaic projects based on spectral analysis,” *Renew. Energy*, 2020, doi: 10.1016/j.renene.2019.06.071.

[74] J. Haas, J. Khalighi, A. de la Fuente, S. U. Gerbersdorf, W. Nowak, and P. J. Chen, “Floating photovoltaic plants: Ecological impacts versus hydropower

operation flexibility," *Energy Convers. Manag.*, vol. 206, no. December 2019, 2020, doi: 10.1016/j.enconman.2019.112414.

[75] A. Gasparatos, C. N. H. Doll, M. Esteban, A. Ahmed, and T. A. Olang, "Renewable energy and biodiversity: Implications for transitioning to a Green Economy," *Renewable and Sustainable Energy Reviews*. 2017, doi: 10.1016/j.rser.2016.08.030.

[76] Y. Choi, "A Case Study on Suitable Area and Resource for Development of Floating Photovoltaic System," *Int. J. Electr. Comput. Electron. Commun. Eng.*, 2014.

[77] T. Guerin, "A case study identifying and mitigating the environmental and community impacts from construction of a utility-scale solar photovoltaic power plant in eastern Australia," *Sol. Energy*, 2017, doi: 10.1016/j.solener.2017.02.020.

[78] "Solar Power Jobs : Exploring the Employment Potential in India's Grid-Connected Solar Market, 2014."

[79] J. E. Lovich and J. R. Ennen, "Wildlife conservation and solar energy development in the desert Southwest, United States," *Bioscience*, 2011, doi: 10.1525/bio.2011.61.12.8.

[80] P. Rosa-Clot, "FPV and environmental compatibility," in *Floating PV Plants*, 2020.

[81] C. S.G., "Impactes ambientais de sistemas fotovoltaicos flutuante. UNIVERSIDADE DE LISBOA." .

[82] Marco Antonio Esteves Galdino and Marta Maria de Almeida Olivieri, "Some Remarks about the Deployment of Floating PV Systems in Brazil," *J. Electr. Eng.*, 2017, doi: 10.17265/2328-2223/2017.01.002.

[83] M. Rosa-Clot and G. M. Tina, "Introduction to PV Plants," in *Submerged and Floating Photovoltaic Systems*, 2018.

[84] World Bank, "Where Sun Meets Water: Floating Solar Market," *World Bank Group, ESMAP SERIS*, 2019.

[85] B. P. Martins, "Techno-economic Evaluation of a Floating PV System for a Wastewater Treatment Facility."

[86] M. Barbuscia, “Economic Viability Assessment of Floating Photovoltaic Energy,” 2017.

[87] L. E. Teixeira, J. Caux, A. Beluco, I. Bertoldo, J. A. S. Louzada, and R. C. Eifler, “Feasibility Study of a Hydro PV Hybrid System Operating at a Dam for Water Supply in Southern Brazil,” *J. Power Energy Eng.*, 2015, doi: 10.4236/jpee.2015.39006.

[88] “Sonoma county is building the largest floating solar project in the US | Greentech Media.”

[89] M. Rosa-Clot and G. M. Tina, “Levelized cost of energy (LCOE) analysis,” in *Floating PV Plants*, 2020.

[90] E. Vartiainen, G. Masson, C. Breyer, D. Moser, and E. Román Medina, “Impact of weighted average cost of capital, capital expenditure, and other parameters on future utility-scale PV levelised cost of electricity,” *Prog. Photovoltaics Res. Appl.*, 2020, doi: 10.1002/pip.3189.

[91] I. S. Rodrigues, G. L. B. Ramalho, and P. H. A. Medeiros, “Potential of floating photovoltaic plant in a tropical reservoir in Brazil,” *J. Environ. Plan. Manag.*, 2020, doi: 10.1080/09640568.2020.1719824.

[92] M. Rosa-Clot and G. M. Tina, *Floating PV plants*. 2020.

[93] International Bank for Reconstruction and Development, “Where Sun Meets Water Floating Solar Market Report,” *Where Sun Meets Water*, 2019.

[94] M. Temiz and N. Javani, “Design and analysis of a combined floating photovoltaic system for electricity and hydrogen production,” *Int. J. Hydrogen Energy*, 2020, doi: 10.1016/j.ijhydene.2018.12.226.

[95] Y. Ren, S. Wei, K. Cheng, and Q. Fu, “Valuation and pricing of agricultural irrigation water based on macro and micro scales,” *Water (Switzerland)*, 2018, doi: 10.3390/w10081044.

[96] Regione Siciliana, “Piano di gestione del distretto idrografico della Sicilia.” 2021.

[97] F. Bontempo Scavo, G. M. Tina, A. Gagliano, and S. Nižetić, “An assessment study of evaporation rate models on a water basin with floating photovoltaic plants,” *Int. J. Energy Res.*, 2020, doi: 10.1002/er.5170.

[98] D. L. King, W. E. Boyson, and J. A. Kratochvil, “Photovoltaic array performance model,” *Sandia Rep. No. 2004-3535*, 2004, doi: 10.2172/919131.

[99] G. Tamizhmani, L. Ji, Y. Tang, L. Petacci, and C. Osterwald, “Photovoltaic Module Thermal/Wind Performance : Long-Term Monitoring and Model Development For Energy Rating,” *NCPV Sol. Progr. Rev. Meet.*, pp. 936–939, 2003.

[100] P. W. Wong, Y. Shimoda, M. Nonaka, M. Inoue, and M. Mizuno, “Semi-transparent PV: Thermal performance, power generation, daylight modelling and energy saving potential in a residential application,” *Renew. Energy*, 2008, doi: 10.1016/j.renene.2007.06.016.

[101] H. L. Cha, B. G. Bhang, S. Y. Park, J. H. Choi, and H. K. Ahn, “Power prediction of bifacial Si PV module with different reflection conditions on rooftop,” *Appl. Sci.*, 2018, doi: 10.3390/app8101752.

[102] N. Shaw and D. Brunt, “Physical and Dynamical Meteorology,” *Math. Gaz.*, 1935, doi: 10.2307/3605892.

[103] R. J. Cole and N. S. Sturrock, “The convective heat exchange at the external surface of buildings,” *Building and Environment*. 1977, doi: 10.1016/0360-1323(77)90021-X.

[104] A. Bejan and A. D. Kraus, *Heat Transfer Handbook*. 2003.

[105] S. W. Churchill, “A comprehensive correlating equation for laminar, assisting, forced and free convection,” *AIChE J.*, 1977, doi: 10.1002/aic.690230103.

[106] D. M. McEligoi, “Fundamentals of momentum, heat and mass transfer,” *Int. J. Heat Mass Transf.*, 1970, doi: 10.1016/0017-9310(70)90063-3.

[107] M. W. P. E. Lamers *et al.*, “Temperature effects of bifacial modules: Hotter or cooler?,” *Sol. Energy Mater. Sol. Cells*, vol. 185, no. May, pp. 192–197, 2018, doi: 10.1016/j.solmat.2018.05.033.

[108] H. L. PENMAN, “Natural evaporation from open water, hare soil and grass,” *Proc. R. Soc. Lond. A. Math. Phys. Sci.*, 1948, doi: 10.1098/rspa.1948.0037.

[109] “FAO Penman-Monteith determination of Evaporation, Chapter 3 - Meteorological data, http://www.fao.org/3/X0490E/x0490e07.htm#TopOfPage.” .

[110] D. L. Ficklin, Y. Luo, I. T. Stewart, and E. P. Maurer, “Development and application of a hydroclimatological stream temperature model within the Soil and Water Assessment Tool,” *Water Resour. Res.*, 2012, doi: 10.1029/2011WR011256.

[111] S. J. Jacobs, A. B. Pezza, V. Barras, J. Bye, and T. Vihma, “An analysis of the meteorological variables leading to apparent temperature in Australia: Present climate, trends, and global warming simulations,” *Glob. Planet. Change*, 2013, doi: 10.1016/j.gloplacha.2013.05.009.

[112] F. B. Giuseppe Marco Tina, Fausto Bontempo Scavo, Leonardo Merlo, “Analysis of water environment on the production of floating photovoltaic plants,” *Renew. Energy*, no. In Press, 2021.

[113] J. H. Lienhard IV and J. H. Lienhard V, “A HEAT TRANSFER TEXTBOOK, fourth edition,” *Phlogist. Press*, 2017.

[114] F. Spertino, A. D’Angola, D. Enescu, P. Di Leo, G. V. Fracastoro, and R. Zaffina, “Thermal-electrical model for energy estimation of a water cooled photovoltaic module,” *Sol. Energy*, vol. 133, pp. 119–140, 2016, doi: 10.1016/j.solener.2016.03.055.

[115] T. Whittaker, M. Folley, and J. Hancock, “Environmental loads, motions, and mooring systems,” in *Floating PV Plants*, 2020.

[116] R. Cazzaniga, “Floating PV structures,” in *Floating PV Plants*, 2020.

[117] G. M. Tina, “Simulation model of photovoltaic and photovoltaic/thermal module/string under nonuniform distribution of irradiance and temperature,” *J. Sol. Energy Eng. Trans. ASME*, vol. 139, no. 2, pp. 1–12, 2017, doi: 10.1115/1.4035152.

[118] S. Z. Golroodbari and W. van Sark, “Simulation of performance differences between offshore and land-based photovoltaic systems,” *Prog. Photovoltaics Res. Appl.*, 2020, doi: 10.1002/pip.3276.

[119] G. M. Tina, F. Bontempo Scavo, L. Merlo, and F. Bizzarri, “Comparative analysis of monofacial and bifacial photovoltaic modules for floating power plants,” *Appl. Energy*, 2021, doi: 10.1016/j.apenergy.2020.116084.

[120] W. Short, D. Packey, and T. Holt, “A manual for the economic evaluation of

energy efficiency and renewable energy technologies," *Renew. Energy*, 1995, doi: NREL/TP-462-5173.

[121] "https://www.mercatoelettrico.org/it/." .

Appendix A: Statistical evaluation indexes

For the verification of the accuracy of the different models implemented, statistical indices have been used which are shown below.

Therefore, with Eq. 141 the root mean square error indicated as *RMSE* was calculated, the percentage error with Eq. 142 indicated as *PE*, the mean bias error with Eq. 143 indicated as *MBE*, the mean absolute error with Eq. 144 indicated as *MAE* and finally the coefficient of determination with Eq. 145 indicated as R^2. The following are the calculation formulas:

$$RMSE = \sqrt{\frac{\sum_{i=1}^{n}(P_i - O_i)^2}{n}} \quad \textbf{Eq. 141}$$

$$PE = 100 \left| \frac{P_{mean} - O_{mean}}{O_{mean}} \right| \quad \textbf{Eq. 142}$$

$$MBE = \frac{\sum_{i=1}^{n}(P_i - O_i)}{n} \quad \textbf{Eq. 143}$$

$$MAE = \left| \frac{\sum_{i=1}^{n}(P_i - O_i)}{n} \right| \quad \textbf{Eq. 144}$$

$$R^2 = \frac{\left[\sum_{i=1}^{n}(P_i - P_{mean})(O_i - O_{mean})\right]^2}{\sum_{i=1}^{n}(P_i - P_{mean})^2 \sum_{i=1}^{n}(O_i - O_{mean})^2} \quad \textbf{Eq. 145}$$

Where P_i and O_i are predicted and observed values. The subscript "*mean*" indicates the mean value of the variable and the letter "*n*" indicates the number of values examined. From the negative or positive sign of *MBE* it is possible to understand if the examined model, respectively, underestimates or overestimates the evaporation with respect to the model or measurements used as a reference.

Acknowledgments

This research was conducted with the financial support of the Italian Ministry of Education (MIUR) by “the Notice 12/2017 for financing the industrial Ph.D.” PON FSE-FESR RICERCA E INNOVAZIONE 2014-2020 AZIONE I.1.

The first and most important thanks goes to the supervisor Prof. Giuseppe Marco Tina, who offered me the opportunity to undertake this research and had the patience to guide me in the three years of my PhD. I will always appreciate the friendship, advice, and skills I have gained from him.

This rewarding journey for life would not have been possible without the support of the company tutor, Ing. Leonardo Merlo of Enel Green Power, thanks to whom I had the good fortune and the pleasure of following innovative projects and various activities with an industrial approach that have enriched me professionally.

A special thanks also goes to the tutor of the foreign university as well as Prof. Sandro Nižetić, head of the LTEF laboratories who allowed me to spend a few months at the University of Split, where I had the opportunity to compare myself with other students and researchers, that enriched my cultural background and perfect my knowledge of the English language.

I would like to acknowledge Enel Green Power team for help and support that gave me during my PhD, in particular I would like to thank Fabrizio Bizzarri who was supervisor.

I would like to thank my girlfriend Lucia from the bottom of my heart for her patience, the affection she has shown me and the many beautiful experiences she has shared with me over the years, also thanks to PhD period. Finally, I would like to thank my family that I know they love me a lot and that they always support and keep me motivated.

Thank you all,

Fausto Bontempo Scavo

La borsa di dottorato è stata cofinanziata con risorse del
Programma Operativo Nazionale Ricerca e Innovazione 2014-2020 (CCI 2014IT16M2OP005),
Fondo Sociale Europeo, Azione I.1 “Dottorati Innovativi con caratterizzazione Industriale”

UNIONE EUROPEA
Fondo Sociale Europeo